
THE UNIVERSITY
*of* EDINBURGH

# Lattice Phenomenology of Heavy Quarks Using Dynamical Fermions


*Ava Khamseh*

Doctor of Philosophy

University of Edinburgh

October 2017

*To the memory of*
*Mir Salavatian*

# Lay Summary

The Standard Model of particle physics describes how three of the four fundamental forces in Nature, *i.e.* the electromagnetic, the weak and the strong forces, allow for elementary particles of matter, such as quarks and electrons, to interact with each other via the force-carrier particles. With the discovery of the Higgs boson in 2012, the Standard Model (SM) is currently known to be the best theory describing subatomic particles and their forces of interaction. However, there are limitations to SM as it cannot explain certain phenomena such as gravitational interactions, dark matter or the abundance of matter over antimatter in the universe, to name a few. For these reasons, Standard Model is believed to only be the low energy limit of a more fundamental theory. Searches for new physics beyond the SM are performed both directly at the high-energy frontier, such as the LHC experiment at CERN, and indirectly at the precision frontier, via experiments such as LHCb.

Charge and parity violation, is a lack of symmetry between particles and antiparticles in the universe which may explain why the universe is made of matter and not antimatter. The interesting structure of quark interactions in the SM allows an asymmetry between matter and antimatter and is believed to contain important information about physics at high energies. One of the aims of the program in precision physics is to verify, using both theory and experiment, whether the mechanism explaining this symmetry violation in the SM is correct. Of particular interest is the heavy quark sector, where there are possible tensions between SM predictions and the experimental data. Lattice Quantum Chromodynamics (LQCD) is a major theoretical tool that, amongst other applications, allows for probing the dynamics of heavy quarks at low

energies, using numerical simulations.

There are two mains parts to this work. The first part develops better theoretical techniques for extracting numerical results from the simulations; in particular with relation to heavy quarks that are nowadays being simulated on the lattice more easily given the computational technology. The second part involves measurements of observables such as masses and decay constants of heavy particles, in order to compare the theoretical predictions with the experimental results, in search of any possible tensions.

# Abstract

The Standard Model of particle physics is believed to be only the low energy limit of a more fundamental theory. In order to determine its range of validity, a major part of theoretical and experimental efforts in physics is dedicated to precision tests of the Standard Model. Lattice QCD is a non-perturbative, first-principles approach to Quantum Field Theory. It plays an important role in flavor physics by providing calculations of non-perturbative strong interaction contributions to weak processes involving quarks. Measurements of hadronic quantities can be used to constrain the Standard Model as well as theories Beyond the Standard Model.

The first part of this thesis contains theoretical developments regarding non-perturbative renormalization. A new renormalization scheme, RI/mSMOM, for fermion bilinear operators in QCD at non-vanishing quark mass is presented. In order to investigate the properties of the mSMOM scheme, an explicit one-loop computation in perturbation theory using dimensional regularization is performed. Numerically, vertex functions are generated on the lattice, with an appropriate projector, based on the RI/SMOM scheme and the renormalization factors are extracted. Quantities measured include renormalization of the axial current $Z_A$, required to renormalize the axial current entering the computation of the decay constant and the renormalization of the bag parameter.

The second part of this report focuses on flavor physics phenomenology on the lattice. It presents results of the first run of the RBC/UKQCD charm project with (2+1)-flavor Domain Wall fermions. Observables and matrix elements are measured on lattices with Iwasaki gauge action. There are two ensembles at the physical point with inverse lattice spacings 1.73 and 2.36 GeV and a third finer ensemble at 2.76 GeV as well as four other auxiliary ensembles with smaller volumes and heavier pion masses which are used to perform the continuum

extrapolations. The quantities measured in the region of the charm quark mass are meson masses, decay constants, the matrix element of the $O_{VV+AA}$ operator, the neutral D-meson mixing parameter B and the SU(3) breaking ratio $\xi$.

# Declaration

Except where otherwise stated, the research undertaken in this thesis was my unaided work, carried out as a member of the RBC/UKQCD collaboration. Where the work was done in collaboration with others, I have made a significant contribution. This work has not been submitted for any other award or professional qualification.

The domain wall ensembles used in this analyses have been generated by the RBC/UKQCD collaboration. The vertex functions in Chapter 3 have been generated by me using the corresponding RBC/UKQCD gauge configurations, and *UKHadron* code written by Peter Boyle. The analyses of masses and decay constants in Chapter 4 as well as the light-light $Z_A$ factors have been cross-checked with Tobi Tsang. The 4-quark renormalization $Z_{B_K}$ on the F1 ensembles in Chapter 3 has been cross-checked with Nicolas Garron. An example bag parameter result has been crossed-checked with Julia Kettle. I have used the analysis code, *ukfit*, developed principally by Peter Boyle with additions by Christopher Kelly.

Some of the results presented in this work, also appear as part of publications listed on the next page.

*A. Khamseh*
July 2017

# List of Publications

Papers:

- P. A. Boyle, L. Del Debbio, A. Khamseh *Massive momentum-subtraction scheme*, *Phys.Rev.* **D95** (2017) 054505, [1611.06908].

- P. A. Boyle, L. Del Debbio, A. Juettner, A. Khamseh, F. Sanfilippo, J. T. Tsang, *The decay constants $f_D$ and $f_{D_s}$ in the continuum limit of $N_f = 2+1$ domain wall lattice QCD*, submitted to *Phys. Rev.* **D**, under review, [1701.02644].

Proceedings:

- P. A. Boyle, L. Del Debbio, N. Garron, A. Juettner, A. Khamseh, M. Marinkovic, F. Sanfilippo, J. T. Tsang, *Charm physics with physical light and strange quarks using domain wall fermions*, PoS LATTICE2014 (2015) 380, [1502.00845].

- P. A. Boyle, L. Del Debbio, A. Juettner, A. Khamseh, F. Sanfilippo, J. T. Tsang*Domain Wall Charm Physics with Physical Pion Masses: Decay Constants, Bag and $\xi$ Parameters*, PoS LATTICE2015 (2016) 336 [1511.09328].

- P. A. Boyle, L. Del Debbio, A. Khamseh *Massive momentum-subtraction scheme*, PoS LATTICE2016 (2016) 193, [1608.07982].

- P. A. Boyle, L. Del Debbio, A. Juettner, A. Khamseh, J. T. Tsang, O. Witzel *Charm Physics with Domain Wall Fermions and Physical Pion Masses*, PoS LATTICE2016 (2016) 278, [1611.06804].

In preparation:

- P. A. Boyle, L. Del Debbio, A. Juettner, A. Khamseh, J. T. Tsang, O. Witzel *Charm Physics with Domain Wall Fermions*, to be submitted to PoS LATTICE2017.
- P. A. Boyle, L. Del Debbio, N. Garron, J. Kettle, A. Khamseh, J. T. Tsang, *BSM Kaon Mixing at the Physical Point*, to be submitted to PoS LATTICE2017.

# Acknowledgements

I will not attempt to list all the various reasons why I feel so extremely grateful to my educator, Luigi Del Debbio, for his mentorship over the past several years, as this would require a dedicated chapter in this thesis, to say the least. His supervision during the course of this PhD made the entire journey truly motivating, pleasant and exciting, making it one of the best periods of my life so far. In short, I can only express my deepest gratitude for his full support and guidance, academic and beyond, that has shaped me as not just a physicist, but more generally as a scientist, and even more importantly as a person.

I am also very thankful to my second supervisor, Peter Boyle, for his patience and support during the course of this PhD. His great enthusiasm for the subject and deep involvement with the collaboration work has always been a continued source of motivation in driving the project forwards swiftly. I am particularly appreciative of him introducing me to the Feynman lectures on computation and all the discussion surrounding this topic.

I wish to thank my collaborators: Andreas Jüttner, Chris Sachrajda, Antonin Portelli, Tobi Tsang, Julia Kettle, Oliver Witzel and Nicolas Garron. A special thanks to Chris Sachrajda and Agostino Patella for deep, several hour discussions regarding the renormalization scheme as well as Claude Duhr, Einan Gardi and Andries Waelkens for their advice on the perturbative calculations.

I am grateful to all friends and officemates: Vlad and David, for the many interesting discussions about various different topics, Susanna for all the weekly super fun times, teaching me the Italian language and culture, as well as Susi, Eliana, Jimbo, Gustav, James, Rafa, Jack, Marco, Mark, Samuel, Øyvind and the rest of the PPT group.

Special thanks to Andries for bearing with me almost everyday in the past four years, listening to all the stories and complaints while providing a constant reservoir of Bouchées and Belgian chocolates. It has been very enjoyable listening to his exciting stories about cycling adventures, news and live tours, with all the things that can go wrong, from all around the world!

I remain eternally grateful to my parents, Khaleh, H., and Maman Feri, who have always been there for me, unconditionally, at every-single-step of the way. I cannot imagine receiving greater love and support.

Finally, I thank Sjoerd, for always being calm, rational and supportive, keeping the hectic moments sane but also for basically being awesome. I very much appreciate all the discussions regarding various parts of the projects ( ... and, no, I do not care which space they live on, nor am I going to make the statements more precise!), which have made the entire experience a great deal more fun.

# Contents

# List of Figures

# List of Tables

# Chapter 1

# Status of the Standard Model

## 1.1 Introduction

The Standard Model (SM) of particle physics is a description, based on quantum field theory, of strong and electromagnetic interactions at energies of order 1 TeV. With the discovery of the Higgs boson in 2012, SM has proved to be a highly successful theory. However, there are limitations to SM. For example, SM does not account for dark matter, gravitational interactions, the hierarchy problem or matter-antimatter asymmetry in the flavor sector. These issues have led us to believe SM should be viewed as an effective field theory (EFT) at the electroweak scale. On the other hand, not having observed any significant indications of New Physics (NP) at high energy colliders, so far, has imposed real challenges in finding deviations from SM predictions. In the case of the matter-antimatter asymmetry, the sources of CP violation provided by the SM do not fully explain the large dominance of matter over antimatter in the universe. CP violation is one motivation for this thesis and is addressed further in the coming chapters.

Flavor physics plays an important role in probing the limits of SM and providing constraints for Beyond the Standard Model (BSM) theories. Absence of deviations from the SM at TeV scale at the high-energy frontier, makes this role even more prominent. Precision measurements of the flavor sector can give access to physics at higher energy scales, of order 200 TeV or higher, by indirectly searching for signatures of NP. Such experiments are complementary to direct searches at the LHC, which was designed to have maximum collision energy of 14 TeV [1]. Precision, however, is required on both theoretical and experimental

fronts in order to resolve possible tensions between SM predictions and the data [2–4]. On the theory side, higher order perturbative QCD calculation are being performed for high energy scales while lattice QCD using dynamical fermions is being used as non-perturbative, first-principles method for obtaining hadronic quantities. These quantities include pion, kaon, $D$- and $B$-meson masses, decay constants, form factors and particle-antiparticle mixing parameters which are then used in determination of CKM matrix elements, allowing to further constrain SM and BSM theories. Other measurements include, the electric dipole moments, $(g-2)_\mu$ and the strong coupling constant $\alpha_s$ [5].

This report focuses mostly on the heavy sector of flavor physics, in particular $D$-mesons masses, decay constants and mixing parameters.

## 1.2 Flavor physics and CP-violation in SM

Before discussing flavor physics experimental and theoretical research currently being carried out, it is worthwhile recalling the fundamental ingredients of the flavor sector of the SM. These are required for describing CP-violation within the SM.

### 1.2.1 The Standard Model Lagrangian

The gauge interactions in the SM are given by the gauge symmetry group $SU(3)_{\rm c} \times SU(2)_{\rm L} \times U(1)_{\rm Y}$ which is spontaneously broken, by the non-zero vacuum expectation value (VEV) of a Higgs scalar particle, to $SU(3)_{\rm c} \times U(1)_{\rm EM}$. The SM Lagrangian reads as follows:

$$\mathcal{L}_{\rm SM} = \mathcal{L}_{\rm kinetic} + \mathcal{L}_{\rm Higgs} + \mathcal{L}_{\rm Yukawa}. \tag{1.1}$$

This is the most general, Lorentz and gauge invariant Lagrangian consistent with nature in terms of particle content, gauge symmetries and the mechanism for spontaneous breaking for the symmetry which gives rise to masses for heavy gauge bosons and fermions. In SM, there are three generations of quarks and leptons. With regards to electroweak interactions, the left-handed quarks and

leptons are $SU(2)_L$ doublets:

$$L^i = \begin{pmatrix} \nu_e \\ e \end{pmatrix}_L , \begin{pmatrix} \nu_\mu \\ \mu \end{pmatrix}_L , \begin{pmatrix} \nu_\tau \\ \tau \end{pmatrix}_L \qquad \text{and} \qquad Q^i = \begin{pmatrix} u \\ d \end{pmatrix}_L , \begin{pmatrix} c \\ s \end{pmatrix}_L , \begin{pmatrix} t \\ b \end{pmatrix}_L . \tag{1.2}$$

The respective right-handed fermions, $u^i_R = (u, c, t)_R$ and $d^i_R = (d, s, b)_R$, transform as singlets under $SU(2)_L$ and do not couple to the weak interactions. For example, the kinetic part of the Lagrangian for left-handed quarks takes the form:

$$\mathcal{L}(Q_L) = i\bar{Q}_{Li}\gamma_\mu\Big(\partial^\mu + \underbrace{\frac{i}{2}g_s G^\mu_a \lambda_a}_{\text{QCD}} + \underbrace{\frac{i}{2}gW^\mu_b\sigma_b + ig'Y_Q B^\mu}_{\text{Electroweak}}\Big)\delta_{ij}Q_{Lj} , \tag{1.3}$$

where the hypercharge $Y_Q = 1/6$ for left-handed quarks, $\lambda_a/2$ are $3 \times 3$ Gell-Mann matrices for triplets and $\sigma_b/2$ are $2 \times 2$ Pauli matrices for doublets. $G^\mu_a$ are eight gluons, $W^\mu_b$ are three weak interaction bosons and $B^\mu$ is the hypercharge boson. $\delta_{ij}$ is explicit to emphasise that this term is proportional to the identity matrix in flavor space *i.e.* its interactions are flavor universal. A similar equation holds for left handed leptons, but the main difference is that leptons do not couple to gluons. Here, we restrict ourselves to terms containing quarks. The SM Lagrangian is symmetric with respect to $CPT$, *i.e.* the combined discrete symmetry transformations, parity $P$, time-reversal $T$ and charge conjugation $C$. Moreover, the part of the Lagrangian shown in Eq. 1.3 is CP-conserving. The Higgs potential term,

$$\mathcal{L}_{\text{Higgs}} = \mu^2 H^\dagger H - \lambda(H^\dagger H)^2 , \tag{1.4}$$

is also CP-conserving, where,

$$H = \begin{pmatrix} H^+ \\ H^0 \end{pmatrix} , \tag{1.5}$$

is a complex doublet. On the other hand, the quark Yukawa term,

$$-\mathcal{L}^{q}_{\text{Yukawa}} = Y^{d}_{ij}\bar{Q}_{Li}Hd_{Rj} + Y^{u}_{ij}\bar{Q}_{Li}\tilde{H}u_{Rj} + \text{h.c.}\ , \tag{1.6}$$

is flavor dependent and CP-violating. This is explicitly discussed in the next section. Note that the indices $i$ and $j$ refer to the 3 different generations, $\tilde{H} = i\sigma_2 H^*$ and $Y_{ij}$'s are $3 \times 3$ Yukawa matrices. $\mathcal{L}^{q}_{\text{Yukawa}}$ is invariant under $SU(3) \times SU(2) \times U(1)$ [6–8].

### 1.2.2 The CKM matrix

Within the SM, mass for fermions and gauge bosons is generated via spontaneous breaking of the $SU(2)_L \times U(1)_Y$ symmetry. Minimizing the Higgs potential,

$$V_H = -\mu^2 H^\dagger H + \lambda (H^\dagger H)^2\ , \tag{1.7}$$

gives, apart from the trivial solution $\langle H \rangle_0 = 0$, the non-trivial solution

$$\langle H^\dagger H \rangle_0 = \frac{v^2}{2} \quad \text{with} \quad v \equiv \sqrt{\frac{\mu^2}{\lambda}}\ . \tag{1.8}$$

Therefore, after symmetry breaking, *i.e.* when $H$ acquires a vacuum expectation value

$$\langle H \rangle_0 = \begin{pmatrix} 0 \\ \\ \frac{v}{\sqrt{2}} + h(x) \end{pmatrix} \tag{1.9}$$

where $h(x)$ represents fluctuations around the minimum $v$. Focusing only on the terms including $v$, Eq. 1.6 contains the quark mass terms:

$$-\mathcal{L}_m = \frac{v}{\sqrt{2}}\bar{d}_L Y^d d_R + \frac{v}{\sqrt{2}}\bar{u}_L Y^u u_R + \text{h.c.}\ , \tag{1.10}$$

where the equation is written in matrix form, with the up- and down-type quarks denoted by $u^i_{L/R} = (u, c, t)_{L/R}$ and $d^i_{L/R} = (d, s, b)_{L/R}$. These mass terms can be diagonalized using unitary matrices $S^u_L, S^d_L, S^u_R, S^d_R$ such that

$$M_d = S^\dagger_{dL} Y_d S_{dR} \quad \text{and} \quad M_u = S^\dagger_{uL} Y_u S_{uR}\ , \tag{1.11}$$

where the matrices $M_d$ and $M_u$ are diagonal. The states then transform as follows:

$$u_L \to S_L^u u_L \quad , \quad u_R \to S_R^u u_R \quad , \quad d_L \to S_L^d d_L \quad , \quad d_R \to S_R^d d_R \cdot \tag{1.12}$$

Therefore the Lagrangian in Eq. 1.10 in the mass basis reads,

$$-\mathcal{L}_m = \bar{d}_L \mathbf{m}_d d_R + \bar{u}_L \mathbf{m}_u u_R + \text{h.c.} \,, \tag{1.13}$$

where $\mathbf{m}_d = v/\sqrt{2} M_d$, $\mathbf{m}_u = v/\sqrt{2} M_u$. More explicitely,

$$\mathbf{m}_u = \begin{pmatrix} m_u & 0 & 0 \\ 0 & m_c & 0 \\ 0 & 0 & m_t \end{pmatrix} \quad , \quad \mathbf{m}_d = \begin{pmatrix} m_d & 0 & 0 \\ 0 & m_s & 0 \\ 0 & 0 & m_b \end{pmatrix} . \tag{1.14}$$

This change of basis modifies the kinetic term, Eq. 1.3, for left-handed quarks that was written in the flavor basis. Note that hypercharge interactions are flavor diagonal and remain unaffected. On the other hand, the off-diagonal element of $W_b^\mu \sigma_b$, *i.e.* $W^1$ and $W^2$ do mix the up- and down-type quarks in the doublets $Q^i$. Defining,

$$W^\pm = \frac{W^1 \mp i W^2}{\sqrt{2}} \,, \tag{1.15}$$

the off-diagonal terms can be written as

$$\bar{Q}_{Li} \frac{g}{2} \gamma^\mu \Big( W_\mu^1 \sigma^1 + W_\mu^2 \sigma^2 \Big) \delta_{ij} Q_{Lj} = \frac{1}{\sqrt{2}} g \Big( \bar{u}_{Li} \not{W}^+ d_{Li} + \bar{d}_{Li} \not{W}^- u_{Li} \Big). \tag{1.16}$$

Under transformations in Eq. 1.12, this takes the form,

$$\frac{1}{\sqrt{2}} g \Big( \bar{u}_{Li} \big( S_{uL}^\dagger S_{dL} \big)^{ij} \not{W}^+ d_{Lj} + \bar{d}_{Li} \big( S_{dL}^\dagger S_{uL} \big)^{ij} \not{W}^- u_{Lj} \Big) \tag{1.17}$$

$$= \frac{1}{\sqrt{2}} g \Big( \bar{u}_{Li} V^{ij} \not{W}^+ d_{Lj} + \bar{d}_{Li} (V^\dagger)^{ij} \not{W}^- u_{Lj} \Big), \tag{1.18}$$

where $V = S_{uL}^{\dagger} S_{dL}$ is the Cabibbo-Koboyashi-Maskawa (CKM) matrix:

$$V_{\text{CKM}} = \begin{pmatrix} V_{ud} & V_{us} & V_{ub} \\ V_{cd} & V_{cs} & V_{cb} \\ V_{td} & V_{ts} & V_{tb} \end{pmatrix} . \tag{1.19}$$

Parameter counting allows us to indicate the source of CP-violation in the SM. A general unitary matrix has 9 real degrees of freedom. The mass matrices remain invariant under global $U(1)^6$ transformations similar to Eq. 1.12. More explicitly, taking $S_{uL} = S_{uR} = \text{diag}(e^{i\alpha_1}, e^{i\alpha_2}, e^{i\alpha_3})$ and $S_{dL} = S_{dR} = \text{diag}(e^{i\beta_1}, e^{i\beta_2}, e^{i\beta_3})$, there are 6 independent transformations that leave the mass matrices in Eq. 1.13 invariant. For the kinetic term, if $V$ is redefined as $V_{ij} \to e^{i(-\alpha_i+\beta_j)} V_{ij}$, these transformations can be used to eliminate phases in $V$. Only five phase differences $-\alpha_i + \beta_j$ are independent, leaving $9 - 5 = 4$ degrees of freedom for $V$. Now, if $V$ were real, it would have been a rotation matrix $O(3)$, with three degrees of freedom. Therefore, the matrix $V$ has four degrees of freedom consisting of: 3 angles, denoted by $\theta_{12}, \theta_{23}, \theta_{13}$ corresponding to rotations in the $ij$-flavor space, and 1 complex phase denoted, by $\delta$ [8]. It is precisely this irremovable phase that allows for CP-violation in the SM. This can be shown more explicitly by observing the CP-violating term in the kinetic part of the Lagrangian, $\bar{u}_L \not{W}^{+} V d_L + \bar{d}_L (V^{\dagger}) \not{W}^{-} u_L$. Under $CP$, Appendix A, the terms in the Lagrangian transform as follows:

$$\begin{aligned} \bar{u}_L \gamma^{\mu} d_L &\xrightarrow{CP} -\bar{d}_L \gamma^{\mu} u_L, \\ \bar{d}_L \gamma^{\mu} u_L &\xrightarrow{CP} -\bar{u}_L \gamma^{\mu} d_L, \\ W_{\mu}^{+} &\xrightarrow{CP} -W_{\mu}^{-} , \end{aligned} \tag{1.20}$$

yielding overall,

$$\bar{u}_L \not{W}^{+} V d_L + \bar{d}_L \not{W}^{-} (V^{\dagger}) u_L \xrightarrow{CP} \bar{d}_L \not{W}^{-} V^{T} u_L + \bar{u}_L \not{W}^{+} (V^{*}) d_L \cdot \tag{1.21}$$

In other words, CP-invariance requires $V^* = V$, which cannot be the case for non-vanishing complex phase $\delta$. It turns out that in order to have CP-violation in the SM, we must have $\theta_{12}, \theta_{23}, \theta_{13} \neq 0$ or $\pi/2$ and $\delta \neq 0, \pi$.

The CKM matrix can also be parameterized as follows:

$$V_{\text{CKM}} = \begin{pmatrix} c_{12}c_{13} & s_{12}c_{13} & s_{13}e^{-i\delta} \\ -s_{12}c_{23} - c_{12}s_{23}s_{13}e^{i\delta} & c_{12}c_{23} - s_{12}s_{23}s_{13}e^{i\delta} & s_{23}c_{13} \\ s_{12}s_{23} - c_{12}c_{23}s_{13}e^{i\delta} & -c_{12}s_{23} - s_{12}c_{23}s_{13}e^{i\delta} & c_{23}c_{13} \end{pmatrix}, \tag{1.22}$$

where $s_{ij} = \sin(\theta_{ij})$ and $c_{ij} = \cos(\theta_{ij})$ with $s_{ij}, c_{ij} \geq 0$. The convention, known as the *standard parameterization*, is chosen to agree with PDG (2016) [9] and it is not independent of the phase convention. An alternative way of writing the CKM matrix, known as the *Wolfenstein parameterization* can be used by defining four other parameters $\lambda, A, \rho, \eta$ such that:

$$\begin{aligned} s_{12} = \lambda, \quad s_{23} = A\lambda^2, \quad s_{13}e^{-i\delta} = A\lambda^3(\rho - i\eta), \\ \rho = \frac{s_{13}}{s_{12}s_{23}}\cos(\delta), \quad \eta = \frac{s_{13}}{s_{12}s_{23}}\sin(\delta)\ \cdot \end{aligned} \tag{1.23}$$

The reason behind this choice is that experimentally, it was found that $s_{13} \ll s_{23} \ll s_{12}$. In other words, mixing becomes smaller if one moves away from the diagonal. This hierarchy can be viewed more explicitly by rewriting the CKM matrix in Eq. 1.22 in terms of parameters in Eq. 1.23 and expanding each element of the matrix in powers of $\lambda$. At order $\mathcal{O}(\lambda^4)$ the matrix takes the form:

$$V_{\text{CKM}} = \begin{pmatrix} 1 - \lambda^2/2 & \lambda & A\lambda^3(\rho - i\eta) \\ -\lambda & 1 - \lambda^2/2 & a\lambda^2 \\ A\lambda^3(1 - \rho - i\eta) & -A\lambda^2 & 1 \end{pmatrix} + \mathcal{O}(\lambda^4)\ \cdot \tag{1.24}$$

There is another advantage to this parameterization. In its exact form *i.e.* without any expansions in $\lambda$, the unitarity condition of the matrix can be viewed graphically as a unitarity triangle in some complex plane. More explicitly, unitarity implies that the rows and columns of the CKM matrix are orthonormal. For example, taking the standard choice,

$$V_{ud}V_{ub}^* + V_{cd}V_{cb}^* + V_{td}V_{tb}^* = 0\ \cdot \tag{1.25}$$

This equation states that three complex numbers are added to give zero. Dividing through by the best experimental measurement of these quantities, $V_{cd}V_{cb}^*$, we get,

$$\frac{V_{ud}V_{ub}^*}{V_{cd}V_{cb}^*} + \frac{V_{cd}V_{cb}^*}{V_{cd}V_{cb}^*} + 1 = 0 \cdot \tag{1.26}$$

Taking $\bar{\rho}$ and $\bar{\eta}$ are a reparameterization of $\rho$ and $\eta$ in such a way as to ensure the relation

$$\bar{\rho} + i\bar{\eta} = -\frac{V_{ud}V_{ub}^*}{V_{cd}V_{cb}^*} \ , \tag{1.27}$$

is independent of the phase convention [9], the triangle can be represented on the $\bar{\rho} - \bar{\eta}$ plane as in Fig. 1 [10], with one side having unit length. Geometrically, phase transformation correspond to the triangle being rotated in the $\bar{\rho} - \bar{\eta}$ plane. Since the sides and the angles of the triangle remain invariant under these transformations, they are independent of the phase conventions and hence correspond to physical observables that can be measured by experiments [11].

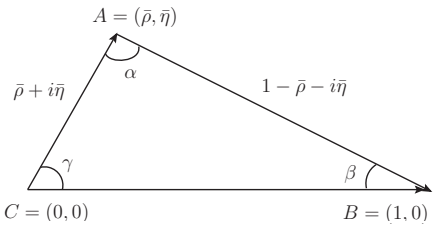


Figure 1.1: Unitarity Triangle in the $\bar{\rho} - \bar{\eta}$ plane.

### 1.2.3 Leptonic decay constants

In this section we discuss how certain CKM matrix elements can be extracted, given experimental measurement of branching fractions and precise theoretical determinations of hadronic matrix elements. In our case, the focus is on leptonic decays of $D$ and $D_s$ mesons via charged $W$-boson exchange. The relevant matrix elements under consideration are then $V_{cd}$ and $V_{cs}$, which can be use to test the unitarity of the second row of the CKM matrix.

In the SM, the decay constants $f_D$ and $f_{D_s}$ are related to the branching ratios

for leptonic decays via:

$$\mathcal{B}\big(D_{(s)} \to l\nu_l\big) = \frac{G_F^2 |V_{cq}|^2 \tau_{D_{(s)}}}{8\pi} f_{D_{(s)}}^2 m_l^2 \; m_{D_{(s)}} \left(1 - \frac{m_l^2}{m_{D_{(s)}}^2}\right) \; , \tag{1.28}$$

where $V_{cq} = V_{cd},\ V_{cs}$ for $D$ and $D_s$ mesons respectively, $\tau_{D_{(s)}}$ is the $D_{(s)}$ meson lifetime, and $G_F$ is the Fermi coupling. The branching ratios on the left hand side are measured experimentally, and later combined with results for meson masses $m_{D_{(s)}}$ and decay constants $f_{D_{(s)}}$ from the lattice to extract the matrix elements $V_{cd}$ and $V_{cs}$. On the lattice, the decays constant $f_D$ and $f_{D_s}$ are computed using the axial current matrix element

$$\langle 0|A_{cq}^{\mu}|D_q(p)\rangle = i f_{D_q} p_{D_q}^{\mu} \; , \tag{1.29}$$

with $q = d, s$ and $A_{cq}^{\mu} = \bar{c}\gamma_\mu\gamma_5 q$. A major part of Chapter 4 is dedicated to the lattice computation of $D$ and $D_s$ mesons masses and decay constants.

### 1.2.4 Neutral meson mixing

This section starts with a general formalism for neutral meson mixing, $M^0 \leftrightarrow \bar{M}^0$. Even though the formalism in describing mixing in neutral meson is similar, the CP-violating phenomenology related to specific systems, *i.e.* kaon, $D$- and $B$-mesons is very different. This is mainly due to the fact that these systems exhibit different decay rates and oscillation. The details particular to each system are discussed in the subsequent sections.

Let $H$ be the effective 2-by-2 Hamiltonian for SM written as:

$$H_{\text{eff}} = H_{\text{QCD+QED}} + H_W \; , \tag{1.30}$$

governing the time-evolution of the two-state system

$$|\psi(t)\rangle = \begin{pmatrix} a(t) \\ \\ b(t) \end{pmatrix} = a(t)|M^0\rangle + b(t)|\overline{M}^0\rangle \; , \tag{1.31}$$

which is the superposition of the eigenstates of $H_{\text{QCD+QED}}$, *i.e.* $|M^0\rangle$ and $|\overline{M}^0\rangle$,

being neutral mesons. In the absence of the electroweak interactions $H_W$, the Hamiltonian $H$ takes the diagonal form:

$$H \to M = \begin{pmatrix} m_{M^0} & 0 \\ 0 & m_{\overline{M}^0} \end{pmatrix}, \tag{1.32}$$

with $m_{M^0} = m_{\overline{M}^0}$ and the off-diagonal element being zero to preserve flavor conservation. However, when electroweak interactions are present, flavor is no longer conserved and quark mixing can occur. Therefore, the off-diagonal elements of $H_{\text{eff}}$ are no longer zero and are associated with flavor changing transitions $M^0 \leftrightarrow \bar{M}^0$. As well as that, weak interactions are responsible for decays, forcing the Hamiltonian to be non-Hermitian, otherwise $H_{\text{eff}}$ can only take into account oscillations and not decays. Requiring the above properties, the two-state Hamiltonian $H_{\text{eff}}$ can be written as:

$$H_{ij} = M_{ij} - \frac{i}{2}\Gamma_{ij} \ , \tag{1.33}$$

where both matrices $\mathbf{M}$ and $\mathbf{\Gamma}$ are Hermitian. Hence, the time evolution of the state $|\psi\rangle$ is described by:

$$i\frac{d}{dt}|\psi(t)\rangle = \Big(\mathbf{M} - \frac{i}{2}\mathbf{\Gamma}\Big)|\psi(t)\rangle \ , \tag{1.34}$$

so that,

$$|\psi(t)\rangle = e^{-i\mathbf{M}t - \frac{1}{2}\mathbf{\Gamma}t}|\psi(0)\rangle \ . \tag{1.35}$$

The effective Hamiltonian $H_{\text{eff}}$ in Eq. 1.30, to second order in perturbation theory can be written as:

$$H_{ij}^W = m_M\delta_{ij} + \frac{\langle M_i^0|H_W|M_j^0\rangle}{2m_M} + \frac{1}{2m_M}\sum_n \frac{\langle M_i^0|H_W|n\rangle\langle n|H_W|M_j^0\rangle}{m_M^{(0)} - E_n + i\epsilon} + \cdots \ . \tag{1.36}$$

The mass-diagonal term, $m_M\delta_{ij}$, corresponds to $H_{\text{QCD+QED}}$ part of the Hamiltonian, taking into account the fact that $M^0$ and $\overline{M}^0$ have the same mass, $m_M$. The second and third terms contribute to both diagonal and off-diagonal elements and

correspond to the weak part of $H_{\text{eff}}$. Note that $E_n$ is the energy of the intermediate state $|n\rangle$. Using Cauchy's theorem,

$$\frac{1}{\omega - E_n + i\epsilon} = \underbrace{P\left(\frac{1}{\omega - E_n}\right)}_{\text{mass term}} - i\underbrace{\pi\delta(E_n - \omega)}_{\text{width term}}, \tag{1.37}$$

where $P\left(\frac{1}{\omega - E_n}\right)$ is the principle value. Then, the off-diagonal elements become,

$$M_{12} = \frac{\langle M^0|H_W^{\Delta F=2}|\overline{M}^0\rangle}{2m_M} + \frac{1}{2m_M} P \sum_n \frac{\langle M^0|H_W^{\Delta F=1}|n\rangle\langle n|H_W^{\Delta F=1}|\overline{M}^0\rangle}{m_M^{(0)} - E_n} + \cdots \ , \tag{1.38}$$

and

$$\Gamma_{12} = \frac{1}{2m_M} \sum_n \langle M^0|H_W|n\rangle\langle n|H_W|\overline{M}^0\rangle 2\pi\delta(E_n - m_M) \ , \tag{1.39}$$

where the first term in Eq. 1.38 describes mixing between $M^0$ and $\overline{M}^0$ with change in flavor $\Delta F = 2$. For example, for kaon mixing the operator would be $\Delta S = 2$ and for B-meson mixing it would be $\Delta B = 2$. If the intermediate states $|n\rangle$ are light, they can lead to long-distance contributions. The structure of the matrix element $\langle M^0|H_W^{\Delta F=2}|\overline{M}^0\rangle$, for the explicit cases of $K$, $D$ and $B$ mesons, is discussed in the upcoming sections.

Returning to the Hamiltonian of Eq. 1.33, due to $CPT$, we have $H_{11} = H_{22}$ and $H_{21} = H_{12}^*$. This allows us to write $M_{11} = M_{22} \equiv m$ and $\Gamma_{11} = \Gamma_{22} \equiv \Gamma$. On the other hand the hermiticity of $\mathbf{M}$ and $\mathbf{\Gamma}$ implies $M_{21} = M_{12}^*$ and $\Gamma_{21} = \Gamma_{12}^*$. This gives the general form:

$$\mathbf{M} - \frac{i}{2}\mathbf{\Gamma} = \begin{pmatrix} A & p^2 \\ q^2 & A \end{pmatrix}, \tag{1.40}$$

for complex $A, p^2, q^2$. Under $CP$ the state transforms as

$$CP|M^0\rangle = \eta_{CP}|\overline{M}^0\rangle, \tag{1.41}$$

where $\eta_{CP}$ is a phase such that $|\eta_{CP}|^2 = 1$ and is allowed to be chosen. Here the convention is $\eta_{CP} = -1$. If CP-invariance is assumed,

$$\langle M^0|H_W|\overline{M}^0\rangle = \langle M^0|(CP)^{-1}CP\ H_W\ (CP)^{-1}CP|\overline{M}^0\rangle = \langle \overline{M}^0|H_W|M^0\rangle, \quad (1.42)$$

which yields $p = q$. Given then $\mathbf{M}$ and $\mathbf{\Gamma}$ are hermitian, it implies $M_{12}$ and $\Gamma_{12}$ are real. However, this is not the case in reality since nature is not CP-invariant. Therefore, to measure CP-violation one has to take into account the imaginary parts of $M_{12}$ and $\Gamma_{12}$. Diagonalizing the matrix in Eq. 1.40, the mass eigenstates are written as,

$$|M_{\frac{1}{2}}\rangle = \frac{1}{\sqrt{|p|^2 + |q|^2}}\Big(p|M^0\rangle \pm q|\overline{M}^0\rangle\Big), \quad (1.43)$$

and

$$\frac{p}{q} = \sqrt{\frac{M_{12} - \frac{i}{2}\Gamma_{12}}{M_{12}^* - \frac{i}{2}\Gamma_{12}^*}}\ . \quad (1.44)$$

For CP-violation, $\frac{p}{q} \neq 1$. Let us denote the two eigenvalues by $m_1 - \frac{i}{2}\Gamma_1$ and $m_2 - \frac{i}{2}\Gamma_2$. Computing the eigenvalues and taking the difference between them we get:

$$\begin{aligned} 2pq =& (m_1 - m_2) - \frac{i}{2}(\Gamma_1 - \Gamma_2) && (1.45)\\ =& 2\left(M_{12} - \frac{i}{2}\Gamma_{12}\right)^{1/2}\left(M_{12}^* - \frac{i}{2}\Gamma_{12}^*\right)^{1/2} && (1.46)\\ \simeq& 2\Re M_{12} - i\Im\Gamma_{12}\ , && (1.47) \end{aligned}$$

where the last approximation is valid if CP-violation is small, *i.e.* $\Im M_{12} \ll \Re M_{12}$ and $\Im\Gamma_{12} \ll \Re\Gamma_{12}$. In other words,

$$\Delta m \equiv m_1 - m_2 \simeq 2\Re M_{12} \quad , \quad \Delta\Gamma \equiv \Gamma_2 - \Gamma_1 \simeq -2\Re\Gamma_{12} \quad (1.48)$$

Taking $\Delta m > 0$, $|M_1\rangle$ should be taken to be heavier than $|M_2\rangle$. Now, given Eq. 1.41 with $\eta_{CP} = -1$, we can define the even and the odd CP eigenstates,

$|M^0_+\rangle$ and $|M^0_-\rangle$:

$$CP|M^0_\pm\rangle = \pm|M^0_\pm\rangle \ , \tag{1.49}$$

as a linear combination of the flavor eigenstates $|M^0\rangle$ and $|\overline{M}^0\rangle$ states, *i.e.*

$$|M^0_\pm\rangle \equiv \frac{1}{\sqrt{2}}\Big(|M^0\rangle \mp |\overline{M}^0\rangle\Big)\cdot \tag{1.50}$$

If $CP$ were to be conserved, *i.e.* ($p = q$), one would have $|M_2\rangle \to |M^0_+\rangle$ and $|M_1\rangle \to |M^0_-\rangle$ which are defined by,

$$|M_{\substack{2\\1}}\rangle \simeq |M^0_\pm\rangle \equiv \frac{1}{\sqrt{2}}\Big(|M^0\rangle \mp |\overline{M}^0\rangle\Big), \tag{1.51}$$

and are consistent with Eq. 1.41. In Nature however, $|M_{\substack{2\\1}}\rangle$ are not pure CP-eigenstates, since it is broken by the weak interactions. Since $M^0$ and $\overline{M}^0$ mix under weak interaction, using Eq. 1.43, Eq. 1.44 and Eq. 1.51 one can write,

$$|M_{\substack{1\\2}}\rangle = \frac{1}{\sqrt{2}\sqrt{1+|\bar{\epsilon}|^2}}\Big((1+\bar{\epsilon})|M^0\rangle \pm (1-\bar{\epsilon})|\overline{M}^0\rangle\Big) \tag{1.52}$$

$$= \frac{1}{\sqrt{1+|\bar{\epsilon}|^2}}\Big(|M^0_\mp\rangle + \bar{\epsilon}|M^0\pm\rangle\Big), \tag{1.53}$$

where $\bar{\epsilon}$ is a small complex parameter such that,

$$\frac{p}{q} = \frac{1+\bar{\epsilon}}{1-\bar{\epsilon}} \ . \tag{1.54}$$

Solving for $\bar{\epsilon}$ and using Eq. 1.52, one can derive explicit expressions relating the physical eigenstates, $|M_1\rangle$ and $|M_2\rangle$ to the flavor eigenstates $|M^0\rangle$ and $|\overline{M}^0\rangle$.

$M^0 - \overline{M}^0$ mixing can be observed experimentally. To obtain the time evolution we start by writing the flavor eigenstates in terms of the mass eigenstates using Eq. 1.43 as:

$$|M^0\rangle = \frac{\sqrt{|p|^2+|q|^2}}{2p}\Big(|M_1\rangle + |M_2\rangle\Big) \quad , \quad |\overline{M}^0\rangle = \frac{\sqrt{|p|^2+|q|^2}}{2q}\Big(|M_1\rangle - |M_2\rangle\Big). \tag{1.55}$$

Then, the time-evolution of the flavor eigenstates is written as

$$|M^0(t)\rangle = \frac{\sqrt{|p|^2+|q|^2}}{2p}\Big(|M_1(t)\rangle + |M_2(t)\rangle\Big) \tag{1.56}$$

$$= \frac{\sqrt{|p|^2+|q|^2}}{2p}\Big(e^{-im_1 t}e^{-\Gamma_1 t}|M_1\rangle + e^{-im_2 t}e^{-\Gamma_2 t}|M_2\rangle\Big). \tag{1.57}$$

Substituting again for $|M_{\substack{1\\2}}\rangle$ using Eq. 1.43 gives,

$$|M^0(t)\rangle = g_+(t)|M^0\rangle + \frac{q}{p}g_-(t)|\overline{M}^0\rangle\cdot \tag{1.58}$$

Similarly,

$$|\overline{M}^0(t)\rangle = \frac{p}{q}g_-(t)|M^0\rangle + g_+(t)|\overline{M}^0\rangle, \tag{1.59}$$

with

$$g_\pm = \frac{1}{2}\Big(e^{-\Gamma_1 t/2}e^{-im_1 t} \pm e^{-\Gamma_2 t/2}e^{-im_2 t}\Big). \tag{1.60}$$

Therefore, the probability amplitude, $P(M^0(0) \to M^0(t))$, of starting with a pure $|M^0\rangle$ state at time $t = 0$ and being at state $M^0(t)$ at some later time $t$, is equal to $|g_+|^2$. Similarly, the probability amplitude, $P(M^0(0) \to \overline{M}^0(t))$, of starting with a pure $|M^0\rangle$ state at time $t = 0$ and being at state $\overline{M}^0(t)$ at some later time $t$, is equal to $|g_-|^2$. These probability amplitudes can be written as:

$$|g_\pm|^2 = \frac{e^{-\Gamma t}}{2}\left(\cosh\left(\frac{\Delta\Gamma t}{2}\right) \pm \cos(\Delta m t)\right), \tag{1.61}$$

where $\Delta m \equiv m_1 - m_2$, $\Delta\Gamma \equiv \Gamma_2 - \Gamma_1$, $m = (m_1 + m_2)/2$ and $\Gamma = (\Gamma_1 + \Gamma_2)/2$.

In general, there are two main types of contributions to mixing. One can write,

$$\Delta m_{\text{theory}} = (\Delta m)^{\text{SD}}_{\text{theory}} + (\Delta m)^{\text{LD}}_{\text{theory}}. \tag{1.62}$$

The first term, *i.e.* the short distance component is

$$(\Delta m)^{\rm SD}_{\rm theory} = 2\Re\langle M^0|H_w^{\rm box}(\mu)|\overline{M}^0\rangle \cdot \tag{1.63}$$

In the equation above, $H_w^{\rm box}$ can be written as:

$$H_w^{\rm box} = C(\mu)O^{\Delta F=2}(\mu) \ , \tag{1.64}$$

where the change in the change in the particular fermion number is equal to two for $M^0 - \overline{M}^0$ mixing. $C(\mu)$ is the Wilson coefficient at a given order in QCD perturbation theory, which is specified in the same renormalization scheme as the operator $O^{\Delta F=2}$. The operator $O^{\Delta F=2}$, is a local four-quark operator. Specific cases for kaons, $D^0$ and $B^0$ mesons are discussed in Sec. 1.2.5 and Sec. 1.2.7. Generically, the short distance contribution $(\Delta m)^{\rm SD}_{\rm theory}$ can be represented by box diagrams similar to Fig. 1.5 and Fig. 1.10. It has been shown in Ref. [12], that the formal way of integrating out the $W$ bosons explicitly via the path integral formulation leads to the same answer as writing down a 4-fermi effective Hamiltonian.

Even though the formalism for meson mixing mentioned above is similar for all neutral mesons, $K^0$, $D^0$, $B^0$ and $B_s^0$, the different masses and weak coupling strengths results in very different phenomenology, some of which are discussed in the following sections. Chapter 4 of this thesis focuses on the lattice computation of such contributions to meson mixing.

### 1.2.5 Mixing in kaon systems

In the case of neutral kaons, $M_1^0$ and $M_2^0$ are denoted by $K_L$ and $K_S$ which stand for "long" and "short", referring to their respective lifetimes. The ratio $\tau_L/\tau_S \simeq 571$. If $CP$ was conserved, $K_S$, being a $CP$-even state according to Eq. 1.49 and Eq. 1.51, would only decay to a $CP$-even state *i.e.* $\pi\pi$ while $K_L$, being an odd state, would only decay to the $CP$-odd state $\pi\pi\pi$. Since the available phase for final state of the former process ($m_K - 2m_\pi \approx 220$ MeV) is greater than that of the latter ($m_K - 3m_\pi \approx 80$ MeV), $K_S$ has a much shorter life-time than $K_L$. However, $K_S$ and $K_L$ are not pure CP-eigenstates. Therefore, any observation of $K_L \approx K_- + \bar{\epsilon}K_+$, decaying into a $\pi\pi$ states is a measure of CP-violation. This

can be seen experimentally in Fig. 1.2 [13], of the decay rate vs time in units of $\tau_s$, the life-time of $K_S$. The experiment starts with kaons in $K^0$ and $\overline{K}^0$ states, and a fast decay to $\pi\pi$ corresponding to $K_S$ even-state. Given the short lifetime of $K_S$, waiting long enough will result in $K_S$ to have decayed away and one expects to detect only $\pi\pi\pi$ states corresponding to a pure $K_L$ state. However, $\pi\pi$ states are also detected, which can only corresponding to transitions $K_L \to \pi\pi$ implying CP-violation. This is known as indirect CP-violation and was first observed in 1964 by Fitch and Cronin where they observed 45 decays of $K_L \to \pi\pi$ in a sample of 22700 kaon decays a long time away from the production time [14].

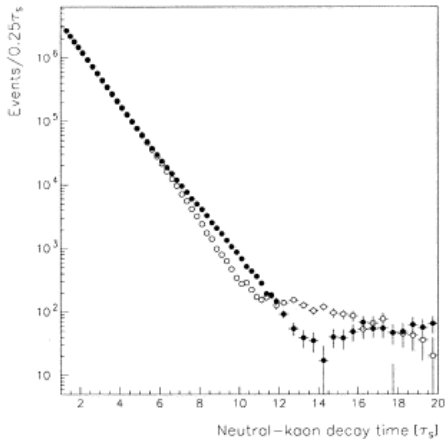


Figure 1.2: CPLEAR experiment: Decay rate vs time in units of $\tau_s$. The open circles correspond to kaon that started as $K^0$, the closed circles correspond to kaons that started as $\overline{K}^0$.

Eq. 1.56-1.61 can be used to plot the respective probabilities, $P(K^0(0) \to K^0(t))$ or $P(K^0(0) \to \overline{K}^0(t))$, of starting with a beam in pure $|K^0\rangle$ state at $t = 0$ and ending up in either $|K^0(t)\rangle$ or $|\overline{K}^0(t)\rangle$ at time $t$. See the left hand plot in Fig. 1.3, where the probabilities are plotted against time in units of $\tau_S$, assuming CP-symmetry. Here, the values for $\Delta m$, $\Delta\Gamma$ and $\Gamma$ are taken from PDG as an input to show a comparison between the probabilities. After a few $K_S$ life-times, one would expect all the $K_s$ to have decayed, leaving a $K_L$ state which is half $|K^0(t)\rangle$ and half $|\overline{K}^0(t)\rangle$. This is indeed observed in the plot, the probabilities reach an equal value at large $t/\tau_s$. These probabilities can be used to construct the asymmetry ratio $\frac{P(K^0\to K^0)-P(K^0\to\overline{K}^0)}{P(K^0\to K^0)+P(K^0\to\overline{K}^0)}$. The probability for the same input values as above is plotted below, on the right hand side of Fig. 1.3, again assuming no CP-violation.

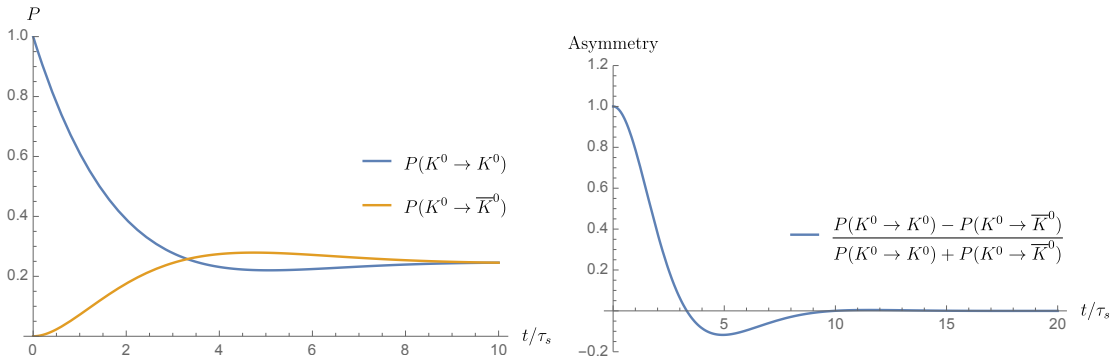


Figure 1.3: The plot on the left shows probability amplitudes $P\big(K^0(t=0) \to K^0(t)\big)$ and $P\big(K^0(t=0) \to \overline{K}^0(t)\big)$. The plot on the right, uses these ingredients to construct the transition probability asymmetry fraction, $\frac{P(K^0 \to K^0) - P(K^0 \to \overline{K}^0)}{P(K^0 \to K^0) + P(K^0 \to \overline{K}^0)}$. Both plots assume no $CP$ violation *i.e.* $p = q \in \mathbb{R}$.

In fact, $\Delta m$ is computed experimentally as a fit parameter of data measuring asymmetries in decay rates as a function of time. The result by CPLEAR allowing for CP-violation in the fit, are presented below in Fig. 1.4. CP-violation is also measured experimentally using such asymmetry ratios, with the form chosen in such as way as to optimize this measurement [15]. It was observed that, at large times, $K_L$ mesons decays more often to $\pi^- e^+ \overline{\nu}_e$ than to $\pi^+ e^- \nu_e$, with the decay rate asymmetry of 0.3% [9].

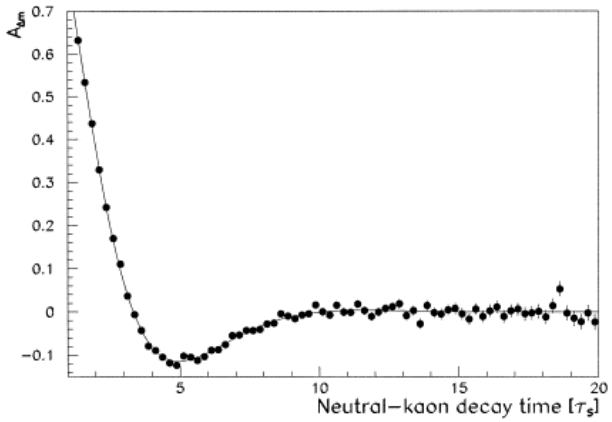


Figure 1.4: CPLEAR experimental results of the asymmetry ratio $A$ vs $t$ in units of $\tau_s$. The data is fitted to the theoretical prediction to obtain the value of $\Delta m$, using $CPT$ only.

### 1.2.6 Short-distance contribution to kaon mixing

Returning to the theoretical description of the short-distance component of $\Delta m$, Eq. 1.63,

$$(\Delta m)^{\text{SD}}_{\text{theory}} = 2\Re\langle K^0|H_W^{\text{box}}|\overline{K}^0\rangle, \tag{1.65}$$

where to lowest order in electroweak theory, the contributions to $K^0 - \overline{K}^0$ oscillations arise from box diagrams presented in Fig. 1.5. Calculations regarding the long-distance contributions *i.e.* the second term in Eq. 1.38 affecting the dispersive part $M_{12}$, and Eq. 1.39 affecting the absorptive part $\Gamma_{12}$, are not the focus of the discussion here but are available in the literature *e.g.* [16–19]. Fig. 1.6 shows these long-distance contributions via on-shell states.

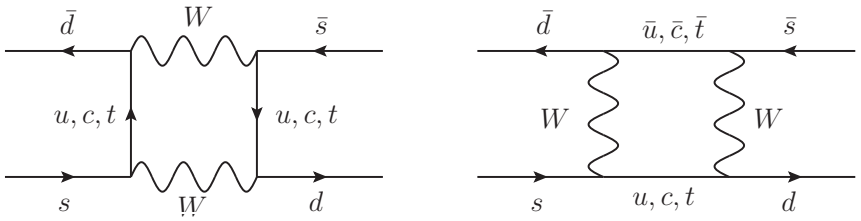


Figure 1.5: Box diagrams contributing to $K^0 - \overline{K}^0$ mixing.

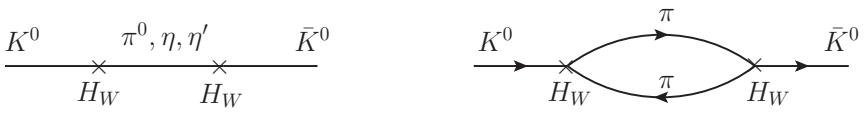


Figure 1.6: Long-distance contributions to $K^0 - \overline{K}^0$ mixing.

It is more common to write $H_W^{\text{box}}$ as a $\Delta S = 2$ operator, hence in the form

$$2m_k M_{12}^* = \langle\overline{K}^0|H_W^{\Delta S=2}|K^0\rangle\cdot \tag{1.66}$$

The above matrix element is computed using operator product expansion (OPE), where one can factorize perturbative and non-perturbative effects. At a given order in QCD perturbations theory, the Wilson coefficient $C(\mu)$ is computed using the same renormalization scheme as the non-perturbative part, hence having the same scale and number of flavors. Explicitely,

$$\langle\overline{K}^0|H_W^{\Delta S=2}(\mu)|K^0\rangle = C(\mu)\langle\overline{K}^0|Q^{\Delta S=2}(\mu)|K^0\rangle, \tag{1.67}$$

where the operator

$$Q^{\Delta S=2} = [\bar{s}\gamma_\mu(1-\gamma_5)d][\bar{s}\gamma_\mu(1-\gamma_5)d] \equiv O_{\mathrm{VV+AA}} - O_{\mathrm{VA+AV}} \ , \tag{1.68}$$

is the four-fermion operator. The matrix element of the operator between the mesonic states $K^0$ and $\overline{K}^0$, needs to be computed non-pertubatively on the lattice. The loop integration for such box diagrams can be computed exactly. In the limit that external momenta and external quark masses as well as mass of the up quark go to zero, and $\mu < m_c$, the result can be written as [5]:

$$\langle \overline{K}^0 | H_W^{\Delta S=2} | K^0 \rangle = \frac{G_F^2 M_W^2}{16\pi^2} \Big[ \lambda_c^2 S_0(x_c)\eta_1 + \lambda_t^2 S_0(x_t)\eta_2 + 2\lambda_c\lambda_t S_0(x_c, x_t)\eta_3 \Big] \times \tag{1.69}$$

$$\left(\frac{g_R(\mu)^2}{4\pi}\right)^{-\gamma_0/(2\beta_0)} \exp\left\{ \int_0^{g_R(\mu)} dg \left( \frac{\gamma(g)}{\beta(g)} + \frac{\gamma_0}{\beta_0} \right) \right\} \langle \overline{K}^0 | Q_R^{\Delta S=2}(\mu) | K^0 \rangle + \text{h.c.} \cdot$$

In the above, $G_F$ is the Fermi coupling, $M_W$ is the $W$-boson mass and $\lambda_a = V_{as}^* V_{ad}$ with $a = c, t$. The functions $S_0(x_c)$, $S_0(x_t)$ and $S_0(x_c, x_t)$ where $x_c = m_c^2/M_W^2$, $x_t = m_t^2/M_W^2$, are the Inami-Lim functions [20] expressing electroweak loop corrections without QCD corrections. Note that the most important contribution to $\Delta m$ comes from the $c$-quark. This is because even though $m_t^2$ is large, the factor $|V_{ts}V_{td}|^2 \sim \lambda^5$ according to Eq. 1.24, which is very small whereas $|V_{cs}V_{cd}|^2 \sim \lambda$. The subscript $R$ in $g_R(\mu)$ and $Q_R^{\Delta S=2}(\mu)$ is written to indicate these quantities represent the renormalized coupling and the renormalized 4-fermi operator in a given renormalization scheme. Typically this is chosen to be the naive dimensional regularization (NDR) of $\overline{\mathrm{MS}}$ [5]. $\eta_1, \eta_2, \eta_3$ contain QCD corrections to the diagrams, explicit expressions can be found in [21–23]. The $\beta$- and $\gamma$- functions are define in the usual sense

$$\frac{dg_R}{d\ln\mu} = \beta(g_R) \quad , \quad \frac{dQ_R^{\Delta S=2}}{d\ln\mu} = -\gamma(g_R) Q_R^{\Delta S=2} \tag{1.70}$$

$$\begin{aligned} \beta(g) &= -\beta_0 \frac{g^3}{(4\pi)^2} - \beta_1 \frac{g^5}{(4\pi)^4} - \cdots \\ \gamma(g) &= \gamma_0 \frac{g^2}{(4\pi)^2} + \gamma_1 \frac{g^4}{(4\pi)^4} + \cdots \end{aligned} \tag{1.71}$$

Explicit expression for $\beta_0, \beta_1, \gamma_0, \gamma_1$ can be found in [5] for different numbers of flavors $N_f$. Eq. 1.69 is valid for $N_f = 3$.

The physical amplitude between the initial and final states cannot depend on the scale $\mu$. As a result the dependence on the scale, $\mu$, must cancel between the Wilson coefficient and operator $\langle \overline{K}^0 | Q_R^{\Delta S=2}(\mu) | K^0 \rangle$. In lattice computations, it is more convenient (see Sec. 4.3) to express $\langle \overline{K}^0 | Q_R^{\Delta S=2}(\mu) | K^0 \rangle$ in terms of the bag parameter, $B_K$, defined as,

$$B_K(\mu) = \frac{\langle \overline{K}^0 | Q_R^{\Delta S=2}(\mu) | K^0 \rangle}{\frac{8}{3} f_K^2 m_K^2}, \tag{1.72}$$

where $f_K$ and $m_K$ are the decay constant and mass of kaon respectively, which can both be determined using lattice computations. The four-quark operator $\langle \overline{K}^0 | Q_R^{\Delta S=2}(\mu) | K^0 \rangle$ is renormalized in some regularization scheme such as RI/SMOM non-perturbatively. The result is converted, via one- or two-loop perturbative matching, to more commonly used schemes such as NDR-$\overline{\text{MS}}$, or the Renormalization Group Independent (RGI) scheme in which

$$\hat{B}_K = \left( \frac{g_R(\mu)^2}{4\pi} \right)^{-\gamma_0/(2\beta_0)} \exp \left\{ \int_0^{g_R(\mu)} dg \left( \frac{\gamma(g)}{\beta(g)} + \frac{\gamma_0}{\beta_0} \right) \right\} B_K(\mu) \tag{1.73}$$

is independent of the scale. At NLO in perturbation theory,

$$\hat{B}_K = \left( \frac{g_R(\mu)^2}{4\pi} \right)^{-\gamma_0/(2\beta_0)} \exp \left\{ 1 + \frac{g_R(\mu)^2}{(4\pi))^2} \left[ \frac{\beta_1 \gamma_0 - \beta_0 \gamma_1}{2\beta_0^2} \right] \right\} B_K(\mu) \cdot \tag{1.74}$$

The details of the renormalization of operators on the lattice is discussed in Chapter 2.

The computation of the kaon bag parameter is an ingredient required for the measurement of CP-violation in $K^0 - \overline{K}^0$ mixing which imposes a constraint on the apex of the unitarity triangle, shown in green in Fig. 1.7, corresponding to the approximate hyperbolas shown in green, $\epsilon_K$. $\epsilon_K$ is the indirect CP violation parameter of the neutral kaon system and receives its dominant contribution from indirect CP violation via state-mixing. Therefore, computing the bag parameters is a crucial ingredient in determining $\epsilon_K$ [24].

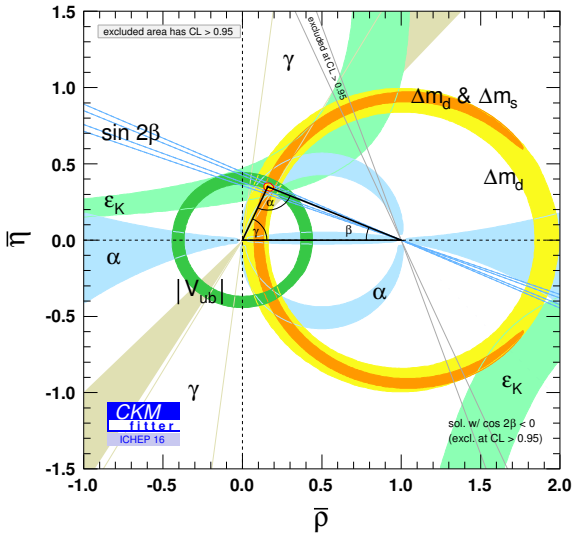


Figure 1.7: CKM unitarity triangle in the $\bar{\rho} - \bar{\eta}$ plane, by CKMfitter (2016).

### 1.2.7 Mixing in $D$ and $B$ systems

Experimentally, $B_d^0 - \overline{B}_d^0$ and $B_s^0 - \overline{B}_s^0$ mixing were discovered by the Argus experiment in 1987 [25] and the CDF collaboration in 2006 [26] respectively. There are many possible decay modes for these systems. As a result $\Gamma$ is very large as compared to the kaon system and so $\Delta\Gamma/\Gamma$ is small. For the $B_d^0$ system [9] we expect mixing via oscillations rather than decays, taking $\Delta\Gamma = 0$. The asymmetry between the probabilities $P(B^0(0) \to B^0(t))$ and $P(B^0(0) \to \overline{B}^0(t))$ can again be constructed, by writing the probability of starting with a pure $|B^0\rangle$ state at $t = 0$ and ending up in either $|B^0(t)\rangle$ or $|\overline{B}^0(t)\rangle$ states at time $t$:

$$\frac{P(B_d^0 \to B_d^0) - P(B_d^0 \to \overline{B}_d^0)}{P(B_d^0 \to B_d^0) + P(B_d^0 \to \overline{B}_d^0)} = \cos(\Delta m_d t) \cdot \tag{1.75}$$

This corresponds to the plot in Fig. 1.8, which is an oscillatory function such that $\Delta m_d$ is the frequency of oscillation. In fact $\Delta m_d$ is determined experimentally by measuring the oscillations frequency of the asymmetry ratio. An example plot below shows the data by the BaBar experiment in 2001 where oscillatory behaviour is observed and then fitted to determine $\Delta m_d$ [27–29]. The most recent results by the LHCb collaborations of $\Delta m_d$ obtained using the asymmetry fraction

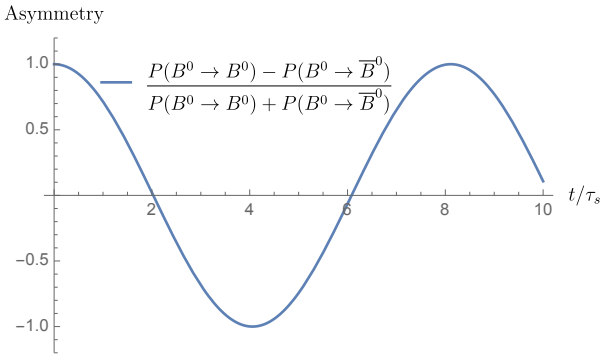


Figure 1.8: Transition probability asymmetry fraction, $\frac{P(B^0 \to B^0) - P(B^0 \to \overline{B}^0)}{P(B^0 \to B^0) + P(B^0 \to \overline{B}^0)}$, assuming no CP-violation *i.e.* $(p = q) \in \mathbb{R}$.

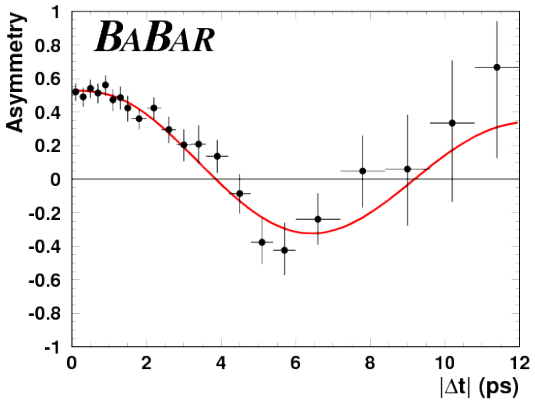


Figure 1.9: Time-dependent asymmetry for $B^0 - \overline{B}^0$, fitted to determine $\Delta m_d$. The x-axis label $|\Delta t|$ refers to the time difference between two $B$-meson decays inferred from the distance between their decay vertices along the beam line.

similar to Eq. 1.75 can be found in [30]. CP-violation in $B$-mesons was reported by Belle and BaBar collaborations in 2001 [31, 32] and the precision has been improved since, with experiments measuring $CP$ both indirectly via mixing and directly via decays.

Mixing in $B_d$ and $B_s$ systems is dominated by short-distance contributions. The reason for this is that the dominant weak coupling of the $b$ quarks is to the $t$ quarks in the box diagrams, shown in Fig. 1.10, is proportional to the square of the mass of the intermediate quarks. As a result, $B - \overline{B}^0$ mixing is dominated by the top intermediate state.

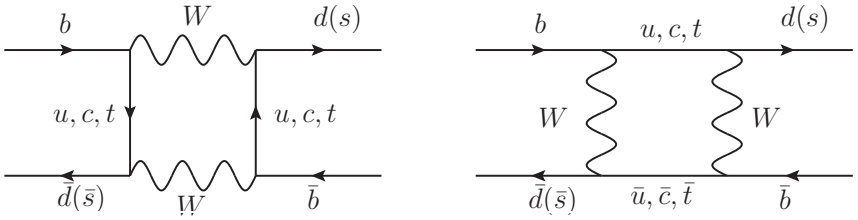


Figure 1.10: Box diagrams contributing to $B^0 - \overline{B}^0$ mixing.

The transition amplitude, in a similar way to Eq. 1.69, can be written as

$$\langle \overline{B}^0_q | H_W^{\Delta B=2} | B^0_q \rangle = \frac{G_F^2 M_W^2}{16\pi^2} \left( \lambda_{tq}^2 S_0(x_t) \eta_{2B} \right) \left( \frac{g_R(\mu)^2}{4\pi} \right)^{-\gamma_0/(2\beta_0)} \times \exp\left\{ \int_0^{g_R(\mu)} dg \left( \frac{\gamma(g)}{\beta(g)} + \frac{\gamma_0}{\beta_0} \right) \right\} \langle \overline{B}^0 | Q_R^q(\mu) | B^0 \rangle + \text{h.c.} \,, \tag{1.76}$$

where $Q_R^q(\mu)$ is the four-fermi operator and $\eta_{2B}$ contains short-distance QCD corrections [21]. Note that $\lambda_{tq} = V_{tq}^* V_{tb}$. The other symbols have their usual meanings. In a similar way to $B_K$ in Eq. 1.72, the bag parameter for the $B$-system is

$$B_{B_q}(\mu) = \frac{\langle \overline{B}^0_q | Q_R^q(\mu) | B^0_q \rangle}{\frac{8}{3} f_B^2 m_B^2}. \tag{1.77}$$

Given this definition, the SM prediction for the $B_q^0$ mass difference is written as

$$\Delta m_q = \frac{G_F^2 m_W^2 m_{B_q}}{6\pi^2} |\lambda_{tq}|^2 S_0(x_t) \eta_{2B} f_{B_q}^2 \hat{B}_{B_q}, \tag{1.78}$$

where $\hat{B}_{B_q}$ is the renormalization group invariant (RGI) $B$ parameter, which at 2-loops takes the form

$$\hat{B}_{B_q} = \left( \frac{g_R(\mu)^2}{4\pi} \right)^{-\gamma_0/(2\beta_0)} \left\{ 1 + \frac{g_R(\mu)^2}{(4\pi)^2} \left[ \frac{\beta_1\gamma_0 - \beta_0\gamma_1}{2\beta_0^2} \right] \right\} B_{B_q}(\mu). \tag{1.79}$$

Given that $\Delta m_{d(s)}$ are known experimentally from the oscillations frequencies mentioned above, and the lattice calculation provides measurements of $f_{B_q}$ and $B_{B_q}$, $\lambda_{tq}$ can be determined from Eq. 1.78. Lattice calculations of the flavor

$SU(3)$-breaking ratio

$$\xi = \frac{f_{B_s}\sqrt{B_{B_s}}}{f_{B_d}\sqrt{B_{B_d}}} \,, \tag{1.80}$$

from which $|V_{td}/V_{ts}|$ can be extracted due to Eq. 1.76 and $\lambda_{tq} = V_{tq}^* V_{tb}$, yields a more precise result than the individual bag parameters. This ratio also has an added advantage that for certain lattice fermion formulations, such as the Domain Wall fermions (DWF), the renormalization factors cancel between the numerator and the denominator and can be dropped. The determination of $|V_{td}/V_{ts}|$ via this ratio, is used to constrain the apex of the CKM triangle corresponding the orange circle in Fig. 1.7.

Experimentally, charm $D^0 - \overline{D}^0$ mixing has been observed in recent years [33]. However, since short- and long-distance effects presented in Fig. 1.11 and Fig. 1.12 respectively are of the same order of magnitude, it is difficult to calculate SM predictions for the mixing parameters $\Delta m_D$ and $\Delta\Gamma$. The reason the short-distance effects in this case are smaller is the following. The mass of the heaviest quark $m_b$ in the box diagram of Fig. 1.11 is not large enough to compensate for the corresponding CKM matrix elements $|V_{ub}V_{cb}|^2 \sim (\lambda^5)^2$ according to Eq. 1.24. This implies that the light quarks dominate the mixing, which are of order $|V_{us}V_{cs}|^2 m_s^2 \sim \lambda^2 m_s^2$ in the box diagram, resulting in small mixing parameters. Therefore, the purpose of searches for $D^0 - \overline{D}^0$ mixing is mostly viewed as a probe for new physics rather than a method for constraining the CKM parameters. CP-violation effects within SM are expected to be very small. As a results, observation of CP-violation in these systems at a higher level than $\mathcal{O}(10^{-3})$ indicates signals for new physics [9]. There will be a programme dedicated to charm physics in the upcoming Belle II experiment [34].

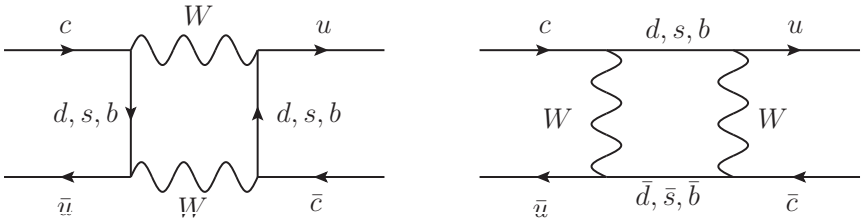


Figure 1.11: Box diagrams contributing to $D^0 - \overline{D}^0$ mixing.

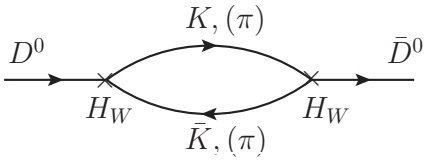


Figure 1.12: Long-distance contributions to $D^0 - \overline{D}^0$ mixing.

## 1.3 Examples of anomalies in the flavor sector

To emphasize the role of probing the flavor sector, in this section we mention examples of current important anomalies present in this sector, such as Lepton Flavor Universality (LFU) ratios $R_D$, $R_{D^*}$, $R_K$ and $R_{K^*}$. We do not go into much detail as these particular anomalies, arising from semi-leptonic decays, are not the subject of this thesis.

Lepton flavor universality in the SM refers to the equality of the electroweak couplings of different flavors of leptons. The LFU ratios are defined as

$$R_M[q^2_{\text{min}}, q^2_{\text{max}}] = \frac{\int_{q^2_{\text{min}}}^{q^2_{\text{max}}} dq^2 \frac{d\Gamma(B\to M\mu^+\mu^-)}{dq^2}}{\int_{q^2_{\text{min}}}^{q^2_{\text{max}}} dq^2 \frac{d\Gamma(B\to Me^+e^-)}{dq^2}} \ , \tag{1.81}$$

where $\Gamma$ is the $q^2$-dependent partial width of the decay, $q^2 = m^2_{ll}$ is the square of the dilepton mass and $M$ is the meson which is the result of the decay, such as $K$, $K^*$, $D$ or $D^*$. These semi-leptonic decays are sensitive to contributions from non SM particles. In the SM, where there is LFU, one expects the ratio in Eq. 1.81 to be equal to one. However, measurements at the LHCb, Belle and BaBar [35–39] show deviations from unity. For example, in the case of $R_K$, LHCb results of $R_K[1\ \text{GeV}^2, 6\ \text{GeV}^2] = 0.754^{+0.090}_{-0.074} \pm 0.036$ differ from the SM expectation by $2.6\sigma$ [40]. There are also recent results by the LHCb collaboration on $R_{K^*}$ indicating 2.4-2.5$\sigma$ deviation from the SM [41].

## 1.4 Current research and challenges

This project has involved lattice computation of $D$- and $D_s$-meson masses, decay constants $f_{D_{(s)}}$ extracted via the axial current matrix element

$$\langle 0|A^{\mu}_{cq}|D_q(p)\rangle = if_{D_q}p^{\mu}_{D_q}, \tag{1.82}$$

with $q = d, s$ and $A^{\mu}_{cq} = \bar{c}\gamma_{\mu}\gamma_5 q$, as well as bag parameters using Domain Wall Fermion (DWF) formulation. The leptonic decays in the charm sector give information on CKM matrix elements $|V_{cd}|$ and $|V_{cs}|$. Computing the bag and $\xi$ parameters in this sector, with the aim of eventually extrapolating the results to the $B$-sector using Heavy Quark Effective Theory (HQET), is an ingredient that provides constraint on the apex of the unitarity triangle via the ratio $|V_{td}/V_{ts}|$, as discussed in the previous section.

Current research has the mass of the quarks being pushed to higher values, to reach $c$ and $b$ quarks, making lattice artefacts more visible. For example, lattices that can be currently simulated have a cut off which is of the same order as the $b$-quark mass. As a result, simulating $b$-quarks directly suffers from large cut-off effects [42]. Charm physics on the lattice also allows us to gain more insight into $B$-physics via direct application of HQET, by making an expansion in inverse heavy quark mass and extrapolating from the charm to the bottom region.

At this stage, it seems necessary to invest more effort into reducing lattice artefacts and improve measurements at the level of both resources and formalism. The former involves *e.g.* developing better algorithms to be able to simulate finer lattices with greater volumes, or using efficient averaging methods [43–45]. The latter involves *e.g.* varying lattice actions, number of sea flavors and using different techniques in extracting the observables etc. In terms of testing a different formalism, a major part of this thesis is dedicated to discussing the development of a new massive renormalization scheme, denoted by RI/mSMOM. The aim here is that by using a massive renormalization scheme, some of the lattice artefacts arising from masses of quarks and appearing as coefficients of $\mathcal{O}(a^2)$ terms would be reduced, giving a smoother extrapolation to the continuum limit. This scheme is discussed in great detail in chapter 3.

# Chapter 2

# Non-perturbative formulation of QCD

The part of this chapter focuses mostly on the theoretical background required to construct QFT on the lattice. The derivations presented here are done for a free theory, *i.e.* not involving gauge fields. An important derivation is that of the fermion propagator on the lattice. A naive discretisation of the Dirac operator leads to extra poles that have no continuum analogue. This implies the need for constructing other types of lattice fermions, such as Wilson, Domain Wall and Overlap fermions to describe the physics correctly. Domain Wall fermions are the type used later on in the simulations and are explained in more detail later in this chapter.

## 2.1 The Basics

In order to construct QFT on the lattice, one has to perform a Wick rotation from Minkowski to Euclidean space-time. The conventions, starting from the space-time 4-vector $x^\mu$ and including Dirac gamma matrices and Fourier transforms are written in Appendix B. This section starts with the naive discretization of the Euclidean action for scalar fields. The propagator is computed as an explicit example and the result is compared with the usual continuum propagator. A similar calculation for the naive fermion propagator is then performed and the problem with the so-called *doublers* is discussed.

### 2.1.1 Free Field Scalar Propagator on the Lattice

In this section, we derive the lattice scalar field propagator starting in momentum space from the discretized Euclidean action. By integrating the 4th component, we examine the pole structure and the large time behaviour of the propagator. We also show the usual continuum dispersion relation is recovered as $a \to 0$.

The continuum Euclidean action in 4 dimensions for the free scalar field reads as follows

$$\begin{aligned} S_E[\phi] =& \int d^4x \left( \frac{1}{2}\partial_\mu\phi(x)\partial_\mu\phi(x) + \frac{1}{2}m^2\phi^2(x) \right) \\ =& \frac{1}{2}\int d^4x \left( -\phi(x)\partial^2\phi(x) + m^2\phi^2(x) \right) , \end{aligned} \tag{2.1}$$

Discretizing and taking the Fourier transform, according to the derivation in App. B.3, the scalar field propagator can be written as

$$\begin{aligned} D_S(x) = \langle\phi(x)\phi(0)\rangle &= \int_{-\pi/a}^{\pi/a} \frac{d^4k}{(2\pi)^4} \frac{e^{ik.x}}{m^2a^2 + \sum_\mu 4\sin^2(\frac{k_\mu a}{2})} \\ &= \int \frac{d^3k}{(2\pi)^3} \int \frac{dk_4}{(2\pi)} \frac{e^{ik.x}}{m^2a^2 + \sum_\mu (2 - 2\cos(k_\mu a))} \\ &= \int \frac{d^3k}{(2\pi)^3} e^{i\mathbf{k}.\mathbf{x}} \int \frac{dk_4}{(2\pi)} \frac{e^{ik_4x_4}}{2M(\mathbf{k})^2 - 2\cos(k_4a)} , \end{aligned} \tag{2.2}$$

where we have defined $2M(\mathbf{k})^2 = m^2a^2 + 8 - \sum_i 2\cos(k_ia)$ noting that $m^2a^2 + 8 - \sum_i 2\cos(k_ia)$ is a positive quantity. The poles are at the points where the denominator vanishes:

$$2M(\mathbf{k})^2 - 2\cos(k_4a) = 2M(\mathbf{k})^2 - \left(e^{ik_4a} + e^{-ik_4a}\right) = 2M(\mathbf{k})^2 - z - z^{-1} = 0 \cdot \tag{2.3}$$

In other words, the integral over $k_4$ can be performed using a contour integration in the $z$ plane with an anti-clockwise contour, $|z| = 1$, and the change of variable $z = e^{ik_4a}$ so that $dk_4 = \frac{dz}{iaz}$. The $z$ in the denominator of the latter expression multiplies Eq. 2.3 which yields,

$$z^2 - 2M^2z + 1 = 0 , \tag{2.4}$$

and hence,

$$z = M^2 \pm \sqrt{M^4 - 1} \cdot \tag{2.5}$$

This quantity is real since $M \geq 1$. However, since the contour $|z| = 1$, is the unit

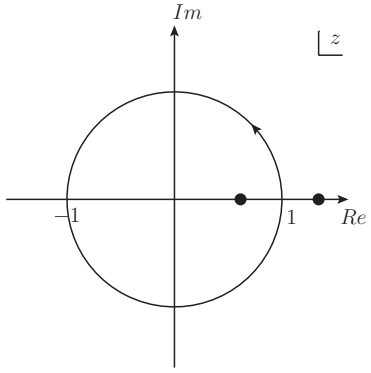


Figure 2.1: $z = e^{ik_4 a}$ contour

circle in the $z$-plane, only one of the poles *i.e.* $z = M^2 - \sqrt{M^4 - 1}$ contributes while the other one lies outside the unit circle, Fig. 2.1. Because $z$ is real and positive, one can write $z = e^{-\omega a}$ where $\omega$ is a positive quantity associated with the energy, as shown in Eq. 2.10. Indeed, the non-contributing pole can be written as,

$$\frac{1}{M^2 - \sqrt{M^4 - 1}} \times \frac{M^2 + \sqrt{M^4 - 1}}{M^2 + \sqrt{M^4 - 1}} = M^2 + \sqrt{M^4 - 1} = e^{\omega a} \cdot \tag{2.6}$$

Hence the integral in Eq. 2.2 is evaluated

$$\int \frac{d^3k}{(2\pi)^3} e^{i\mathbf{k}.\mathbf{x}} \frac{2\pi i}{-ia2\pi} \frac{e^{-\omega x_4}}{e^{-\omega a} - e^{\omega a}} = \frac{1}{a} \int \frac{d^3k}{(2\pi)^3} e^{i\mathbf{k}.\mathbf{x}} \frac{e^{-\omega x_4}}{2\sinh(\omega a)} \cdot \tag{2.7}$$

Also, from Eq. 2.4 it can readily been seen that,

$$\cosh(\omega a) = \frac{1}{2}(e^{\omega a} + e^{-\omega a}) = M^2 \cdot \tag{2.8}$$

Expanding the both sides of the equation above up to order $\mathcal{O}(a^2)$ yields,

$$1 + \frac{\omega^2 a^2}{2} = \frac{1}{2}\left[m^2a^2 + 8 - \sum_i 2(1 - \frac{(k_i a)^2}{2})\right] = \frac{1}{2}\left[m^2a^2 + 2 + \mathbf{k}^2a^2\right] \cdot \quad (2.9)$$

Therefore, in the continuum limit $am \ll 1$, $ak_i \ll 1$, we recover Lorentz invariance and the expected dispersion relation:

$$\omega(\mathbf{k}) \to \sqrt{m^2 + \mathbf{k}^2}\ , \quad (2.10)$$

and the expression for the energy in the continuum is recovered. Moreover, observing Eq. 2.7, which is a sum of exponentials $\exp(-\omega t)$, implies that for large $t = n_t a$ the exponential with the smallest value of $\omega$ *i.e.* $\omega = m$ dominates. Therefore,

$$D_s \to e^{-m \times n_t a} \quad , \quad \text{for} \quad t \to \infty \cdot \quad (2.11)$$

This gives the correlation length $\xi$ as:

$$\xi = \frac{1}{am} \cdot \quad (2.12)$$

This is also true for the interaction theory. Note that we wish the continuum limit $m$ to remain finite. Comparing the above to the notion of correlation length in statistical physics, we see that there is a critical point, *i.e.* $a \to 0$, where the correlation length $\xi$ diverges. In other words, the continuum limit corresponds to a second order transition of a statistical system.

### 2.1.2 Restoration of rotational invariance in 2-dimensions

It would be interesting to see, in a simple example, how rotational invariance is restored when the continuum limit is taken. We take a 2-dimensional example for simplicity, and show explicitly discretization effects in the form of $\mathcal{O}(a^2)$ and $\mathcal{O}(a^4)$ terms for this case.

Let us now consider the propagator for the free scalar field in 2-dimensions

which can be written as follows in lattice units [46],

$$D_F(x) = \langle \phi(x)\phi(0)\rangle = \int \frac{d^2p}{(2\pi)^2} \frac{e^{ip.x}}{m^2 + 4 - 2\cos(p_1) - 2\cos(p_2)} \cdot \tag{2.13}$$

Consider two cases: $x \to \infty$ along a lattice direction where $x = nt, t \to \infty$ with $n = (1,0)$ or along the diagonal with $n = (1,1)/\sqrt{2}$:

1. For $n = (1,0)$ and denoting $2b = m^2 + 4 - 2\cos(p_2)$, Eq. 2.13 reads

$$\begin{aligned} D_F &= \int_{-\pi}^{\pi} \frac{dp_2}{2\pi} \int_{-\pi}^{\pi} \frac{dp_1}{2\pi} \frac{e^{ip_1 t}}{2b - 2\cos(p_1)} = \int_{-\pi}^{\pi} \frac{dp_2}{2\pi} \frac{e^{-\omega t}}{2\sinh(\omega)} \\ &= \int_{-\pi}^{\pi} \frac{dp_2}{2\pi} \frac{1}{2\sinh(\omega)} e^{-t\left[\ln(b(p_2)+\sqrt{b(p_2)^2-1})\right]} , \end{aligned} \tag{2.14}$$

where the first integral is done by finding the relevant pole in exactly the same way as in the previous section with $\cosh(\omega) = b$ and $\omega = \ln\left(b + \sqrt{b^2-1}\right)$. For $t$ large, one can use the saddle point method to evaluate the leading contribution to the integral. To this end, we need to find the point(s) at which the first derivative of $\omega(b(p_2)) = \ln\left(b(p_2) + \sqrt{b(p_2)^2-1}\right)$ with respect to $p_2$ vanishes. Note that in order to keep the algebra simpler, there is no need to derive an explicit form for the derivative. It merely suffices to identify the point at which the derivative vanishes. Taking

$$\frac{d\omega}{db} = \frac{\partial\omega}{\partial b}\frac{\partial b}{\partial p_2} = \frac{1 + \frac{2b(p_2)}{2\sqrt{b(p_2)^2-1}}}{b(p_2) + \sqrt{b(p_2)^2-1}} \sin(p_2) = 0 \cdot \tag{2.15}$$

It is clear from the definition of $b$ that $b > 1$ meaning the fraction in the above expression is always greater that zero. Hence, within the Brillouin zone, the solution to the equation corresponds to $p_2 = 0$. This implies

$$b_0 = \frac{m^2}{2} + 1 \quad \Rightarrow \quad \cosh(\omega) = \frac{m^2}{2} + 1 \cdot \tag{2.16}$$

Eq. 2.14 is then equal to

$$D_F \simeq \frac{1}{2\sinh(\omega(b))}\Big|_{b_0 = m^2/2+1} e^{-t\omega(b_0)} \int \frac{dp_2}{2\pi} e^{-\frac{1}{2}t\omega''(b_0)(b(p_2)-b_0)^2} \propto e^{-t\omega(b_0)} . \tag{2.17}$$

The correlation length $\xi(n)$ in direction $n$ is identified by $D_F \propto e^{-t/\xi(n)}$ so in this case, $\xi^{-1}(n) = \omega$.

2. For $n = (1,1)/\sqrt{2}$, changing variables to $\Sigma = \frac{p_1+p_2}{2}$ and $\Delta = \frac{p_1-p_2}{2}$, Eq. 2.13 becomes

$$\begin{aligned} &\int_\pi^\pi \frac{dp_1 dp_2}{(2\pi)^2} \frac{e^{it(p_1+p_2)/\sqrt{2}}}{m^2+4-4\cos(\frac{p_1-p_2}{2})\cos(\frac{p_1+p_2}{2})} \\ &\propto \int d\Sigma d\Delta \frac{e^{i\sqrt{2}\Sigma t}}{m^2+4-4\cos\Delta\cos\Sigma} \propto \int d\Delta g(\Delta) e^{-t\sqrt{2}\omega'} \\ &\propto \int d\Delta g(\Delta) e^{-t\sqrt{2}\ln(b(\Delta)+\sqrt{b^2(\Delta)-1})} \end{aligned} \tag{2.18}$$

where

$$\omega' = \ln(b+\sqrt{b^2-1}) \quad , \quad b = \frac{m^2+4}{4\cos\Delta} \cdot \tag{2.19}$$

Using the same saddle point method as in the previous part, the integral is dominated by $\Delta_0$ such that $\sin\Delta_0 = 0$ *i.e.* $\cos\Delta_0 = 1$ implying

$$D_F \propto e^{-t\sqrt{2}\omega'} \ , \tag{2.20}$$

with

$$\cosh(\omega') = b_0 = 1 + \frac{m^2}{4} \cdot \tag{2.21}$$

In this case, the correlation length, $\xi'^{-1}(n) = \sqrt{2}\omega'$.

Taking the ratio of the two correlation lengths,

$$\frac{\xi'}{\xi} = \frac{\omega}{\sqrt{2}\omega'} = 1 - \frac{m^2}{48} + \mathcal{O}(m^4) \cdot \tag{2.22}$$

In non-lattice units $m \to ma$ and at this finite lattice spacing, the ratio is away from unity, with the discretization effects identified explicitly at order $a^2$. However, $\frac{\xi'}{\xi} \to 1$ as $ma \to 0$ which implies the recovery of the rotational invariance.

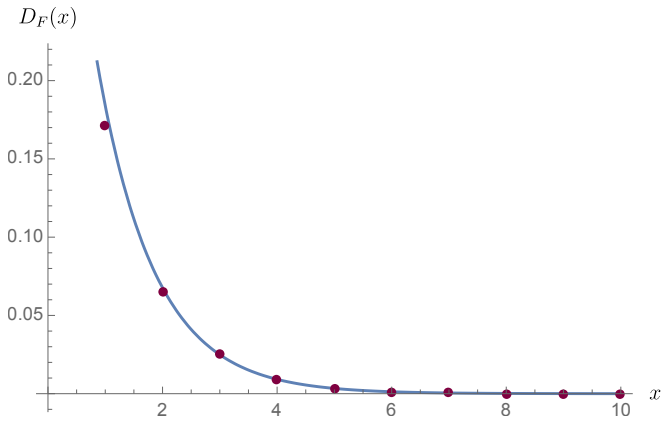


Figure 2.2: 1-D Lattice and Continuum Scalar Propagators

### 2.1.3 Comparison of Lattice and Continuum Propagators

We now compare the lattice formulation of the scalar propagator to the continuum in infinite volume. It is known that the continuum scalar field propagator in four dimensions can be written in terms of the modified Bessel function $K_1$ [47]. Here we merely quote the results for the continuum case,

$$D_F^C(x,n) = \int_{-\infty}^{\infty} \frac{d^n p}{(2\pi)^n} \frac{e^{ipx}}{m^2+p^2} = (2\pi)^{-n/2} \left[\frac{(x^2)^{1/2}}{m}\right]^{1-n/2} K_{1-n/2}\left[m(x^2)^{1/2}\right], \tag{2.23}$$

and the lattice case

$$D_F^L(x,n) = \int_{-\pi/a}^{\pi/a} \frac{d^n p}{(2\pi)^n} \frac{e^{ipx}}{m^2+\hat{p}^2} = \int_0^{\infty} d\alpha\; e^{-m^2\alpha} \left\{ \prod_{\mu=1}^{n} e^{-\frac{2\alpha}{a^2}} (\frac{1}{a}) I_{\frac{x_\mu}{a}}\left(\frac{2\alpha}{a^2}\right) \right\}, \tag{2.24}$$

where

$$\hat{p}^2 = \frac{4}{a^2} \sum_{\mu=1}^{n} \sin^2\left(\frac{p_\mu a}{2}\right), \tag{2.25}$$

and $I_{\frac{x_\mu}{a}}$ is the modified Bessel function of the first kind. The plot in Fig. 2.2 shows the Mathematica [48] implementation of the above propagators in one dimension for particular values of $x$. As it can observed, the discretized lattice

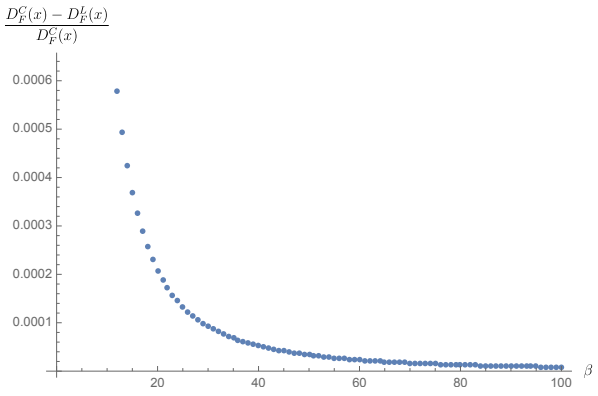


Figure 2.3: Relative difference between lattice and continuum scalar propagators

points, in red, agree with the continuum propagator drawn in blue. Examining the deviation of the lattice points from the continuum one would be able to analyse the discretization errors properly and recover the full continuum limit. In order to discuss continuum physics properly, one has to work in a region where the physics is insensitive to the cut off (*i.e.* of order $\ll 1/a$). This is better illustrated with an example: Let us take $mx$ to be fixed at a value say, $\alpha = mx$, change the ratio $\beta = \frac{x}{a}$ which takes different values over a range, in which case $am = \frac{\alpha}{\beta}$ and then compare the relative difference between lattice and continuum results. This is presented in the following graph for a particular value of $\alpha$. As it can be seen in Fig. 2.3, the relative difference, *i.e.* the error, decrease as $x$ increases.

### 2.1.4 Free Field Naive Fermion Propagator on the Lattice

In this section, we examine the dispersion relation for the case of the naive fermion propagator in the continuum limit and discuss the problem of "*fermion doublers*".

The continuum Euclidean action in four dimensions for the free fermion field reads as follows:

$$S_E[\psi, \bar{\psi}] = \int d^4x \left(\bar{\psi}(x)\gamma_\mu \partial_\mu \psi(x) + m\bar{\psi}(x)\psi(x)\right) \cdot \tag{2.26}$$

The continuum action can be discretized using the Finite Difference Approxima-

tion for the derivatives discussed in Appendix B. This gives,

$$\begin{aligned}
S_E[\psi,\bar{\psi}] =& a^4 \sum_x \bar{\psi}(x) \left[\gamma_\mu \frac{\psi(x+a\hat{\mu}) - \psi(x-a\hat{\mu})}{2a}\right] + m\bar{\psi}(x)\psi(x) \\
=& \frac{a^4}{(2\pi)^2} \sum_x \int_{kk'} e^{-ikx} \Bigg\{ \tilde{\bar{\psi}}(k)\gamma_\mu \frac{1}{2a} \left[\left(e^{ik'(x+a\hat{\mu})} - e^{ik'(x-a\hat{\mu})}\right)\right] \tilde{\psi}(k') \\
& \qquad + m e^{ikx'} \tilde{\bar{\psi}}(k)\tilde{\psi}(k') \Bigg\} \\
=& \frac{a^4}{(2\pi)^2} \sum_x \int_{kk'} \tilde{\bar{\psi}}(k) e^{-ikx} \gamma_\mu \frac{1}{2a} e^{ik'x} \left(e^{ik'_\mu a} - e^{-ik'_\mu a}\right) \tilde{\psi}(k') \\
& \qquad + m e^{-ikx+ikx'} \tilde{\bar{\psi}}(k)\tilde{\psi}(k') \\
=& \frac{a^4}{(2\pi)} \int_{kk'} \tilde{\bar{\psi}}(k)\delta(k-k') \left(\frac{i}{a}\gamma_\mu \sin(k'_\mu a)\tilde{\psi}(k') + m\tilde{\bar{\psi}}(k)\tilde{\psi}(k')\right) \\
=& \frac{a^4}{(2\pi)} \int_k \tilde{\bar{\psi}}(k) \left[m + \gamma_\mu \frac{i\sin(k_\mu a)}{a}\right] \tilde{\psi}(k) \ ,
\end{aligned} \tag{2.27}$$

where $x = na$ and index $\mu$ is summed over. Therefore, the lattice fermion propagator in momentum space is:

$$\tilde{D}_F(k) = \frac{1}{m\mathbb{I} + i\gamma_\mu \frac{\sin(k_\mu a)}{a}} \ . \tag{2.28}$$

In the continuum limit Minkowski space, one must recover the usual fermion propagator. Therefore in the limit as $a \to 0$,

$$\tilde{D}_F(k) \to \frac{1}{m + i\gamma_\mu k_\mu} \xrightarrow{\text{Minkowski}} \frac{1}{-(\gamma_0 k_0 - \underline{\gamma}.\underline{k} - m)} = -\frac{1}{\not{k} - m} \ , \tag{2.29}$$

where we have used the conversion conventions for $\gamma$ matrices and the momentum 4-vector as spelled out in Appendix B. The results agree with Eq. B.18 as expected.

In order to examine the dispersion relation, we start by finding the inverse Fourier transform of the lattice propagator. Note that the integral is over the

first Brillouin zone and we work in infinite volume.

$$\begin{aligned}\tilde{D}_F = \langle\psi(x)\bar{\psi}(0)\rangle &= \int \frac{d^4k}{(2\pi)^4}\frac{e^{ikx}}{m+\frac{i}{a}\sin(k_\mu a)\gamma_\mu}\times\frac{m-\frac{i}{a}\sin(k_\mu a)\gamma_\mu}{m-\frac{i}{a}\sin(k_\mu a)\gamma_\mu} \\ &= \int \frac{dk^4}{2\pi}\frac{d^3\mathbf{k}}{(2\pi)^3}\frac{ma^2-ia\sin(k_\mu a)\gamma_\mu}{m^2a^2+\sum_\mu \sin^2(k_\mu a)}e^{ik_4x_4}e^{i\mathbf{k}.\mathbf{x}}\ ,\end{aligned} \tag{2.30}$$

where the $\mu$ index is summed, $\gamma_\mu\gamma_\mu = \mathbb{I}$ is used and we have multiplied top and bottom by $a^2$. Now the relevant poles in the denominator have to be identified. Note, however, that we are integrating with respect to $dk^4$, so the contour in the $k^4$ space need to be considered. Because the integral is over the first Brillouin zone, the real part of $k^4$ must satisfy $-\pi/a < k^4 < \pi/a$. Defining $z = e^{ik_4a}$ the denominator becomes

$$\underbrace{m^2a^2+\sum_{i=1}^{3}\sin^2(k_ia)}_{M^2}+\frac{-1}{4}(z^2+z^{-2}-2) = 0\ . \tag{2.31}$$

The numerator and the denominator are then multiplied by $-4z^2$ and equation

$$z^4 - 2(1+2M^2)z^2 + 1 = 0\ , \tag{2.32}$$

is solved to obtain

$$z^2 = (1+2M^2) \pm 2M\sqrt{M^2+1} = (-M\pm\sqrt{1+M^2})^2\ . \tag{2.33}$$

Hence the four solutions for $z$ are:

$$z = \begin{cases} M+\sqrt{1+M^2} = e^{\omega a} \\ M-\sqrt{1+M^2} = -e^{-\omega a} \\ -M+\sqrt{1+M^2} = e^{-\omega a} \\ -M-\sqrt{1+M^2} = -e^{\omega a}\ , \end{cases} \tag{2.34}$$

where $\omega$ is defined such that $M+\sqrt{1+M^2} = e^{\omega a}$. The main task now is to identify the relevant poles. We are changing variables from $k \to z$, which means that the relevant poles have to be identified in the complex $z$ plane. The limits of the $k$ integral run from $-\pi/a$ to $\pi/a$ which correspond to $z$ running once around

the unit circle. Note that,

$$dk = \frac{dz}{iaz} \cdot \tag{2.35}$$

Therefore, using Eq. 2.32 and Eq. 2.35 we have an overall factor of $z$ in the numerator. Clearly, the only poles that contribute are the ones that lie within

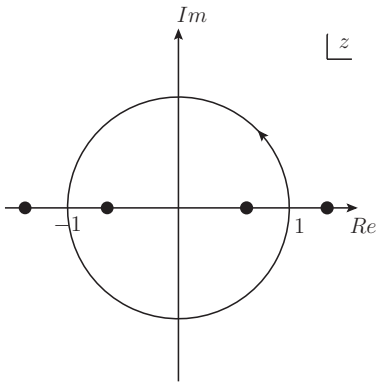


Figure 2.4: $z = e^{ik_4 a}$ contour

the unit circle $0 \leq |z| \leq 1$, *i.e.* $z = \pm e^{-\omega a}$. We now use the residue theorem. Finding the coefficients for the poles at:

1. $z = e^{ik_4 a} = e^{-wa}$, the numerator becomes,

$$\begin{aligned} &-4z\left[ma^2 - ia\sum_{i=1}^{3}\sin(k_i a)\gamma_i - ia\frac{1}{2i}\left[e^{-\omega a} - e^{\omega a}\right]\gamma_4\right] \\ =&-4e^{-\omega x_4}\left[ma^2 - ia\sum_{i=1}^{3}\sin(k_i a)\gamma_i + a\sinh(\omega a)\gamma_4\right], \end{aligned} \tag{2.36}$$

and the denominator,

$$(z - e^{\omega a})(z + e^{-\omega a})(z + e^{\omega a}) = 2e^{-\omega a}(e^{-\omega a} - e^{\omega a})(e^{-\omega a} + e^{\omega a}) \tag{2.37}$$

$$= -4e^{-\omega a}\sinh(2\omega a) \cdot \tag{2.38}$$

2. $z = e^{ik_4 a} = -e^{-wa}$ the numerator becomes,

$$(-)^{x_4/a} 4e^{-\omega x_4} \left[ ma^2 - ia \sum_{i=1}^{3} \sin(k_i a)\gamma_i - a \sinh(\omega a)\gamma_4 \right] \cdot \tag{2.39}$$

Note that since $e^{ika} = -e^{-\omega a}$, raising both sides to the power of $x_4/a$ yields $e^{ikx_4} = (-)^{x_4/a} e^{-\omega x_4}$. The denominator reads,

$$-2e^{-\omega a}(e^{-\omega a} + e^{\omega a})(-e^{-\omega a} + e^{\omega a}) = 4e^{-\omega a} \sinh(2\omega a) \cdot \tag{2.40}$$

Finally, summing the residues results in

$$\tilde{D}_F = \int \frac{d^3\mathbf{k}}{(2\pi)^3} \frac{e^{i\mathbf{k}.\mathbf{x} - \omega x_4}}{\sinh(2\omega a)} \Bigg\{ \left[ ma - i \sum_{i=1}^{3} \sin(k_i a)\gamma_i + \sinh(\omega a)\gamma_4 \right] + (-)^{x_4/a} \left[ ma - i \sum_{i=1}^{3} \sin(k_i a)\gamma_i - \sinh(\omega a)\gamma_4 \right] \Bigg\} \cdot \tag{2.41}$$

For $e^{-\omega a} = -M + \sqrt{1+M^2}$ where $M = \sqrt{m^2 a^2 + \sum_{i=1}^{3} \sin^2(k_i a)}$, expanding both sides for lattice spacing $a \to 0$ up to order $a^2$ yields,

$$1 - \omega a = -a\sqrt{m^2 + \mathbf{k}^2} + \sqrt{1 + a^2(m^2 + \mathbf{k}^2)} = -a\sqrt{m^2 + \mathbf{k}^2} + 1 + \mathcal{O}(a^2) \ , \tag{2.42}$$

*i.e.*

$$\omega(\mathbf{k}) \to \sqrt{m^2 + \mathbf{k}^2} \cdot \tag{2.43}$$

So far, we have seen that the free naive lattice fermion propagator satisfies the continuum limit, Eq. 2.29 as well as the seemingly correct dispersion relation. However, let us observe the denominator of Eq. 2.30, explicitly written in Eq. 2.31. In the massless limit, the denominator vanishes when $k_i = n_i \pi/a$ where $n_i$ can only be either 0 or 1, on the spacial direction as well as $k_4 = n_i \pi/a$ for the same values, given that $k \in (-\pi/a, \pi/a]$. This leads to $2^4$ poles, in contrast to the continuum case where there is a single pole at $k^\mu = (0,0,0,0)$. Hence the energy $\omega$ is equal to zero at more points than just the rest frame. This is known as the "*fermion doubler problem*". In the next sections we discuss methods to overcome

this problem.

### 2.1.5 Free Field Wilson Fermion Propagator

Consider the following lattice action for massless fermions,

$$S = \sum_{x,y} \bar{\psi}(x) D(x-y) \psi(y) \cdot \tag{2.44}$$

According to the Nielsen-Ninomiya theorem, the properties below cannot hold simultaneously [49]:

1. $D(x)$ is local *i.e.* $\tilde{D}(p)$ is a periodic, analytic function of $p_\mu$.
2. $\tilde{D}(p) \propto \gamma_\mu p_\mu$ for $a|p_\mu| \ll 1$
3. $\tilde{D}(p)$ is invertible for $p_\mu \neq 0$
4. $\{\gamma_5, \tilde{D}(p)\} = 0$

Note that violating locality results in discontinuities in the derivatives of the propagator. The second and third cases are related to having a single flavor of Dirac fermions in the continuum limit. We have come across the third case in our discussion of the doubling problem. Any attempt to solve this issue involves violation of one of the other conditions. The last point is a statement about chiral symmetry which will be discussed later on.

There is a simple method by which one can resolve the doubling problem. This method involves adding a term to the mass. It is clear that introducing a mass term breaks chiral symmetry. As a result, the Nielsen-Ninomiya theorem still holds. However, we still need to check that the continuum fermion propagator and the continuum dispersion relation still hold with the addition of this term. Let

$$M(k) = m + \frac{1}{a}\sum_{\mu=1}^{4}(1-\cos(k_\mu a)) = \underbrace{m + \frac{1}{a}\sum_{i=1}^{3}(1-\cos(k_i a)) + \frac{1}{a}}_{\Omega(\mathbf{k})} - \frac{1}{a}\cos(k_4 a) \ , \tag{2.45}$$

where the $k_4$-independent part is denoted by $\Omega(\mathbf{k})$. Note that the Wilson term in position space, found by taking inverse Fourier transform, takes the form:

$$-a\sum_{\mu=1}^{4}\frac{\delta_{x+\hat{\mu},m}-2\delta_{x,y}+\delta_{x-\hat{\mu},y}}{2a^2}\ , \tag{2.46}$$

which is a discretization of $-(a/2)\partial_\mu\partial_\mu$. Therefore, due to the pre-factor $a$, the Wilson term goes to zero when the continuum limit $a \to 0$ is taken. Using the relabelling in Eq. 2.45, one can observe that the form of the propagator is the same as that in Eq. 2.30 *i.e.*

$$\tilde{D}_F = \langle\psi(x)\bar{\psi}(0)\rangle = \int \frac{dk^4}{2\pi}\frac{d^3\mathbf{k}}{(2\pi)^3}\frac{Ma^2 - ia\sin(k_\mu a)\gamma_\mu}{M^2a^2+\sum_\mu \sin^2(k_\mu a)}e^{ik_4x_4}e^{i\mathbf{k}.\mathbf{x}}\ . \tag{2.47}$$

The denominator can be written as follows:

$$\begin{aligned} M^2a^2+\sum_\mu \sin^2(k_\mu a) =& a^2\left[\Omega^2 - \frac{2}{a}\Omega\cos(k_4a)+\frac{1}{a^2}\cos^2(k_4a)\right] \\ &+\sum_i \sin^2(k_ia)+1-\cos^2(k_4a) \\ =& a^2\Omega^2 - 2a\Omega\cos(k_4a)+\sum_{i=1}^{3}\sin^2(k_ia)+1\ , \end{aligned} \tag{2.48}$$

which vanishes when the right hand side is zero. Therefore,

$$\begin{aligned} \cos(k_4a) =& \frac{a^2\Omega^2+\sum_i\sin^2(k_ia)+1}{2\Omega a} \\ =& \frac{\left[ma+\sum_i(1-\cos(k_ia))+1\right]^2+1+\sum_i\sin^2(k_ia)}{2\left[ma+\sum_i(1-\cos(k_ia))+1\right]} \equiv \cosh(\omega a)\ . \end{aligned} \tag{2.49}$$

One can check that with the above identification, the energy $\omega$ makes sense by taking the continuum limit of the above expression (also see Eq. 2.43). Note however, that the exact relation between $\omega$ and $k_4$ is more subtle and is addressed in detail when the poles are computed below. Expanding the left hand side for small $a$ gives,

$$1+\frac{1}{2}(\mathbf{k}^2+m^2)a^2+\mathcal{O}(a^4)\ . \tag{2.50}$$

On the other hand the expansion of $\cosh(\omega a) = 1 + \frac{\omega^2 a^2}{2}$. Comparing the two equations implies

$$\omega(\mathbf{k}) \to \sqrt{m^2 + \mathbf{k}^2} \ , \tag{2.51}$$

as required. Now, as before, we start by changing variables to $z = e^{ik_4 a}$ in Eq. 2.48. Note that the relevant integral is now over a unit circle in the complex $z$ plane and $dk^4 = \frac{dz}{iaz}$. The $z$ in the denominator of the measure multiplies the term in Eq. 2.48 to give

$$\begin{aligned} & z\left(a^2\Omega^2 - a\Omega\left(z + z^{-1}\right) + \sum_i \sin^2(k_i a) + 1\right) = 0 \\ \Rightarrow & -2\underbrace{\left(\frac{a^2\Omega^2 + \sum_i \sin^2(k_i a) + 1}{2a\Omega}\right)}_{\lambda} z + z^2 + 1 = 0 \ , \end{aligned} \tag{2.52}$$

which in turn implies,

$$z = \lambda \pm \sqrt{\lambda^2 - 1} \cdot \tag{2.53}$$

Note that it is important to keep track of the factor $\frac{-1}{ia^2\Omega}$. At this stage, a few checks need to be made:

1. Because $\Omega > 0$, it immediately implies that $\lambda > 0$. For $z$ to be real, we must have $\lambda \geq 1$. This condition is also satisfied for $a\Omega > 0$ which can be easily verified by plotting $\lambda$ as a function of $a\Omega$. This is shown in Fig. 2.5(a).[1]

2. Only one pole *i.e.* $z = \lambda - \sqrt{\lambda^2 - 1}$ lies within the unit circle for $\lambda > 1$, right graph in Fig. 2.5(b).

3. Now, we need to consider how to write $z$ as a function of $\omega$ correctly. $z = \pm e^{\omega a}$ results in a divergent integral for large time due to the term $e^{ik_4 x_4} = e^{\omega x_4}$. Therefore, $z \neq \pm e^{\omega a}$.

4. The only other possibilities are $z = \pm e^{-\omega a}$ corresponding to $k = i\omega$ and $k = i\omega + \pi$. Since the solution $0 < \lambda - \sqrt{\lambda^2 - 1} < 1$ for $\lambda > 1$ (from the

[1] To plot the graph, $\lambda$ is merely treated as a mathematical function of $a\Omega$ without considering its dependence on any physical parameter such as $m$. When $k_i = 0$ or $\pi$, $\sin(k_i a)$ in the numerator for $\lambda$ vanishes while $a\Omega$ takes a minimum or a maximum value respectively.

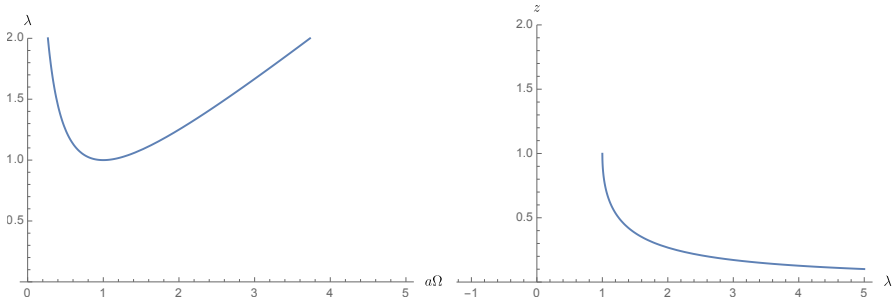


Figure 2.5: Plots of $\lambda$ vs $a\Omega$ and $z$ vs $\lambda$

plot), $z \neq -e^{-\omega a}$ leaving only one possibility: $z = e^{-\omega a}$ *i.e.* $k = i\omega$.

Hence, there is only one contributing pole corresponding to $z = \lambda - \sqrt{\lambda^2 - 1} \equiv e^{-\omega a}$. Substituting back into Eq. 2.47 and using the residue theorem,

$$\tilde{D}_F = \langle \psi(x)\bar{\psi}(0)\rangle \tag{2.54}$$

$$= \frac{1}{2a^2}\int \frac{d^3\mathbf{k}}{(2\pi)^3} \frac{\Omega a^2 - a\cosh(\omega a) - ia\sum_{i=1}^{3}\sin(k_i a)\gamma_i + a\gamma_4 \sinh(\omega a)}{\Omega \sinh(\omega a)} e^{-\omega x_4} e^{i\mathbf{k}.\mathbf{x}} \cdot \tag{2.55}$$

The leading contribution to the integral, as $x_4 = t$ increases, corresponds to the lowest possible value of $\omega$.

$$D_F \to e^{-m \times n_t a} \quad , \quad \text{for} \quad t \to \infty \cdot \tag{2.56}$$

We can explicitly check that the doubling problem has been solved. Observing Eq. 2.45 and Eq. 2.48, we see that in the massless limit, the denominator only vanishes for $k^\mu = (0,0,0,0)$ and there are no doublers. With the mass present, expanding both sides of $e^{-\omega a} \equiv z = \lambda - \sqrt{\lambda^2 - 1}$ for small $a$ gives,

$$1 - \omega a = 1 - ma + \mathcal{O}(a^2) \quad \Longrightarrow \quad \omega(\mathbf{k} = 0) = m \ , \tag{2.57}$$

as expected.

## 2.2 Chiral Symmetry and Domain Wall Fermions

### 2.2.1 Chiral Symmetry

Before discussing what chiral symmetry is, let us recall the representations of the Lorentz group for spin-1/2 particles. Using the chiral (Weyl) representation of the gamma matrices in Minkowski space [50]

$$\gamma^\mu = \begin{pmatrix} 0 & \sigma^\mu \\ \bar{\sigma}^\mu & 0 \end{pmatrix}, \tag{2.58}$$

where

$$\sigma^\mu \equiv (1, \underline{\sigma}) \quad \text{and} \quad \bar{\sigma}^\mu \equiv (1, -\underline{\sigma}) \cdot \tag{2.59}$$

The generators for infinitesimal boost and rotations are:

$$\sigma^{0i} = \frac{i}{4}[\gamma^0, \gamma^i] = \frac{i}{2}\begin{pmatrix} -\sigma^i & 0 \\ 0 & \sigma^i \end{pmatrix} = \frac{i}{2}\gamma^0\gamma^i \ , \tag{2.60}$$

$$\sigma^{ij} = \frac{i}{4}[\gamma^i, \gamma^j] = -\frac{i}{4}\begin{pmatrix} 2i\epsilon_{ijk}\sigma_k & 0 \\ 0 & 2i\epsilon_{ijk}\sigma_k \end{pmatrix} = \frac{1}{2}\epsilon_{ijk}\Sigma_k \cdot \tag{2.61}$$

The fact that both of these have a block-diagonal form implies that the Dirac representations is reducible. Therefore, one can consider each block separately and form a 2-dimensional representation,

$$\psi = \begin{pmatrix} \psi_L \\ \psi_R \end{pmatrix}, \tag{2.62}$$

where $\psi_L$ and $\psi_R$ are known as left-handed and right-handed Weyl spinors, each transforming under a separate irreducible representation of the Lorentz group. Then an invariant Lagrangian can be built, using combinations of spinor fields $\psi$ and the gamma matrices, from which the Dirac equation can be derived. For the

case of the massless Dirac equation we have,

$$(i\gamma^\mu\partial_\mu)\begin{pmatrix}\psi_L\\ \\ \psi_R\end{pmatrix}=0 \quad \Rightarrow \quad \begin{pmatrix}0 & i\sigma^\mu\partial_\mu\\ \\ i\bar{\sigma}^\mu\partial_\mu & 0\end{pmatrix}\begin{pmatrix}\psi_L\\ \\ \psi_R\end{pmatrix}=0\ . \tag{2.63}$$

In other words,

$$(E-\underline{\sigma}.\underline{p})\psi_R=0 \quad \Rightarrow \quad (\underline{\sigma}.\underline{p})\psi_R=+E\psi_R \quad \Rightarrow \quad (\underline{\sigma}.\underline{\hat{p}})\psi_R=+\psi_R\ , \tag{2.64}$$

where we have used that fact that for massless particles $|\underline{p}|=E$. Similarly,

$$(\underline{\sigma}.\underline{\hat{p}})\psi_L=-\psi_L\ , \tag{2.65}$$

meaning that $\psi_L$ and $\psi_R$ are eigenstates of the helicity operator

$$h=\frac{1}{2}\begin{pmatrix}\underline{\sigma}.\underline{\hat{p}} & 0\\ \\ 0 & \underline{\sigma}.\underline{\hat{p}},\end{pmatrix}, \tag{2.66}$$

with eigenvalues $-1/2$ and $+1/2$ respectively. The existence of a mass term in the Lagrangian would mix the two components which is the reason the massless case is being considered here. It is important to note that since massless particles have no rest frames, if a particle has helicity $1/2$ in one frame, it will have the same value in all frames. Therefore it can be said that for massless particles helicity (*i.e.* chirality) is an intrinsic property. This is clearly not the case for massive particles, since observers in different frames can measure different helicities. It is also worth mentioning that using the basis in Eq. 2.58 for the gamma matrices made the reducibility manifest which would not have been the case if we had chosen a different basis. As well as that, $\gamma^5$ takes the diagonal form:

$$\gamma^5=\begin{pmatrix}-1 & 0\\ \\ 0 & 1\end{pmatrix}, \tag{2.67}$$

with the usual relation $\{\gamma^5, \gamma^\mu\} = 0$. We can now construct the projection operators $P_R$ and $P_L$ such that:

$$P_R = \frac{1+\gamma^5}{2} = \begin{pmatrix} 0 & 0 \\ 0 & 1 \end{pmatrix}, \tag{2.68}$$

$$P_L = \frac{1-\gamma^5}{2} = \begin{pmatrix} 1 & 0 \\ 0 & 0 \end{pmatrix}. \tag{2.69}$$

It is easy to see,

$$P_R \begin{pmatrix} \psi_L \\ \psi_R \end{pmatrix} = \begin{pmatrix} 0 \\ \psi_R \end{pmatrix}, \tag{2.70}$$

*i.e.* $P_R$ project to the right-handed component. Similarly

$$P_L \begin{pmatrix} \psi_L \\ \psi_R \end{pmatrix} = \begin{pmatrix} \psi_L \\ 0 \end{pmatrix}, \tag{2.71}$$

and

$$\gamma^5 \begin{pmatrix} 0 \\ \psi_R \end{pmatrix} = \begin{pmatrix} 0 \\ \psi_R \end{pmatrix} \quad , \quad \gamma^5 \begin{pmatrix} \psi_L \\ 0 \end{pmatrix} = - \begin{pmatrix} \psi_L \\ 0 \end{pmatrix}. \tag{2.72}$$

The massless Dirac Lagrangian takes the form

$$\mathcal{L} = i\bar{\psi}\not{D}\psi = i \begin{pmatrix} \psi_R^\dagger & \psi_L^\dagger \end{pmatrix} \begin{pmatrix} 0 & \sigma^\mu \partial_\mu \\ \bar{\sigma}^\mu \partial_\mu & 0 \end{pmatrix} \begin{pmatrix} \psi_L \\ \psi_R \end{pmatrix} = i\psi_R^\dagger \sigma^\mu D_\mu \psi_R + i\psi_L^\dagger \bar{\sigma^\mu} D_\mu \psi_L \,. \tag{2.73}$$

However, including a mass term would mix the right- and left-handed parts:

$$m\bar{\psi}\psi = m\left(\psi_R^\dagger\psi_L + \psi_L^\dagger\psi_R\right) \cdot \tag{2.74}$$

The Dirac Lagrangian has an exact $U(1)$ symmetry $\psi \to e^{i\alpha}\psi$ under which the left- and right-handed components rotate with the same phase. This is known as the "vector symmetry". According to Noether's theorem, we can associate to every symmetry a conserved current. In other words for an infinitesimal field transformation $\phi \to \phi + \epsilon\delta\phi$:

$$J^\mu = -\frac{\partial\mathcal{L}}{\partial(\partial_\mu\phi)}\delta\phi \quad \text{and} \quad \partial_\mu J^\mu = -\delta\mathcal{L} \cdot \tag{2.75}$$

In this case $\psi \to (\mathbb{I} + i\alpha)\psi = \psi + i\alpha\psi \quad \Rightarrow \quad \delta\psi = i\psi$ , therefore

$$J^\mu = \bar{\psi}\gamma^\mu\psi \quad , \quad \partial_\mu J^\mu = 0 \ , \tag{2.76}$$

where we have used the Dirac equation when computing the divergence of $J$. The associated conserved charge is of the following form:

$$Q = \int d^3x\ J^0 = \int d^3x\ \psi^\dagger\psi = \int d^3x\ (\psi_L^\dagger\psi_L + \psi_R^\dagger\psi_R) = (N_L - \bar{N}_L) + (N_R - \bar{N}_R)\cdot \tag{2.77}$$

Hence,

$$Q = (N_L + N_R) - (\bar{N}_L + \bar{N}_R) \cdot \tag{2.78}$$

Physically this means that the fermion number is conserved. For the case $m = 0$, the Lagrangian has yet another symmetry where the left- and right-handed components rotate with opposite phase $\psi \to e^{i\alpha\gamma_5}\psi$. This is known as "axial symmetry" $U(1)_A$.

$$J_A^\mu = \bar{\psi}\gamma^\mu\gamma_5\psi \quad , \quad \partial_\mu J_A^\mu = 2im\bar{\psi}\gamma_5\psi \cdot \tag{2.79}$$

The corresponding classically conserved charge is

$$Q_A = \int d^3x\psi^\dagger\gamma_5\psi = \int d^3x\psi_L^\dagger\psi_L - \psi_R^\dagger\psi_R \cdot \tag{2.80}$$

Therefore,

$$Q_A = (N_L - \bar{N}_L) - (N_R - \bar{N}_R) \cdot \tag{2.81}$$

This implies that when the divergence of $J$ vanishes, the difference in the number of (unpaired) left- and right-handed fermions remains constant.

### 2.2.2 The axial anomaly

It is possible to relax the condition for chiral symmetry written in Sec. 2.1.5, *i.e.* $\{D, \gamma_5\} = 0$, on the lattice according to the Ginsparg-Wilson relation [51]:

$$\{D, \gamma_5\} = aD\gamma_5 D \ , \tag{2.82}$$

for a given Dirac operator $D$. This condition allows for the recovery of the correct chiral symmetry in the continuum limit as $a \to 0$. An example of a lattice Dirac operator satisfying this relation is discussed in Sec. 2.2.6 in more detail.

The axial transformation on the lattice takes the form:

$$\psi \to \exp\left(i\alpha\gamma_5\left(\mathbb{1} - \frac{a}{2}D\right)\right)\psi \quad , \quad \bar{\psi} \to \bar{\psi}\exp\left(i\alpha\left(\mathbb{1} - \frac{a}{2}D\right)\gamma_5\right) \cdot \tag{2.83}$$

This transformation leaves the Lagrangian for massless fermions, *i.e.* $\bar{\psi}D\psi$, invariant, given Eq. 2.82. Generalizing the above transformation to multiple flavors with $M$ being the flavor matrix, taking a infinitesimal transformation for small $\alpha$ and keeping only the leading term in $\alpha$, we have

$$\psi \to \left(\mathbb{1} + i\alpha M\gamma_5\left(\mathbb{1} - \frac{a}{2}D\right)\right) \quad , \quad \bar{\psi} \to \bar{\psi}\left(\mathbb{1} + i\alpha M\left(\mathbb{1} - \frac{a}{2}D\right)\gamma_5\right) \cdot \tag{2.84}$$

The flavor matrix $M$, can be chosen to be the identity $\mathbb{1}_{N_f}$, representing the singlet case or one of the generators of $\mathrm{SU}(N_f)$ for the non-singlet case. Noting that $\psi$ and $\bar{\psi}$ are Grassmann variables, the fermionic measure in the path integral transforms as,

$$\mathcal{D}[\psi, \bar{\psi}] \ \to \ \mathcal{D}[\psi, \bar{\psi}] \det\left[\mathbb{1} + i\alpha M\gamma_5\left(\mathbb{1} - \frac{a}{2}D\right)\right] \det\left[\mathbb{1} + i\alpha M\left(\mathbb{1} - \frac{a}{2}D\right)\gamma_5\right] \tag{2.85}$$

$$= \mathcal{D}[\psi, \bar{\psi}] \det\left[\mathbb{1} + i\alpha M\gamma_5\left(\mathbb{1} - \frac{a}{2}D\right)\right]^2 \cdot \tag{2.86}$$

To obtain the second line, we have multiplied the argument of the second determinant in the first line by $1 = \gamma_5^2$ and used the cyclic property of the determinant. Using the formula $\det[A] = \exp(\mathrm{tr}[\ln A])$, expanding the logarithm in powers of $\alpha$ and then expanding the exponential to leading order we obtain

$$\begin{aligned}\det\left[\mathbb{1} + i\alpha M\gamma_5\left(\mathbb{1} - \frac{a}{2}D\right)\right]^2 =& 1 + 2i\alpha\ \mathrm{tr}\left[M\gamma_5\left(\mathbb{1} - \frac{a}{2}D\right)\right] + \mathcal{O}(\alpha^2) \\ =& 1 - 2i\alpha \times \frac{a}{2}\ \mathrm{tr}_F[M]\mathrm{tr}[\gamma_5 D]\cdot\end{aligned} \tag{2.87}$$

Note that the first trace, over $M$, is only over flavor indices while the second is over position, Dirac and color matrices. We have also used trace over the Dirac indices $\mathrm{tr}_D[\gamma_5] = 0$ to write the last equation. For the flavor non-singlet case, where $M$ is one of the $\mathrm{SU}(N_f)$ generators, $\mathrm{tr}_F[M] = 0$. However, the flavor-singlet case $M = \mathbb{1}_{N_f}$, is non-trivial as the trace does not vanish. Here, we clearly observe the non-invariant term which makes the transformation of the measure non-trivial for the flavor-singlet case, making it the source of the axial anomaly. It can be shown that this term is equivalent to the topological charge [52], which is the lattice QFT version of the classical charge derived in Eq. 2.81.

### 2.2.3 Domain Wall: The Model

The following is based on the Shaposhnikov-Rubakov model [53]. Consider a Minkowski space with four spatial dimensions and one time component with ordinary particles confined inside a potential-well which is flat in the three spatial dimensions and very narrow in the extra spatial dimension. The extra dimension is denoted by the index "5" to avoid confusion. A particle created in a high energy collision whose energy exceeds the depth of the well can come out of the well and propagate in the extra direction as well. This particle, however, cannot be detected by our measuring apparatus since it is sitting inside the well and the process will seem to violate energy-momentum conservation. Note that the usual four dimensional space-time plane now acts like a "Domain Wall", as shown in Fig. 2.6, splitting the extra dimension into two parts *i.e.* section above or below the 4D plane.

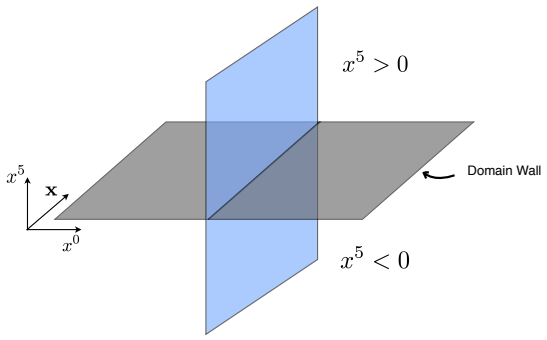


Figure 2.6: Domain Wall

To understand this model more, consider the following scalar Lagrangian [2]:

$$\mathcal{L} = \frac{1}{2}\partial_\mu\phi\partial^\mu\phi + \frac{1}{2}m^2\phi^2 - \frac{\lambda}{4}\phi^4 \quad , \quad \mu = 0, 1, 2, 3, 5 \cdot \tag{2.88}$$

Note that the potential

$$V(\phi) = \frac{1}{2}m^2\phi^2 + \frac{\lambda}{4}\phi^4 \ , \tag{2.89}$$

is the familiar Higgs potential. Suppose that $\phi(x^5)$ in the extra spatial dimension $x^5$ is independent of $\phi$ at the other three $\mathbf{x} = (x^1, x^2, x^3)$. The energy of the system in the extra direction can then be written as

$$H = \frac{1}{2}\left(\frac{d\phi(x^5)}{dx^5}\right)^2 + \frac{\lambda}{4}\left(\phi^2 - \frac{m^2}{\lambda}\right)^2 \ , \tag{2.90}$$

where we have completed the square and ignored the shift in the energy by $-m^2/4\lambda$. Since $H$ is greater than or equal to zero, we can solve a first order differential equation for $\phi(x^5)$ to obtain its value at the minimum of $H$ *i.e.* when $H = 0$,

$$\frac{d\phi(x^5)}{dx^5} = \sqrt{\frac{\lambda}{2}}\left(\phi^2 - \frac{m^2}{\lambda}\right) \quad \Rightarrow \quad \int \frac{1}{\phi^2 - m^2/\lambda}d\phi = \int \sqrt{\frac{\lambda}{2}}dx^5 \cdot \tag{2.91}$$

[2]Note there is no index "4", the time direction is indexed by "0" and the extra spatial dimension is indexed by "5".

Hence,

$$\phi(x^5) = \frac{m}{\sqrt{\lambda}} \tanh\left(\frac{mx^5}{\sqrt{2}}\right) \cdot \tag{2.92}$$

For sufficiently large $m$, the above functions takes the form a step function and $H$, which involves the first derivative of $\phi(x^5)$, takes the form of a delta function.

Using the Euler-Lagrange equations, the equation of motion for $\phi(x^5)$ is

$$\partial^2\phi(x^5) - m^2\phi(x^5) + \lambda\phi^3(x^5) = 0 \cdot \tag{2.93}$$

Since $\phi(x^5)$ is the classical solution for the extra independent direction, it is from now on denoted by $\phi^{\rm cl}$ so that

$$\phi = \phi^{\rm cl} + \phi' \ , \tag{2.94}$$

where $\phi'$ describes the fluctuations about the classical solutions. The equation of motion for $\phi'$ now reads:

$$\partial^2\phi' - m^2\phi'(x) + \lambda\left(\phi^{\rm cl}\right)^2\phi' = 0 \ , \tag{2.95}$$

where we have used $\partial^2\phi^{\rm cl} - m^2\phi^{\rm cl} + \lambda(\phi^{\rm cl})^3 = 0$ and kept only first order terms in $\phi'$ for the cubic part. One can check by substitution that one solution to the above equation is of the form

$$\phi'(x^0, \mathbf{x}, x^5) = \left(\frac{d\phi^{\rm cl}(x^5)}{dx^5}\right) e^{-i\mathbf{k}.\mathbf{x}+iEx^0} \quad , \quad E^2 = \mathbf{k}^2 \cdot \tag{2.96}$$

The planewave part of the solution (the massless Klein-Gordon equation), corresponds to a massless scalar particle living in 3+1-dimensions *i.e.* confined to the domain wall. Indeed the derivative of $\phi(x^5)$ in Eq. 2.92 looks like a narrow bump at a point in $x^5$ and nearly flat otherwise. At low energies the particle cannot escape this bump in the 5th direction and remains confined to 3+1-dimensions.

There are two other solutions to Eq. 2.95, one describing massive particles

which are also confined inside the wall and another which corresponds to massive particle that are not confined. However, for the purpose of our discussion, we are only interested in the massless case explained above.

### 2.2.4 Domain Wall Fermions in Euclidean Space-Time

The model in the previous section can be extended to account for massless fermions living in 3+1-dimensions [49, 54, 55]. We start by treating the classical field $\phi^{\mathrm{cl}}(x^5) = hV(s)$ as a potential in the extra dimension, calling the coordinate along the latter $s$, and writing the Dirac equation as

$$\left[\gamma^\mu D_\mu + \gamma^5 \partial_s + hV(s)\right] \psi(x_\mu, s) = 0 \cdot \tag{2.97}$$

This equation has a solution:

$$\psi(x^0, \mathbf{x}, s) = \exp\left(-h \int_0^s V(s')ds'\right) \times \psi(x^4, \mathbf{x}) \ , \tag{2.98}$$

where $h > 0$ and so it is normalizable. One can easily check by substitution that $\psi(x^4, \mathbf{x}, s)$ satisfies the above equation if and only if $\psi(x^4, \mathbf{x})$ is a right-handed spinor, $\psi(x^4, \mathbf{x}) \equiv \psi_R(x^4, \mathbf{x})$ satisfying the corresponding massless Dirac equation, $\sigma_\mu D_\mu \psi_R(x^0, \mathbf{x}) = 0$, which is clearly confined to domain wall *i.e.* the usual 3+1-dimensions. Note that there is nothing special about $\psi(x^4, \mathbf{x})$ being right-handed. If we had chosen the potential term such that $h < 0$ then the exponent would have had an opposite sign, requiring a left-handed massless spinor $\psi(x^0, \mathbf{x})$ for the equation to be satisfied.

The potential can now be taken to be of the form of a step function. Moreover we can choose it to be a function of mass such that

$$m(s) = \begin{cases} m & s > 0 \\ -m & s < 0 \end{cases} \tag{2.99}$$

where $m > 0$. Now let $\psi_n(x)$ be an eigenstate of the covariant derivative operator $\not{D}$:

$$\not{D}\psi_n = -\lambda_n \psi_n \cdot \tag{2.100}$$

Then, using Eq. ?? and Eq. ?? one has

$$\begin{cases} \sigma_\mu D_\mu \psi_{R,n}(x) = -\lambda_n \psi_{R,n}(x) \ , \\ \bar{\sigma}_\mu D_\mu \psi_{L,n}(x) = -\lambda_n \psi_{L,n}(x) \ . \end{cases} \tag{2.101}$$

At this stage, we can expand the right- and left-handed components in 5-dimensions *i.e.* $\psi_R(x,s)$ and $\psi_L(x,s)$ in the eigenstates of $\not{D}$ and make use of separation of variables to separate the usual 3+1-dimension from the extra component $s$:

$$\begin{cases} \psi_L(x,s) = \sum_n b_n(s)\psi_{L,n}(x) \ , \\ \psi_R(x,s) = \sum_n f_n(s)\psi_{R,n}(x) \ . \end{cases} \tag{2.102}$$

Eq. 2.97 can now be written out explicitly to give

$$\left[ \begin{pmatrix} 0 & \sigma_\mu D_\mu \\ \bar{\sigma}_\mu D_\mu & 0 \end{pmatrix} + \begin{pmatrix} -1 & 0 \\ 0 & 1 \end{pmatrix} \partial_s + \begin{pmatrix} m(s) & 0 \\ 0 & m(s) \end{pmatrix} \right] \begin{pmatrix} \psi_L(x,s) \\ \psi_R(x,s) \end{pmatrix} = 0 \ , \tag{2.103}$$

which implies

$$\begin{cases} D_\mu \sigma_\mu \psi_R(x,s) + (-\partial_s + m(s))\, \psi_L(x,s) = 0 \\ D_\mu \bar{\sigma}_\mu \psi_L(x,s) + (\partial_s + m(s))\, \psi_R(x,s) = 0 \end{cases} \tag{2.104}$$

Expanding above in eigenbasis of $\not{D}$ using Eq. 2.102 and separation of variables yields,

$$\begin{cases} [-\partial_s + m(s)] b_n(s) = \lambda_n f_n(s) \\ [\partial_s + m(s)] f_n(s) = \lambda_n b_n(s) \end{cases} \tag{2.105}$$

So far it can be said that the spectrum consists of an infinite tower of massive Dirac fermions with mass of order $m$. However, the solution when the eigenvalue $\lambda = 0$ is,

$$f_0(s) = N \exp\left( - \int_0^s m(s')ds' \right) = N e^{-m|s|} \ , \tag{2.106}$$

which is localised near $s = 0$ falling off exponentially on either side. Hence, there is a single massless right-handed fermion localised near the mass defect (*i.e.* the domain wall) as mentioned earlier in Eq. 2.98. Moreover, the other solution,

$$b_0(s) = N \exp\left(+\int_0^s m(s')ds'\right), \tag{2.107}$$

is of course not normalizable since it grows exponentially in $|s|$ and it is discarded. Having said that, this is no longer an issue if we consider finite volume with periodic boundary conditions such that $\psi(x_\mu, s + 2s_0) = \psi(x_\mu, s)$ where $s$ is defined to be $-s_0 < s < s_0$. The two zero mode solutions are now given by:

$$f_0(s) = N_f \exp\left(-\int_{-s_0}^s m(s')ds'\right) \quad , \quad b_0(s) = N_b \exp\left(+\int_{-s_0}^s m(s')ds'\right). \tag{2.108}$$

Analysing the second equation further, for

$$\begin{cases} s < 0 : \int_{-s_0}^s -m = -m(s + s_0) \Rightarrow e^{-m(s+s_0)} \text{ is 1 when } s = -s_0 \ , \\ s > 0 : \int_0^s m = ms \Rightarrow e^{ms} \text{ is maximum when } s = s_0 \ . \end{cases} \tag{2.109}$$

Therefore, we accept both solutions at finite volume.

### 2.2.5 Domain Wall Fermions on the Lattice

The aim of this section is to use the Domain Wall formalism discussed in Sec. 2.2.3 and Sec. 2.2.4 to construct the theory of Domain Wall Fermions on the lattice [49]. If the discretization is done naively, one again ends up with doublers just as in the naive case discussed in Sec. 2.1.4. However, adding a Wilson term $\frac{r}{2}\nabla^*\nabla$, as in Eq. 2.46, for each of the dimensions and treating it is as a mass term, removes the doublers. In this notation, $\nabla$ and $\nabla^*$ are the forward and backward lattice difference operators respectively. Let the Wilson term be a mass term, independent of $s$ but dependent on the wavenumber $k$ denoted by $\Delta m(k)$. In other words, $\Delta m(k)$ is a $k$-dependent spatially constant mass which is added to the step function mass $m(s) = m\epsilon(s)$. Thus, for an infinite extra dimension,

$$f_0(s, k) = N \exp\left(-\int_0^s m(s')ds' + \Delta m(k)\right). \tag{2.110}$$

One can check that for $|\Delta m| < m$ Eq. 2.110 is normalizable for all $s$. However, for $|\Delta m| > m$ and $s < 0$, the solutions becomes more and more extended in the extra dimensions until it fails to be normalizable. Let us examine this in more detail. Using separation of variables, the zero-mode solutions take the form,

$$\psi(x,s) = e^{ipx}\phi_\pm(s)\psi_\pm(x) \qquad \text{with} \qquad \gamma_5\psi_\pm(x) = \pm\psi(x)\ , \tag{2.111}$$

where $\psi_\pm(x)$ are constant 4-component chiral spinors satisfying the usual massless 4-d Dirac equation. Note that $\psi_\pm$ are eigenstates of $\gamma_5$ and transform independently under Lorentz transformations. Then for $r = 1$ in the Wilson term $\frac{r}{2}\nabla^*\nabla$,

$$\not{p}_4\psi_\pm = 0 \qquad \text{and} \qquad -\phi_\pm(s \mp 1) + (m_{\text{eff}} + 1)\phi_\pm(s) = 0\ , \tag{2.112}$$

where $m_{\text{eff}} = m\epsilon(s) + \sum_\mu(1 - \cos p_\mu) \equiv m\epsilon(s) + F(p)$, and $F(p) = \Delta m$, with $\epsilon(s)$ being the step function. To derive the latter, the Wilson term $\frac{1}{2}\nabla^*\nabla$ is added for each direction. The $s$ dependent part of the equation of motion, together with the Wilson term in the other four directions in momentum space, takes the following form:

$$\begin{aligned}
0 = &\pm\frac{1}{2a}\left[(\phi_\pm(s+\hat{\mu}_s)) - (\phi_\pm(s-\hat{\mu}_s))\right] \\
&+ \left[m\epsilon(s) + \frac{-\delta_{s+\hat{\mu}_s,s'} + 2\delta_{s,s'} - \delta_{s-\hat{\mu}_s,s'}}{2a} + \frac{1}{a}\sum_{\mu=1}^{4}(1-\cos(k_i a))\right]\phi_\pm(s) \\
&= \pm\frac{1}{2a}\left[(\phi_\pm(s+\hat{\mu}_s)) - (\phi_\pm(s-\hat{\mu}_s))\right] + m\epsilon(s)\phi_\pm(s) \\
&\quad + \frac{-\phi_\pm(s+\hat{\mu}_s) + 2\phi_\pm(s) - \phi_\pm(s-\hat{\mu}_s)}{2a} + \frac{1}{a}\sum_{\mu=1}^{4}(1-\cos(k_i a))\phi_\pm(s) \\
&= -\phi_\pm(s \mp 1) + (m_{\text{eff}}(s) + 1)\phi_\pm(s)\ ,
\end{aligned} \tag{2.113}$$

where the $\pm$ is due to the action of $\gamma_5$ on $\psi_\pm$. The solutions take the form $\phi_\pm(s) = z_\pm^s$ where

$$z_\pm = (1 + m_{\text{eff}}(s))^\mp = (1 + m\epsilon(s) + F(p))^\pm\ . \tag{2.114}$$

This can be readily seen by substituting for $\phi_{\pm}(s) = z_{\pm}^{s}$ with $z_{\pm} = (1 + m_{\text{eff}}(s))^{\mp}$ in the RHS of Eq. 2.113. The solutions are normalizable if $|z|^{\epsilon(s)} < 1$ since

$$\begin{cases} \text{For} \quad s > 0 \quad |z| < 1 \quad \text{so that} \quad \phi = z^{s} \quad \text{is normalizable.} \\ \text{For} \quad s < 0 \quad \frac{1}{|z|} < 1 \quad \text{so that} \quad \phi = z^{-|s|} \quad \text{is normalizable.} \end{cases} \tag{2.115}$$

Examining the $\phi_{-}$ solution, one can see that for $s > 0$, $|1 + m + F(p)| > 1$ and for $s < 0$, $|1 + m + F(p)|$ could be less than 1 when $F(p) = 0$ which implies $\phi_{-}(s)$ is not a valid solutions. The same check shows that the normalizablity condition is always satisfied for $\phi_{+}(s)$ when $s > 0$. For $s < 0$, for the solution to be normalizable, one would need $\frac{1}{|z|} < 1$ *i.e.* $|1 - m + F| < 1$ resulting in the following constraint for the value of $m$:

$$F(p) < m < 2 + F(p) \tag{2.116}$$

the case where $0 < m < 2$ corresponds to a single right-handed mode at $\boldsymbol{p} = 0$. For the details of how the spectrum behaves see chapter 3 of [49].

### 2.2.6 Overlap fermions

In the continuum, the massless QCD Lagrangian has a global symmetry given by the transformation $\psi \to e^{i\alpha\gamma_5}\psi$ as discussed in an earlier section. This can be summarized as:

$$\{D, \gamma_5\} = 0 \ , \tag{2.117}$$

where $D = \gamma_\mu(\partial_\mu + iA_\mu)$ is the massless Dirac operator. The corresponding equation for chiral fermions on the lattice was derived by Ginsparg and Wilson [51]:

$$\{D, \gamma_5\} = aD\gamma_5 D \ , \tag{2.118}$$

where $D$ is the massless lattice Dirac operator. Such an operator leads to a chirally symmetric action in the continuum limit. It was later shown by Neuberger [56]

that the solution to the Ginsparg-Wilson Eq. 2.118 is given by

$$aD = \mathbb{1} + \gamma_5 \epsilon(\mathcal{H}(-m)) \tag{2.119}$$

$$= \mathbb{1} + \gamma_5 \frac{\mathcal{H}(-m)}{\sqrt{H(-m)^2}} \tag{2.120}$$

$$= \mathbb{1} + \frac{D_w - m}{\sqrt{(D_w - m)^\dagger (D_W - m)}} \tag{2.121}$$

which is known as the *overlap* operator. In the above, $\epsilon(\mathcal{H}(-m))$ is the sign-function and $\mathcal{H}(-m) = \gamma_5(D_W - m) = \gamma_5 \left( \not{D} - \frac{r}{2} D^2 - m \right)$ where $D_\mu$ and $D^2$ are the symmetric covariant derivative and covariant Laplacian Wilson term on the lattice respectively. The doublers are taken care of by the Wilson term.

It can be checked explicitly that in the continuum limit Eq. 2.121 reduces to the usual massless continuum Dirac operator as expected. In the case of the free theory, $\mathcal{H}(-m) = \gamma_5 \left( \not{\partial} - \frac{r}{2}\partial^2 - m \right)$ so that,

$$\begin{aligned}
\frac{D_w - m}{\sqrt{(D_w - m)^\dagger (D_w - m)}} &= \left( \not{\partial} - \frac{r}{2}\partial^2 - m \right) \left[ \left( \not{\partial} - \frac{r}{2}\partial^2 - m \right)^\dagger \left( \not{\partial} - \frac{r}{2}\partial^2 - m \right) \right]^{-1/2} \\
&\approx \left( \not{\partial} - \frac{r}{2}\partial^2 - m \right) \left[ -\partial^2 + m\not{\partial} + \frac{r}{2} m\partial^2 - m\not{\partial} + \frac{r}{2} m\partial^2 + m^2 \right]^{-1/2} \\
&= \frac{1}{m} \left( \not{\partial} - \frac{r}{2}\partial^2 - m \right) \left[ -\frac{\partial^2}{m^2} + \frac{\not{\partial}}{m} + \frac{r}{m}\partial^2 - \frac{\not{\partial}}{m} + 1 \right]^{-1/2} \\
&\approx \frac{\not{\partial}}{m} - 1 + \cdots \cdot
\end{aligned} \tag{2.122}$$

Therefore, the massless overlap operator in continuum limit reduces to the usual massless Dirac operator:

$$D_{\text{ov}} \to \frac{\not{\partial}}{am} \, , \tag{2.123}$$

where $am$ is a finite multiplicative factor. The key point here is that Nielsen-Ninomiya no-go theorem can be bypassed by taking the chiral transformation not to have their usual definition of continuum on the lattice as in Eq. 2.117, but instead a different form as in Eq. 2.118, whilst insisting only on producing the continuum result when $a \to 0$ [57]. The locality of the overlap operator, however, is not immediately obvious due to the inverse square root term. Strict locality

condition implies that the non-zero terms in the sum

$$D\psi(x) = a^4 \sum_y D(x,y)\psi(y) \ , \tag{2.124}$$

come from the points $y$ in a finite neighbourhood of $x$, and that the kernel $D(x,y)$ only depends on the gauge fields variables near $x$. Due to the form of the overlap operator Eq. 2.121, containing the inverse square root term, it is clear that the operator is not local in the above restricted sense. Having said that, this definition of locality can be generalised. It has been proved in [58], that $D_{\text{ov}}$ is local with exponentially decaying tails. As long as the decay rate can be shown to be proportional to $1/a$, this generalised form of locality is as good as the strict sense from the point of the continuum limit.

In our simulations, we have used Shamir and Möbius domain wall fermions, discussed in the next section. It has been demonstrated in [59] that there exists a regime, in terms of the inverse lattice spacing, such that DWFs have the acceptable degree of locality. It is also worth mentioning that that the overlap formulation of lattice fermions can also be derived from the domain wall formulation [60].

### 2.2.7 Shamir and Möbius Domain Wall Fermions

The particular type of domain wall fermions used for simulation of the physical point lattices in the recent RBC/UKQCD charm project is known the *Möbius* domain wall fermions [61–63]. This has had the effect of suppressing residual chiral symmetry breaking whilst reducing the computational cost of having a large domain wall height $L_s$. We state some of the key properties in this section. The details are discussed in [64]. The Möbius kernel is,

$$H_M = \gamma_5 \frac{(b+c)D_w}{\frac{2}{a} + (b-c)D_w} \ , \tag{2.125}$$

with $D_w(M)$ being the usual Wilson matrix

$$D_w(M) = M + 4 - \frac{1}{2}\left((1-\gamma_\mu)U_\mu(x)\delta_{x+\mu,y} + (1+\gamma_\mu)U_\mu^\dagger(y)\delta_{x-\mu,y}\right) \cdot \tag{2.126}$$

Then, $D_{\text{Möb}}$ is taken to be

$$D_{\text{Möb}} = \frac{1+m}{2} + \frac{1-m}{2}\gamma_5 \frac{(1+H_M)^{L_s} - (1-H_M)^{L_s}}{(1+H_M)^{L_s} + (1-H_M)^{L_s}} \ . \tag{2.127}$$

which is an approximation to the massive overlap operator. Notice that

$$\epsilon(H_M, L_s) = \frac{(1+H_M)^{L_s} - (1-H_M)^{L_s}}{(1+H_M)^{L_s} + (1-H_M)^{L_s}} \tag{2.128}$$

is an approximation to the sign function, such that

$$\lim_{L_s \to \infty} \epsilon(H_M, L_s) = \text{sgn}(H_M) \tag{2.129}$$

To see this, one can simply consider the two cases where $H_M > 0$ and $H_M < 0$. In the former case, we can divide the numerator and denominator by $(1+H_M)^{L_s}$. Then the ratio $\frac{(1-H_M)^{L_s}}{(1+H_M)^{L_s}} \to 0$ as $L \to \infty$ implying $\epsilon(H_M) \to +1$. On the other hand, if $H_M < 0$, we can divide the numerator and denominator by $(1-H_M)^{L_s}$ so that $\frac{(1+H_M)^{L_s}}{(1-H_M)^{L_s}} \to 0$ as $L \to \infty$ implying $\epsilon(H_M) \to -1$, leading to the definition of the sign function. Another point to note is that changing Möbius parameters $b+c$ while fixing $b-c=1$, makes the Möbius kernel proportional to the Shamir kernel [54, 55, 65] used for the non-physical point ensembles in our simulations. In other words, the two formulations merely differ in their approximation to the sign function and in the limit where $L_s \to \infty$, both Möbius and Shamir formulations in the action reduce to the action formed using the overlap operator [64]. For a review of the properties of generalized DWFs with Möbius kernel and the mapping between such fermions and overlap fermions see Ref. [63].

## 2.3 QCD path integral

Given the fermionic $S_F$ and gauge $S_G$ actions, the Euclidean QCD path integral is written as:

$$Z = \int \mathcal{D}[\psi, \bar{\psi}] \mathcal{D}[U] e^{-S_F[\psi,\bar{\psi},U] - S_G[U]} \ , \tag{2.130}$$

where

$$\mathcal{D}[\psi,\bar{\psi}] = \prod_x \prod_{f,\alpha,c} d\psi^{(f)}(x)_{\alpha,c}\, d\bar{\psi}^{(f)}(x)_{\alpha,c} \quad , \quad \mathcal{D}[U] = \prod_x \prod_{\mu=1}^{4} dU_\mu(x) \ , \quad (2.131)$$

with $x$ being the lattice sites, $f$ the fermion flavor, $\alpha$ the spinor index and $c$ the color index. $\psi$ and $\bar{\psi}$ are Grassmann variables which are integrated out and end up as a fermionic determinant. The quark flavors included in the computation of this determinant are knows as the *sea quarks* which are interpreted as those particles that participate in virtual creation and annihilation in the loops. In this context, we refer to the quark flavors not included in this determinant as *valence quarks*, meaning they are too heavy to be generated from the vacuum as particle anti-particle pairs. The path integral as a function of the gauge fields is now:

$$Z = \prod_{x,\mu} \int dU_\mu \det D[U] e^{-S_G[U]} \ , \quad (2.132)$$

where $D$ is the Dirac matrix. A generic correlator of fields $\langle O \rangle$ can be expressed as,

$$\langle O \rangle = \prod_{x,\mu} \int dU_\mu \det D[U] e^{-S_G[U]} O[U] \ \cdot \quad (2.133)$$

The integral can be viewed as a sum over all possible gauge field configurations. Using a Monte Carlo simulation, the above expression can be approximated by taking an average over $N$ gauge field configurations $U_i$, where $i = 1, \cdots, N$

$$\langle O \rangle \approx \frac{1}{N} \sum_{i=1}^{N} O[U_i] \quad (2.134)$$

with $U_i$'s drawn according to the Boltzmann probability distribution

$$P[U_i] = \det D[U_i] e^{-S_G[U_i]}. \quad (2.135)$$

There are different types of Monte Carlo algorithms that can be used for generating the gauge fields configurations. For the charm project, the exact hybrid Monte Carlo (HMC) algorithm has been used. Discussing the properties and techniques used are beyond the scope of the current thesis. For details and

the choice of parameters, see Ref. [64].

Computing the fermionic determinant in Eq. 2.133 is non-trivial. Setting the determinant to unity is known as the *quenched approximation*. Most of lattice results in the 1980s and 1990s were obtained in this approximation and predicted the ground state spectrum of hadrons with light quarks [66]. However, as mentioned before, this approximation ignores the quarks in the sea sector and there is an unknown systematic error of order 15% empirically [67, 68]. A simulation which includes the determinant and hence the vacuum structure of fermions is knowns as a *dynamical* simulation.

## 2.4 RBC/UKQCD charm project - Run I

In this section we state the parameters used in our RBC/UKQCD charm project simulations and list the ensembles used to perform fits of meson masses and bag parameters.

The gauge field ensembles used are generated with the Iwasaki gauge action [69, 70]. These ensembles are isospin symmetric and have $N_f = 2 + 1$ dynamical flavors. There are three different lattice spacing in the range $0.11 - 0.07$ fermi which we denote by **C**ourse, **M**edium and **F**ine. As mentioned in Sec. 2.2.7, for the quark fields we have used domain wall fermion actions with Shamir (SDWF) or Möbius (MDWF) kernels. Performing the continuum extrapolation whilst having different actions has been discussed and justified in Ref. [64] in great detail. For the case of Wilson fermions, the explicit symmetry breaking allows for a dimension-5 clover term, which introduces $\mathcal{O}(a)$ discretization effects. The equivalent to such a term, in the DWF formulation, is of order $\mathcal{O}(a^2 m_{\text{res}})$ which is always less than $10^{-3}$ or even smaller [71], hence it can be neglected. Furthermore, the existence of chiral symmetry for DWF, implies all terms containing odd powers of the lattice spacing can be ignored. Apart from the $\mathcal{O}(a^2)$ terms that are explicitly fitted in the global fit ansatz, the next to leading order discretization effects enter at $\mathcal{O}(a^4)$, and are shown to be negligible in Ref. [64]. Moreover, in section II.A of Ref. [64], the equivalence of Shamir and Möbius DWF are discussed in great detail. Finally, additional numerical evidence for the closeness of Shamir

| Name | type | $L/a$ | $T/a$ | $a^{-1}$[GeV] | $m_\pi$[MeV] | hits/conf | confs | total |
|---|---|---|---|---|---|---|---|---|
| C0 | MDWF | 48 | 96 | 1.7295(38) | 139.15(36) | 48 | 88 | 4224 |
| C1 | SDWF | 24 | 64 | 1.7848(50) | 339.789(12) | 32 | 100 | 3200 |
| C2 | SDWF | 24 | 64 | 1.7848(50) | 430.648(14) | 32 | 101 | 3232 |
| M0 | MDWF | 64 | 128 | 2.3586(70) | 139.35(46) | 32 | 80 | 2560 |
| M1 | SDWF | 32 | 64 | 2.3833(86) | 303.248(14) | 32 | 83 | 2656 |
| M2 | SDWF | 32 | 64 | 2.3833(86) | 360.281(16) | 16 | 77 | 1232 |
| F1 | MDWF | 48 | 96 | 2.774(10) | 234.297(10) | 48 | 82 | 3936 |

Table 2.1: The parameters used in simulating the $N_f = 2+1$ ensembles. C stands for coarse, M for medium and F for fine. Note that amongst the large lattices, **C0** and **M0** are at the physical point while **F1** is at a heavier pion mass. The column "hits/conf" gives the number of measurement on each configuration where "hits" is the number of time planes used as sources, with the quark propagators computed using $\mathbb{Z}(2) \times \mathbb{Z}(2)$ stochastic wall sources. These measurements are averaged into one bin before any fits are performed. The label "confs" gives the total number of configurations. The column "total" is the product of the two.

and Möbius ensembles were found by comparing the renormalization factors of quark masses $Z_m$ and the kaon bag parameter $Z_{B_K}$, computed on both ensembles with Shamir and Möbius fermions in their action. The difference was observed to be very small, *i.e.* , 0.2% or less for $Z_m$ and 0.25% for $Z_{B_K}$ [64].

Parameters of the ensembles and quarks used in the simulation are presented in Tables 2.1 and 2.2. The details of parameters and properties for all the stated ensembles, apart from **F1**, can be found in Ref. [64], where $m_\pi$, $m_K$ and $m_\Omega$ has been used as experimental input in order to determine the lattice scale and the physical light-quark masses. More specifically, given a fixed bare coupling, $m_u = m_d$ and $m_s$ are adjusted until $m_\pi/m_\Omega$ and $m_K/m_\Omega$ take on their physical values [64]. The **F1** ensemble was generated specifically for the RBC/UKQCD charm and bottom physics programs, the details of which can be found in Ref. [72]. The quark propagators have all been computed using $\mathbb{Z}(2) \times \mathbb{Z}(2)$ stochastic wall sources [73].

The simulation parameters in the valence sector for light and strange quarks

| Name | DWF | $M_5$ | $L_s$ | $am_l^{\text{uni}}$ | $am_s^{\text{uni}}$ | $am_s^{\text{sim}}$ | $am_s^{\text{phys}}$ | $\frac{\Delta m_s}{m_s^{\text{phys}}}$ |
|---|---|---|---|---|---|---|---|---|
| C0 | MDWF | 1.8 | 24 | 0.00078 | 0.0362 | 0.0362 | 0.03580(16) | 0.0112(45) |
| C1 | SDWF | 1.8 | 16 | 0.005 | 0.04 | 0.03224, 0.04 | 0.03224(18) | - |
| C2 | SDWF | 1.8 | 16 | 0.01 | 0.04 | 0.03224 | 0.03224(18) | - |
| M0 | MDWF | 1.8 | 12 | 0.000678 | 0.02661 | 0.02661 | 0.02539(17) | 0.0476(70) |
| M1 | SDWF | 1.8 | 16 | 0.004 | 0.03 | 0.02477, 0.03 | 0.02477(18) | - |
| M2 | SDWF | 1.8 | 16 | 0.006 | 0.03 | 0.02477 | 0.02477(18) | - |
| F1 | MDWF | 1.8 | 12 | 0.002144 | 0.02144 | 0.02144 | 0.02132(17) | -0.0056(80) |

Table 2.2: Domain wall parameters for the light and strange quarks of all ensembles. $am_l$ and $am_s$ are bare quark masses in lattice units. The suffix "uni" refers to the sea and valence quark having the same mass.

are presented in Table 2.2, while those for the heavy quarks near the charm mass region are shown in Table 2.3. The light quarks masses are unitary *i.e.* sea quarks and valence quarks have the same mass. For ensembles **C1**, **C2**, **M1** and **M2** where the value of the physical strange quark mass was known [64] prior to running the measurements, the simulated strange quark mass was partially quenched to agree with the physical value. For the other ensembles the unitary value was chosen. To determine the charm parameters, $M_5$, $L_s$ and the charm mass range for the simulations, quenched DWF studies were performed [74, 75]. Altering $M_5$, the negative mass parameter in the 4D Wilson operator, changes the cut-off effects while $L_s$ affects the residual breaking of chiral symmetry. These studies, which focused on the pseudoscalar heavy-heavy and strange-heavy decay constants, indicated that the cut-off effects are minimal for $M_5 \approx 1.6$ while the residual chiral symmetry breaking effects are suppressed for $L_s = 12$. Rapid increase in discretization effects were observed as the mass of the input heavy quark was increased to values above $am_h \approx 0.4$. For this reason, all the valence heavy quark masses are chosen to be $m_h \leq 0.4$, as it can been seen from Table 2.3.

We state the lattice Ward Identities for DWFs and a measure of chiral symmetry breaking, known as the *residual mass*, in Sec. 3.9. After explaining the RI/SMOM renormalization scheme, we present numerical results of the

| Name | $M_5$ | $L_s$ | $am_h^{\text{bare}}$ |
|---|---|---|---|
| C0 | 1.6 | 12 | 0.3, 0.35, 0.4 |
| C1 | 1.6 | 12 | 0.3, 0.35, 0.4 |
| C2 | 1.6 | 12 | 0.3, 0.35, 0.4 |
| M0 | 1.6 | 12 | 0.22, 0.28, 0.34, 0.4 |
| M1 | 1.6 | 12 | 0.22, 0.28, 0.34, 0.4 |
| M2 | 1.6 | 12 | 0.22, 0.28, 0.34, 0.4 |
| F1 | 1.6 | 12 | 0.18, 0.23, 0.28, 0.33, 0.4 |

Table 2.3: Möbius domain wall parameters for the heavy quarks of all ensembles. The bare quark masses $am_h$, are in lattice units.

renormalization factors on each ensemble. These renormalization factors are required for renormalizing matrix elements such as the axial current and the bag parameter obtained from these simulations in Sec. 3.11. The data analysis and fitting procedures leading to the predictions for the meson masses and the decay constants as well as the bag and $\xi$ parameters are presented in Chapter 4.

## 2.5 Statistical Methods

In this section we discuss statistical techniques used in calculation and propagation of statistical errors in our fitting analyses. To this end, we use a *resampling* method such as *jacknife* and *boostrap*. A resampling is a procedure in which a distribution of $N$ independent raw measurements of a quantity $\{y_i \ ; \ i = 1, \cdots, N\}$, is resampled in a particular way to create a new distribution of means $\{\overline{y}_i \ ; \ i = 1, \cdots, \overline{N}\}$. For jackknife, we discard one of the original $N$ original measurements and take an average over the remaining $N-1$ measurements. We repeat this for all the $N$ samples resulting in $\overline{N} = N$ new sample of averages $\overline{y}_i$. The error on this mean is estimated as,

$$\sigma^2 = \frac{N-1}{N} \sum_{i=1}^{n} \left( \overline{y}_i - \langle \overline{y} \rangle \right) \cdot \tag{2.136}$$

In bootstrap resampling, we draw $N$ samples from the original raw data, randomly and allowing for replacement. This process is repeated $\overline{N} = N_{\text{boot}}$ times, with $N_{\text{boot}} \sim \mathcal{O}(500)$. To obtain the error on the mean, the $\{\overline{y}_i;\ i = 1, \cdots, N_{\text{boots}}\}$ are sorted in ascending order. The $16^{\text{th}}$ and $84^{\text{th}}$ percentiles are then selected bounding the 68% confidence region.

The fitting procedure for a Green's function is then as follows:

1. Given that successive gauge field configurations are generally correlated, groups of such measurements are averaged together, known as *binning*, leaving a set of $N$ measurements which are taken to be independent for the rest of the analysis.

2. Measurement of the Green's functions are made on each of these configurations.

3. The covariance matrix $M_{t,t'}$

$$M_{t,t'} = \mathcal{N} \sum_{n=1}^{N} \left(C^{(n)}(t) - \overline{C}(t)\right) \left(C^{(n)}(t') - \overline{C}(t')\right) \ , \tag{2.137}$$

   is then computed. In our analysis, *frozen* covariance is used *i.e.* the covariance matrix is built once using the binned raw data, for which $\mathcal{N} = \frac{1}{N(N-1)}$ in Eq. 2.137, and is then kept fixed and used to perform the fits. Some analysis codes have the frozen covariance matrix computed using the bootstrap or jackknife resampled data, after step four below. In such cases, the normalization factor is $\mathcal{N} = (N-1)/N$ for jackknife, and $\mathcal{N} = 1/N_{\text{boot}}$ for bootstrap resampling. The sums is also over the corresponding sample number. The average, $\overline{C}(t)$, in these cases corresponds to jackknife or boostrap average. Alternatively, if the covariance matrix is recomputed for every $\overline{y}_i$, then the matrix is said to be *unfrozen* or *dynamical*. This is not used in any part of our analysis.

4. The binned data are resampled using jackknife or bootstrap procedures explained above.

5. The fit is performed by minimizing the $\chi^2$ function:

$$\chi^2(p_1, p_2, \cdots) = \sum_{t,t'} \Big(\overline{y}_i(t) - \langle y(t, p_1, p_2, \cdots)\rangle\Big) M^{-1}_{t,t'} \Big(\overline{y}_i(t') - \langle y(t', p_1, p_2, \cdots)\rangle\Big) \ , \tag{2.138}$$

with respect to the parameters of the fit, $p_1$ and $p_2$ etc. and the function in minimized for every resampled data point $\overline{y}_i$ *i.e.* $\overline{N}$ times. This gives a distribution for parameters $p_1$, $p_2$ etc., from which an estimate of the average and standard error can be derived using the appropriate formula for jackknife or bootstrap.

The diagonal elements of the covariance matrix Eq. 2.137 give the variance $M_{t,t} = \sigma_t^2$ for each time $t$. The correlation matrix is then defined as:

$$\tilde{M}_{t,t'} = \frac{M_{t,t'}}{\sigma_t \sigma_{t'}} \ , \tag{2.139}$$

which is equal to the covariance matrix normalized by the variances, having unity for the diagonal elements. A *correlated fit* is one that takes into account the full correlation between the time slices fitted in Eq. 2.138 for $M^{-1}_{t,t'}$. If the estimate of the covariance matrix is poor due to not having sufficient data, then the inversion will be unstable for correlated fits. For our analyses, we use frozen *uncorrelated fits* which implies replacing the correlation matrix with the identity matrix *i.e.* ignoring the off-diagonal elements of $M_{t,t'}$.

# Chapter 3

# Renormalization

Lattice QCD is a method by which Quantum Field Theory can be regulated non-perturbatively, with a momentum cut-off that is inversely proportional to the lattice spacing $a$. When the continuum limit is eventually taken, one encounters the usual ultraviolet divergences at high frequencies unless they have been removed via a certain renormalization scheme. Non-perturbative renormalization Momentum Subtraction (MOM) schemes have been introduced in [76, 77] and have been in use for a number of years. These schemes specify conditions, at the chiral limit of QCD, to determine the renormalization of the fermions wave function, fermion mass and composite operators such as the fermions bilinears. In other words, these schemes are mass-independent implying that the renormalization conditions are independent of the fermion mass. The renormalization scale $\mu$ in MOM schemes should be within the so-called "renormalization window":

$$a\Lambda_{\rm QCD} \ll a\mu \ll \pi \ , \tag{3.1}$$

where $a\Lambda_{\rm QCD}$ can be thought of as *e.g.* as the mass of the heaviest quark involved in the simulations or the corresponding meson mass being measured in lattice units $a$. The upper bound exist to guarantee the discretization effects are under control, by taking $\mu \ll \pi/a$, where the inverse lattice spacing $a^{-1}$ defines the UV cut-off. The reason for the lower bound is related to the fact that a physical amplitude $\mathcal{A}$, as a weak matrix element between physical initial and final states,

$|i\rangle$ and $|f\rangle$, can be written using operator product expansion (OPE) as,

$$\mathcal{A} = \langle f|H_W|i\rangle = C\left(\frac{\mu}{M_W}\right)\langle f|O_R(\mu)|i\rangle \ , \tag{3.2}$$

where Wilson coefficient $C$ is scale dependent and takes into account the short-distance processes and are computed in perturbation theory. The second term in the right hand side of Eq. 3.2 is a long-distance quantity which can be computed non-perturbatively on the lattice. The subscript $R$ denotes the fact that the operator $O(\mu)$ has been renormalized. The scale dependence from the renormalized operator must therefore cancel that of the coefficient $C(\mu)$ to render the physical amplitude $\mathcal{A}$ independent of scale. An explicit example of such a quantity was mentioned in Eq. 1.67 for kaon mixing. $C(\mu)$ is a perturbative quantity, which is computed at a scale $\mu$ with $\mu \gg \Lambda_{\rm QCD}$, implying the lower bound to the renormalization window in Eq. 3.1. Moreover, $C(\mu)$ has to be computed in the same scheme as the operator $O_R$. Recent lattice studies have begun investigating the nonperturbative dynamics of heavy quarks like charm and bottom. In current simulations the mass of the heavy quarks is often of the same order of magnitude as the UV cutoff, $a^{-1}$. As a consequence, it is not possible to reach a regime where there is a clear separation between the fermion mass, the renormalization scale, and the cutoff. Therefore, when studying heavy quarks, it may be interesting to introduce a massive scheme, i.e. a scheme where the renormalization conditions are imposed at some finite value of the renormalized mass. We have developed such a massive renormalization scheme, denoted by RI/mSMOM, for fermion bilinear operators in QCD with non-exceptional momentum kinematics similar to the standard RI/SMOM scheme. The momenta are said to be non-exceptional if no partial sum of the incoming momenta $p_i$ vanishes [78]. In contrast to RI/SMOM where the renormalization conditions are imposed at the chiral limit, our scheme allows for the renormalization conditions to be set at some mass scale $m$, which we are free to choose. In the limit where $m \to 0$, our scheme reduces to SMOM. Using a mass dependent scheme for a theory containing massive quarks has the benefit of preserving the continuum WI by taking into account terms of order $m/\mu$, which would otherwise violate the WI when a massless scheme is used. We have shown that the WI for the case of both degenerate and non-degenerate

masses are satisfied non-perturbatively, giving $Z_V = 1$ and $Z_A = 1$. In order to gain a better understanding of the properties of the mSMOM scheme we have performed an explicit one-loop computation in perturbation theory using dimensional regularization. RI/mSMOM can be implemented numerically, in order to obtain non-perturbative determinations of the renormalization constants of certain composite operators. The details of the operators are discussed on the upcoming sections. The massive renormalization constants will automatically subtract some lattice artefacts $O(a^2m^2)$, and could potentially lead to smoother extrapolations to the continuum limit of phenomenologically relevant observables. However, to verify this statement, a dedicated numerical study is required.

The first part of this chapter starts by summarizing the kinematics and the form of the vertex functions used. This is followed by presenting the vector and axial Ward Identities (WI) from which the renormalization conditions for the RI/mSMOM scheme are derived. Afterwards, some of the important features of the perturbative calculation using Dimensional Regularization (dim-reg) are discussed and certain calculations are presented in detail. In the second part of this chapter, numerical results for the renormalization of vertex functions and the 4-quark operators in the SMOM scheme are presented.

## 3.1 The kinematics

Let us start by summarizing the kinematics used. Starting with the correlators of fermion bilinears with two external off-shell fermions in momentum space:

$$G^a_\Gamma(p_3, p_2) = \langle O^a_\Gamma(q)\bar{\psi}(p_3)\psi(p_2)\rangle\,, \tag{3.3}$$

where $O^a_\Gamma = \bar{\psi}\Gamma\tau^a\psi$ is a flavor non-singlet fermion bilinear, and $\Gamma$ spans all the elements of the basis of the Clifford algebra, which we denote as $\Gamma = \mathrm{S}, \mathrm{P}, \mathrm{V}, \mathrm{A}, \mathrm{T}$. Note that $\tau^a$ denotes a generic generator of rotations in flavor space. The corresponding vertex function in position-space together with conventions for the propagator, the Fourier transforms and the Dirac gamma matrices are spelled out in detail in App. C.1. The four dimensional vectors $p_2$ and $p_3$ are respectively the incoming and outgoing momenta of the external fermions, and momentum conservation requires $q = p_2 - p_3$. The kinematics adopted in this work is the one

used in Ref. [77]:

$$p_2^2 = p_3^2 = q^2 = -\mu^2 \,. \tag{3.4}$$

Note that asymmetric or exceptional kinematics where $p_2^2 = p_3^2 = -\mu^2$, $p_2 = p_3$ and $q = 0$, suffers from infrared effect that are substantially suppressed using the non-exceptional kinematics in Eq. 3.4 [77, 78]. Following the convention in the paper above, we denote this symmetric point by the shorthand "sym". These are presented pictorially in Fig. 3.1.

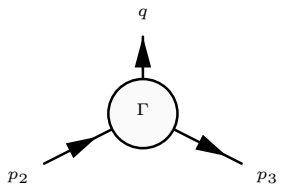


Figure 3.1: Kinematics used for the correlators of fermion bilinears.

For the purpose of illustration, we can consider the case of a fermion doublet

$$\psi = \begin{pmatrix} \psi_1 \\ \\ \psi_2 \end{pmatrix} \,, \quad \overline{\psi} = \begin{pmatrix} \overline{\psi}_1 & \overline{\psi}_2 \end{pmatrix} , \tag{3.5}$$

with mass matrix

$$\mathcal{M} = \begin{pmatrix} m_1 & 0 \\ \\ 0 & m_2 \end{pmatrix} . \tag{3.6}$$

Note that in the mass degenerate case, we simply have $\mathcal{M} = m\mathbb{1}$. If we choose $\tau^a = \tau^+ = \frac{\sigma^+}{2} = \frac{1}{2}(\sigma^1 + i\sigma^2)$, then the bilinear $O_\Gamma^a = \bar{\psi}\Gamma\tau^a\psi$ takes the form $O_\Gamma = \overline{\psi}_1\Gamma\psi_2$.

The infinitesimal vector and axial non-singlet SU(2) chiral transformation are as follows

$$\delta\psi(x) = i\Big[\alpha_V(x)\tau^a\Big]\psi(x) \,, \quad \delta\overline{\psi}(x) = -i\overline{\psi}(x)\Big[\alpha_V(x)\tau^a\Big], \tag{3.7}$$

and

$$\delta\psi(x) = i\Big[\alpha_A(x)\tau^a\gamma^5\Big]\psi(x)\,, \quad \delta\overline{\psi}(x) = i\overline{\psi}(x)\Big[\alpha_A(x)\tau^a\gamma^5\Big]\,. \tag{3.8}$$

In our conventions, bare quantities are written without any suffix, while their renormalized counterparts are identified by a suffix $R$. The renormalization conditions are usually expressed in terms of amputated correlators

$$\Lambda^a_\Gamma(p_2,p_3) = S(p_3)^{-1}G^a_\Gamma(p_3,p_2)S(p_2)^{-1}\,, \tag{3.9}$$

where $S(p)$ is the fermion propagator in Minkowski space:

$$S(p) = \frac{i}{\not{p} - m - \Sigma(p) + i\epsilon}\,. \tag{3.10}$$

Note that for each leg being amputated, the fermion propagator with the corresponding flavor needs to be used.

## 3.2 Vector and axial Ward Identities

We now show, as an example, the derivation of the axial WI for the amputated vertex function in Minkowski space, under the symmetry transformation Eq. 3.8. The corresponding computation in the Euclidean space is presented in App. C.3, as well as Minkowski and Euclidean vector WIs.

Let us consider the Dirac Lagrangian,

$$\mathcal{L} = i\bar{\psi}\not{D}\psi - m\bar{\psi}\psi\ , \tag{3.11}$$

where the covariant derivative $D_\mu$ is:

$$D_\mu = \partial_\mu + ig\not{\mathcal{A}}_\mu\ . \tag{3.12}$$

We take the probe to be the operator,

$$O(x_3,x_2) = \psi(x_3)\bar{\psi}(x_2), \tag{3.13}$$

and apply the infinitesimal axial transformations in Eq. 3.8. Under the symmetry transformation, the change in the expectation value $\delta\langle O(x_3, x_2)\rangle = 0$:

$$\begin{aligned} 0 &= \frac{\delta}{\delta\alpha(x)}\langle O(x_3,x_2)\rangle = \frac{\delta}{\delta\alpha(x)}\left[\int \mathcal{D}[\bar{\psi},\psi]e^{iS[\mathcal{L}]}O(x_3,x_2)\right] \\ &= \int \mathcal{D}[\bar{\psi},\psi]e^{iS[\mathcal{L}]}\frac{\delta O(x_3,x_2)}{\delta\alpha(x)} \quad + i\int \mathcal{D}[\bar{\psi},\psi]e^{iS[\mathcal{L}]}\frac{\delta S[\mathcal{L}]}{\delta\alpha(x)}O(x_3,x_2)\cdot \end{aligned} \tag{3.14}$$

For the variation in the operator we have,

$$\frac{\delta O(x_3,x_2)}{\delta\alpha(x)} = i\delta(x-x_3)\gamma^5\psi(x_3)\bar{\psi}(x_2) + i\delta(x-x_2)\psi(x_3)\bar{\psi}(x_2)\gamma^5\cdot \tag{3.15}$$

For the variation of the action,

$$\begin{aligned} &\frac{\delta}{\delta\alpha(x)}\Bigg[\int d^4x'\Bigg( -(\bar{\psi}(x')\delta\alpha(x')\gamma^5)(\not{\partial}+ig\not{A})\psi(x') - \bar{\psi}(x')(\not{\partial}+ig\not{A})\Big(\alpha(x')\gamma^5\psi(x')\Big) \\ &\qquad -2mi\ \delta\alpha(x')\ \bar{\psi}(x')\gamma^5\psi(x')\Bigg)\Bigg] \\ &= -\bar{\psi}(x)\gamma^5\gamma^\mu D_\mu\psi(x) + \frac{\delta}{\delta\alpha(x)}\left[\int d^4x'\alpha(x')\partial_\mu A^\mu(x')\right] - \bar{\psi}(x)\gamma^\mu\gamma^5 D_\mu\psi(x) \\ &\quad -2mi\bar{\psi}(x)\gamma^5\psi(x) \\ &= -\bar{\psi}(x)\{\gamma^5,\gamma^\mu\}D_\mu\psi(x) + \partial_\mu A^\mu - 2mi\bar{\psi}(x)\gamma^5\psi(x) \\ &= \partial_\mu A^\mu - 2mi\bar{\psi}(x)\gamma^5\psi(x), \end{aligned} \tag{3.16}$$

where we have denoted the axial operator $A^\mu(x) = \bar{\psi}(x)\gamma^\mu\gamma^5\psi(x)$. Note that in getting to the last line we have assumed $\{\gamma^5,\gamma^\mu\} = 0$ which is true in 4-dimensions. However, using dimensional regularization, the dimensions are extended to a generic value $d$ which is then set to be $d = 4-2\epsilon$. In this case, $\gamma_5$ is ill-defined and must be generalized to $d$-dimensions. The general form of $\gamma_5$ was proposed by 't Hooft and Veltman [79]. Calculations using this convention are discussed in detail, later in this chapter. However, since we are mostly interested in flavor non-singlet quantities, we do not need to worry about extending the definition of $\gamma_5$ to arbitrary dimensions [79, 80]. If one were

interested in flavor singlet currents, then a precise definition of $\gamma_5$ in dimensional regulation is mandatory.

Therefore, the Minkowski axial WI in position space can be written as:

$$i\delta(x-x_3)\gamma^5\langle\psi(x_3)\bar{\psi}(x_2)\rangle + i\delta(x-x_2)\langle\psi(x_3)\bar{\psi}(x_2)\rangle\gamma^5 \tag{3.17}$$

$$= -i\partial_\mu\langle A^\mu(x)\psi(x_3)\bar{\psi}(x_2)\rangle + 2mi\langle\bar{\psi}(x)i\gamma^5\psi(x)\psi(x_3)\bar{\psi}(x_2)\rangle \tag{3.18}$$

In terms of the quark propagator $S(x_3 - x_2) = \langle\psi(x_3)\bar{\psi}(x_2)\rangle$ and the vertex function as in Eq. 3.3, the above reads,

$$i\delta(x-x_3)\gamma^5 S(x_3-x_2) + i\delta(x-x_2)S(x_3-x_2)\gamma^5 \tag{3.19}$$

$$= -i\partial_\mu G^\mu_{\mathrm{A}}(x_3-x, x_2-x) + 2miG_{\mathrm{P}}(x_3-x, x_2-x) \tag{3.20}$$

Taking the Fourier transform according to Eq. C.2 and placing the operator at the origin $x = 0$, *i.e.* an implicit $\int d^4x\delta(x)$, the LHS of Eq. 3.19 becomes,

$$\begin{aligned}
&\int d^4x_2 d^4x_3 \left(i\delta(-x_3)\gamma^5 S(x_3-x_2) + i\delta(-x_2)S(x_3-x_2)\gamma^5\right)e^{ip_3.x_3}e^{-ip_2.x_2} \\
=&\int d^4x_2\ i\gamma^5 S(-x_2)e^{-ip_2.x_2} \ + \ \int d^4x_3\ iS(x_3)\gamma^5 e^{ip_3.x_3} \\
=&i\gamma^5 S(p_2) + iS(p_3)\gamma^5\ \cdot
\end{aligned} \tag{3.21}$$

For the first term on the RHS of Eq. 3.19 we have the following, which we evaluate at $x = 0$ after differentiation,

$$\begin{aligned}
&-i\partial_\mu \int d^4x_2 d^4x_3\ G^\mu_{\mathrm{A}}(x_3-x, x_2-x)e^{ip_3.x_3}e^{-ip_2.x_2} \\
=&-i\partial_\mu \int d^4x'_2 d^4x'_3\ G^\mu_{\mathrm{A}}(x'_3, x'_2)e^{ip_3.(x'_3+x)}e^{-ip_2.(x'_2+x)} \\
=&-i(ip_3 - ip_2)_\mu \int d^4x'_2 d^4x'_3\ G^\mu_{\mathrm{A}}(x'_3, x'_2)e^{ip_3.x'_3}e^{-ip_2.x'_2} \\
=&-q.G_{\mathrm{A}}(p_3, p_2)\ ,
\end{aligned} \tag{3.22}$$

giving the axial WI in momentum space,

$$q.G_{\mathrm{A}}(p_3,p_2) = 2miG_{\mathrm{P}}(p_3,p_2) - i\gamma^5 S(p_2) - iS(p_3)\gamma^5\ \cdot \tag{3.23}$$

Multiplying on the left by $S(p_3)^{-1}$ and on the right by $S(p_2)^{-1}$, the Ward identity for the amputated vertex function in momentum space takes the form:

$$q.\Lambda_{\mathrm{A}}(p_2,p_3) = 2mi\Lambda_{\mathrm{P}}(p_2,p_3) - iS(p_3)^{-1}\gamma^5 - i\gamma^5 S(p_2)^{-1} \cdot \tag{3.24}$$

To obtain the vector WI, one starts from the transformations in Eq. C.21 computes the change in the action and the probe, similar to what we have done above. The result of the amputated vertex function in momentum space reads:

$$q.\Lambda_{\mathrm{V}}(p_2,p_3) = iS(p_2)^{-1} - iS(p_3)^{-1} \cdot \tag{3.25}$$

The explicit computation for both Minkowski and Euclidean spaces are presented in App. C.2 and App. C.3.

## 3.3 Non-perturbative renormalization

The vector and axial Ward identities in terms of the fermion propagator and the amputated vertex function in Euclidean momentum space is repeated below for clarity:

$$q \cdot \Lambda^a_{\mathrm{V}} = iS(p_2)^{-1} - iS(p_3)^{-1}\,, \tag{3.26}$$

$$q \cdot \Lambda^a_{\mathrm{A}} = 2mi\Lambda^a_{\mathrm{P}} - \gamma_5 iS(p_2)^{-1} - iS(p_3)^{-1}\gamma_5\,. \tag{3.27}$$

The quark mass breaks chiral symmetry explicitly. This breaking is visible in the axial WI, Eq. 3.27. Note that the vertex functions are all taken to be non-singlet for the rest of this discussion, and the flavor index $a$ is suppressed to keep the notation simple. In this section, all the vertex functions are mass-degenerated *i.e.* either both quarks are light (massless) or both are heavy. As a result the fermions propagators entering the WI in each case are the same in terms of the quark fields but differ in terms of their momentum associated to each external legs only. The renormalized quantities are defined as follows:

$$\psi_R = Z_q^{1/2}\psi\,, \quad m_R = Z_m m\,, \quad M_R = Z_M M \quad O_{\Gamma,R} = Z_\Gamma O_\Gamma\,, \tag{3.28}$$

where $m$ and $M$ denote the masses of the light and heavy quark respectively. The renormalized propagator and amputated vertex functions are

$$S_R(p) = Z_q S(p)\,, \quad \Lambda_{\Gamma,R}(p_2,p_3) = \frac{Z_\Gamma}{Z_q}\Lambda_\Gamma(p_2,p_3)\,, \tag{3.29}$$

where $q = l, H$ for light and heavy quarks respectively. Note that our conventions for defining the fermion propagator are slightly different from the ones used in Ref. [77]; using our own conventions, the RI/SMOM conditions are

$$\lim_{m_R\to 0}\frac{1}{12p^2}\mathrm{Tr}\left[iS_R(p)^{-1}\ \not{p}\right]\Big|_{p^2=-\mu^2} = 1\,, \tag{3.30}$$

$$\lim_{m_R\to 0}\frac{1}{12m_R}\left\{\mathrm{Tr}\left[-iS_R(p)^{-1}\right]\big|_{p^2=-\mu^2} - \frac{1}{2}\,\mathrm{Tr}\left[(q\cdot\Lambda_{\mathrm{A},R})\,\gamma_5\right]\big|_{\mathrm{sym}}\right\} = 1\,, \tag{3.31}$$

$$\lim_{m_R\to 0}\frac{1}{12q^2}\mathrm{Tr}\left[(q\cdot\Lambda_{\mathrm{V},R})\ \not{q}\right]\big|_{\mathrm{sym}} = 1\,, \tag{3.32}$$

$$\lim_{m_R\to 0}\frac{1}{12q^2}\mathrm{Tr}\left[(q\cdot\Lambda_{\mathrm{A},R})\,\gamma_5\ \not{q}\right]\big|_{\mathrm{sym}} = 1\,, \tag{3.33}$$

$$\lim_{m_R\to 0}\frac{1}{12i}\mathrm{Tr}\left[\Lambda_{\mathrm{P},R}\gamma_5\right]\big|_{\mathrm{sym}} = 1\,, \tag{3.34}$$

$$\lim_{m_R\to 0}\frac{1}{12}\mathrm{Tr}\left[\Lambda_{\mathrm{S},R}\right]\big|_{\mathrm{sym}} = 1\,. \tag{3.35}$$

There are several important properties to note about these conditions.

Firstly, RI/SMOM is a momentum-subtraction scheme. This means that the renormalization conditions are set by projecting the vertex functions in such a way that the renormalization constants satisfy their tree-level value. Take Eq. 3.30 as an example. At tree-level, using Eq. 3.10,

$$\begin{aligned}\lim_{m_R\to 0}\frac{1}{12p^2}\mathrm{Tr}\left[iS_R(p)^{-1}\ \not{p}\right]\Big|_{p^2=-\mu^2} &= \lim_{m_R\to 0}\frac{Z_q^{-1}}{12p^2}\mathrm{Tr}\left[iS(p)^{-1}\ \not{p}\right]\Big|_{p^2=-\mu^2} \\ = \lim_{m_R\to 0}\frac{Z_q^{-1}}{12p^2}\mathrm{Tr}\left[(\not{p}-m)\ \not{p}\right]\Big|_{p^2=-\mu^2} &= \lim_{m_R\to 0} Z_q^{-1} = 1\ ,\end{aligned} \tag{3.36}$$

as expected. Then, for the vector at tree-level we have,

$$\begin{aligned}\lim_{m_R\to 0}\frac{1}{12q^2}\mathrm{Tr}\left[(q\cdot\Lambda_{\mathrm{V},R})\ \not{q}\right]\big|_{\mathrm{sym}} &= \lim_{m_R\to 0}\frac{1}{12q^2}\frac{Z_q}{Z_V}\mathrm{Tr}\left[(q\cdot\Lambda_{\mathrm{V}})\ \not{q}\right]\big|_{\mathrm{sym}} \\ = \lim_{m_R\to 0}\frac{1}{12q^2}\frac{Z_q}{Z_V}\mathrm{Tr}\left[\not{q}\ \not{q}\right]\big|_{\mathrm{sym}} &= \lim_{m_R\to 0}\frac{Z_q}{Z_V} = 1\ ,\end{aligned} \tag{3.37}$$

where we have used $\Lambda^{\mu}_{\rm V} = \gamma^{\mu}$ at tree-level. Given that $Z_q = 1$ at tree-level, as shown in Eq. 3.36, it implies that $Z_{\rm V} = 1$ at tree-level. Similar arguments hold for all the other conditions.

Secondly, these renormalization conditions ensure that the renormalized bilinears obey vector and axial renormalized Ward identities like the ones in Eqs. 3.26, and 3.27, and the renormalization constants satisfy the same properties as in the $\overline{\rm MS}$ scheme, namely

$$Z_{\rm V} = Z_{\rm A} = 1, \quad Z_{\rm P} = Z_{\rm S}, \quad Z_m Z_{\rm P} = 1\,. \tag{3.38}$$

These properties have been clearly shown in Ref. [77]. Here we present $Z_{\rm A} = 1$ and the conservation of the renormalized axial WI as examples. Starting from Eq. 3.27, and writing the bare quantities in terms of the renormalized ones using Eq. 3.28 gives,

$$\frac{1}{Z_A} q \cdot \Lambda_{{\rm A},R} = \frac{1}{Z_m Z_{\rm P}} 2 m_R i \Lambda_{{\rm P},R} - \gamma_5 i S_R(p_2)^{-1} - i S_R(p_3)^{-1} \gamma_5 \ , \tag{3.39}$$

where the $Z_q$ factors have cancelled from both sides of the equation. Multiplying both sides by $\gamma^5 \not{q}$ and $\frac{1}{12q^2}$, taking the trace yields and the limit $m_R \to 0$,

$$\begin{aligned}
\frac{1}{12q^2}\frac{1}{Z_A}{\rm Tr}\left[(q\cdot\Lambda_{{\rm A},R})\,\gamma_5\,\not{q}\right]\big|_{\rm sym} =& \frac{1}{12q^2}{\rm Tr}\left[\big(-\gamma_5 i S_R(p_2)^{-1} - i S_R(p_3)^{-1}\gamma_5\big)\gamma_5\,\not{q}\right]\big|_{\rm sym} \\
=& \frac{1}{12q^2}{\rm Tr}\left[\big(i S_R(p_2)^{-1} - i S_R(p_3)^{-1}\big)\,\not{q}\right]\big|_{\rm sym} \\
=& \frac{1}{12q^2}{\rm Tr}\left[\big(i S_R(q)^{-1}\big)\,\not{q}\right]\big|_{\rm sym} = 1
\end{aligned} \tag{3.40}$$

where the last equality comes from Eq. 3.30. Therefore, using the renormalization condition for the axial vertex function Eq. 3.33 for the LHS of Eq. 3.40, we get $Z_{\rm A} = 1$. If instead, we multiply Eq. 3.27 by $\gamma^5$, and apply the same procedure, we obtain $Z_m Z_{\rm P} = 1$ using the condition in Eq. 3.31. Plugging $Z_{\rm A} = 1$ and $Z_m Z_{\rm P} = 1$ into Eq. 3.39 we see that the renormalized WI is clearly satisfied:

$$q \cdot \Lambda_{{\rm A},R} = m_R i \Lambda_{{\rm P},R} - \gamma_5 i S_R(p_2)^{-1} - i S_R(p_3)^{-1}\gamma_5 \cdot \tag{3.41}$$

A similar procedure can be performed to obtain $Z_{\rm V} = 1$. Starting from the bare

vector WI Eq. 3.26, and rewriting the bare quantities in terms of the renormalized ones we obtain,

$$\frac{1}{Z_{\rm V}} q \cdot \Lambda^a_{{\rm V},R} = iS_R(p_2)^{-1} - iS_R(p_3)^{-1} \tag{3.42}$$

Multiplying the above equation by $\not{q}$, taking the trace and using the condition in Eq. 3.32 we get,

$$\lim_{M_R \to \overline{m}} \frac{1}{Z_{\rm V}} \frac{1}{12q^2} {\rm Tr}\left[ (q \cdot \Lambda_{{\rm V},R})\ \not{q} \right]\big|_{\rm sym} = \lim_{M_R \to \overline{m}} \frac{1}{12q^2} {\rm Tr}\left[ iS_R(q)^{-1}\ \not{q} \right]\big|_{\rm sym} = 1 \cdot \tag{3.43}$$

Finally, using the vector renormalization condition in Eq. 3.32, one obtains that $Z_{\rm V} = 1$. Again, it can be observed that with $Z_{\rm V} = 1$, the renormalized vector WI, Eq. 3.42 is indeed satisfied. All These properties have been checked using a one-loop calculation in massless continuum perturbation theory in Ref. [77].

While the renormalization conditions in the RI/SMOM scheme are imposed in the chiral limit, the RI/mSMOM scheme is defined by imposing a similar set of conditions at some fixed value of a reference renormalized mass that we denote by $\overline{m}$ [81]:

$$\lim_{M_R \to \overline{m}} \frac{1}{12p^2} {\rm Tr}\left[ iS_R(p)^{-1}\ \not{p} \right]\Big|_{p^2=-\mu^2} = 1\,, \tag{3.44}$$

$$\lim_{M_R \to \overline{m}} \frac{1}{12M_R} \left\{ {\rm Tr}\left[ -iS_R(p)^{-1} \right]\big|_{p^2=-\mu^2} - \frac{1}{2}\ {\rm Tr}\left[ (q \cdot \Lambda_{{\rm A},R})\, \gamma_5 \right]\big|_{\rm sym} \right\} = 1\,, \tag{3.45}$$

$$\lim_{M_R \to \overline{m}} \frac{1}{12q^2} {\rm Tr}\left[ (q \cdot \Lambda_{{\rm V},R})\ \not{q} \right]\big|_{\rm sym} = 1\,, \tag{3.46}$$

$$\lim_{M_R \to \overline{m}} \frac{1}{12q^2} {\rm Tr}\left[ (q \cdot \Lambda_{{\rm A},R} - 2M_R i\Lambda_{{\rm P},R})\, \gamma_5\ \not{q} \right]\big|_{\rm sym} = 1\,, \tag{3.47}$$

$$\lim_{M_R \to \overline{m}} \frac{1}{12i} {\rm Tr}\left[ \Lambda_{{\rm P},R} \gamma_5 \right]\big|_{\rm sym} = 1\,, \tag{3.48}$$

$$\lim_{M_R \to \overline{m}} \left\{ \frac{1}{12} {\rm Tr}\left[ \Lambda_{{\rm S},R} \right] - \frac{1}{6q^2} {\rm Tr}\left[ 2iM_R \Lambda_{P,R} \gamma_5 \not{q} \right] \right\}\Bigg|_{\rm sym} = 1\,. \tag{3.49}$$

Comparing with the SMOM prescription where the renormalization conditions were imposed at the chiral limit $m_R \to 0$, the renormalization conditions in the

mSMOM scheme are imposed at $M_R \to \overline{m}$, a new scale that one is free to choose. It can be observed that only the renormalization conditions for the axial and scalar vertex functions have been modified by terms proportional to $M_R$, which therefore vanish in the chiral limit. Therefore, the mSMOM prescription reduces to the SMOM one as $\overline{m}$ is set to zero. As usual the renormalization conditions are satisfied by the tree-level values of the field correlators. The properties listed in Eq. 3.38 also hold for the mSMOM scheme. This implies that the renormalized WIs are satisfied. We now show all of these features in more detail.

Let us first focus on the modified conditions for the axial vertex function, Eq. 3.47, and check $Z_{\rm A} = 1$ at tree-level:

$$\begin{aligned} &\lim_{M_R \to \overline{m}} \frac{1}{12q^2} \mathrm{Tr}\left[ (q \cdot \Lambda_{{\rm A},R} - 2M_R i \Lambda_{{\rm P},R})\, \gamma_5 \not{q} \right]\big|_{\rm sym} \\ &= \lim_{M_R \to \overline{m}} \frac{1}{12q^2} \mathrm{Tr}\left[ \left( Z_{\rm A} \not{q} \gamma^5 + 2 Z_M Z_{\rm P} M \gamma^5 \right) \gamma_5 \not{q} \right]\big|_{\rm sym} \\ &= \lim_{M_R \to \overline{m}} Z_{\rm A} = 1 \ , \end{aligned} \tag{3.50}$$

as required, where we have used $Z_q = 1$, $\Lambda_{\rm P} = i\gamma^5$ and $\Lambda_{\rm A} = \gamma^\mu \gamma^5$ at tree-level. We follows the same procedure as Eq. 3.40, but now it is repeated for the massive scheme. Two independent equations can be obtained by multiplying Eq. 3.39 by $\gamma^5 \not{q}$ and by $\gamma_5$ respectively, taking the trace, and evaluating correlators at the symmetric point. In the first case, using Eqs. (3.44) and (3.47), we obtain

$$(Z_{\rm A} - 1) = \left( 1 - \frac{Z_{\rm A}}{Z_M Z_{\rm P}} \right) C_{mP} \, , \tag{3.51}$$

where

$$C_{m\rm P} = \lim_{M_R \to \overline{m}} \frac{1}{12q^2} \mathrm{Tr}\left[ 2iM_R \Lambda_{{\rm P},R} \gamma_5 \not{q} \right]\big|_{\rm sym} \ . \tag{3.52}$$

The second equation instead gives

$$\begin{aligned} \frac{1}{Z_{\rm A}} \mathrm{Tr}\left[ (q \cdot \Lambda_{{\rm A},R})\, \gamma_5 \right]\big|_{\rm sym} =& \frac{2M_R}{Z_M Z_{\rm P}} \mathrm{Tr}\left[ (i\Lambda_{{\rm P},R})\, \gamma_5 \right]\big|_{\rm sym} \\ &- \mathrm{Tr}\left[ \gamma_5 i S_R(p_2)^{-1} \gamma_5 \right]\big|_{\rm sym} - \mathrm{Tr}\left[ i S_R(p_3)^{-1} \right]\big|_{\rm sym} \ . \end{aligned} \tag{3.53}$$

For the first term on the RHS of Eq. 3.53, we can use the renormalization in Eq. 3.48 and for the second term, we can use Eq. 3.45 for each propagator. This yields,

$$\frac{1}{Z_{\mathrm{A}}}\,\mathrm{Tr}\left[(q\cdot\Lambda_{\mathrm{A},R})\,\gamma_5\right]\big|_{\mathrm{sym}} = -\frac{24M_R}{Z_M Z_{\mathrm{P}}} + 24M_R + \mathrm{Tr}\left[(q\cdot\Lambda_{\mathrm{A},R})\,\gamma_5\right]\big|_{\mathrm{sym}}\ . \tag{3.54}$$

Rearranging gives,

$$(Z_{\mathrm{A}}-1)C_{qA} = -2Z_{\mathrm{A}}\left(1-\frac{1}{Z_M Z_{\mathrm{P}}}\right)\,, \tag{3.55}$$

where we have introduced one more constant

$$C_{q\mathrm{A}} = \lim_{M_R\to\overline{m}}\frac{1}{12M_R}\mathrm{Tr}\left[q\cdot\Lambda_{\mathrm{A},R}\gamma_5\right]\big|_{\mathrm{sym}}\ . \tag{3.56}$$

It is easy to verify that $Z_{\mathrm{A}} = 1$, $Z_M Z_{\mathrm{P}} = 1$ is a solution of the system. Rearranging for $Z_{\mathrm{A}}/(Z_M Z_{\mathrm{P}})$ in Eq. 3.55 and substituting the result into Eq. 3.51, gives $Z_{\mathrm{A}} = 1$. Substituting back to any of the two equations results in $Z_M Z_{\mathrm{P}} = 1$ making the solution unique. Notice that because of the modified renormalization condition for the renormalization of the axial vertex function, the computation of $Z_{\mathrm{A}}$ and $Z_M Z_{\mathrm{P}}$ are coupled in the mSMOM scheme. The results $Z_{\mathrm{A}} = 1$, $Z_M Z_{\mathrm{P}} = 1$ imply that the renormalized axial WI, using the modified condition in the massive scheme is satisfied. In particular, $Z_{\mathrm{A}} = 1$ implies that $Z_{\mathrm{A}}$ does not depend on the renormalization scale $\mu$.

The renormalization condition for the scalar vertex function $\Lambda_{\mathrm{S}}$ in Eq. 3.49, however, has been determined by performing a 1-loop computation in perturbation theory, as discussed in Sec. 3.4.9. To prove $Z_{\mathrm{P}} = Z_{\mathrm{S}}$ we start from the non-degenerate vector Ward identity, which is an extension of Eq. (3.26) with $m_1 \neq m_2$,

$$q\cdot\Lambda_{\mathrm{V}} = (m_1-m_2)\Lambda_{\mathrm{S}} + iS_{q_1}(p_2,m_1)^{-1} - iS_{q_2}(p_3,m_2)^{-1}, \tag{3.57}$$

where $q_1$ and $q_2$ refer to two different quark flavors with masses $m_1$ and $m_2$ respectively. Note that since the field renormalization condition is set in the limit $m\to\overline{m}$ and the momenta are symmetric, $Z_q$ is the same for both quark fields $q_1$

and $q_2$. Writing the above equation in terms of the renormalized quantities, we have

$$\begin{aligned} q \cdot Z_q^{-1} Z_{\mathrm{V}}\ \Lambda_{\mathrm{V},R} =& Z_q^{-1} Z_M Z_{\mathrm{S}} (m_{1,R} - m_{2,R}) \Lambda_{\mathrm{S},R} \\ &+ i Z_q^{-1} S_{q_1,R}(p_2, m_1)^{-1} - i Z_q^{-1} S_{q_2,R}(p_3, m_2)^{-1}, \end{aligned} \tag{3.58}$$

where we have used the property that the mass difference $(m_1 - m_2)$ is renormalized by $Z_M$, given that it is obtained in the limit $m \to \overline{m}$ for both quarks, as shown in Ref. [78]. Since it is already shown that $Z_{\mathrm{V}} = 1$ and the renormalized WI is satisfied, it implies that $Z_M Z_{\mathrm{S}} = 1$. Using $Z_M Z_{\mathrm{P}} = 1$, we finally obtain $Z_{\mathrm{P}} = Z_{\mathrm{S}}$. Hence we recover the equality between the two renormalization constants. This also holds non-perturbatively in the SMOM scheme (its validity had been previously shown at 1-loop in perturbation theory in Ref. [77]).

We have showed that mSMOM inherits the good properties of the SMOM scheme presented in Eq. 3.38, in particular the renormalized WIs at all scales $\mu$ are satisfied.

## 3.4 Perturbative computation I

In order to understand the details of the RI/mSMOM scheme we present an explicit one-loop computation of the fermions self-energy and all the bilinear vertex functions. For simplicity we regularize the theory using dimensional regularization, and evaluate the relevant diagrams including their dependence on the bare mass $m$. Because we are mostly interested in flavor non-singlet quantities, we do not need to worry about extending the definition of $\gamma_5$ to arbitrary dimensions [79, 80]. Using the naive definition of $\gamma_5$ keeps the computation simpler. However, if one were interested in flavor singlet currents, then a precise definition of $\gamma_5$ in dimensional regulation is mandatory. To this end, we also present a 1-loop calculation using the 't Hooft-Veltman convention for $\gamma_5$ in this chapter. This leads to extra Feynman diagrams that have to be computed and is discussed in detail.

The 1-loop diagram, Fig. 3.3, in the perturbative calculation of the vertices

corresponds to the following integral:

$$\Lambda_{\Gamma}^{(1)} = -ig^2 C_2(F) \int_k \frac{\gamma_\mu [\not{p}_3 - \not{k} + m] \Gamma [\not{p}_2 - \not{k} + m] \gamma^\mu}{k^2 [(p_2 - k)^2 - m^2][(p_3 - k)^2 - m^2]} \ , \tag{3.59}$$

where $\Gamma = \mathrm{S}, \mathrm{P}, \mathrm{V}, \mathrm{A}$. The strategy for computing these vertex functions is

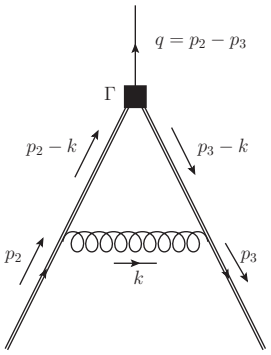


Figure 3.2: Diagram representing the non-amputated vertex function at 1-loop in perturbative QCD.

as follows: First, the scalar, vector and tensor parts of the above integral are extracted and the integrals are written in terms of scalar integrals. Then, all the scalar master integrals are computed and are used to calculate each vertex $\Lambda_{\Gamma}^{(1)}$. It is important to organize the terms in the numerator with respect to their unique Dirac structure. The loop integration is a standard computation, performed in $D = 4 - 2\epsilon$ using dimensional regularization, while for the integration over the Feynman parameters we have used certain techniques which have been developed in the past few years, see Ref. [82–84]. We discuss some of the techniques in the upcoming sections.

### 3.4.1 The basis integrals

We list the set of scalar basis integrals that are ingredients to the full vertex function integrals. As discussed later, there are several methods by which one can compute some of these integrals. As a result this set may not be the minimal basis, however it is complete. All the other integrals can be written as a linear combinations of the basis integrals. Observing Eq. 3.59, one of the integrals

required is

$$I_{111} = g^2 \int_k \frac{1}{k^2[(p_2-k)^2-m^2][(p_3-k)^2-m^2]} \,, \tag{3.60}$$

which turns out to be the most complex integral to compute and its calculation is discussed in detail. Let us first explain the notation. In what follows, the subscripts on each integral $I_{XYZ}$ refer to the power of each propagator present in the denominator. More explicitly, the first subscript counts the powers of $k^2$ in the denominator, the second counts that of $(p_2-k)^2-m^2$ and the third $(p_3-k)^2-m^2$. For example in Eq. 3.60, there is one power of each propagator in the denominator, hence the notation $I_{111}$. Powers of the propagator in the numerator are written in the subscript with a negative sign. The other scalar integrals required are: $I_{011}, I_{101}, I_{001}, I_{-111}, I_{1-11}$. It turns out that the last two integrals can be written as a linear combination of the other 4. Notice also that $I_{101} = I_{110}$ if $p_3$ is relabelled to $p_2$. The same is true for $I_{001} = I_{010}$. Hence the minimal basis would be $\{I_{111}, I_{011}, I_{101}, I_{001}\}$. The calculation of the first of these is discussed in the next section while the rest are standard integrals with the results shown in App. C.4.

### 3.4.2 The scalar integral

We wish to compute the integral in Eq. 3.60. Introducing as usual a set of Feynman parameters $x_1, x_2, x_3$, the integral can be recast in the following form:

$$I_{111} = g^2\Gamma(3) \int_k \int_0^1 \left(\prod_{i=1}^{3} \mathrm{d}x_i\right) \delta\left(1 - \sum_{i=1}^{3} x_i\right) \times \frac{1}{\left(x_1 k^2 + x_2\left[(p_2-k)^2-m^2\right] + x_3\left[(p_3-k)^2-m^2\right]\right)^3} \,. \tag{3.61}$$

The denominator can be written as a polynomial in $k$. The coefficients are then simplified using the symmetric kinematics $p_2^2 = p_3^2 = (p_2-p_3)^2 = -\mu^2$, implying also that $p_2.p_3 = -\frac{1}{2}\mu^2$. Making the change of variable,

$$l = k - \frac{x_2 p_2 + x_3 p_3}{x_1 + x_2 + x_3} \,, \tag{3.62}$$

introducing the function,

$$M^2 = \left(\frac{x_2 p_2 + x_3 p_3}{x_1 + x_2 + x_3}\right)^2 + \frac{x_2 + x_3}{x_1 + x_2 + x_3}\left(\mu^2 + m^2\right) , \tag{3.63}$$

and performing a Wick rotation to Euclidean space yields:

$$I_{111} = -ig^2\Gamma(3)\int_0^1 \left(\prod_{i=1}^3 \mathrm{d}x_i\right)\delta\left(1 - \sum_{i=1}^3 x_i\right)\frac{1}{(x_1 + x_2 + x_3)^3}\int_\ell \frac{1}{\left(\ell^2 + M^2\right)^3} \ . \tag{3.64}$$

The loop integral can now be performed in closed form in $D$ dimensions. We can use,

$$\frac{1}{(l^2 + m^2)^3} = \frac{1}{\Gamma(3)}\int_0^\infty d\lambda \lambda^2 e^{-\lambda(l^2 + M^2)} , \tag{3.65}$$

to first perform the gaussian integral over $l$ and then the integral over $\lambda$. In this particular case the integral is finite, there are no $1/\epsilon$ singularities as $\epsilon \to 0$. This gives,

$$I_{111} = -i\frac{\alpha}{4\pi}\int_0^1 \left(\prod_{i=1}^3 \mathrm{d}x_i\right)\delta\left(1 - \sum_{i=1}^3 x_i\right)\frac{1}{(x_1 + x_2 + x_3)^3}\frac{1}{M^2} \ , \tag{3.66}$$

where we defined $g \to g\mu^\epsilon$ and $\alpha = g^2/4\pi$ to obtain the previous equation. The denominator in the integrand can be expressed as

$$\mu^2(x_1 + x_2 + x_3)\left[\ x_2x_3 + x_1x_2 + x_1x_3 + u\left(x_1x_2 + x_1x_3 + x_2^2 + x_3^2 + 2x_2x_3\right)\right] , \tag{3.67}$$

where we have introduced $u = m^2/\mu^2$. Using the Cheng-Wu theorem Ref. [82], applied to the case where we choose the constraint to be $\delta(1 - x_3)$, two integrations over the Feynman parameters can be easily done, yielding

$$\begin{aligned} I_{111} = &- i\frac{\alpha}{4\pi}\frac{1}{\mu^2} \times \\ &\int_0^\infty \mathrm{d}x_2 \ \frac{-\log\left[-u(x_2+1)^2 - x_2\right] + \log\left[-(x_2+1)(u+1)\right] + \log(x_2+1)}{x_2(x_2+1) + 1} \ . \end{aligned} \tag{3.68}$$

Note that this integral can be readily computed numerically for the case where $m = 0$. The result of the numerical integration of the above integral is 2.34239 which agrees with the number quoted in Ref. [77].

For our purposes the analytic expression for $I_{111}$ as a function of the mass is actually desirable. We find the two roots, $d_1, d_2$, of $x_2$ in the denominator and use the symmetry between the roots *i.e.* $d_1 = 1/d_2$ to reduce the number of parameters in the integral. This makes the computation easier for Mathematica and the packages used within. Similarly, the numerator takes the form,

$$\begin{aligned} &\log(x^2 + 2x + 1 + \frac{\omega}{u}x) + \log(-u) - 2\log(x+1) - \log(-u-1) \\ =&\log(x^2 + (2 + \frac{\omega}{u})x + 1) - 2\log(x+1) + \log(u) - i\pi - \log(u+1) + i\pi \ , \end{aligned} \tag{3.69}$$

which is shown not to have any imaginary parts. Defining $r = 1/u = \mu^2/m^2$, the roots of the argument of the log are

$$n_1 = \frac{1}{2}\left(-2 - r - \sqrt{r^2+4r}\right) \quad , \quad n_2 = \frac{1}{2}\left(-2 - r + \sqrt{r^2+4r}\right) \ . \tag{3.70}$$

Again, there is a symmetry between the roots: $n_1 = \frac{1}{n_2}$. The numerator can therefore be written as,

$$\log(x - n_1) + \log(x - n_2) = \log(x - n_1) + \log(x - \frac{1}{n_1}) \tag{3.71}$$

$$= \log(x - n_1) + \log(n_1 x - 1) - \log(n_1) \ . \tag{3.72}$$

The integral becomes, $-i\frac{\alpha}{4\pi}\frac{1}{\mu^2}\times$

$$\int_0^\infty dx \ \frac{\log(x - n_1) + \log(n_1 x - 1) - \log(n_1) - 2\log(x+1) + \log(u) - \log(u+1)}{(x - d_1)(x - \frac{1}{d_1})} \ . \tag{3.73}$$

In order to avoid later complications with the upper limit of the integral being at infinity, we make the change of variables:

$$x \mapsto y \, , \quad x = \frac{y}{1-y} \ .$$

The problem is then reduced to an integral that can be computed explicitly: $I_{111} = i\frac{\alpha}{4\pi}\frac{1}{\mu^2}\times$

$$\int_0^1 \mathrm{d}y \frac{\log(\frac{y}{1-y} - n_1) + \log(n_1\frac{y}{1-y} - 1) - \log(n_1) - 2\log(\frac{y}{1-y} + 1) + \log(u) - \log(u+1)}{(y + (y-1)d_1)(y + \frac{y-1}{d_1})}\,, \tag{3.74}$$

where $d_1 = \frac{1}{2}\left(-1 + i\sqrt{3}\right), n_1 = \frac{1}{2}\left(-2 - 1/u - \sqrt{1/u^2 + 4/u}\right)$. The final result is a lengthy expression, which we report for completeness,

$$\begin{aligned} I_{111} =& \frac{\alpha}{4\pi}\frac{1}{\mu^2}\frac{1}{\sqrt{3}}\Bigg\{ i\frac{\pi}{3}(-2i\pi - 2\log(1+u)) \\ &+ \log\left[-\frac{2u+1-\sqrt{1+4u}}{2}\right]\log\left[\frac{4+(i\sqrt{3}-1)(1-\sqrt{4u+1})}{4-(i\sqrt{3}+1)(1-\sqrt{4u+1})}\right] \\ &+ \log\left[-\frac{(1+\sqrt{4u+1})^2}{4}\right]\log\left[\frac{4+(i\sqrt{3}-1)(1+\sqrt{4u+1})}{4-(i\sqrt{3}+1)(1+\sqrt{4u+1})}\right] \\ &+ 2\ \mathrm{Li}\left[\frac{4u}{4u-\left(i\sqrt{3}-1\right)\left(1+\sqrt{4u+1}\right)}\right] - \mathrm{Li}\left[\frac{4u}{4u+\left(i\sqrt{3}+1\right)\left(1+\sqrt{4u+1}\right)}\right] \\ &+ \mathrm{Li}\left[\frac{4u+2+2\sqrt{4u+1}}{4u+\left(i\sqrt{3}+1\right)\left(1+\sqrt{4u+1}\right)}\right] - \mathrm{Li}\left[\frac{4u+\left(i\sqrt{3}+1\right)\left(1+\sqrt{4u+1}\right)}{4(1+u)}\right]\Bigg\}. \end{aligned} \tag{3.75}$$

As a partial check of our massive computation, the limit $u \to 0$ of the expression above is numerically evaluated, and shown to reproduce again the value 2.34391 from Ref. [77]. Here we denote

$$I_{111} = -\frac{i\alpha}{4\pi}\frac{1}{\mu^2}C_0\left(\frac{m^2}{\mu^2}\right)\,, \tag{3.76}$$

so that $C_0|_{m=0} = 2.34391$.

### 3.4.3 Integral with $k^\mu$ in the numerator

The integral with $k^\mu$ in the numerator,

$$I^\mu = g^2\int_k \frac{k^\mu}{k^2[(p_2-k)^2 - m^2][(p_3-k)^2 - m^2]}\,, \tag{3.77}$$

can be reduced to scalar integrals by taking all possible linear combinations and solving simultaneous equations. The only two scales in the problem with a vector index are $p_2^\mu$ and $p_3^\mu$. Therefore, we expect $I^\mu$ to be of the form

$$I^\mu = Ap_2^\mu + Bp_3^\mu \cdot \tag{3.78}$$

Dotting with $p_2^\mu$ and $p_3^\mu$ gives the following simultaneous equations:

$$\begin{cases} p_{2\mu} I^\mu = \mu^2 \left(-A - \frac{1}{2}B\right) \ , \\ p_{3\mu} I^\mu = \mu^2 \left(-B - \frac{1}{2}A\right) \ . \end{cases} \tag{3.79}$$

One computes the LHS of Eq. 3.79 starting with

$$p_{2\mu} I^\mu = g^2 \int_k \frac{p_2.k}{k^2[(p_2-k)^2 - m^2][(p_3-k)^2 - m^2]} \cdot \tag{3.80}$$

Using $-2(p_2.k) = (p_2-k)^2 - m^2 - p_2^2 - k^2 + m^2$,

$$\begin{aligned} p_{2\mu} I^\mu =& \frac{-g^2}{2} \int \frac{1}{k^2[(p_3-k)^2 - m^2]} + \frac{\mu^2 + m^2}{k^2[(p_2-k)^2 - m^2][(p_3-k)^2 - m^2]} \\ & + \frac{-1}{[(p_2-k)^2 - m^2][(p_3-k)^2 - m^2]} \\ =& -\frac{1}{2}\left(I_{101} + (\mu^2 + m^2) I_{111} - I_{011}\right) \cdot \end{aligned} \tag{3.81}$$

The second term is the scalar integral computed in Sec. 3.4.2. We also have the results for the first and the last terms in Appendix C. Due to the symmetry between $p_2$ and $p_3$ we only need to compute this integral once. Going back to Eq. 3.79 and solving for $A$ and $B$ gives,

$$A = B = \frac{2p_{2\mu} I^\mu}{-3\mu^2} = \frac{2p_{3\mu} I^\mu}{-3\mu^2} \implies I^\mu = A(p_2^\mu + p_3^\mu) = \frac{2p_{2\nu} I^\nu (p_2^\mu + p_3^\mu)}{-3\mu^2} \cdot \tag{3.82}$$

Hence,

$$I^\mu = \frac{(p_2^\mu + p_3^\mu)}{-3\mu^2}\left(-I_{101} - (\mu^2 + m^2) I_{111} + I_{011}\right) \cdot \tag{3.83}$$

### 3.4.4 Integral with $k^\mu k^\nu$ in the numerator

Using a similar method to Sec. 3.4.3, the integral

$$I^{\mu\nu} = g^2 \int_k \frac{k^\mu k^\nu}{k^2[(p_2-k)^2-m^2][(p_3-k)^2-m^2]} \tag{3.84}$$

can be reduced to scalar integrals by taking all possible linear combinations and solving simultaneous equations. Knowing the possible scales in the problem, we expect $I^{\mu\nu}$ to be of the form

$$I^{\mu\nu} = Ag^{\mu\nu} + B(p_2^\mu p_2^\nu + p_3^\mu p_3^\nu) + C(p_2^\mu p_3^\nu + p_3^\mu p_2^\nu) \cdot \tag{3.85}$$

To obtain the coefficients $A, B$ and $C$, Eq. 3.85 is contracted with $g^{\mu\nu}$, $p_2^\mu p_2^\nu$ and $p_2^\mu p_3^\nu$. On the LHS, each integral is then written as a linear combination of the basis integrals which are already computed. This gives three simultaneous equations with three unknowns, for which we solve. The details of this computation is presented in App. C.5.

### 3.4.5 Fermion self-energy

The fermion self energy at 1-loop

$$-i\Sigma^{(1)} = -g^2 C_2(F) \int_k \frac{\gamma_\alpha[\not{p}_2 - \not{k} + m]\gamma^\alpha}{k^2[(p_2-k)^2-m^2]} \tag{3.86}$$

shown in Fig. 3.3, can be computed directly by using the Feynman parameterization, writing the denominator as a polynomial in $k$ and making a change of variable in the standard way. However, the computation simplifies if one,

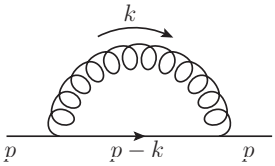


Figure 3.3: Fermion self-energy at 1-loop in perturbative QCD.

instead, notes that the integrand can be written as a linear combination of the basis integrals which have already been computed. To this end, the coefficient $F$

has to be determined:

$$g^2 \int_k \frac{k^\mu}{k^2[(p_2-k)^2-m^2]} = F p_2^\mu \ , \tag{3.87}$$

with $p_2^\mu$ being the only external scale appearing in the integral that can carry the index $\mu$. The computation is very similar to that in Sec. 3.4.3, as is not repeated here. The details are written out App. C.6. Using

$$\gamma^\mu\gamma_\mu = d \quad , \quad \gamma^\mu\gamma^\nu\gamma_\mu = (2-d)\gamma^\nu \ , \tag{3.88}$$

The final answer is:

$$\Sigma(p) = \frac{\alpha}{4\pi} C_2(F) \left[ \not{p} \left( -\frac{1}{\epsilon} - 1 + \gamma_E + \frac{m^2}{\mu^2} + \frac{m^4}{\mu^4} \ln\left(\frac{m^2}{m^2+\mu^2}\right) + \ln\left(\frac{m^2+\mu^2}{\tilde{\mu}^2}\right)\right) \right.$$
$$\left. + m\left( \frac{4}{\epsilon} + 6 - 4\gamma_E + \frac{4m^2}{\mu^2} \ln\left(\frac{m^2}{m^2+\mu^2}\right) - 4\ln\left(\frac{m^2+\mu^2}{\tilde{\mu}^2}\right)\right)\right] , \tag{3.89}$$

where $\gamma_E$ is the Euler-Mascheroni constant, we have replaced $p^2 = -\mu^2$, and denoted $\tilde{\mu}$ the scale introduced by dimensional regularization through the rescaling of the gauge coupling $g \to g\tilde{\mu}^\epsilon$. This scale can later on be set to equal $\mu$.

Eq. (3.44) yields the renormalization constant for the fermion field in the mSMOM scheme:

$$Z_q = 1 + \frac{\alpha}{4\pi} C_2(F) \left[ \frac{1}{\epsilon} + 1 - \gamma_E - \frac{\bar{m}^2}{\mu^2} - \frac{\bar{m}^4}{\mu^4} \ln\left(\frac{\bar{m}^2}{\bar{m}^2+\mu^2}\right) - \ln\left(\frac{\bar{m}^2+\mu^2}{\tilde{\mu}^2}\right)\right] . \tag{3.90}$$

The effect of the change of scheme is a redefinition of the finite part of the renormalization constant $Z_q$. As expected on dimensional grounds, the dependence on the reference mass $\bar{m}$ only enters via the dimensionless ratio $\bar{m}/\mu$. The limit for $\bar{m} \to 0$ is well defined and reproduces the result of the massless scheme [77].

### 3.4.6 Vector vertex

Let us now consider the vertex functions, and discuss how the ingredients of the previous sections are used in this computation. We also discuss in detail the structure of the vector correlator $\Lambda_{\rm V}$. The one-loop contribution to the vertex for the case of massive fermions is

$$\Lambda_{\rm V}^{(1)\sigma}(p_2,p_3) = -ig^2 C_2(F)\int_k \frac{\gamma_\alpha\left[\not{p}_3 - \not{k} + m\right]\gamma^\sigma\left[\not{p}_2 - \not{k} + m\right]\gamma^\alpha}{k^2\left[(p_3-k)^2-m^2\right]\left[(p_2-k)^2-m^2\right]}\,. \tag{3.91}$$

As mentioned before, the first step in the computation of the above vertex function is to organize the terms in the numerator in such a way that the full integral can be written in terms of a scalar, a vector and a tensor integral in $k^\mu$, *i.e.*

$$I^\sigma = K^\sigma(p_2,p_3)I_{111} + K^{\sigma,\mu}I_\mu + K^{\sigma,\mu\nu}(p_2,p_3)I_{\mu\nu}\,\cdot \tag{3.92}$$

After some manipulations,

$$K^\sigma(p_2,p_3) = \Big[ -2p_2^\sigma \not{p}_3 - 2p_3^\sigma \not{p}_2 - \mu^2\gamma^\sigma - 2i\epsilon^{\rho\alpha\sigma\beta}\gamma_\rho\gamma^5 p_{3\alpha}p_{2\beta} \tag{3.93}$$

$$+ 4mp_3^\sigma + 4mp_2^\sigma - 2m^2\gamma^\sigma\Big], \tag{3.94}$$

$$\begin{aligned} K^{\sigma,\mu}(p_2,p_3) = \Big[&(2-2\epsilon)\left[(p_2^\sigma+p_3^\sigma)\gamma^\mu + (\not{p}_2+\not{p}_3)g^{\sigma\mu} - (p_2^\mu+p_3^\mu)\gamma^\sigma\right] \\ &+ (-2-2\epsilon)i\epsilon^{\rho\mu\sigma\alpha}\gamma_\rho\gamma^5(p_{3\alpha}-p_{2\alpha}) - (8-4\epsilon)mg^{\mu\sigma}\Big], \end{aligned} \tag{3.95}$$

and

$$K^{\sigma,\mu\nu}(p_2,p_3) = (-2+2\epsilon)\left(g^{\mu\sigma}\gamma^\nu + g^{\sigma\nu}\gamma^\mu - g^{\mu\nu}\gamma^\sigma\right)\,\cdot \tag{3.96}$$

The integrals $I_{111}$, $I_\mu$, $I_{\mu\nu}$ have been calculated. See Eq. 3.74, Eq. 3.83 and Eq. 3.85 together with Eq. C.75-C.77. Putting all the ingredients together, the integral Eq. 3.91 which transforms as a four-vector under Lorentz transformations

can be expressed in terms of just five form factors.

$$\Lambda_{\mathrm{V}}^{(1)\sigma}(p_2,p_3)=\frac{\alpha}{4\pi}C_2(F)\left[A_{\mathrm{V}}\frac{1}{\mu^2}\left(i\epsilon^{\sigma\rho\alpha\beta}\gamma_\rho\gamma^5 p_{3\alpha}p_{2\beta}\right)+B_{\mathrm{V}}\gamma^\sigma+C_{\mathrm{V}}\frac{1}{\mu^2}\left(p_2^\sigma\ \not{p}_2+p_3^\sigma\ \not{p}_3\right)+\right.$$
$$\left.+D_{\mathrm{V}}\frac{1}{\mu^2}\left(p_2^\sigma\ \not{p}_3+p_3^\sigma\ \not{p}_2\right)+E_{\mathrm{V}}\frac{1}{\mu}\left(p_2^\sigma+p_3^\sigma\right)\right]. \tag{3.97}$$

The form factors $A_{\mathrm{V}},\ldots,E_{\mathrm{V}}$ only depend on the Lorentz invariants, and are computed analytically. At the symmetric point, they are given by the following expressions.

$$A_{\mathrm{V}}=\frac{4}{3}\left[\left(\frac{1}{2}-\frac{m^2}{\mu^2}\right)C_0\left(\frac{m^2}{\mu^2}\right)+\left(1+\frac{m^2}{\mu^2}\right)\log\left(\frac{m^2}{m^2+\mu^2}\right)\right.$$
$$\left.-\sqrt{1+4\frac{m^2}{\mu^2}}\log\left(\frac{\sqrt{1+4\frac{m^2}{\mu^2}}-1}{\sqrt{1+4\frac{m^2}{\mu^2}}+1}\right)\right], \tag{3.98}$$

where the expression for $C_0\left(\frac{m^2}{\mu^2}\right)$ can be found in Eq. 3.75 and Eq. 3.76. Although the last two terms in the expression are separately divergent in the massless limit, these divergences cancel, yielding a finite expression when $m\to 0$, which agrees with the results in Ref. [77]. Similarly for the other form factors we find:

$$B_{\mathrm{V}}=\frac{1}{\epsilon}-\gamma_E+\frac{1}{3}\left[-C_0\left(\frac{m^2}{\mu^2}\right)\left(1-4\frac{m^2}{\mu^2}-2\frac{m^4}{\mu^4}\right)+2\left(3-\frac{m^2}{\mu^2}\right)\frac{m^2}{\mu^2}\log\left(\frac{m^2}{m^2+\mu^2}\right)\right.$$
$$+\left(1-4\frac{m^2}{\mu^2}\right)\log\left(\frac{m^2}{\tilde{\mu}^2}\right)-4\left(1-\frac{m^2}{\mu^2}\right)\log\left(\frac{m^2+\mu^2}{\tilde{\mu}^2}\right)$$
$$\left.-\left(1-2\frac{m^2}{\mu^2}\right)\sqrt{1+4\frac{m^2}{\mu^2}}\log\left(\frac{\sqrt{1+4\frac{m^2}{\mu^2}}-1}{\sqrt{1+4\frac{m^2}{\mu^2}}+1}\right)\right]; \tag{3.99}$$

$$C_{\mathrm{V}}=-\frac{2}{3}\left[\left(1-\frac{m^2}{\mu^2}\right)\frac{m^2}{\mu^2}\log\left(\frac{m^2}{m^2+\mu^2}\right)+\left(1-2\frac{m^2}{\mu^2}\right)\sqrt{1+4\frac{m^2}{\mu^2}}\right.$$
$$\left.\times\log\left(\frac{\sqrt{1+4\frac{m^2}{\mu^2}}-1}{\sqrt{1+4\frac{m^2}{\mu^2}}+1}\right)+\left(2-\frac{m^2}{\mu^2}\right)-2C_0\left(\frac{m^2}{\mu^2}\right)\frac{m^2}{\mu^2}\left(1+\frac{m^2}{\mu^2}\right)\right.$$

$$- \left(1 - 4\frac{m^2}{\mu^2}\right) \log\left(\frac{m^2}{\tilde{\mu}^2}\right) + \left(1 - 4\frac{m^2}{\mu^2}\right) \log\left(\frac{m^2+\mu^2}{\tilde{\mu}^2}\right)\Bigg] \; ; \tag{3.100}$$

$$D_{\rm V} = \frac{2}{3}\left[\left(1 + C_0\left(\frac{m^2}{\mu^2}\right)\right)\left(1 - 2\frac{m^2}{\mu^2}\right) - 2\left(1 + \frac{m^2}{\mu^2}\right)\frac{m^2}{\mu^2}\log\left(\frac{m^2}{m^2+\mu^2}\right)\right] ; \tag{3.101}$$

$$E_{\rm V} = -\frac{4}{3}\frac{m}{\mu}\Bigg[C_0\left(\frac{m^2}{\mu^2}\right)\left(1 - 2\frac{m^2}{\mu^2}\right) + 2\log\left(\frac{m^2}{m^2+\mu^2}\right) + 2\frac{m^2}{\mu^2}\log\left(\frac{m^2}{m^2+\mu^2}\right) - 2\sqrt{1+4\frac{m^2}{\mu^2}}\log\left(\frac{\sqrt{1+4\frac{m^2}{\mu^2}}-1}{\sqrt{1+4\frac{m^2}{\mu^2}}+1}\right)\Bigg] ; \tag{3.102}$$

which all agree with the results in Ref. [77] when the limit $m \to 0$ is taken.

### 3.4.7 Pseudoscalar vertex

For the pseudoscalar vertex function at one-loop we have:

$$\Lambda_{\rm P}^{(1)}(p_2,p_3) = g^2 C_2(F) \int_k \frac{\gamma_\alpha \left[\not{p}_3 - \not{k} + m\right]\gamma^5\left[\not{p}_2 - \not{k} + m\right]\gamma^\alpha}{k^2\left[(p_3-k)^2 - m^2\right]\left[(p_2-k)^2 - m^2\right]} \, . \tag{3.103}$$

Decomposing the integral into scalar, vector and tensor parts with respect to the loop-momentum $k^\mu$,

$$I^\sigma = K_5(p_2,p_3) I_{111} + K_5^\mu I_\mu + K_5^{\mu\nu}(p_2,p_3) I_{\mu\nu} \; , \tag{3.104}$$

with

$$K_5(p_2,p_3) = \gamma^5\Big[2(\omega-2)\mu^2 + (d-4)\not{p}_3\not{p}_2 + (2-d)m(\not{p}_3 - \not{p}_2) - dm^2\Big], \tag{3.105}$$

$$K_5^\mu(p_2,p_3) = \gamma^5\Bigg[-4(p_2^\mu + p_3^\mu) - (d-4)\not{p}_3\gamma^\mu - (d-4)\gamma^\mu\not{p}_2\Bigg], \tag{3.106}$$

and

$$K_5^{\mu\nu}(p_2,p_3)=\gamma^5\Big(4g^{\mu\nu}+(d-4)\gamma^\mu\gamma^\nu\Big)\cdot \tag{3.107}$$

Putting the ingredients together and setting $d=4-2\epsilon$, we see the one-loop structure of this vertex is simpler as compared to the vector case:

$$\Lambda_{\rm P}^{(1)}(p_2,p_3)=\frac{i\alpha}{4\pi}C_2(F)\left[B_{\rm P}\left(\gamma^5\right)+E_{\rm P}\frac{1}{\mu}(\gamma^5)\left(\not{p}_2-\not{p}_3\right)\right]. \tag{3.108}$$

The form factors are:

$$B_{\rm P}=4\left[\frac{1}{\epsilon}-\gamma_E+\frac{3}{2}-\frac{1}{2}C_0\left(\frac{m^2}{\mu^2}\right)+\frac{m^2}{\mu^2}\log\left(\frac{m^2}{m^2+\mu^2}\right)-\log\left(\frac{m^2+\mu^2}{\tilde{\mu}^2}\right)\right]; \tag{3.109}$$

$$E_{\rm P}=-\frac{m}{\mu}2C_0\left(\frac{m^2}{\mu^2}\right). \tag{3.110}$$

Using the renormalization condition Eq. (3.48), we have

$$\lim_{M_R\to\overline{m}}\frac{1}{12i}{\rm Tr}\left[\Lambda_{{\rm P},R}\gamma_5\right]\big|_{\rm sym}=\lim_{m_R\to\overline{m}}\frac{1}{12i}{\rm Tr}\left[\frac{Z_{\rm P}}{Z_q}\Lambda_P\gamma^5\right]\Bigg|_{\rm sym}=1, \tag{3.111}$$

giving

$$\begin{aligned}Z_{\rm P}=\Bigg\{1+\frac{\alpha}{4\pi}C_2(F)\Bigg[&-3\left(\frac{1}{\epsilon}-\gamma_E\right)-5+2C_0\left(\frac{m^2}{\mu^2}\right)+3\ln\left(\frac{\overline{m}^2+\mu^2}{\tilde{\mu}^2}\right)\\&-\frac{\overline{m}^2}{\mu^2}\left(1-4\ln\left(1+\frac{\mu^2}{\overline{m}^2}\right)-\frac{\overline{m}^2}{\mu^2}\ln\left(1+\frac{\mu^2}{\overline{m}^2}\right)\right)\Bigg]\Bigg\}.\end{aligned} \tag{3.112}$$

The above result reduces to Ref. [77] in the massless limit. Note that $Z_{\rm P}$ is scale dependent; setting $\tilde{\mu}=\mu$, we find that the dependence on the scale only appears through the combination $\mu/\overline{m}$.

### 3.4.8 Axial vertex

The computation of the axial vertex follows very closely the one of the vector vertex presented above. The starting expression

$$\Lambda_{\mathrm{A}}^{(1)\sigma}(p_2,p_3) = -ig^2 C_2(F)\int_k \frac{\gamma_\alpha\left[\not{p}_3 - \not{k} + m\right]\gamma^\sigma\gamma^5\left[\not{p}_2 - \not{k} + m\right]\gamma^\alpha}{k^2\left[(p_3-k)^2-m^2\right]\left[(p_2-k)^2-m^2\right]}\ , \tag{3.113}$$

It is decomposed as follows:

$$I^\sigma = K_5^\sigma(p_2,p_3)I_{111} + K_5^{\sigma,\mu}I_\mu + K_5^{\sigma,\mu\nu}(p_2,p_3)I_{\mu\nu}\ , \tag{3.114}$$

where, with $d = 4-2\epsilon$,

$$\begin{aligned} K^\sigma(p_2,p_3) = \Bigg[ & 2\gamma^5\left(p_2^\sigma\not{p}_3 + p_3^\sigma\not{p}_2 + \frac{\mu^2}{2}\gamma^\sigma\right) - 2i\epsilon^{\rho\alpha\sigma\beta}\gamma_\rho p_{3\alpha}p_{2\beta} \\ & + 4m\gamma^5 p_2^\sigma - 4m\gamma^5 p_3^\sigma - 2m^2\gamma^5\gamma^\sigma\Bigg], \end{aligned} \tag{3.115}$$

$$\begin{aligned} K^{\sigma,\mu}(p_2,p_3) = \Bigg[ & (-2+2\epsilon)\gamma^5\left((p_2^\sigma + p_3^\sigma)\gamma^\mu + (\not{p}_2 + \not{p}_3)g^{\sigma\mu} - (p_2^\mu + p_3^\mu)\gamma^\sigma\right) \\ & - (2+2\epsilon)i\epsilon^{\rho\mu\sigma\alpha}\gamma_\rho(p_{3\alpha} - p_{2\alpha}) - 2\epsilon m\gamma^5[\gamma^\mu,\gamma^\sigma]\Bigg], \end{aligned} \tag{3.116}$$

$$K^{\sigma,\mu\nu}(p_2,p_3) = (2-2\epsilon)\gamma^5\left(g^{\mu\sigma}\gamma^\nu + g^{\sigma\nu}\gamma^\mu - g^{\mu\nu}\gamma^\sigma\right)\ . \tag{3.117}$$

The integral can again be parametrized in terms of five form factors, which we denote $A_{\mathrm{A}},\ldots,E_{\mathrm{A}}$,

$$\begin{aligned} \Lambda_{\mathrm{A}}^{(1)\sigma}(p_2,p_3) = \frac{\alpha}{4\pi}C_2(F)\Bigg[ & A_{\mathrm{A}}\frac{1}{\mu^2}\left(i\epsilon^{\sigma\rho\alpha\beta}\gamma_\rho p_{3\alpha}p_{2\beta}\right) + B_{\mathrm{A}}\gamma^\sigma\gamma^5 + C_{\mathrm{A}}\frac{1}{\mu^2}\gamma^5\left(p_2^\sigma\ \not{p}_2 + p_3^\sigma\ \not{p}_3\right) \\ & + D_{\mathrm{A}}\frac{1}{\mu^2}\gamma^5\left(p_2^\sigma\ \not{p}_3 + p_3^\sigma\ \not{p}_2\right) + E_{\mathrm{A}}\frac{1}{\mu}\gamma^5\left(p_2^\sigma - p_3^\sigma\right)\Bigg] \end{aligned} \tag{3.118}$$

All the possible Lorentz structures expected for an axial vertex function are included such that $\sigma$ is the free index, unless the form factor turns out to be zero, *e.g.* in this case the term proportional to $\gamma^5\sigma^{\mu\nu}$. For the non-zero axial form factors we find:

$$A_{\mathrm{A}} = \frac{4}{3}\Bigg[\left(\frac{1}{2}-\frac{m^2}{\mu^2}\right)C_0\left(\frac{m^2}{\mu^2}\right)+\frac{m^2}{\mu^2}\log\left(\frac{m^2}{m^2+\mu^2}\right)-\log\left(\frac{m^2+\mu^2}{\tilde{\mu}^2}\right) - \sqrt{1+4\frac{m^2}{\mu^2}}\log\left(\frac{\sqrt{1+4\frac{m^2}{\mu^2}}-1}{\sqrt{1+4\frac{m^2}{\mu^2}}+1}\right)\Bigg]; \tag{3.119}$$

$$B_{\mathrm{A}} = \frac{1}{\epsilon}-\gamma_E+\frac{1}{3}\Bigg[-C_0\left(\frac{m^2}{\mu^2}\right)\left(1+8\frac{m^2}{\mu^2}-2\frac{m^4}{\mu^4}\right)+\left(3-\frac{m^2}{\mu^2}\right)2\frac{m^2}{\mu^2}\log\left(\frac{m^2}{m^2+\mu^2}\right) + \left(1-4\frac{m^2}{\mu^2}\right)\log\left(\frac{m^2}{\tilde{\mu}^2}\right)-4\left(1-\frac{m^2}{\mu^2}\right)\log\left(\frac{m^2+\mu^2}{\tilde{\mu}^2}\right) - \left(1-2\frac{m^2}{\mu^2}\right)\sqrt{1+4\frac{m^2}{\mu^2}}\log\left(\frac{\sqrt{1+4\frac{m^2}{\mu^2}}-1}{\sqrt{1+4\frac{m^2}{\mu^2}}+1}\right)\Bigg]; \tag{3.120}$$

$$C_{\mathrm{A}} = -\frac{2}{3}\Bigg[\left(4-\frac{m^2}{\mu^2}\right)\frac{m^2}{\mu^2}\log\left(\frac{m^2}{m^2+\mu^2}\right)-\left(1-2\frac{m^2}{\mu^2}\right)\sqrt{1+4\frac{m^2}{\mu^2}} \times\log\left(\frac{\sqrt{1+4\frac{m^2}{\mu^2}}-1}{\sqrt{1+4\frac{m^2}{\mu^2}}+1}\right)-\left(2-\frac{m^2}{\mu^2}\right)+2C_0\left(\frac{m^2}{\mu^2}\right)\frac{m^2}{\mu^2}\left(1+\frac{m^2}{\mu^2}\right) + \left(1-4\frac{m^2}{\mu^2}\right)\log\left(\frac{m^2}{\tilde{\mu}^2}\right)-\left(1-4\frac{m^2}{\mu^2}\right)\log\left(\frac{m^2+\mu^2}{\tilde{\mu}^2}\right)\Bigg]; \tag{3.121}$$

$$D_{\mathrm{A}} = -\frac{2}{3}\left[\left(1+C_0\left(\frac{m^2}{\mu^2}\right)\right)\left(1-2\frac{m^2}{\mu^2}\right)-2\left(1+\frac{m^2}{\mu^2}\right)\frac{m^2}{\mu^2}\log\left(\frac{m^2}{m^2+\mu^2}\right)\right]; \tag{3.122}$$

$$E_{\rm A} = \frac{m}{\mu} 4C_0 \left(\frac{m^2}{\mu^2}\right) . \tag{3.123}$$

Again, in the massless limit $m \to 0$, the above coefficients coincide with the corresponding results in Ref. [77].

### 3.4.9 Scalar vertex

In this section we discuss the mSMOM renormalization condition for the scalar vertex.

$$\Lambda_{\rm S}^{(1)}(p_2,p_3) = -ig^2 C_2(F) \int_k \frac{\gamma_\alpha \left[\not{p}_3 - \not{k} + m\right] \left[\not{p}_2 - \not{k} + m\right] \gamma^\alpha}{k^2 \left[(p_3-k)^2 - m^2\right] \left[(p_2-k)^2 - m^2\right]} . \tag{3.124}$$

Decomposing gives,

$$\Lambda_{\rm S}^{(1)}(p_2,p_3) = -ig^2 C_2(F) \Bigg[ K(p_2,p_3) I_{111} + K^\mu I_\mu + K^{\mu\nu}(p_2,p_3) I_{\mu\nu} \Bigg], \tag{3.125}$$

where,

$$K(p_2,p_3) = \Big[ 2(\omega-2)\mu^2 + (d-4)\not{p}_3\not{p}_2 + (2-d)m(\not{p}_3 + \not{p}_2) + dm^2 \Big], \tag{3.126}$$

$$K^\mu(p_2,p_3) = \Bigg[ -4(p_2^\mu + p_3^\mu) - (d-4)\not{p}_3\gamma^\mu - (d-4)\gamma^\mu\not{p}_2 - 2m(2-d)\gamma^\mu \Bigg], \tag{3.127}$$

$$K^{\mu\nu}(p_2,p_3) = \Big( 4g^{\mu\nu} + (d-4)\gamma^\mu\gamma^\nu \Big) \cdot \tag{3.128}$$

We set $d = 4 - 2\epsilon$. The one-loop structure of this vertex is

$$\Lambda_{\rm S}^{(1)}(p_2,p_3) = \frac{\alpha}{4\pi} C_2(F) \left[ B_{\rm S} + E_{\rm S} \frac{1}{\mu} \left(\not{p}_2 + \not{p}_3\right) \right] . \tag{3.129}$$

The form factors are:

$$
\begin{aligned}
B_{\mathrm{S}} =& 4\left(\frac{1}{\epsilon}-\gamma_E\right)+6-\left(8\frac{m^2}{\mu^2}+2\right)C_0\left(\frac{m^2}{\mu^2}\right) \\
&+\frac{4m^2}{\mu^2}\ln\left(\frac{m^2}{m^2+\mu^2}\right)-4\ln\left(\frac{m^2+\mu^2}{\tilde{\mu}^2}\right),
\end{aligned}
\tag{3.130}
$$

$$
\begin{aligned}
E_{\mathrm{S}} =& -\frac{4}{3}\frac{m}{\mu}\Bigg[C_0\left(\frac{m^2}{\mu^2}\right)\left(-\frac{1}{2}+\frac{m^2}{\mu^2}\right)-\left(1+\frac{m^2}{\mu^2}\right)\log\left(\frac{m^2}{m^2+\mu^2}\right) \\
&+\sqrt{1+4\frac{m^2}{\mu^2}}\log\left(\frac{\sqrt{1+4\frac{m^2}{\mu^2}}-1}{\sqrt{1+4\frac{m^2}{\mu^2}}+1}\right)\Bigg].
\end{aligned}
\tag{3.131}
$$

Using the renormalization condition Eq. (3.49), and the fact that $Z_m Z_{\mathrm{P}} = 1$, yields

$$
\begin{aligned}
&\lim_{m_R\to\overline{m}}\left\{\frac{1}{12}\mathrm{Tr}\left[\frac{Z_S}{Z_q}\Lambda_S\right]+\frac{1}{6q^2}\mathrm{Tr}\left[\frac{Z_m Z_{\mathrm{P}}}{Z_q}2im\Lambda_P\gamma_5\not{q}\right]\right\}\Bigg|_{\mathrm{sym}} \\
&=\lim_{m_R\to\overline{m}} Z_q^{-1}\Bigg\{Z_S\Bigg(1+C_2(F)\frac{\alpha}{4\pi}\Bigg[4\left(\frac{1}{\epsilon}-\gamma_E\right)+6-\left(8\frac{m^2}{\mu^2}+2\right)C_0\left(\frac{m^2}{\mu^2}\right) \\
&\qquad+\frac{4m^2}{\mu^2}\ln\left(\frac{m^2}{m^2+\mu^2}\right)-4\ln\left(\frac{m^2+\mu^2}{\tilde{\mu}^2}\right)\Bigg)+\frac{8m^2}{\mu^2}C_0\left(\frac{m^2}{\mu^2}\right)\Bigg]\Bigg\}=1\,.
\end{aligned}
\tag{3.132}
$$

After introducing

$$
\begin{aligned}
\mathcal{P} = 1+C_2(F)\frac{\alpha}{4\pi}\Bigg[&4\left(\frac{1}{\epsilon}-\gamma_E\right)+6-2C_0\left(\frac{m^2}{\mu^2}\right)+\frac{4m^2}{\mu^2}\ln\left(\frac{m^2}{m^2+\mu^2}\right) \\
&-4\ln\left(\frac{m^2+\mu^2}{\tilde{\mu}^2}\right)\Bigg],
\end{aligned}
\tag{3.133}
$$

we obtain

$$Z_S\left(\mathcal{P}-\frac{\alpha}{4\pi}C_2(F)\frac{8m^2}{\mu^2}C_0\left(\frac{m^2}{\mu^2}\right)\right)=Z_q\left(1-\frac{1}{Z_q}C_2(F)\frac{\alpha}{4\pi}\frac{8m^2}{\mu^2}\right)$$
$$=Z_q\left(1-C_2(F)\frac{\alpha}{4\pi}\frac{8m^2}{\mu^2}+\mathcal{O}(\alpha^2)\right)\ .$$

Hence,

$$\begin{aligned}Z_S=&Z_q\mathcal{P}^{-1}\left(1-C_2(F)\frac{\alpha}{4\pi}\frac{8m^2}{\mu^2}+\mathcal{O}(\alpha^2)\right)\left(1+\frac{\alpha}{4\pi}C_2(F)\frac{8m^2}{\mu^2}\frac{C_0\left(\frac{m^2}{\mu^2}\right)}{\mathcal{P}}\right)\\ =&Z_q\mathcal{P}^{-1}\left(1-C_2(F)\frac{\alpha}{4\pi}\frac{8m^2}{\mu^2}+\mathcal{O}(\alpha^2)\right)\left(1+\frac{\alpha}{4\pi}C_2(F)\frac{8m^2}{\mu^2}C_0\left(\frac{m^2}{\mu^2}\right)+\mathcal{O}(\alpha^2)\right)\\ =&Z_{\rm P}\,.\end{aligned}\tag{3.134}$$

We can rewrite the above expression explicitly as:

$$\begin{aligned}Z_S=&\left\{1+\frac{\alpha}{4\pi}C_2(F)\left[-3\left(\frac{1}{\epsilon}-\gamma_E\right)-5+2C_0\left(\frac{m^2}{\mu^2}\right)+3\ln\left(\frac{\overline{m}^2+\mu^2}{\tilde{\mu}^2}\right)\right.\right.\\ &\left.\left.-\frac{\overline{m}^2}{\mu^2}\left(1-4\ln\left(1+\frac{\mu^2}{\overline{m}^2}\right)-\frac{\overline{m}^2}{\mu^2}\ln\left(1+\frac{\mu^2}{\overline{m}^2}\right)\right)\right]\right\}\\ =&Z_{\rm P}\ ,\end{aligned}\tag{3.135}$$

which clearly depends on the ratio $\frac{m^2}{\mu^2}$. It is possible to show non-perturbatively that $Z_mZ_S=1$ using the vector WI with a suitable probe. See *e.g.* Ref. [78] for a detailed discussion.

### 3.4.10 Mass Renormalization

The mass renormalization can be computed following the mSMOM prescription:

$$\lim_{m_R\to\overline{m}}\frac{1}{12m_R}\left\{\mathrm{Tr}\left[-iS_R^{-1}\right]-\frac{1}{2}\mathrm{Tr}\left[q_\mu\Lambda^\mu_{A,R}\gamma^5\right]\right\}\Bigg|_{\rm sym}=1.\tag{3.136}$$

We prove that $Z_m Z_{\rm P}$ has to be equal to 1, i.e.

$$\begin{aligned}
&\lim_{m_R\to\overline{m}} \frac{1}{12 Z_m m}\left\{ {\rm Tr}\left[ -iZ_q^{-1}S^{-1}\right] - \frac{1}{2}{\rm Tr}\left[ Z_{\rm A} Z_q^{-1} q_\mu \Lambda^\mu_{A,R}\gamma^5\right]\right\}\Big|_{\rm sym} \\
&= \lim_{m_R\to\overline{m}} \frac{Z_m^{-1}}{12m}\left\{ Z_q^{-1}(12m)(1+\Sigma_S(p^2)) - \frac{1}{2}Z_{\rm A}Z_q^{-1}(12)C_2(F)\frac{\alpha}{4\pi}4mC_0\left(\frac{m^2}{\mu^2}\right)\right\}\Big|_{\rm sym}
\end{aligned} \tag{3.137}$$

Setting $Z_{\rm A}=1$, we have

$$\begin{aligned}
Z_m =& Z_q^{-1}\Bigg[1+\frac{\alpha}{4\pi}C_2(F)\Bigg(4\left(\frac{1}{\epsilon}-\gamma_E\right)+6+\frac{4m^2}{\mu^2}\ln\left(\frac{m^2}{m^2+\mu^2}\right) \\
&- 4\ln\left(\frac{m^2+\mu^2}{\tilde{\mu}^2}\right) - 2C_0\left(\frac{m^2}{\mu^2}\right)\Bigg)\Bigg] \\
=& 1+\frac{\alpha}{4\pi}C_2(F)\Bigg[3\left(\frac{1}{\epsilon}-\gamma_E\right)+5-2C_0\left(\frac{m^2}{\mu^2}\right) \\
&+\frac{\overline{m}^2}{\mu^2}\left(1+4\ln\left(\frac{\overline{m}^2}{\overline{m}^2+\mu^2}\right)-\frac{\overline{m}^2}{\mu^2}\ln\left(\frac{\overline{m}^2}{\overline{m}^2+\mu^2}\right)\right) \\
&-3\ln\left(\frac{\overline{m}^2+\mu^2}{\tilde{\mu}^2}\right)\Bigg] = Z_{\rm P}^{-1}\,.
\end{aligned} \tag{3.138}$$

### 3.4.11 Vector Ward identity

The results in the Sec. 3.4.6 and Sec. 3.4.5 need to satisfy the vector Ward identity. This requirement provides a stringent test of our computations. At one-loop the Ward identity, Eq. 3.26, becomes

$$q\cdot\Lambda_{\rm V}^{(1)} = \Sigma(p_3)-\Sigma(p_2)\,. \tag{3.139}$$

Using the results in Sec. (3.4.6), the LHS of Eq. 3.139 is readily evaluated

$$\begin{aligned}
\frac{\alpha}{4\pi}C_2(F)\;\not{q}\Bigg\{&\frac{1}{\epsilon}-\gamma_E+1-\log\left(\frac{m^2+\mu^2}{\tilde{\mu}^2}\right) \\
&-\frac{m^2}{\mu^2}\left(1-\frac{m^2}{\mu^2}\left[1-\frac{m^2}{\mu^2}\log\left(\frac{m^2}{m^2+\mu^2}\right)\right]\right)\Bigg\}\,.
\end{aligned} \tag{3.140}$$

Likewise, for the RHS of Eq. 3.139, the results in Sec. 3.4.5 yield exactly the same expression, so that the vector Ward identity is indeed satisfied.

As discussed in the previously, the vector Ward identity implies that $Z_V = 1$. This can be checked explicitly from our one-loop calculation. Using the renormalization condition Eq. (3.46) yields

$$\lim_{M_R\to\overline{m}} \frac{1}{12q^2}\mathrm{Tr}\left[(q\cdot\Lambda_{\mathrm{V},R})\ \not{q}\right]|_{\mathrm{sym}} = \lim_{m_R\to\overline{m}} \frac{1}{12q^2}\mathrm{Tr}\left[\frac{Z_V}{Z_q}(q\cdot\Lambda_V)\ \not{q}\right]\Bigg|_{\mathrm{sym}} = 1, \tag{3.141}$$

which, using Eq. (3.90), implies

$$\begin{aligned} Z_{\mathrm{V}} =& Z_q\left[1+\frac{\alpha}{4\pi}C_2(F)\left(\frac{1}{\epsilon}+1-\gamma_E-\frac{\bar{m}^2}{\mu^2}-\frac{\bar{m}^4}{\mu^4}\ln\left(\frac{\bar{m}^2}{\bar{m}^2+\mu^2}\right)-\ln\left(\frac{\bar{m}^2+\mu^2}{\tilde{\mu}^2}\right)\right)\right]^{-1} \\ =& 1. \end{aligned} \tag{3.142}$$

### 3.4.12 Axial Ward identity

The axial Ward identity also needs to be fulfilled in our check at 1-loop. This constraint becomes

$$q\cdot\Lambda_{\mathrm{A}}^{(1)} = 2mi\Lambda_{\mathrm{P}} + \gamma_5\Sigma(p_2) + \Sigma(p_3)\gamma_5 \tag{3.143}$$

Using the results in Sec. (3.4.8), the LHS of Eq. (3.143) can be evaluated

$$\begin{aligned} -\frac{\alpha}{4\pi}C_2(F)\gamma^5\Bigg\{\not{q}\Bigg[&\frac{1}{\epsilon}-\gamma_E+1-\frac{4m^2}{\mu^2}C_0\left(\frac{m^2}{\mu^2}\right)-\frac{m^2}{\mu^2}-\frac{m^4}{\mu^4}\ln\left(\frac{m^2}{m^2+\mu^2}\right) \\ &-\ln\left(\frac{m^2+\mu^2}{\tilde{\mu}^2}\right)\Bigg]-4mC_0\left(\frac{m^2}{\mu^2}\right)\Bigg\}. \end{aligned} \tag{3.144}$$

Similarly, for the RHS of Eq. (3.143) , the results in Sec. 3.4.5 and Sec. 3.4.7 yield exactly the same expression, so that the axial Ward identity is indeed satisfied.

As discussed in the previous section, the axial Ward identity implies that $Z_{\mathrm{A}} = 1$. This can be checked explicitly from our one-loop calculation. Note that

the modified renormalization condition Eq. (3.47) is critical to get $Z_{\rm A} = 1$.

$$\begin{aligned}
&\lim_{M_R\to\overline{m}} \frac{1}{12q^2}\mathrm{Tr}\left[\left(q\cdot\Lambda_{{\rm A},R} - 2m_R i\Lambda_{{\rm P},R}\right)\gamma_5\, \not{q}\right]\Big|_{\rm sym} \qquad (3.145)\\
&= \lim_{M_R\to\overline{m}} \frac{1}{12q^2}\mathrm{Tr}\left[\left(\frac{Z_{\rm A}}{Z_q} q\cdot\Lambda_A - \frac{Z_{\rm P}Z_m}{Z_q} 2im\Lambda_P\right)\gamma^5 \not{q}\right]\Big|_{\rm sym}\\
&= \lim_{M_R\to\overline{m}} \frac{1}{12q^2}\frac{1}{Z_q}\mathrm{Tr}\Bigg\{ Z_{\rm A}\Bigg(q^2 + \frac{\alpha}{4\pi}C_2(F)q^2\Bigg[\frac{1}{\epsilon} - \gamma_E + 1 - \frac{4m^2}{\mu^2}C_0\left(\frac{m^2}{\mu^2}\right) - \frac{m^2}{\mu^2}\\
&\qquad - \frac{m^4}{\mu^4}\ln\left(\frac{m^2}{m^2+\mu^2}\right) - \ln\left(\frac{m^2+\mu^2}{\tilde{\mu}^2}\right)\Bigg]\Bigg)\\
&\qquad + C_2(F)\frac{\alpha}{4\pi}q^2\frac{4m^2}{\mu^2}C_0\left(\frac{m^2}{\mu^2}\right)\Bigg\}\Big|_{\rm sym} = 1,
\end{aligned}$$

where we have used $Z_m Z_{\rm P} = 1$. Substituting Eq. (3.90), yields

$$Z_{\rm A} = 1\,. \qquad (3.146)$$

## 3.5 Perturbative computation II

The 't Hooft-Veltman convention for $\gamma_5$, generalizes this matrix for arbitrary dimensions $d$ [79]:

$$\begin{aligned}
&\{\gamma_5, \gamma^\mu\}, \quad \text{if } \mu = 0,1,2,3, \qquad (3.147)\\
&[\gamma_5, \gamma^\mu], \quad \text{otherwise},\\
&(\gamma_5)^2 = 1, \quad \gamma_5^\dagger = \gamma_5.
\end{aligned}$$

This is only Lorentz invariant for the first four dimensions and not the entire space, however it also gives the correct axial anomaly. When considering the flavor-singlet axial current, it is essential to use this convention for $\gamma_5$. Even though we have not considered the flavor-singlet case, as a check, we redo the 1-loop computation for the pseudoscalar and axial vertices using this convention. Such a 1-loop calculation also gives insight for attempting to extend the mSMOM renormalization scheme for flavor-singlet operators. Due to the different commutation and anti-commutation relations depending on whether

$\mu \leq 3$ or $\mu > 3$, the axial WI needs to be re-derived and now contains extra terms corresponding to extra 1-loop diagrams that have to be recomputed.

We follow the notation first introduced by Breitenlohner & Maison in Ref. [80] and re-expressed in [85]. Dimensions $\mu \leq 3$ are denoted with a bar and $\mu > 3$ are denoted with a hat. Explicitly:

$$\hat{g}_{\mu\nu} = \begin{cases} g_{\mu\nu}, & \text{if } \mu, \nu \geq 4 \\ 0, & \text{otherwise;} \end{cases} \tag{3.148}$$

and

$$\bar{g}_{\mu\nu} = \begin{cases} g_{\mu\nu}, & \text{if } \mu, \nu < 4, \\ 0, & \text{otherwise.} \end{cases} \tag{3.149}$$

For a vector:

$$\begin{cases} \hat{p}^{\mu} = \hat{g}^{\mu\nu} p_{\nu}, \\ \bar{p}^{\mu} = \bar{g}^{\mu\nu} p_{\nu}. \end{cases} \tag{3.150}$$

Furthermore, let

$$\hat{\delta}^{\mu}_{\nu} = \begin{cases} \delta^{\mu}_{\nu}, & \text{if } \mu, \nu \geq 4 \\ 0, & \text{otherwise;} \end{cases} \tag{3.151}$$

and

$$\bar{\delta}^{\mu}_{\nu} = \begin{cases} \delta^{\mu}_{\nu}, & \text{if } \mu, \nu < 4 \\ 0, & \text{otherwise;} \end{cases} \tag{3.152}$$

Appendix C.7 is dedicated to the manipulation of the $\gamma$ matrices in this convention, in particular those that are required in the 1-loop computation of the pseudoscalar, the axial and other vertices appearing in the axial WI.

### 3.5.1 Axial WI in the 't Hooft-Veltman convention

Returning to Sec. 3.2, where we derived the axial WI explicitly starting from the variation of the action, we see that the term appearing in the line before last in

Eq. 3.16, *i.e.*

$$-\bar{\psi}(x)\{\gamma^5,\gamma^\mu\}D_\mu\psi(x)+\partial_\mu A^\mu-2mi\bar{\psi}(x)\gamma^5\psi(x)\ , \tag{3.153}$$

contains an anti-commutator term. This term is no longer zero for $\mu > 3$ but instead equals

$$-2\bar{\psi}(x)\gamma^5\hat{\gamma}^\mu D_\mu\psi(x)+\partial_\mu A^\mu-2mi\bar{\psi}(x)\gamma^5\psi(x)\ \cdot \tag{3.154}$$

This yields the axial WI:

$$\begin{aligned} & i\delta(x-x_3)\gamma^5\langle\psi(x_3)\bar{\psi}(x_2)\rangle+i\delta(x-x_2)\langle\psi(x_3)\bar{\psi}(x_2)\rangle\gamma^5 \\ =&-i\partial_\mu\langle A^\mu(x)\psi(x_3)\bar{\psi}(x_2)\rangle+2mi\langle\bar{\psi}(x)i\gamma^5\psi(x)\psi(x_3)\bar{\psi}(x_2)\rangle \\ +&\underbrace{i\langle\bar{\psi}(x)\gamma^5\hat{\gamma}^\mu\big(\partial_\mu\psi(x)\big)\psi(x_3)\bar{\psi}(x_2)\rangle-i\langle\big(\partial_\mu\bar{\psi}(x)\big)\gamma^5\hat{\gamma}^\mu\psi(x)\psi(x_3)\bar{\psi}(x_2)\rangle}_{} \\ &\underbrace{-2g\langle\bar{\psi}(x)\gamma^5\hat{\gamma}^\mu\not{A}_\mu\psi(x)\psi(x_3)\bar{\psi}(x_2)\rangle}_{\text{new Feynman rules needed}}\cdot \end{aligned} \tag{3.155}$$

The terms indicated appear as a result of the 't Hooft-Veltman convention and yield new vertices that have to be computed. Let us start with the first term and perform a Wick contraction,

$$\begin{aligned} &\langle\bar{\psi}(x)\gamma^5\hat{\gamma}^\mu\big(\partial_\mu\psi(x)\big)\psi(x_3)\bar{\psi}(x_2)\rangle \\ =&+\langle\psi(\overbrace{x_3)\bar{\psi}(x}\gamma^5\hat{\gamma}^\mu\big(\partial_\mu\psi(\overbrace{x)\big)\bar{\psi}(x_2}\rangle\ \cdot \end{aligned} \tag{3.156}$$

The momentum space value, placing the operator at the origin using a delta function becomes,

$$\begin{aligned} &\int d^4x\ \delta(x)\int d^4x_2d^4x_3\ S(x_3-x)\gamma^5\hat{\gamma}^\mu\bigg(\partial_\mu S(x-x_2)\bigg)e^{ip_3.x_3}e^{-ip_2.x_2} \\ =&\int d^4x\ \delta(x)\bigg[\int d^4x_3\ S(x_3-x)e^{ip_3.x_3}\ \gamma^5\hat{\gamma}^\mu\ \times(-)(-)(-ip_2)\int d^4x_2\ S(x-x_2)e^{-ip_2.x_2}\bigg] \\ =&-ip_{2\mu}\int d^4x_3\ S(x_3)e^{ip_3.x_3}\ \gamma^5\hat{\gamma}^\mu\ \int d^4x_2\ S(-x_2)e^{-ip_2.x_2} \\ =&-ip_{2\mu}S(p_3)\ \gamma^5\hat{\gamma}^\mu\ S(p_2)\ \cdot \end{aligned} \tag{3.157}$$

This has to be multiplied by an overall factor $i$ in Eq. 3.155, giving,

$$+p_{2\mu}S(p_3)\ \gamma^5\hat{\gamma}^\mu\ S(p_2)\ \cdot \tag{3.158}$$

Following a similar procedure for the other vertex, $\langle\big(\partial_\mu\bar{\psi}(x)\big)\gamma^5\hat{\gamma}^\mu\psi(x)\psi(x_3)\bar{\psi}(x_2)\rangle$, gives $+ip_{3\mu}S(p_3)\ \gamma^5\hat{\gamma}^\mu\ S(p_2)$ which will be multiplied by $-i$ according to Eq. 3.155. After amputation, *i.e.* multiplying on the left with $S(p_3)^{-1}$ and on the right with $S(p_2)^{-1}$, the tree-level value for this vertex becomes,

$$+\ (p_2+p_3)_\mu\gamma^5\hat{\gamma}^\mu\ , \tag{3.159}$$

corresponding to the diagram in Fig. 3.4.

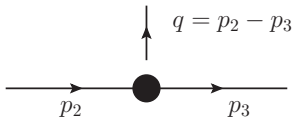


Figure 3.4: Diagram representing the tree level contribution to the operator $\langle\bar{\psi}(x)\hat{\gamma}^\mu\gamma^5 D_\mu\psi(x)\rangle$.

Returning to Eq. 3.155 the contribution to $\langle\bar{\psi}(x)\hat{\gamma}^\mu\gamma^5 D_\mu\psi(x)\psi(x_3)\bar{\psi}(x_2)\rangle$ at tree-level is in fact zero since in the absence of any poles we can simply take $\hat{p}=0$. The 1-loop contribution is then expressed as

$$\Lambda^{(1)}_{\hat{a}\ \text{anom}} = -ig^2C_2(F)\int_k \frac{\gamma_\alpha[\not{p}_3-\not{k}+m](\hat{\not{p}}_2+\hat{\not{p}}_3-2\hat{\not{k}})\gamma^5[\not{p}_2-\not{k}+m]\gamma^\alpha}{k^2[(p_2-k)^2-m^2][(p_3-k)^2-m^2]}\ , \tag{3.160}$$

which corresponds to the diagram:

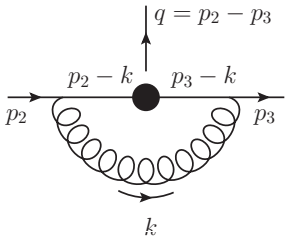


Figure 3.5: Diagram representing one loop contribution to the operator $\langle\bar{\psi}(x)\hat{\gamma}^\mu\gamma^5 D_\mu\psi(x)\rangle$.

The last term in the WI Eq. 3.155 *i.e.* $-2g\langle\bar{\psi}(x)\gamma^5\hat{\gamma}^\mu\not{A}_\mu\psi(x)\psi(x_3)\bar{\psi}(x_2)\rangle$, has

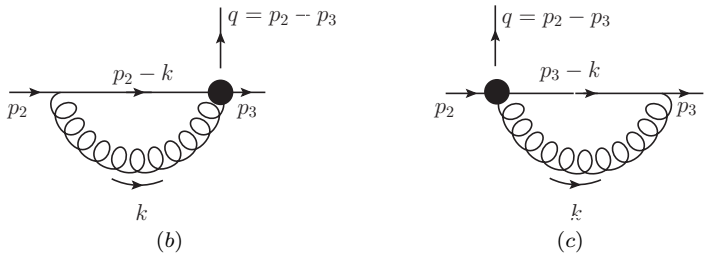


Figure 3.6: Diagrams representing one loop contribution to the operator $-2g\langle\bar{\psi}(x)\tau^a\gamma^5\hat{\gamma}^\mu\mathscr{A}_\mu\psi(x)\psi(x_3)\bar{\psi}(x_2)\rangle$.

its first contribution appearing at 1-loop in the following combination:

$$(-ig)(-2g)\int d^4x\ \delta(x)\ d^4x_2\ e^{-ip_2.x}\ d^4x_3\ e^{ip_3.x}\ d^4z \\ \bar{\psi}(z)\mathscr{A}_\rho(z)\gamma^\rho\psi(z)\bar{\psi}(x)\gamma^5\hat{\gamma}^\mu\mathscr{A}(x)_\mu\psi(x)\psi(x_3)\bar{\psi}(x_2)\ . \tag{3.161}$$

Performing the contractions, setting $x = 0$ using a delta-function and taking the Fourier transform, we get,

$$(2ig^2)\int_p S(p_3)\gamma^\rho S(p_3-p)\gamma^5\hat{\gamma}^\mu S(p_2)\Delta_{\rho\mu}(p)\ . \tag{3.162}$$

For the details of the computation see App. C.7.3. After amputating the vertex by multiplying on the left with $S(p_3)^{-1}$ and on the right with $S(p_2)^{-1}$, we have,

$$\Lambda^{(1)}_{\hat{c}\ \text{anom}} = (2ig^2)(-i)(i)\int_k \frac{\hat{\gamma}_\mu[\not{p}_3 - \not{k} + m]\gamma^5\hat{\gamma}^\mu}{k^2[(p_3-k)^2-m^2]}\ . \tag{3.163}$$

Similarly, for the other equivalent contribution,

$$\Lambda^{(1)}_{\hat{b}\ \text{anom}} = 2ig^2C_2(F)\int_k \frac{\hat{\gamma}_\mu\gamma^5[\not{p}_2 - \not{k} + m]\hat{\gamma}^\mu}{k^2[(p_2-k)^2-m^2]}\ . \tag{3.164}$$

These vertices are shown in Fig. 3.6. We discuss the computation of these vertices in the upcoming sections.

### 3.5.2 Axial and pseudoscalar vertices recomputed

The axial current contribution has to be recomputed using the new convention,

$$\Lambda_{\mathrm{A}}^{(1)\sigma}(p_2,p_3) = -ig^2 C_2(F)\int_k \frac{\gamma_\alpha\left[\not{p}_3 - \not{k}+m\right]\bar{\gamma}^\sigma\gamma^5\left[\not{p}_2-\not{k}+m\right]\gamma^\alpha}{k^2\left[(p_3-k)^2-m^2\right]\left[(p_2-k)^2-m^2\right]}\,. \tag{3.165}$$

Using the previous calculation in the naive case, we know that the coefficients multiplying the scalar and the vector terms in $k$, *i.e.* $K_5^\sigma$ and $K_5^{\sigma,\mu}$ in Eq. 3.114, are finite. This implies that there is no need to recompute these using the new convention since parts proportional to $\hat{\not{p}}_2, \hat{\not{p}}_3$ can be safely set to zero in the absence of any $1/\epsilon$ poles. We therefore need to consider the term in the numerator of the form $k_\mu k_\nu$. Again, the part of the integral proportional to $(\bar{p}_2^\sigma\ \not{p}_2 + \bar{p}_3^\sigma\ \not{p}_3)$ and $(\bar{p}_2^\sigma\ \not{p}_3 + \bar{p}_3^\sigma\ \not{p}_2)$ are finite and we can carry forward the result from the naive case. This shows that we only need to recompute the contribution proportional to $g_{\mu\nu}$ which contains a $1/\epsilon$ pole. The result is:

$$\begin{aligned}\Lambda_{\mathrm{A}}^{(1)\sigma}(p_2,p_3) = \frac{\alpha}{4\pi}C_2(F)\Bigg[A_{\mathrm{A}}\frac{1}{\mu^2}\left(i\epsilon^{\sigma\rho\alpha\beta}\gamma_\rho p_{3\alpha}p_{2\beta}\right) + B_{\mathrm{A}}\gamma^\sigma\gamma^5 + \\ + C_{\mathrm{A}}\frac{1}{\mu^2}\gamma^5\left(p_2^\sigma\ \not{p}_2 + p_3^\sigma\ \not{p}_3\right) + \\ + D_{\mathrm{A}}\frac{1}{\mu^2}\gamma^5\left(p_2^\sigma\ \not{p}_3 + p_3^\sigma\ \not{p}_2\right) + E_{\mathrm{A}}\frac{1}{\mu}\left(p_2^\sigma - p_3^\sigma\right)\Bigg]\,.\end{aligned} \tag{3.166}$$

where coefficients $A_{\mathrm{A}}, C_{\mathrm{A}}, D_{\mathrm{A}}$ and $E_{\mathrm{A}}$ are the same as in Sec. 3.4.8, while the coefficient of $\bar{\gamma}^\sigma\gamma^5$ now becomes,

$$\begin{aligned}B_{\mathrm{A}} = \frac{1}{\epsilon} - \gamma_E + 4 + \frac{1}{3}\Bigg[&-C_0\left(\frac{m^2}{\mu^2}\right)\left(1+8\frac{m^2}{\mu^2}-2\frac{m^4}{\mu^4}\right) \\ &+\left(3-\frac{m^2}{\mu^2}\right)\frac{2m^2}{\mu^2}\log\left(\frac{m^2}{m^2+\mu^2}\right) \\ &+\left(1-4\frac{m^2}{\mu^2}\right)\log\left(\frac{m^2}{\tilde{\mu}^2}\right) - 4\left(1-\frac{m^2}{\mu^2}\right)\log\left(\frac{m^2+\mu^2}{\tilde{\mu}^2}\right) \\ &-\left(1-2\frac{m^2}{\mu^2}\right)\sqrt{1+4\frac{m^2}{\mu^2}}\log\left(\frac{\sqrt{1+4\frac{m^2}{\mu^2}}-1}{\sqrt{1+4\frac{m^2}{\mu^2}}+1}\right)\Bigg]\,.\end{aligned} \tag{3.167}$$

The extra number, "4" above, is the only extra addition to the naive case Eq. 3.167, which means the change in the convention has had a finite, non-zero contribution to the integral.

Similar arguments hold for the pseudoscalar integral using the new convention. The result is similar to Sec. 3.4.7,

$$\Lambda^{(1)}_{\mathrm{P}}(p_2,p_3) = \frac{i\alpha}{4\pi}C_2(F)\left[B_{\mathrm{P}}\left(\gamma^5\right) + E_{\mathrm{P}}\frac{1}{\mu}(\gamma^5)\left(\bar{\not{p}}_2 - \bar{\not{p}}_3\right)\right], \tag{3.168}$$

with a different form factor $B_{\mathrm{P}}$ as compared to Eq. 3.169,

$$B_{\mathrm{P}} = 4\left[\frac{1}{\epsilon} - \gamma_E + \frac{7}{2} - \frac{1}{2}C_0\left(\frac{m^2}{\mu^2}\right) + \frac{m^2}{\mu^2}\log\left(\frac{m^2}{m^2+\mu^2}\right) - \log\left(\frac{m^2+\mu^2}{\tilde{\mu}^2}\right)\right]. \tag{3.169}$$

Again, we see a finite contribution that is different compared to the naive case.

### 3.5.3 Integral $\Lambda^{(1)}_{\hat{a}\ \mathbf{anom}}$

One of the main ingredients in computing

$$\Lambda^{(1)}_{\hat{a}\ \mathrm{anom}} = -ig^2C_2(F)\int_k \frac{\gamma_\alpha[\not{p}_3 - \not{k} + m](\hat{\not{p}}_2 + \hat{\not{p}}_3 - 2\hat{\not{k}})\gamma^5[\not{p}_2 - \not{k} + m]\gamma^\alpha}{k^2[(p_2-k)^2-m^2][(p_3-k)^2-m^2]}, \tag{3.170}$$

is the term containing three $k$s in the numerator,

$$I^{\mu\sigma\nu} = \int_k \frac{k^\mu k^\sigma k^\nu}{k^2[(p_2-k)^2-m^2][(p_3-k)^2-m^2]}\cdot \tag{3.171}$$

This integral is symmetric both under the exchange of $p_2 \leftrightarrow p_3$ and permutations of indices $\mu,\sigma,\nu$. Therefore it is expected to be of the form:

$$\begin{aligned} I^{\mu\sigma\nu} =& A\left[g^{\mu\sigma}(p_2^\nu + p_3^\nu) + g^{\mu\nu}(p_2^\sigma + p_3^\sigma) + g^{\sigma\nu}(p_2^\mu + p_3^\mu)\right] + B\left[p_2^\mu p_2^\sigma p_2^\nu + p_3^\mu p_3^\sigma p_3^\nu\right] \\ &+ C\left[(p_2^\mu p_3^\sigma p_2^\nu + p_2^\nu p_3^\mu p_2^\sigma + p_2^\sigma p_3^\nu p_2^\mu) + (p_3^\mu p_2^\sigma p_3^\nu + p_3^\nu p_2^\mu p_3^\sigma + p_3^\sigma p_2^\nu p_3^\mu)\right]\cdot \end{aligned} \tag{3.172}$$

The constants $A, B$ and $C$ can be determined by appropriately contracting the indices and solving a set of simultaneous equations in the same spirit as Sec. 3.4.3 and Sec. 3.4.4. The full detail of this computation can be found in App. C.7.4. The terms containing two $k$'s in the numerator have a divergent contribution proportional to $g^{\mu\nu}$ as we have seen before, hence have to be computed. The details of the calculations can be seen in App. C.7.5. The final result of $\Lambda^{(1)}_{\hat{a}\ \text{anom}}$ is:

$$\Lambda^{(1)}_{\hat{a}\ \text{anom}} = \frac{\alpha}{4\pi}\gamma^5 C_2(F)\left[\frac{3}{\epsilon}(\hat{\not{p}}_2 + \hat{\not{p}}_3) + 2(\bar{\not{p}}_3 - \bar{\not{p}}_2) + 8m\right]. \tag{3.173}$$

### 3.5.4 Integrals $\Lambda^{(1)}_{\hat{b}\ \textbf{anom}}$ and $\Lambda^{(1)}_{\hat{c}\ \textbf{anom}}$

For the integral $\Lambda^{(1)}_{\hat{b}\ \text{anom}}$ in Eq. 3.164, we use the results Eq. C.81 computed for Eq. C.79. Simplifying the numerator,

$$\begin{aligned}\hat{\gamma}_\mu\gamma^5\bar{\gamma}^\sigma\hat{\gamma}^\mu + \hat{\gamma}_\mu\gamma^5\hat{\gamma}^\sigma\hat{\gamma}^\mu =& \gamma^5\left(\hat{\gamma}_\mu\bar{\gamma}^\sigma\hat{\gamma}^\mu + \hat{\gamma}_\mu\hat{\gamma}^\sigma\hat{\gamma}^\mu\right) = \gamma^5\Big((4-d)\bar{\gamma}^\sigma + (6-d)\hat{\gamma}^\sigma\Big)\\ =& \gamma^5\Big(2\epsilon\bar{\gamma}^\sigma + (2+2\epsilon)\hat{\gamma}^\sigma\Big)\end{aligned} \tag{3.174}$$

Therefore, the term in the numerator with $\not{p}_2$ gives

$$\frac{i\alpha}{4\pi}\gamma^5\left[2\bar{\not{p}}_2 + \frac{2}{\epsilon}\hat{\not{p}}_2\right], \tag{3.175}$$

where the finite part vanishes as $\hat{p}_2 \to 0$. The $-\not{k}$ part gives,

$$-\frac{i\alpha}{4\pi}\gamma^5\left[\bar{\not{p}}_2 + \frac{1}{\epsilon}\hat{\not{p}}_2\right]. \tag{3.176}$$

The $m$ part gives,

$$\frac{i\alpha}{4\pi}\gamma^5\left[\frac{1}{\epsilon} + \text{finite}\right](d-4)m = \frac{i\alpha}{4\pi}\gamma^5(-2m)\ . \tag{3.177}$$

Putting it all together we obtain,

$$\frac{\Lambda^{(1)}_{\hat{b}\ \text{anom}}}{iC_2(F)} = 2\frac{i\alpha}{4\pi}\gamma^5\left[\bar{\not{p}}_2 + \frac{1}{\epsilon}\hat{\not{p}}_2 - 2m\right]. \tag{3.178}$$

For $\Lambda^{(1)}_{\hat{c}\ \text{anom}}$, Eq. 3.163, in the numerator we have the term

$$\begin{aligned}\hat{\gamma}_\mu\bar{\gamma}^\sigma\hat{\gamma}^\mu\gamma^5 + \hat{\gamma}_\mu\hat{\gamma}^\sigma\hat{\gamma}^\mu\gamma^5 =&\gamma^5\big(-\hat{\gamma}_\mu\bar{\gamma}^\sigma\hat{\gamma}^\mu + \hat{\gamma}_\mu\hat{\gamma}^\sigma\hat{\gamma}^\mu\big) = \gamma^5\Big(-(4-d)\bar{\gamma}^\sigma + (6-d)\hat{\gamma}^\sigma\Big)\\ =&\gamma^5\Big(-2\epsilon\bar{\gamma}^\sigma + (2+2\epsilon)\hat{\gamma}^\sigma\Big).\end{aligned} \tag{3.179}$$

The $\bar{\not{p}}_3$ part becomes,

$$\frac{i\alpha}{4\pi}\gamma^5\left[-2\bar{\not{p}}_3 + \frac{2}{\epsilon}\hat{\not{p}}_3\right]. \tag{3.180}$$

The $-\not{k}$ part gives

$$-\frac{i\alpha}{4\pi}\gamma^5\left[-\bar{\not{p}}_3 + \frac{1}{\epsilon}\hat{\not{p}}_3\right], \tag{3.181}$$

and the $m$ part remains the same as the previous case. Therefore,

$$\frac{\Lambda^{(1)}_{\hat{c}\ \text{anom}}}{iC_2(F)} = 2\frac{i\alpha}{4\pi}\gamma^5\left[-\bar{\not{p}}_3 + \frac{1}{\epsilon}\hat{\not{p}}_3 - 2m\right]. \tag{3.182}$$

Adding the two graphs,

$$\Lambda^{(1)}_{\hat{b}\ \text{anom}} + \Lambda^{(1)}_{\hat{c}\ \text{anom}} = \frac{\alpha}{4\pi}C_2(F)\gamma^5\left[-2(\bar{\not{p}}_2 - \bar{\not{p}}_3) - \frac{2}{\epsilon}(\hat{\not{p}}_2 + \hat{\not{p}}_3) + 8m\right]. \tag{3.183}$$

### 3.5.5 Bare axial WI check at 1-loop

The bare axial WI at 1-loop it takes the form

$$\begin{aligned}q.\Lambda^{a(1)}_A(p_1,p_2) =&2mi\Lambda^{a(1)}_P(p_1,p_2) + \tau^a\gamma_5\Sigma(p_2) + \Sigma(p_3)\tau^a\gamma_5\\ &+\Lambda^{a(1)}_{\hat{a}\ \text{anom}} + \Lambda^{a(1)}_{\hat{b}\ \text{anom}} + \Lambda^{a(1)}_{\hat{c}\ \text{anom}}\ .\end{aligned} \tag{3.184}$$

For the propagator terms at 1-loop we have,

$$\begin{aligned}
&\gamma_5\Sigma(p_2)+\Sigma(p_3)\gamma_5 \\
=&\frac{\alpha}{4\pi}\gamma^5 C_2(F)\Bigg[\frac{-\bar{\not{q}}-(\hat{\not{p}}_2+\hat{\not{p}}_3)}{\epsilon} \\
&\qquad +\bar{\not{q}}\left(-1+\gamma_E+\frac{m^2}{\mu^2}+\frac{m^4}{\mu^4}\ln\left(\frac{m^2}{m^2+\mu^2}\right)+\ln\left(\frac{m^2+\mu^2}{\tilde{\mu}^2}\right)\right) \\
&\qquad +2m\left(4\left(\frac{1}{\epsilon}-\gamma_E\right)+6+\frac{4m^2}{\mu^2}\ln\left(\frac{m^2}{m^2+\mu^2}\right)-4\ln\left(\frac{m^2+\mu^2}{\tilde{\mu}^2}\right)\right)\Bigg],
\end{aligned} \tag{3.185}$$

and

$$\begin{aligned}
\bar{q}.\Lambda_A^{\bar{\sigma}(1)} = \frac{\alpha}{4\pi}\gamma^5 C_2(F)\Bigg[\bar{\not{q}}\Bigg(&-\frac{1}{\epsilon}+\gamma_E+\frac{4m^2}{\mu^2}C_0+\log\left(\frac{m^2+\mu^2}{\tilde{\mu}^2}\right)+\frac{m^2}{\mu^2} \\
&+\frac{m^4\log\left(\frac{m^2}{m^2+\mu^2}\right)}{\mu^4}-5\Bigg)+4mC_0\Bigg].
\end{aligned} \tag{3.186}$$

Given the ingredients, it is easy to check that the WI, Eq. 3.184, is indeed satisfied.

## 3.6 The 't Hooft-Veltman modified renormalization conditions

The renormalization conditions for the axial current and the mass have always been derived starting from considering the axial WI and multiplying it with an appropriate projector, *i.e.* $\gamma^5\not{q}$ and $\gamma^5$ respectively. Afterwards, simplifications may be made using the other renormalization conditions such as those for the field and pseudoscalar vertex. Here, we carry the same logic forward. Firstly, note that the conditions for the field, vector, pseudoscalar and scalar renormalization will remain unaltered. However, we have seen that using the 't Hooft-Veltman $\gamma^5$ conventions changes the finite part of the pseudoscalar vertex which means that $Z_P$ will be different; explicitly, starting from

$$\lim_{M_R\to\overline{m}}\frac{1}{12i}\mathrm{Tr}\left[\Lambda_{\mathrm{P},R}\gamma_5\right]\big|_{\mathrm{sym}} = \lim_{m_R\to\overline{m}}\frac{1}{12i}\mathrm{Tr}\left[\frac{Z_{\mathrm{P}}}{Z_q}\Lambda_P\gamma^5\right]\Bigg|_{\mathrm{sym}} = 1, \tag{3.187}$$

we obtain

$$Z_{\rm P} = \Bigg\{ 1 + \frac{\alpha}{4\pi} C_2(F) \Bigg[ -3\left(\frac{1}{\epsilon} - \gamma_E\right) - 13 + 2C_0\left(\frac{m^2}{\mu^2}\right) - \frac{\overline{m}^2}{\mu^2}\left(1 - 4\ln\left(1+\frac{\mu^2}{\overline{m}^2}\right) - \frac{\overline{m}^2}{\mu^2}\ln\left(1+\frac{\mu^2}{\overline{m}^2}\right)\right) + 3\ln\left(\frac{\overline{m}^2+\mu^2}{\tilde{\mu}^2}\right)\Bigg]\Bigg\}. \tag{3.188}$$

Finally let us write out the new set of renormalization conditions for the mass and the axial current. For the axial current we have

$$\begin{aligned} &\lim_{M_R\to\overline{m}} \frac{1}{12q^2}\mathrm{Tr}\left[(q\cdot\Lambda_{\mathrm{A},R} - 2M_R i\Lambda_{\mathrm{P},R})\,\gamma_5\,\not{q}\right]\Big|_{\rm sym} \\ &= \lim_{M_R\to\overline{m}} \frac{1}{12q^2}\mathrm{Tr}\left[\Big(-\gamma_5 iS_R(p_2)^{-1} - iS_R(p_3)^{-1}\gamma_5\Big)\gamma_5\,\not{q}\right]\Big|_{\rm sym} \\ &+ \lim_{M_R\to\overline{m}} \frac{1}{12q^2}\mathrm{Tr}\left[Z_q^{-1}\Big(\Lambda_{\hat{a}\ \mathrm{anom}} + \Lambda_{\hat{b}\ \mathrm{anom}} + \Lambda_{\hat{c}\ \mathrm{anom}}\Big)\gamma_5\,\not{q}\right]\Big|_{\rm sym}\ . \end{aligned} \tag{3.189}$$

The first term on the right hand side is indeed the term that reduces to unity in the naive $\gamma^5$ convention. However, in the 'tHooft-Veltman convention, passing the $\gamma^5$ through the inverse propagator introduces hatted terms corresponding to $\gamma^\mu$ with $\mu \geq 4$. It is important to note that as far as the usual four dimensional, *i.e.* barred, termed are concerned, there is no difference between this condition and what we previously had for the naive case. The extra terms are purely an artefact of the definition of $\gamma^5$. Since we have designed the conditions directly using the bare WI, the hatted terms arising from commuting the $\gamma^5$ with the inverse propagator cancel with the corresponding terms coming from $\Lambda_{\hat{a}\ \mathrm{anom}} + \Lambda_{\hat{b}\ \mathrm{anom}} + \Lambda_{\hat{c}\ \mathrm{anom}}$ order by order in perturbation theory. Note also that these terms are zero at tree-level. More explicitly, the left hand side of Eq. 3.189 at 1-loop now reads

$$\begin{aligned} &\lim_{M_R\to\overline{m}} \frac{1}{12q^2}\mathrm{Tr}\left[(q\cdot\Lambda_{\mathrm{A},R} - 2m_R i\Lambda_{\mathrm{P},R})\,\gamma_5\,\not{q}\right]\Big|_{\rm sym} \\ &= \lim_{M_R\to\overline{m}} \frac{1}{12q^2}\mathrm{Tr}\left[\left(\frac{Z_{\rm A}}{Z_q} q\cdot\Lambda_A - \frac{Z_{\rm P}Z_m}{Z_q} 2im\Lambda_P\right)\gamma^5\not{q}\right]\Big|_{\rm sym} \end{aligned} \tag{3.190}$$

$$= \lim_{M_R\to\overline{m}} \frac{1}{12q^2}\frac{1}{Z_q}\mathrm{Tr}\Bigg\{ Z_{\mathrm{A}}\Bigg( q^2 + \frac{\alpha}{4\pi}C_2(F)q^2\Bigg[\frac{1}{\epsilon} - \gamma_E + 5 - \frac{4m^2}{\mu^2}C_0\left(\frac{m^2}{\mu^2}\right) - \frac{m^2}{\mu^2} - \frac{m^4}{\mu^4}\ln\left(\frac{m^2}{m^2+\mu^2}\right) - \ln\left(\frac{m^2+\mu^2}{\tilde{\mu}^2}\right)\Bigg]\Bigg) + C_2(F)\frac{\alpha}{4\pi}q^2\frac{4m^2}{\mu^2}C_0\left(\frac{m^2}{\mu^2}\right)\Bigg\}\Bigg|_{\mathrm{sym}}, \tag{3.191}$$

where we have taken $Z_m Z_{\mathrm{P}} = 1$, checked to be consistent in Eq. 3.193. The right hand side of Eq. 3.189 takes the form

$$\begin{aligned}
&\lim_{M_R\to\overline{m}} \frac{1}{12q^2}Z_q^{-1}\mathrm{Tr}\Bigg\{ 1 + \frac{\alpha}{4\pi}C_2(F)\Bigg[\frac{+\bar{\not{q}} - (\hat{\not{p}}_2 + \hat{\not{p}}_3)}{\epsilon} \\
&\qquad - \bar{\not{q}}\left(-1 + \gamma_E + \frac{m^2}{\mu^2} + \frac{m^4}{\mu^4}\ln\left(\frac{m^2}{m^2+\mu^2}\right) + \ln\left(\frac{m^2+\mu^2}{\tilde{\mu}^2}\right)\right)\Bigg] \\
&\qquad + \frac{\alpha}{4\pi}C_2(F)\left[\frac{1}{\epsilon}(\hat{\not{p}}_2 + \hat{\not{p}}_3) + 4(\bar{\not{p}}_2 - \bar{\not{p}}_3) + 16m\right]\bar{\not{q}}\Bigg\} \\
&= \lim_{M_R\to\overline{m}} Z_q^{-1}\Bigg\{ 1 + \frac{\alpha}{4\pi}C_2(F)\left[\frac{1}{\epsilon} - \gamma_E + 5 - \frac{m^2}{\mu^2} - \frac{m^4}{\mu^4}\ln\left(\frac{m^2}{m^2+\mu^2}\right) - \ln\left(\frac{m^2+\mu^2}{\tilde{\mu}^2}\right)\right],
\end{aligned} \tag{3.192}$$

where the $Z_q^{-1}$ cancels on both sides of the equation and gives $Z_{\mathrm{A}} = 1$.

Finally, to obtain the mass renormalization and check that $Z_m Z_{\mathrm{P}} = 1$, we modify Eq. 3.45 keeping in mind bare WI with a $\gamma^5$ projector. This gives,

$$\begin{aligned}
&\lim_{M_R\to\overline{m}} \frac{1}{12}\left\{ \mathrm{Tr}\left[q\cdot\Lambda_{\mathrm{A},R}\gamma_5\right]\big|_{q^2=-\mu^2} - 2\ \mathrm{Tr}\left[M_R i\Lambda_{\mathrm{P},R}\gamma_5\right]\big|_{\mathrm{sym}}\right\} \\
&= \lim_{M_R\to\overline{m}} \frac{1}{12}\mathrm{Tr}\ \Big[\Big( -\gamma_5 iS_R(p_2)^{-1} - iS_R(p_3)^{-1}\gamma_5\Big)\gamma_5\Big]\Big|_{\mathrm{sym}} \\
&\quad + \lim_{M_R\to\overline{m}} \frac{1}{12}\mathrm{Tr}\ \Big[Z_q^{-1}\Big(\Lambda_{\hat{a}\ \mathrm{anom}} + \Lambda_{\hat{b}\ \mathrm{anom}} + \Lambda_{\hat{c}\ \mathrm{anom}}\Big)\gamma_5\Big]\Big|_{\mathrm{sym}}\ .
\end{aligned} \tag{3.193}$$

Using $Z_A = 1$, the LHS of Eq. 3.193 at 1-loop becomes,

$$\lim_{M_R \to \overline{m}} Z_q^{-1} \Bigg\{ \frac{\alpha}{4\pi} C_2(F) \Bigg( 4mC_0 \Bigg) + 2Z_M Z_P \Bigg[ m + \frac{\alpha}{4\pi} m \Bigg( 4 \left( \frac{1}{\epsilon} - \gamma_E \right) + 14 - 2C_0 + 4\frac{m^2}{\mu^2} \log \left( \frac{m^2}{m^2 + \mu^2} \right) - 4 \log \left( \frac{m^2 + \mu^2}{\tilde{\mu}^2} \right) \Bigg) \Bigg] \Bigg\}.$$

The RHS of Eq. 3.193 takes the form,

$$\lim_{M_R \to \overline{m}} Z_q^{-1} \Bigg\{ 2m + \frac{\alpha}{4\pi} C_2(F) \Bigg[ - \frac{\hat{\not{p}}_2 + \hat{\not{p}}_3}{\epsilon} + 2m \Bigg( 4 \left( \frac{1}{\epsilon} - \gamma_E \right) + 6 + 4\frac{m^2}{\mu^2} \log \left( \frac{m^2}{m^2 + \mu^2} \right) - 4 \log \left( \frac{m^2 + \mu^2}{\tilde{\mu}^2} \right) \Bigg) \Bigg] + \frac{\alpha}{4\pi} C_2(F) \left[ \frac{\hat{\not{p}}_2 + \hat{\not{p}}_3}{\epsilon} + 16m \right] \Bigg\}. \tag{3.194}$$

Putting them together, $Z_q^{-1}$ on both sides cancels giving $Z_m Z_{\mathrm{P}} = 1$.

## 3.7 Mass non-degenerate scheme

We will now consider the renormalization scheme for the case of non-singlet, mass non-degenerate vertex functions in Minkowski space. Note that according to Eq. 3.5, we collect the two fermion fields in a flavor doublet:

$$\psi = \begin{pmatrix} H \\ \\ l \end{pmatrix}, \quad \overline{\psi} = \begin{pmatrix} \overline{H} & \overline{l} \end{pmatrix}, \tag{3.195}$$

with the non-degenerate mass matrix

$$\mathcal{M} = \begin{pmatrix} M & 0 \\ \\ 0 & m \end{pmatrix}. \tag{3.196}$$

In what follows we will be interested in fermion bilinears of the form $O^+ = \overline{H}\Gamma l$ by choosing the flavor rotation matrix to be $\tau^a = \tau^+ = \frac{\sigma^+}{2} = \frac{1}{2}(\sigma^1 + i\sigma^2)$. For clarity, we will leave the flavor index " + " explicit in the Ward identities, but will suppress it for the rest of the section to keep the notation simple. We have used curly letters $(\mathcal{V}, \mathcal{A}, \mathcal{P}, \mathcal{S})$ to denote the heavy-light bilinears. The vector and axial Ward identities are as follows:

$$q \cdot \Lambda^+_{\mathcal{V}} = (M - m)\Lambda^+_{\mathcal{S}} + iS_H(p_2)^{-1} - iS_l(p_3)^{-1}. \tag{3.197}$$

$$q \cdot \Lambda^+_{\mathcal{A}} = (M + m)i\Lambda^+_{\mathcal{P}} - \gamma_5 iS_H(p_2)^{-1} - iS_l(p_3)^{-1}\gamma_5\,, \tag{3.198}$$

where $M$ and $m$ are masses of the heavy and the light quarks respectively.

### 3.7.1 Modified renormalization conditions

The RI/mSMOM scheme for the heavy-light mixed case is defined by imposing the following set of conditions at some reference mass $\overline{m}$:

$$\lim_{\substack{m_R\to 0\\ M_R\to\overline{m}}} \frac{1}{12q^2}\mathrm{Tr}\left[(q\cdot\Lambda_{\mathcal{V},R} - (M_R - m_R)\Lambda_{\mathcal{S},R})\ \not{q}\right]\big|_{\mathrm{sym}} \tag{3.199}$$

$$= \lim_{\substack{m_R\to 0\\ M_R\to\overline{m}}} \frac{1}{12q^2}\mathrm{Tr}\left[\left(i\zeta^{-1}S_{H,R}(p_2)^{-1} - i\zeta S_{l,R}(p_3)^{-1}\right)\not{q}\right]\,,$$

$$\lim_{\substack{m_R\to 0\\ M_R\to\overline{m}}} \frac{1}{12q^2}\mathrm{Tr}\left[(q\cdot\Lambda_{\mathcal{A},R} - (M_R + m_R)i\Lambda_{\mathcal{P},R})\,\gamma_5\ \not{q}\right]\big|_{\mathrm{sym}}$$

$$= \lim_{\substack{m_R\to 0\\ M_R\to\overline{m}}} \frac{1}{12q^2}\mathrm{Tr}\big[\big(-i\gamma^5\zeta^{-1}S_{H,R}(p_2)^{-1} - i\zeta S_{l,R}(p_3)^{-1}\gamma^5\big)\gamma_5\ \not{q}\big]\,, \tag{3.200}$$

$$\lim_{\substack{m_R\to 0\\ M_R\to\overline{m}}} \frac{1}{12i}\mathrm{Tr}\left[\Lambda_{\mathcal{P},R}\gamma_5\right]\big|_{\mathrm{sym}} \tag{3.201}$$

$$= \lim_{\substack{m_R\to 0\\ M_R\to\overline{m}}} \left\{ \frac{1}{12(M_R + m_R)} \left\{ \mathrm{Tr}\left[-i\zeta^{-1}S_{H,R}(p)^{-1}\right]\big|_{p^2=-\mu^2} - \frac{1}{2}\,\mathrm{Tr}\left[(q\cdot\Lambda_{\mathcal{A},R})\,\gamma_5\right]\big|_{\mathrm{sym}} \right\} +$$

$$\frac{1}{12(M_R+m_R)}\left\{\mathrm{Tr}\left[-i\zeta S_{l,R}(p)^{-1}\right]\big|_{p^2=-\mu^2}-\frac{1}{2}\,\mathrm{Tr}\left[(q\cdot\Lambda_{\mathcal{A},R})\,\gamma_5\right]\big|_{\mathrm{sym}}\right\}\Bigg\}\,. \tag{3.202}$$

where $\zeta$ denotes the ratio of the light to the heavy field renormalizations, i.e. $\zeta=\frac{\sqrt{Z_l}}{\sqrt{Z_H}}$. In the degenerate mass, $\zeta=1$ and the mixed mSMOM prescription reduces to the mSMOM and SMOM one. The renormalization conditions for $Z_l, Z_H$ and $Z_m$ remain unaltered as they are independently determined from the corresponding degenerate, massive and massless schemes of the previous sections. As usual the renormalization conditions are satisfied by the tree level values of the field correlators.

### 3.7.2 Renormalization constants

The properties of the renormalization constants in this scheme are obtained once again from the Ward identities. We multiply the vector Ward identity Eq. 3.197 by $\not{q}$, take the trace and write the bare quantities in terms of the renormalized ones as follows:

$$\begin{aligned}&Z_H^{1/2}Z_l^{1/2}\mathrm{Tr}\left[\frac{1}{Z_{\mathcal{V}}}\,(q\cdot\Lambda_{\mathcal{V},R})\,\not{q}\right]\\ =&Z_H^{1/2}Z_l^{1/2}\mathrm{Tr}\left[\left(i\zeta^{-1}S_{H,R}(p_2)^{-1}-i\zeta S_{l,R}(p_3)^{-1}+\frac{\frac{M_R}{Z_M}-\frac{m_R}{Z_m}}{Z_{\mathcal{S}}}\Lambda_{\mathcal{S},R}\right)\not{q}\right]\,.\end{aligned} \tag{3.203}$$

Using Eq. C.154 we get

$$\begin{aligned}&\left(\frac{1}{Z_{\mathcal{V}}}-1\right)\mathrm{Tr}\left[\left(i\zeta^{-1}S_{H,R}(p_2)^{-1}-i\zeta S_{l,R}(p_3)^{-1}\right)\not{q}\right]\\ =&\left(\frac{-(M_R-m_R)}{Z_{\mathcal{V}}}+\frac{\frac{M_R}{Z_M}-\frac{m_R}{Z_m}}{Z_{\mathcal{S}}}\right)\mathrm{Tr}\left[\Lambda_{\mathcal{S},R}\,\not{q}\right]\,,\end{aligned} \tag{3.204}$$

which has a solution when $Z_{\mathcal{V}}=1$ and

$$Z_{\mathcal{S}}=\frac{\frac{M_R}{Z_M}-\frac{m_R}{Z_m}}{M_R-m_R}\,. \tag{3.205}$$

For the axial current we follow a similar procedure, starting from the bare mixed axial Ward identity Eq. 3.198. Multiplying by $\gamma^5\not{q}$ and $\gamma_5$ respectively

and taking the trace gives two independent equations. In the first case, we use Eq. C.156 and obtain

$$\begin{aligned}&(1-\frac{1}{Z_{\mathcal{A}}})\mathrm{Tr}\left[\left(-i\gamma^5\zeta^{-1}S_{H,R}(p_2)^{-1}-i\zeta S_{l,R}(p_3)^{-1}\gamma^5\right)\gamma^5\not{q}\right]\\&=\left(\frac{M_R+m_R}{Z_{\mathcal{A}}}-\left(\frac{M_R}{Z_M Z_{\mathcal{P}}}+\frac{m_R}{Z_m Z_{\mathcal{P}}}\right)\right)Tr\left[\left(i\Lambda_{\mathcal{P}}\right)\gamma^5\not{q}\right]\ .\end{aligned} \tag{3.206}$$

The latter equation is satisfied by $Z_{\mathcal{A}}=1$ and

$$Z_{\mathcal{P}}=\frac{\frac{M_R}{Z_M Z_{\mathcal{P}}}+\frac{m_R}{Z_m Z_{\mathcal{P}}}}{M_R+m_R}\,. \tag{3.207}$$

Note that in the degenerate mass limit, we recover $Z_m Z_{\mathrm{P}}=1$.

In the second case, where we take the trace with $\gamma^5$, we make use of Eq. C.157, giving

$$\begin{aligned}&\left(\frac{1}{Z_{\mathcal{A}}}-\frac{\left(\frac{M_R}{Z_M Z_{\mathcal{P}}}+\frac{m_R}{Z_m Z_{\mathcal{P}}}\right)}{M_R+m_R}\right)\mathrm{Tr}\left[\left(q\cdot\Lambda_{\mathcal{A},R}\right)\gamma^5\right]\\&=\left(1-\frac{\left(\frac{M_R}{Z_M Z_{\mathcal{P}}}+\frac{m_R}{Z_m Z_{\mathcal{P}}}\right)}{M_R+m_R}\right)\left(\mathrm{Tr}\left[-i\zeta^{-1}S_{H,R}(p_2)^{-1}-i\zeta S_{l,R}(p_3)^{-1}\right]\right)\ ,\end{aligned} \tag{3.208}$$

which has solutions $Z_{\mathcal{A}}=1$ and $Z_{\mathcal{P}}$ as in Eq. 3.207. One can easily check that this solution is unique.

### 3.7.3 Finiteness of the $\zeta$ ratio

We need to show that the ratio $\zeta$ is finite since it appears together with the renormalized propagators on the right hand sides of Eq. C.154 and Eq. C.156 while the left hand sides of these equations only contain renormalized vertices and mass. For $\zeta=\frac{\sqrt{Z_l}}{\sqrt{Z_H}}$ to be finite, the coefficient of the divergent part $Z_H$ has to be mass independent in order to cancel with the same term in $Z_l$. We will argue that this has to be the case order by order in perturbation theory.

The fermion propagator can be written as:

$$S(p) = \frac{i}{\not{p} - m + i\epsilon - \Sigma(p)}\,, \tag{3.209}$$

where the self-energy $\Sigma(p)$ is decomposed into

$$\Sigma(p) = \not{p}\Sigma_V(p^2) + m\Sigma_S(p^2)\,. \tag{3.210}$$

Assuming that the theory is regulated using dimensional regularization, let us examine all possible coefficients multiplying the divergent terms that can appear in the self-energy at any given order in perturbation theory. Note that $\Sigma_V(p^2)$ and $\Sigma_S(p^2)$ are dimensionless scalars, which means the terms appearing in the coefficient of the divergent part can only be a function of $\ln\left(\frac{p^2}{m^2}\right)$, $\frac{p^2}{m^2}$, $\frac{m^2}{p^2}$ or a number.

As argued in Ref. [86], all UV divergences can be subtracted using *local* counter-terms only. In other words, the field renormalization used to remove the divergences cannot contain terms which are functions of $\ln\left(\frac{p^2}{m^2}\right)$ and $\frac{m^2}{p^2}$, since these are non-local. The term $\frac{p^2}{m^2}$ cannot occur either since it is IR divergent in the limit $m \to 0$ whereas we had used off-shell conditions from the beginning and therefore do not expect any IR divergences. The only remaining option is a coefficient proportional to 1 which has be the same number in both the massive and massless cases since in the absence of IR divergences $Z_H$ to reduces to $Z_l$.

Another way to argue that the divergent part of the massive self-energy has to be mass independent is the fact that a massless renormalization scheme removes all the divergences. Therefore $Z_H$ and $Z_l$ must have the same coefficient for their divergent terms as argued in Ref. [87].

## 3.8 Lattice regularization

We start this section by showing that, when dealing with composite operators, power divergent mixings with lower dimensional operators are independent of the renormalization scale $\mu$, following Ref. [88]. This is true order-by-order in perturbation theory. We then discuss the statement in the case of chiral symmetry being broken by a regulator which appears as part of the axial WI.

### 3.8.1 Power divergent operators

Consider a composite operator $O(x)$ which we need to renormalize in order to make it finite. In this process the operator will mixing with other equal or lower dimensional operators with the same symmetry properties. For simplicity, we take an example of an operator $O(x)$ that only mixes with another lower dimensional operator $\tilde{O}(x)$:

$$O_R(x) = Z_O \left[ O(x) + \frac{\tilde{Z}}{a}\tilde{O}(x) \right] \cdot \tag{3.211}$$

The coefficients $Z_O$ and $\tilde{Z}$ are dimensionless and are chosen such that the Green's function

$$G^{(O_R,n)}(x, x_1, ..., x_n) = \left[Z_\phi(g_0, a\mu)\right]^{n/2} \langle O_R \phi_0(x_1)...\phi_0(x_n)\rangle \ , \tag{3.212}$$

is finite for $a \to 0$ and a massless theory is assumed. We could then apply the Callan-Symanzik differential operator, $\mu\frac{d}{d\mu}|_{g_0,a}$ on both sides of the above equation. The RHS of Eq. 3.212 gives,

$$\begin{aligned}
&\frac{n}{2}\mu\frac{dZ_\phi}{d\mu}Z_\phi^{n/2-1}\langle O_R(x)\phi_0(x_1)...\phi_0(x_n)\rangle \\
&+\left[\mu\frac{d}{d\mu}Z_O\right] Z_O^{-1} Z_O Z^{n/2}\langle O(x)\phi_0(x_1)...\phi_0(x_n)\rangle \\
&+Z_\phi^{n/2}\frac{Z_O}{a}\left[\mu\frac{d}{d\mu}\tilde{Z}\right]\langle\tilde{O}(x)\phi_0(x_1)...\phi_0(x_n)\rangle \\
&= \left(n\gamma_\phi(g) + \gamma_O(g)\right) G^{(O_R,n)}(x, x_1, ..., x_n) + Z_\phi^{n/2}\frac{Z_O}{a}\left[\mu\frac{d}{d\mu}\tilde{Z}\right]\langle O_R\phi_0(x_1)...\phi_0(x_n)\rangle \ ,
\end{aligned} \tag{3.213}$$

where $\gamma_\phi(g) \equiv \frac{1}{2}\mu\frac{d}{d\mu}|_{g_o,a}\log(Z_\phi(g_0,a))$ and $\gamma_O(g) \equiv \mu\frac{d}{d\mu}|_{g_o,a}\log(Z_O(g_0,a))$. The LHS becomes,

$$\left(\mu\frac{\partial}{\partial\mu} + \beta(g)\frac{\partial}{\partial g}\right) G^{(O_R,n)}(x, x_1, ..., x_n) \ , \tag{3.214}$$

which is a finite quantity. This would imply that the right hand side must also be finite and so the term proportional to $1/a$, which diverges as $a \to 0$, must vanish:

$$\mu\frac{d}{d\mu}|_{g_0,a}\ \tilde{Z} = 0 \cdot \tag{3.215}$$

Hence, power divergent mixings with lower dimensional operators are independent of the renormalization scale $\mu$ and do not contribute to anomalous dimensions.

### 3.8.2 Axial WI with operator insertions on the lattice

Continuum chiral symmetry is broken when lattice is used as a regulator. For Wilson fermions the breaking arises from higher-dimensional operators that are present in the action [78]. For DWF fermions the breaking corresponds to finiteness of the fifth dimension and is exponentially suppressed [49]. Generically, we expect the non-singlet axial WI on the lattice to be of the form:

$$\begin{aligned}\nabla^*_\mu \langle A^a_\mu(x)\psi(y)\bar{\psi}(z)\rangle &= 2m\langle P^a(x)\psi(y)\bar{\psi}(z)\rangle + \text{contact terms} \\ &+\langle X^a(x)\psi(y)\bar{\psi}(z)\rangle\,,\end{aligned} \tag{3.216}$$

such that the chiral symmetry breaking term arising from regularization, $X^a(x) = aO_5(x)$, is at least of order $a$. The reason for this is that if the lattice discretized quantities, such as the Dirac operator, are to agree with those in the classical continuum limit, the chiral symmetry breaking terms due to this discretization must go to zero as $a \to 0$. The operators appearing in Eq. 3.216 need to be renormalized. Power divergences arising from mixing of the higher dimensional operator, $O_5(x)$, are required to be subtracted. In this case [88]:

$$O^a_{5R}(x) = Z_5\left[O^a_5(x) + \frac{\overline{m}}{a}P^a(x) + \frac{Z_\mathrm{A}-1}{a}\nabla^*_\mu A^a_\mu(x)\right]. \tag{3.217}$$

As we have seen in Sec. 3.8.1, such power divergences do not depend on the renormalization scale $\mu$. Hence the axial current renormalization $Z_\mathrm{A}$ can only depend on the coupling, the regulator and the mass of the fermions involved, entering as a dimensionless parameter $am$, *i.e.* ,

$$A^a_{R,\mu} = Z_\mathrm{A}\,(g, am)\,A^a_\mu\,\cdot \tag{3.218}$$

The same argument holds if we use local currents rather than the conserved one on the lattice. Again, the local current is expected to be different from the conserved one by operators appearing at $\mathcal{O}(a)$. These operators need to be renormalized as well but the final results yields a $Z_\mathrm{A}$ that is independent of $\mu$.

## 3.9 WI for domain wall fermions

The non-singlet vector and axial Ward Identities (WI) in domain wall frame work has been derived for Shamir [55] and Möbius fermions [64]. We are not going to reproduce all the results here, but merely summarize the main points.

Given the choices of simulation parameters such as the heavy valence quark masses $am$, the extent of the fifth dimension $L_s$, and the negative Wilson mass $M_5$, we quote the result for the axial WI:

$$a\Delta_\mu^- \langle P(x) A_\mu^{\text{cons}}(y)\rangle = \langle P(x)\big(2amP(y) + 2J_{5q}(y)\big)\rangle, \tag{3.219}$$

where $P(x) = \bar{q}(x)\gamma^5 q(x)$ is the pseudoscalar density, with $q(x)$ being the surface 4-D fields. $A_\mu^{\text{cons}}(y)$ is the domain wall 5-D conserved axial current, which depends on the link between the two sites $x$ and $x+\mu$. $\Delta_\mu^-$ is the lattice backward derivative and $am$ is the bare quark mass in lattice units. The quantity $J_{5q}$ is the pseudoscalar density of the center of the 5th dimensions. Explicit expressions for these quantities can be found in [55, 89]. The *residual mass*, which provides an estimate of residual chiral symmetry breaking due to finite $L_s$, is defined as:

$$am_{\text{res}} = \frac{\sum_{\mathbf{x}} \langle J_{5q}(x) P(0)\rangle}{\sum_{\mathbf{x}} \langle P(x) P(0)\rangle} \ . \tag{3.220}$$

We expect the renormalization factors for conserved quantities such as vector and axial currents satisfying the corresponding WIs, to be independent of scale $\mu$. More details have been discussed in Sec. 3.8.2. Often, in lattice simulations, local currents are also simulated and are later used to extract the relevant renormalization constants. These local currents differ from the conserved ones by operators appearing at $\mathcal{O}(a)$, see for example [78] for Wilson fermions. For DWF, $Z_{A^{\text{cons}}} = 1 + \mathcal{O}(\text{mres})$ and the renormalization constant for the local 4-D current $A_\mu^a = \bar{q}(x)\gamma_\mu\gamma_5\tau^a q(x)$, defined on the lattice sites $x$ can be extracted via the ratio:

$$Z_{A^{\text{local}}} \approx \frac{Z_{A^{\text{local}}}}{Z_{A^{\text{cons}}}} = \frac{\langle \sum_{\boldsymbol{x}} A^{\text{cons}}(\boldsymbol{x}, t) P(0)\rangle}{\langle \sum_{\boldsymbol{x}} A^{\text{local}}(\boldsymbol{x}, t) P(0)\rangle} \ . \tag{3.221}$$

The conserved and local current correlation functions,

$$C\left(t+\frac{1}{2}\right) = \langle \sum_{\boldsymbol{x}} A^{\text{cons}}(\boldsymbol{x},t)P(0)\rangle \ , \tag{3.222}$$

and

$$L(t) = \langle \sum_{\boldsymbol{x}} A^{\text{cons}}(\boldsymbol{x},t)P(0)\rangle \ , \tag{3.223}$$

are not defined at the same temporal coordinate, with the former being defined at the midpoint of the links and the latter and the sites. By taking appropriate ratios of the two, $\mathcal{O}(a)$ terms can be removed, whilst also reducing the error at $\mathcal{O}(a^2)$ level [64, 89]:

$$Z_{\text{A}}^{\text{local}} = \frac{1}{2}\left[\frac{C(t-1/2)+C(t+1/2)}{2L(t)} + \frac{2C(t+1/2)}{L(t-1)+L(t+1)}\right]. \tag{3.224}$$

## 3.10 Numerical implementation for mSMOM

In lattice studies involving $D$- and $B$-mesons, the renormalization of the axial current is of particular importance since it is required to normalize correctly the matrix element entering the computation of the decay constant. For example, the decay constants of $D$-mesons $f_D$ and $f_{D_s}$ are determined using

$$\langle 0|A^{\mu}_{cq}|D_q(p)\rangle = f_{D_q} p^{\mu}_{D_q},$$

where $q = d, s$ and the axial current $A^{\mu}_{cq} = \bar{c}\gamma_{\mu}\gamma_5 q$ has to be renormalized. Since the quark content contains a heavy and a light quark, we can use the mass-non-degenerate mSMOM scheme introduced in Sec. 3.7. The renormalization conditions in Euclidean space are specified in App. C.8. Our aim is to extract the axial current renormalization $Z_{\mathcal{A}}$ for the mixed heavy-light vertex function. We start by writing all the ingredients needed before giving the final answer. The field renormalizations $Z_l$ and $Z_H$ are computed using SMOM and mSMOM schemes respectively. If the *local* axial current is simulated on the lattice, the corresponding renormalization factor, $Z_{\text{A}^{\text{local}}}$, for the heavy-heavy and light-light vertex functions can be extracted by taking appropriate ratios of the

respective local and conserved hadronic expectations values. Note that the correlations functions of the local and conserved axial currents only differ by finite contributions which vanish in continuum limit.

Here we will now take the assumption that both quarks are constructed with chiral fermion actions, for which an explicit representation of their partially conserved, point split, axial current is available [64, 89]. We will use this to renormalize the mass degenerate local axial current bilinear operators via the WI as a component in our numerical strategy to determine the renormalization of the mixed axial current. For domain wall fermions $Z_{\mathrm{A}}^{\mathrm{local}}$ is obtained by fitting Eq. 3.224 to a constant in the temporal extent. To obtain $Z_M$, we use the mSMOM renormalization condition Eq. C.149 to write

$$Z_M = \frac{Z_H^{-1}}{12M} \left\{ \mathrm{Tr}\left[S(p)^{-1}\right]\big|_{p^2=-\mu^2} + \frac{1}{2} Z_{\mathrm{A}}\, \mathrm{Tr}\left[(iq\cdot\Lambda_{\mathrm{A}})\,\gamma_5\right]\big|_{\mathrm{sym}} \right\} . \tag{3.225}$$

where $Z_{\mathrm{A}}$ is the renormalization constant for the heavy-heavy local current, if that is chosen, and is computed as in Eq. 3.224. The trace of the bare vertex functions and the propagators with an appropriate projector is numerically evaluated on the lattice. Similarly for $Z_m$, which is obtained from the SMOM scheme and the corresponding value of $Z_A$ for the light-light current. The renormalization constant for the mass degenerate pseudoscalar density, $Z_{\mathrm{P}}$ which can be obtained using Eq. C.148 and Eq. C.152 in the mSMOM scheme:

$$Z_{\mathrm{P}} = \frac{i}{p^2} \frac{\mathrm{Tr}\left[iS(p)^{-1}\ \not{p}\right]\big|_{p^2=\mu^2}}{\mathrm{Tr}\left[\Lambda_{\mathrm{P}}\gamma_5\right]\big|_{\mathrm{sym}}} . \tag{3.226}$$

Now, we can write down the equation which allows us to extract $Z_{\mathcal{A}}$. Recall that curly letters refer to heavy-light mixed vertices. From the renormalization conditions stated in Eq. C.151 and Eq. C.156 we have

$$\left(\frac{C_{\mathcal{A}(Mm)} + C_{Mm\mathcal{P}}}{\Delta_{H-L}}\right)_{\mathrm{mixed}} = 1 = \Big(C_{\mathrm{A}(MM)} + C_{M\mathrm{P}}\Big) C_{\mathrm{A}(mm)} , \tag{3.227}$$

where the numerator of the left hand side contains the heavy-light mixed

vertex functions

$$C_{\mathcal{A}(Mm)} = \lim_{\substack{m_R\to 0\\ M_R\to\bar{m}}} \frac{1}{12q^2}\mathrm{Tr}\left[q\cdot\Lambda_{\mathcal{A},R}\gamma_5\ \not{q}\right]\big|_{\mathrm{sym}} \quad , \tag{3.228}$$

$$C_{Mm\mathcal{P}} = \lim_{\substack{m_R\to 0\\ M_R\to\bar{m}}} \frac{1}{12q^2}\mathrm{Tr}\left[(M_R+m_R)\Lambda_{\mathcal{P},R}\gamma_5\ \not{q}\right]\big|_{\mathrm{sym}} \ , \tag{3.229}$$

and the difference between the inverse propagators

$$\Delta_{H-L} = \lim_{\substack{m_R\to 0\\ M_R\to\bar{m}}} \frac{1}{12q^2}\mathrm{Tr}\left[\left(+i\gamma^5\zeta^{-1}S_{H,R}(p_2)^{-1} + i\zeta S_{l,R}(p_3)^{-1}\gamma^5\right)\gamma_5\ \not{q}\right] = \frac{1}{2}\left(\zeta^{-1}+\zeta\right). \tag{3.230}$$

On the right hand side of Eq. 3.227 we have the heavy-heavy vertex functions,

$$C_{\mathrm{A}(MM)} = \lim_{M_R\to\bar{m}} \frac{1}{12q^2}\mathrm{Tr}\left[q\cdot\Lambda_{\mathrm{A},R}\gamma_5\ \not{q}\right]\big|_{\mathrm{sym}} \quad , \tag{3.231}$$

$$C_{M\mathrm{P}} = \lim_{M_R\to\bar{m}} \frac{1}{12q^2}\mathrm{Tr}\left[2M_R\Lambda_{\mathrm{P},R}\gamma_5\ \not{q}\right]\big|_{\mathrm{sym}} \ , \tag{3.232}$$

and the light-light vertex function

$$C_{\mathrm{A}(mm)} = \lim_{m_R\to 0} \frac{1}{12q^2}\mathrm{Tr}\left[q\cdot\Lambda_{\mathrm{A},R}\gamma_5\ \not{q}\right]\big|_{\mathrm{sym}} \quad . \tag{3.233}$$

The quantity $\zeta$ appearing in $\Delta_{H-L}$ is computed using the renormalization conditions for the light and heavy fields Eq. C.148 and taking the ratio:

$$\zeta = \left(\frac{\mathrm{Tr}\left[iS_l(p)^{-1}\ \not{p}\right]\big|_{p^2=\mu^2}}{\mathrm{Tr}\left[iS_H(p)^{-1}\ \not{p}\right]\big|_{p^2=\mu^2}}\right)^{1/2} . \tag{3.234}$$

We rewrite the renormalized quantities in terms of the bare ones. Note that the aim is to extract $Z_{\mathcal{A}}$. On the left hand side of Eq. 3.227 we have

$$Z_H^{-1/2}Z_l^{-1/2}\left(\mathrm{Tr}\left[\left(Z_{\mathcal{A}}\ q\cdot\Lambda_{\mathcal{A}} + (Z_M M + Z_m m)Z_{\mathcal{P}}\Lambda_{\mathcal{P}}\right)\gamma_5\ \not{q}\right]\big|_{\mathrm{sym}}\right), \tag{3.235}$$

with $Z_l$ and $Z_H$ are already computed using SMOM and mSMOM schemes

respectively, together with $\Delta_{H-L}$ which we have computed using Eq. 3.234.

Let us now focus on the right hand side of Eq. 3.227,

$$Z_H^{-1} Z_l^{-1} \text{ Tr } [(Z_{\text{A}}\ q \cdot \Lambda_{\text{A}} + Z_M Z_{\text{P}}\ 2M\Lambda_{\text{P}})\,\gamma_5\ \ \not{q}]|_{\text{sym}}\Big|_{\text{HH}} \text{ Tr } [(Z_{\text{A}}\ q \cdot \Lambda_{\text{A},R})\,\gamma_5\ \ \not{q}]|_{\text{sym}}\Big|_{\text{ll}} \ . \tag{3.236}$$

Therefore, all the quantities appearing in Eq. 3.227 are known apart from two, $Z_{\mathcal{A}}$ which is the main quantity we are looking for and $Z_{\mathcal{P}}$, which are yet to be extracted. They can both be obtained by solving the set of simultaneous equations using Eq. 3.227 and the renormalization condition for the pseudoscalar Eq. C.157:

$$\begin{cases} C_{\mathcal{A}} Z_{\mathcal{A}} + C_{\mathcal{P}} Z_{\mathcal{P}} = C \ , \\ C'_{\mathcal{A}} Z_{\mathcal{A}} + C'_{\mathcal{P}} Z_{\mathcal{P}} = C' \ , \end{cases} \tag{3.237}$$

with

$$C_{\mathcal{A}} = Z_H^{-1/2} Z_l^{-1/2} \left( \text{Tr } [(q \cdot \Lambda_{\mathcal{A}})\,\gamma_5\ \ \not{q}]|_{\text{sym}} \right) \frac{2}{\zeta^{-1} + \zeta} \ , \tag{3.238}$$

$$C_{\mathcal{P}} = Z_H^{-1/2} Z_l^{-1/2} \left( \text{Tr } [((Z_M M + Z_m m) Z_{\mathcal{P}} \Lambda_{\mathcal{P}})\,\gamma_5\ \ \not{q}]|_{\text{sym}} \right) \frac{2}{\zeta^{-1} + \zeta} \ , \tag{3.239}$$

$$C = \Big( C_{\text{A}(MM)} + C_{M\text{P}} \Big) C_{\text{A}(mm)} \ . \tag{3.240}$$

where all the ingredients in $C$ have already been computed. Together with,

$$C'_{\mathcal{A}} = -\text{ Tr } [(iq \cdot \Lambda_{\mathcal{A}})\,\gamma_5]]_{\text{sym}} \ , \tag{3.241}$$

$$C'_{\mathcal{P}} = \frac{1}{12i} \text{Tr } [\Lambda_{\mathcal{P}} \gamma_5]]_{\text{sym}} \ , \tag{3.242}$$

$$C' = \frac{1}{12(M_R + m_R)} \left\{ \text{Tr } \left[ S_H(p)^{-1} \right]\big|_{p^2 = -\mu^2} + \text{Tr } \left[ S_l(p)^{-1} \right]\big|_{p^2 = -\mu^2} \right\} \ . \tag{3.243}$$

Putting then all together, Eq. 3.237 is solved to obtain $Z_{\mathcal{P}}$ and $Z_{\mathcal{A}}$.

## 3.11 Lattice results for NPR

As mentioned earlier, in order to describe continuum physics, quantities regulated on the lattice have to be renormalized before the cut-off is removed. One such quantity, in the case of the charm project, is the axial current matrix element from which the decay constant is extracted. This can be done using in massless renormalization scheme, RI/SMOM, conditions if the conserved current is used. However, since we have simulated the local axial current, we would need to extract $Z_{\mathrm{A}}$ according to Eq. 3.224. The results are shown in Sec. 3.11.1. We then present results for the amputated bilinear vertex functions, in the RI/SMOM scheme, and discuss some of their features. Finally, we discuss the renormalization of the 4-quark operator in RI/SMOM and its matching the the MS-bar scheme.

### 3.11.1 Axial current renormalization

Table 3.1 shows the results for the local light-light axial vertex function renormalization, for all the ensembles, according to Eq. 3.224. These results are in agreement with their previous determinations, Ref. [64]. The renormalization constants are used to renormalize the corresponding axial current matrix element required to compute the decay constants. An example of a fit to a constant for $Z_{\mathrm{A}}(t)$ in the light-light limit, for the C0 ensemble, is shown in Fig. 3.7. Given that we have used a mixed action current, in the sense that a different value of $M_5$ has been used for the light and strange quarks *i.e.* $M_5 = 1.8$ as compared with the heavy quarks *i.e.* $M_5 = 1.6$, the usual domain wall axial Ward identity Eq. 3.219 is not satisfied. In the free theory, this modification in the action imposes a modest change, in for example the fermion propagator, appearing at next to leading order *i.e.* $\mathcal{O}(a^2)$. As a result, one might hope that the impact on the renormalization constants is small. To measure this difference, we compute the projected amputated axial vertex function, denoted by $\mathcal{P}[\Lambda_{\mathrm{A}}]$, in the non-exceptional RI/SMOM scheme for the following three cases where both legs of the vertex have $M_5 = 1.6$ or both have $M_5 = 1.8$ or when one side has $M_5 = 1.6$ and the other has $M_5 = 1.8$. We then take the ratio of these. The deviation from unity is taken has a systematic error associated with the *mixed* choice in the action. The details of this measurement are presented in Sec. 3.11.2.

| Ensemble | $Z_{\mathrm{A}}^{ll}$ |
|---|---|
| C0 | 0.711970(66) |
| C1 | 0.71721(12) |
| C2 | 0.71790(10) |
| M0 | 0.743441(37) |
| M1 | 0.744868(85) |
| M2 | 0.745190(84) |
| F1 | 0.761108(34) |

Table 3.1: Axial vertex renormalization factor $Z_{\mathrm{A}}$ for all the ensembles. The results are obtained by fitting time dependence in Eq. 3.224 to a constant. The fit for the C0 ensemble has been plotted in Fig. 3.7 as an example.

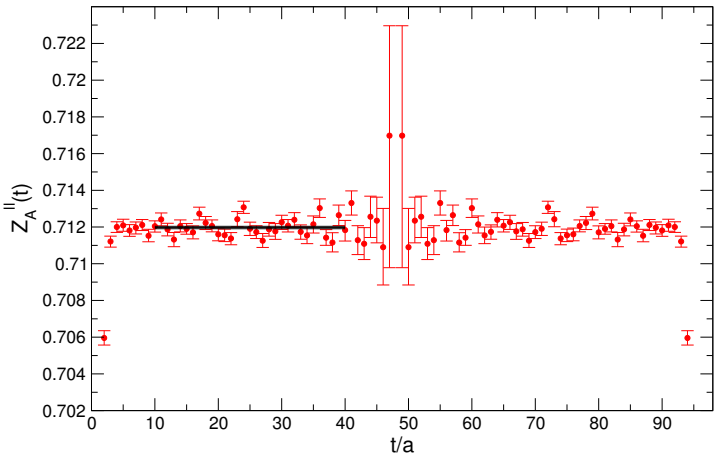


Figure 3.7: $Z_{\mathrm{A}}$ fit on the C0 ensemble. That data is folded with respect to the middle of the time extent.

### 3.11.2 Bilinear vertex functions

In this section, we describe the steps involved in generating the projected amputated vertex functions. We take the axial vertex as a particular example. The process for the other vertices is similar. We then present the numerical results for some of the vertex functions and the renormalization constants extracted.

The projected axial vertex functions are generated according to the SMOM renormalization condition Eq. 3.33:

$$\lim_{m_R \to 0} \frac{1}{12q^2} \mathrm{Tr}\left[(q \cdot \Lambda_{\mathrm{A},R})\, \gamma_5\, \not{q}\right]\big|_{\mathrm{sym}} = 1, \tag{3.244}$$

where $\Lambda_{\mathrm{A},R}$ is the amputated axial vertex function and the subscript $R$, as before,

denotes a renormalizzed quantity. The momentum $q$ out of the vertex satisfies the symmetric non-exceptional condition $p_2^2 = p_2^3 = q^2$. The momenta are determined by

$$ap_\mu = n_\mu \frac{2\pi}{L_\mu/a} \ , \tag{3.245}$$

for every lattice size $L$ such that the magnitude of $p$ is around 2 GeV for an integer $n$. Note that in order to reach the intermediate momenta we use twisting [90–92]:

$$ap_\mu = \left(n_\mu + \frac{\theta_\mu}{2}\right) \frac{2\pi}{L_\mu/a} \ , \tag{3.246}$$

with some details discussed in App. B.4. Eq. 3.244 can be written in terms of the bare amputated vertex function, the field renormalization $Z_q$ and the axial operator renormalization $Z_A$ as follows,

$$\lim_{m_R \to 0} \frac{1}{12q^2} \frac{Z_{\rm A}}{Z_q} {\rm Tr}\left[(q \cdot \Lambda_{\rm A})\, \gamma_5 \not{q}\right]\Big|_{\rm sym} = 1 \ . \tag{3.247}$$

The bare amputated projected vertex:

$$\mathcal{P}[\Lambda_A] \equiv \lim_{m_R \to 0} \frac{1}{12q^2} {\rm Tr}\left[(q \cdot \Lambda_{\rm A})\, \gamma_5 \not{q}\right]\Big|_{\rm sym} \ , \tag{3.248}$$

is what is computed numerically on the lattice, for equal light quark masses , assumed to be sufficiently close to the chiral limit.

In our case, the measurement of $\mathcal{P}[\Lambda_A]$ has been taken on each of the ensembles C2, M1 and F1. Tables 3.2, 3.3 and 3.4 present the ratios of $\mathcal{P}[\Lambda_{\rm A}]$, for different combinations of actions i.e. $(M_5^1, M_5^2) = (1.8, 1.8), (1.6, 1.8), (1.6, 1.6)$ at around 2 GeV. The data has been generated using ten gauge field configurations which leads to sufficiently precise results. We see that the ratio $\frac{\mathcal{P}[\Lambda_{\rm A}](1.8,1.8)}{\mathcal{P}[\Lambda_{\rm A}](1.6,1.6)}$ on each of the ensembles has the largest deviation from unity as compared to the other ratio combinations, which is expected since both the quark fields entering the bilinear have different actions between the numerator and the denominator.

The main feature emerging from this study is that the deviation from unity is at most of order 0.4% across a range of momenta around 2 GeV. This is negligible on the scale of our other uncertainties and for the purposes of the present charm

| $(ap)^2$ | $p\,[\mathrm{GeV}]$ | $\frac{\mathcal{P}[\Lambda_\mathrm{A}](1.8,1.8)}{\mathcal{P}[\Lambda_\mathrm{A}](1.6,1.6)}$ | $\frac{\mathcal{P}[\Lambda_\mathrm{A}](1.6,1.8)}{\mathcal{P}[\Lambda_\mathrm{A}](1.6,1.6)}$ | $\frac{\mathcal{P}[\Lambda_\mathrm{A}](1.8,1.8)}{\mathcal{P}[\Lambda_\mathrm{A}](1.6,1.8)}$ |
|---|---|---|---|---|
| 1.037 | 1.817 | 0.996816(35) | 0.998149(32) | 0.998664(12) |
| 1.133 | 1.900 | 0.996878(41) | 0.998180(33) | 0.998695(14) |
| 1.234 | 1.982 | 0.996943(37) | 0.998220(29) | 0.998721(17) |
| 1.339 | 2.065 | 0.997009(31) | 0.998263(23) | 0.998743(17) |
| 1.448 | 2.148 | 0.997084(28) | 0.998312(20) | 0.998770(15) |

Table 3.2: The ratios of projected amputated vertex function for the axial currents with different actions on the C2 ensemble. The quark mass for both fields is taken to be $am_l = 0.01$.

| $(ap)^2$ | $p\,[\mathrm{GeV}]$ | $\frac{\mathcal{P}[\Lambda_\mathrm{A}](1.8,1.8)}{\mathcal{P}[\Lambda_\mathrm{A}](1.6,1.6)}$ | $\frac{\mathcal{P}[\Lambda_\mathrm{A}](1.6,1.8)}{\mathcal{P}[\Lambda_\mathrm{A}](1.6,1.6)}$ | $\frac{\mathcal{P}[\Lambda_\mathrm{A}](1.8,1.8)}{\mathcal{P}[\Lambda_\mathrm{A}](1.6,1.8)}$ |
|---|---|---|---|---|
| 0.583 | 1.820 | 0.996774(55) | 0.998139(53) | 0.998508(24) |
| 0.637 | 1.903 | 0.996805(66) | 0.998132(45) | 0.998516(32) |
| 0.694 | 1.985 | 0.996773(66) | 0.998143(34) | 0.998520(28) |
| 0.753 | 2.068 | 0.996702(88) | 0.998143(28) | 0.998522(26) |
| 0.814 | 2.151 | 0.996658(85) | 0.998138(22) | 0.998524(22) |

Table 3.3: The ratios of projected amputated vertex function for the axial currents with different actions on the M1 ensemble. The quark mass for both fields is taken to be $am_l = 0.004$.

project, we can simply include it as a sub-dominant systematic error.

For completeness, we present some of the other numerical results related to the vertex function. For SMOM, $Z_\mathrm{A} = Z_\mathrm{V}$ and $Z_\mathrm{S} = Z_\mathrm{P} = 1/Z_m$ in the continuum limit. This implies that, given the renormalization conditions in Eq. 3.32 to Eq. 3.35, we expect $\mathcal{P}[\Lambda_\mathrm{V}] = \mathcal{P}[\Lambda_\mathrm{A}]$ and $\mathcal{P}[\Lambda_\mathrm{S}] = \mathcal{P}[\Lambda_\mathrm{P}]$ at high momenta. This is confirmed in Fig. 3.8, taking F1 ensemble as an example, where the projected amputated vertex functions simulated are plotted vs momenta ranging from around 2 to above 3 GeV. Notice that the vector and axial vertex functions are almost scale invariant while pseudoscalar and scalar vertices clearly show a scale dependence. As well as that, we observe that for large values of momentum, *i.e.* getting closer to the continuum, $\mathcal{P}[\Lambda_\mathrm{P}]$ approaches $\mathcal{P}[\Lambda_\mathrm{S}]$.

### 3.11.3 4-quark operator renormalization

As already mentioned in Chapter 1, the bare four-quark operator *e.g.* $\langle\overline{K}^0|Q_R^{\Delta S=2}|K^0\rangle$ has to be renormalized in some regularization scheme such as RI/SMOM non-

| $(ap)^2$ | $p$ [GeV] | $\frac{\mathcal{P}[\Lambda_A](1.8,1.8)}{\mathcal{P}[\Lambda_A](1.6,1.6)}$ | $\frac{\mathcal{P}[\Lambda_A](1.6,1.8)}{\mathcal{P}[\Lambda_A](1.6,1.6)}$ | $\frac{\mathcal{P}[\Lambda_A](1.8,1.8)}{\mathcal{P}[\Lambda_A](1.6,1.8)}$ |
|---|---|---|---|---|
| 0.482 | 1.926 | 0.996779(23) | 0.9982202(85) | 0.998555(11) |
| 0.516 | 1.990 | 0.996744(26) | 0.9982053(99) | 0.998539(12) |
| 0.548 | 2.054 | 0.996728(24) | 0.9981981(91) | 0.998525(97) |
| 0.583 | 2.118 | 0.996716(19) | 0.9981914(85) | 0.9985203(79) |
| 0.619 | 2.183 | 0.996719(19) | 0.998189(10) | 0.9985242(64) |

Table 3.4: The ratios of projected amputated vertex function for the axial currents with different actions on the F1 ensemble. The quark mass for both fields is taken to be $am_l = 0.002144$.

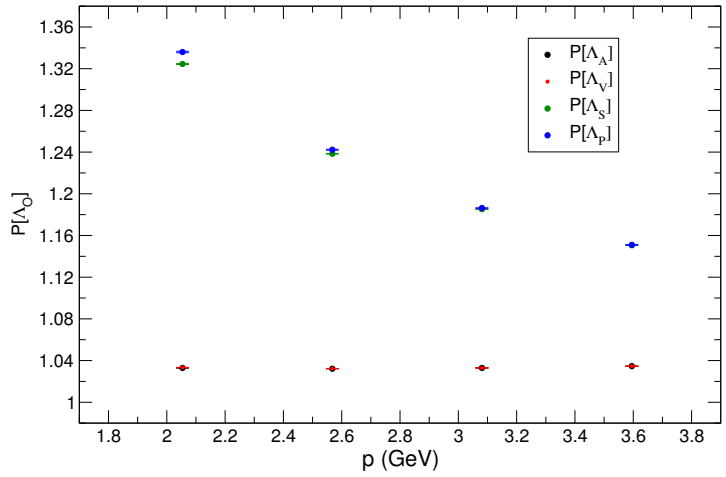


Figure 3.8: Projected amputated vertex functions on the F1 ensemble plotted againts momentum in GeV.

perturbatively. The result is then converted, via one- or two-loop perturbative matching, to a more commonly used schemes such as NDR-$\overline{\text{MS}}$. In this section, we first state the renormalization condition for 4-quark operators in RI/SMOM and then present the corresponding numerical results on the F1 ensemble as well as the conversion to NDR-$\overline{\text{MS}}$.

The RI/SMOM renormalization condition for the 4-quark operator, $O_{\text{VV+AA}}$, in *e.g.* $B_K$, involves amputating four fermionic fields. We therefore have [24],

$$\lim_{m_R\to 0}\frac{1}{12}\text{Tr}\left[\mathbf{P}^{(A)}_{\substack{\alpha\beta\gamma\delta\\ijkl}}\Lambda_{\text{O},R}\right]\Big|_{\text{sym}} = \lim_{m_R\to 0}\frac{1}{12}\text{Tr}\left[Z_q^{-2}Z_{\text{O}}\mathbf{P}^{(A)}_{\substack{\alpha\beta\gamma\delta\\ijkl}}\Lambda_{\text{O}}\right]\Big|_{\text{sym}} = 1\ , \quad (3.249)$$

where the projectors onto tree-level value are given in two schemes known as $\gamma^\mu$

and $\not{q}$ schemes are as follows:

$$\mathbf{P}^{(\gamma^\mu)}_{\substack{\alpha\beta\gamma\delta\\ijkl}} = \frac{1}{256N(N+1)}\left[(\gamma^\nu)_{\beta\alpha}(\gamma_\nu)_{\delta\gamma} + (\gamma^\nu\gamma^5)_{\beta\alpha}(\gamma_\nu\gamma^5)_{\delta\gamma}\right]\delta_{ij}\delta_{kl}\ , \tag{3.250}$$

$$\mathbf{P}^{(\not{q})}_{\substack{\alpha\beta\gamma\delta\\ijkl}} = \frac{1}{64q^2N(N+1)}\left[(\not{q})_{\beta\alpha}(\not{q})_{\delta\gamma} + (\not{q}\gamma^5)_{\beta\alpha}(\not{q}\gamma^5)_{\delta\gamma}\right]\delta_{ij}\delta_{kl}\ , \tag{3.251}$$

where $N = 3$ is the number of colors. The non-exceptional symmetric condition implies the in and out momenta should satisfy $p_2^2 = p_3^2 = (p_2 - p_3)^2 = q^2$ where we take,

$$d(p_2)\overline{s}(-p_3) \ \rightarrow\ \overline{d}(-p_2)s(p_3)\ . \tag{3.252}$$

In other words having computed the bare projected amputated vertex function $\mathcal{P}[\Lambda_{\rm O}]$, the relation

$$\frac{Z_{\rm O}}{Z_q^2}\mathcal{P}[\Lambda_{\rm O}] = 1\ , \tag{3.253}$$

can be used to extract the 4-quark operator renormalization factor $Z_{\rm O}$, where in our case O=VV+AA operator discussed in Sec. 1.2.5. We now recall the kaon bag parameter:

$$B^{\rm bare} = \frac{\langle K^0(\Delta T)|O_{\rm VV+AA}(t)|\overline{K}^0(0)\rangle}{\frac{8}{3}\langle K^0(\Delta T - t)|A_0(0)\rangle\langle A_0(t)|\overline{K}^0(0)\rangle}\ , \tag{3.254}$$

where $\Delta T$ is the time separation between the source and sink operators, see Sec. 4.4 for the details. The renormalization $Z_{B_K}$ is obtained, using RI/SMOM conditions Eq. 3.249 for the 4-quark operator and Eq. 3.33 for the axial vertex function, and taking the ratio:

$$Z_{B_K} = \frac{Z_{VV+AA}}{Z_A^2} = \frac{\mathcal{P}[\Lambda_A]^2}{\mathcal{P}[\Lambda_{VV+AA}]}\ . \tag{3.255}$$

Note that the factors of $Z_q$ have cancelled between the numerator and the denominator.

We have generated vertex functions with light quarks on the F1 ensemble with momenta starting from 2 GeV to more than 3 GeV. Fig. 3.9 shows $Z_{B_K}$ for each

of the momenta simulated.

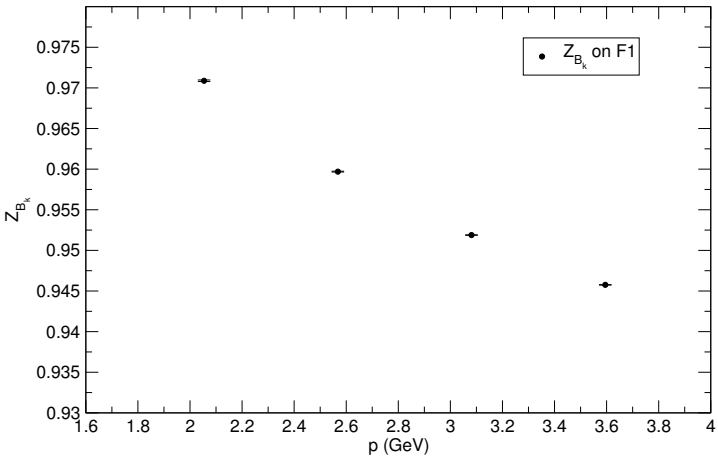


Figure 3.9: $Z_{B_k}$ for four different values of momenta on the F1 ensemble.

By fitting the last three data point to a line, we determine the value

$$Z_{B_K}^{\mathrm{RI}} = 0.952766(35) \ , \tag{3.256}$$

in RI/SMOM, at precisely 3 GeV on the F1 ensemble. It now remains to obtain the equivalent value in the more commonly used NDR-$\overline{\mathrm{MS}}$ scheme. The non-amputated vertex function is renormalized as:

$$\mathrm{O}_R^{\mathrm{RI}} = Z_{\mathrm{O}}^{\mathrm{RI}} \mathrm{O} \ , \tag{3.257}$$

where the label "RI" refers to the renormalization in the RI/SMOM scheme. In a similar way, the renormalization in NDR-$\overline{\mathrm{MS}}$ is generically written as:

$$\mathrm{O}_R^{\overline{\mathrm{MS}}} = Z_{\mathrm{O}}^{\overline{\mathrm{MS}}} \mathrm{O} \cdot \tag{3.258}$$

Taking the ratio of these two equations gives rise to the definition of the conversion factor between the two schemes, denoted by $C_B$, *i.e.*

$$\mathrm{O}_R^{\overline{\mathrm{MS}}}(\mu) = C_B(p^2/\mu^2)\mathrm{O}_R^{\mathrm{RI}}(p) \quad , \quad C_B = \frac{Z_{\mathrm{O}}^{\overline{\mathrm{MS}}}}{Z_{\mathrm{O}}^{\mathrm{RI}}} \cdot \tag{3.259}$$

Using the RI/SMOM renormalization condition for the amputated vertex func-

| $p$ | $Z_{B_K}^{\rm RI}$ | $Z_{B_K}^{\rm MS}$ |
|---|---|---|
| 2.56, 3.08, 3.59 | 0.953680(35) | 0.957781(35) |
| 3.08, 3.59 | 0.952766(35) | 0.956864(35) |
| 2.56, 3.59 | 0.954393(41) | 0.958498(41) |

Table 3.5: $Z_{B_K}$ in RI/SMOM and $\overline{\rm MS}$ at 3 GeV fitted using different momenta points.

tion, Eq. 3.253,

$$\mathcal{P}[\Lambda_{{\rm O},R}]^{\rm RI} = \frac{Z_{\rm O}^{\rm RI}}{(Z_q^{\rm RI})^2}\mathcal{P}[\Lambda_{\rm O}] = 1 \quad \text{and} \quad \mathcal{P}[\Lambda_{{\rm O},R}]^{\overline{\rm MS}} = \frac{Z_{\rm O}^{\overline{\rm MS}}}{(Z_q^{\overline{\rm MS}})^2}\mathcal{P}[\Lambda_{\rm O}] \ , \tag{3.260}$$

we obtain

$$C_B = Z_{\rm O}^{\overline{\rm MS}}\frac{\mathcal{P}[\Lambda_{\rm O}]}{(Z_q^{\rm RI})^2} = \mathcal{P}[\Lambda_{{\rm O},R}]^{\overline{\rm MS}}\frac{(Z_q^{\overline{\rm MS}})^2}{(Z_q^{\rm RI})^2} \ \cdot \tag{3.261}$$

Hence,

$$\frac{(C_q)^2}{C_B}P^{ij,kl}\Lambda_{\alpha\beta,\gamma\delta}^{\overline{\rm MS},ij,kl} = 1 \tag{3.262}$$

where $C_q = \frac{Z_q^{\overline{\rm MS}}}{Z_q^{RI}}$. At one loop order $C_q$ is known at 1- and 2-loops [24, 77, 93, 94], therefore, the above equation can be used to compute the matching coefficient $C_B$. Our final results for $Z_{B_k}$ at 3 GeV is therefore,

$$Z_{B_K}^{\rm MS} = 0.956864(35) \ \cdot \tag{3.263}$$

In order to check the results further, we have examined performing the above fit and interpolation while taking different momenta points into account. More specifically, we have performed the interpolation to 3 GeV in three different ways. First by taking the last three points, resulting in Eq. 3.256 and Eq. 3.263 and then taking only the last two points into account, as well as taking the two middle points. Table. 3.5 summarizes the results. As it can be seen, the results only differ at sub-percent level, implying the final interpolation to be independent of the momenta chosen to perform the fit.

Finally, it is possible to obtain the Renormalization Group Invariant (RGI) factors $Z_{B_K}^{\rm RGI}$. Following the discussion in Sec. 1.2.6, we can related the $Z_{B_K}^{\rm RGI}$ renormalization factor to $Z_{B_K}^{A}(\mu)$ in some scheme $A$, here RI/SMOM, via a

perturbative factor according to using Eq. 1.73 and Eq. 1.74 which we denote by $\omega_A^{-1}(\mu)$ for simplicity. Therefore, we write,

$$Z_{B_K}^{\mathrm{RGI}} = \omega_A^{-1}(\mu) Z_{B_K}^{A}(\mu) \cdot \tag{3.264}$$

Note that the perturbative factor $\omega_A^{-1}(\mu)$ has to be computed in the same scheme as $Z_{B_K}^{A}(\mu)$ in order to cancel the $\mu$ dependence. $Z_{B_K}^{\mathrm{RGI}}$ has been computed numerically for the previous momenta, and the result of the interpolation to 3 GeV is marked in red in Fig. 3.10. We observed that the RGI points do not lie on a completely flat line. This can be due to truncation in the perturbative series or the fact that perturbation theory breaks down at low energies. The same behaviour is seen in other analyses, *e.g.* Ref. [95], where $Z_{B_K}$ in different RI/SMOM schemes is analysed extensively. As the momentum increases, however, the slope is expected to decrease until it becomes flat, *i.e.* , independent of scale $\mu$. For more details see Ref. [95].

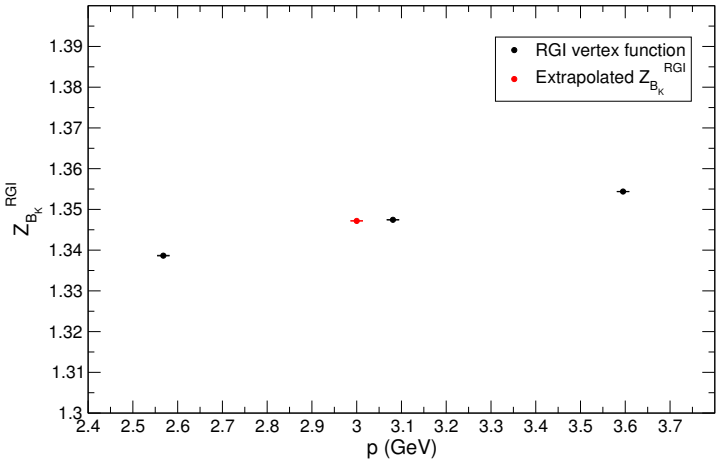


Figure 3.10: The black points denote $Z_{B_k}^{\mathrm{RGI}}$ for the three values of momenta, used for interpolation to 3GeV, on the F1 ensemble. The red point is the interpolated value at 3 GeV.

# Chapter 4

# Lattice Phenomenology

For all the ensembles listed in Sec. 2.4, quantities such as meson masses, decay constants, bag and $\xi$ parameters are extracted. In order to gain a better understanding of the numerical results, we discuss analytical computations of meson two-point and three-point functions from which masses and matrix element can be extracted. We then use these, to describe how the fits over the data points are performed. Parts of this analysis, including the mesons masses and decay constants have led to the results in our charm paper, Ref. [72], while the bag and $\xi$ parameters will potentially appear as part of a future publication.

## 4.1 Meson Correlator

### 4.1.1 Numerical simulation of the meson correlator

A two-point correlator $C_{\Gamma\Gamma'}$ can be constructed using interpolating operators $O_\Gamma(t,\mathbf{y})$ and $O^\dagger_{\Gamma'}(0,\mathbf{x})$ as follows:

$$C_{\Gamma\Gamma'}(t) = \sum_{\mathbf{x},\mathbf{y}} \langle O_\Gamma(t,\mathbf{y}) O^\dagger_{\Gamma'}(0,\mathbf{x})\rangle \ , \tag{4.1}$$

where,

$$O(y) = \bar{q}^{\alpha_1}_{c_1}(y)\Gamma_{\alpha_1\beta_1} q'^{\beta_1}_{c_1}(y) \ , \tag{4.2}$$

$$O'^{\dagger}(x) = \bar{q}'_{\substack{\alpha_2 \\ c_2}}(x)\Gamma'_{\alpha_2\beta_2}q_{\substack{\beta_2 \\ c_2}}(x) \cdot \tag{4.3}$$

In this notation, the Greek subscripts $\alpha, \beta$ indicate spinor indices while Latin subscripts $c_1, c_2$ correspond to color indices. $\Gamma$ and $\Gamma'$ are chosen to be any combination of $\Gamma_{\mathrm{A}} = \gamma_0\gamma_5$ and $\Gamma_{\mathrm{P}} = \gamma_5$, for our simulations of pseudoscalar correlators. Let us focus on the expectation value,

$$\begin{aligned}\langle O(y)O'^{\dagger}(x)\rangle =& \Gamma_{\alpha_1\beta_1}\Gamma'_{\alpha_2\beta_2}\langle \bar{q}_{\substack{\alpha_1 \\ c_1}}(y)q'_{\substack{\beta_1 \\ c_1}}(y)\bar{q}'_{\substack{\alpha_2 \\ c_2}}(x)q_{\substack{\beta_2 \\ c_2}}(x)\rangle \\ =& -\Gamma_{\alpha_1\beta_1}\Gamma'_{\alpha_2\beta_2}D_q^{-1}(x-y)_{\substack{\beta_2\alpha_1 \\ c_2c_1}}D_{q'}^{-1}(y-x)_{\substack{\beta_1\alpha_2 \\ c_1c_2}} \\ =& -\operatorname{tr}\Big[\Gamma' D_q^{-1}(x-y)\Gamma D_{q'}^{-1}(y-x)\Big],\end{aligned} \tag{4.4}$$

where the minus sign is due to Grassmann algebra. In the second equality we have used the fact that the Wick contraction between quark-antiquark pairs can only be performed within the same flavor. Hence the fermionic expectation value factorizes with respect to each flavor $q$, $q'$, leading to the two, inverse Dirac matrices *i.e.* propagators above. This relation can be simplified further using $\gamma_5$ hermiticity for 4D propagators, $\gamma^5 D^{-1}\gamma^5 = D^{-1\dagger}$. Therefore, in numerically computing the pseudoscalar correlation function Eq. 4.1, we need to compute quark propagators. The quark propagators are computed with $\mathbb{Z}(2) \times \mathbb{Z}(2)$ stochastic wall sources [73]. In order to improve the statistics, different number of time planes are used as sources and the results, on a given gauge configuration, are averaged into one bin before any fits are performed. The number of time planes on each configuration is stated in Table. 2.1 with column under the heading "hits/conf". In general, the process of inverting the Dirac matrices to obtain the propagators can have a high numerical cost. In our simulations, light and strange quark propagator inversions were performed using the HDCD algorithm [43] while for heavy quarks a CG inverter was used. We will not delve into the details of these algorithms and their properties, as it is beyond the scope of this thesis.

### 4.1.2 Analytical form of the meson correlator

Let us now examine how meson masses and matrix elements can be extracted. Consider the following two-point function, constructed from interpolating opera-

tors as in Eq. 4.2 and Eq. 4.3:

$$\langle O(y)O'^{\dagger}(x)\rangle = C(x-y)\ , \tag{4.5}$$

which is a function of $x-y$ due to translational invariance. So we can write it as

$$\langle O(x)O'^{\dagger}(0)\rangle = C(x)\ \cdot \tag{4.6}$$

Inserting a complete set of hadronic states gives,

$$|n\rangle\langle n| := \int \frac{d^4p}{(2\pi)^4}\delta(p^2-m_n^2)|n,p\rangle\langle n,p| = \int \frac{d^3p}{(2\pi)^3}\frac{1}{2E_n}\ |n,p\rangle\langle n,p|\ \cdot \tag{4.7}$$

Note that $|n\rangle$ are the eigenstates of the Hamiltonian operator, therefore they must be physical and on-shell. Given that quarks are confined and the observables are mesons and baryons, these states describe composite particles such as pion, $\rho, \eta, \cdots$. Therefore, with zero momentum projection in Minkowski space, we have

$$\begin{aligned}
&\sum_n \int d^3\mathbf{x}\ \langle 0|O(x)|n\rangle\langle n|O'^{\dagger}(0)|0\rangle = \sum_n \int d^3\mathbf{x}\ \langle 0|e^{iP.x}O(0)e^{-iP.x}|n\rangle\langle n|O'^{\dagger}(0)|0\rangle \\
=&\sum_n \int \frac{d^3p}{(2\pi)^3}\frac{1}{2E}\int d^3\mathbf{x}\langle 0|O(0)|n,p\rangle\langle n,p|O'^{\dagger}(0)|0\rangle e^{i\mathbf{p_n}.\mathbf{x}}e^{-iE_nt} \\
=&\sum_n \frac{1}{2E_n}\langle 0|O(0)|n,\mathbf{p}=0\rangle\langle n,\mathbf{p}=0|O'^{\dagger}(0)|0\rangle e^{-iE_nt}\ \cdot
\end{aligned} \tag{4.8}$$

In order to obtain the third equality, the integral over spatial $x$ is performed to give a delta function, followed by the integral over $d^3p$ leading to the 3-momentum being $\mathbf{p}=0$. After performing the Wick rotation, with $t=-it_E$, the Euclidean space correlator at large $t$ takes the form,

$$C(t) = \frac{1}{2m}\langle 0|O(0)|n,\mathbf{p}=0\rangle\langle n,\mathbf{p}=0|O'^{\dagger}(0)|0\rangle e^{-mt_E} + \cdots = \mathcal{N}e^{-mt_E} + \cdots\ , \tag{4.9}$$

where the pre-factor $A_0$,

$$\mathcal{N} = \frac{1}{2m}\langle 0|O(0)|n,\mathbf{p}=0\rangle\langle n,\mathbf{p}=0|O'^{\dagger}(0)|0\rangle\ \cdot \tag{4.10}$$

In other words, when $t$ becomes large, the major contribution comes from the lowest energy state $E_0 = m$, where $m$ is the mass of the lightest pseudoscalar meson given the specific quark structure $q, q'$.

### 4.1.3 Pseudoscalar masses and decay constants

As mentioned before in Sec. 4.1, the operators $O$, Eq. 4.2 and $O'^{\dagger}$, Eq. 4.3 can have any combination of $\Gamma, \Gamma' = \{\Gamma_{\rm A}, \Gamma_{\rm P}\}$. The coefficient, $\mathcal{N}$, of the exponential decay from which we extract the pseudoscalar meson mass in Eq. 4.9, can be any of $\mathcal{N}_{PP}, \mathcal{N}_{AA}, \mathcal{N}_{AP}$ with the generic form stated in Eq. 4.10. Note that Eq. 4.9 could have been also derived directly in Euclidean space, for periodic finite time extent $T$, starting from the Euclidean correlator

$$\langle O(\mathbf{x}, t) O'^{\dagger}(0) \rangle_T = \frac{1}{Z} \mathrm{Tr} \left[ e^{-(T-t)\hat{H}} O(\mathbf{x}) e^{-t\hat{H}} O^{\dagger}(0) \right], \tag{4.11}$$

where $Z = \mathrm{tr}\left[e^{-TH}\right]$ is the partition function and $H$ is the hamiltonian. Inserting a complete set of states, applying a zero momentum projection as above, pulling out a factor $E^{-TE_0}$ and expanding the numerator and denominator gives, as a leading term:

$$C(t) = \mathcal{N}_{PP,AA} e^{-mt} + \mathcal{N}_{PP,AA} e^{-m(T-t)} = 2\mathcal{N}_{PP,AA} e^{-mT/2} \cosh((T/2 - t)m) \ , \tag{4.12}$$

for $PP$ and $AA$ channels that are symmetric under $T$ reversal. For the $AP$ channel, which picks up a minus sign under time reflection [66],

$$C(t) = \mathcal{N}_{AP} e^{-mt} - \mathcal{N}_{AP} e^{-m(T-t)} = 2\mathcal{N}_{AP} e^{-mT/2} \sinh((T/2 - t)m) \cdot \tag{4.13}$$

$C(t)$ is computed numerically as discussed in Sec. 4.1.1. One has to fit this data a correct fit function to extract the meson mass $m$ and the matrix elements stated above. For example, in the range where cosh can be approximated by an exponential, *i.e.* away from the centre where $t \approx T/2$, one can define a quantity known as the *effective mass*,

$$m_{\rm eff} = \ln \frac{C(t)}{C(t+1)} \ , \tag{4.14}$$

where the contributions of the excited states are neglected since the fit is taken to be over an effective mass plateau at $m_{\text{eff}} = E_0$. Another, perhaps more accurate, method of extracting the mass is to take into account the periodicity and fit using hyperbolic cosine for $PP$ and $AA$ channels, or hyperbolic sine for the $AP$ channel, rather than a logarithm:

$$m_{\text{eff}} = \cosh^{-1}\left[\frac{C(t+1)+C(t-1)}{2C(t)}\right] \cdot \tag{4.15}$$

Having extracted the mass the fit code can plug in the numbers and obtain the coefficients in Eq. 4.12 and Eq. 4.13. In our analysis however, we have directly fitted the correlator. In the case of a one-state fit, which only takes into account the ground state meson mass $m$ whilst ignoring the excited states, we fit directly for two parameters $m$ and the coefficient $\mathcal{N}$ with ansatz as stated on the LHS of Eq. 4.12 and Eq. 4.13. It is also possible to perform simultaneous multi-channel fits including all $PP, AA$ and $AP$ to improve the statistics. Moreover, instead of taking the ground state into account only, one can perform a two-state fit which takes into account the effect of the first excited state. The ansatz, taking into account the next to leading order term in Eq. 4.8, is expected to be of the form:

$$C(t) = \mathcal{N}^{(0)}e^{-m_0 t} \pm \mathcal{N}^{(0)}e^{-m_0(T-t)} + \mathcal{N}^{(1)}e^{-m_1 t} \pm \mathcal{N}^{(1)}e^{-m_1(T-t)} + \cdots \ , \tag{4.16}$$

which would be a four parameter fit. To capture the effect the excited states, the two-state fit must begin at lower values of $t_{\text{min}}$. We discuss the details of the fits in Sec. 4.2 , where we present the numerical results.

In the Standard Model the decay constant for pseudoscalar mesons $M^0$ is obtained as follows:

$$f_M = \frac{\langle 0|\bar{q}'\gamma_0\gamma_5 q|M(0)\rangle}{m_M} \cdot \tag{4.17}$$

For the particular case of the charmed mesons we are measuring,

$$f_{D_q} = \frac{\langle 0|\bar{c}\gamma_0\gamma_5 q|D_q(0)\rangle}{m_{D_q}} \ , \qquad \text{where } q = d, s \cdot \tag{4.18}$$

Therefore, we need to extract the axial matrix elements as well as the meson

mass to obtain the decay constant. Suppose we have already performed a fit to extract the matrix element $\mathcal{N}_{AA}$ and the meson mass in Eq. 4.12. Then, the decay constant in lattice units can be computed using

$$f_{D_q} = \sqrt{\frac{2\mathcal{N}_{AA}}{N^3\ m_{D_q}}}\ , \tag{4.19}$$

where $m$ is the meson mass in lattice units and $N = N_x = N_y = N_z$ is the number of lattice points in a particular spatial direction. The latter arises due to the lattice being of a finite volume, Eq. B.33. An equivalent way of extracting the decay constant is via the ratio

$$f_{D_q} = \sqrt{\frac{2\mathcal{N}_{AP}^2}{N^3\ m_{D_q} N_{PP}}}\ . \tag{4.20}$$

Since the pseudoscalar matrix elements $\mathcal{N} = \frac{1}{2m_{D_q}}|\langle 0|\bar{c}\gamma_5 q(0)|n, \mathbf{p} = 0\rangle|^2$ cancel between the numerator and the denominator, the expression reduces to Eq. 4.20.

## 4.2 Numerical results for $m_{D_q}$ and $f_{D_q}$

In this section, we present numerical results for charmed meson masses and decay constants on the 7 ensembles listed in Sec. 2.4. These are shown in Table. 4.1 for heavy-light mesons, and Table. 4.1 for the heavy-strange mesons. Fig. 4.1 shows an example of the plot of effective mass vs time in lattice units for $am_h = 0.3$ on the C0 ensemble. Note that it is the two-point correlator that is simultaneously fitted for $AA, PP$ and $AP$ channels according to fit functions stated in Eq. 4.12 and Eq. 4.13. However we plot the effective mass to demonstrate the plateau better. The fit range is chosen such that it has $t_{\text{min}}$ away from the excited states, well within the plateau region, while $t_{\text{max}}$ is away from the center of the lattice where there is more noise. The behaviour of $\chi^2$ is notated not to fluctuate too much whilst varying $t_{\text{min}}$ and $t_{\text{max}}$. As mentioned earlier, alternatively, one can perform a double exponential fit taking into account the effect of the excited states according to Eq. 4.16. Examples of the excited states contributions in our cases include *e.g.* $D_{l,s} + 2\pi$ and $2K + \pi$, for more details see Ref. [96]. A double exponential fit has been plotted in Fig. 4.2 as an example for the heavy-light

meson with $am_h = 0.3$ on the C0 ensemble. One may wish to perform double exponential fits, since the data is generally less noisy further away from the center of the lattice. The result of the double exponential fit in our case, however, was in good agreement with the single exponential fit without a significant increase in the precision of the fit result. Therefore, for the rest of the analysis we use single exponential fits to extract the meson masses. It is also worth noting that correlated fits were also attempted. However, the correlation matrix turned out not to be stable for a reliable inversion. The fits presented here are, therefore, all uncorrelated fits with the correlation matrix assumed to be diagonal.

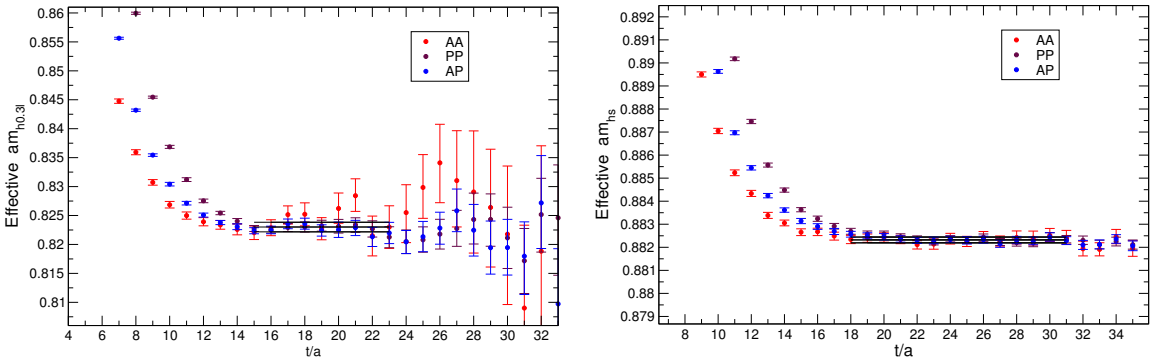


Figure 4.1: Heavy-light (left) and heavy-strange (right) effective mass plots, for heavy quark mass $am_h = 0.3$, on the C0 ensemble. The two-point correlator in $AA, PP$ and $AP$ channels have been fitted simultaneously.

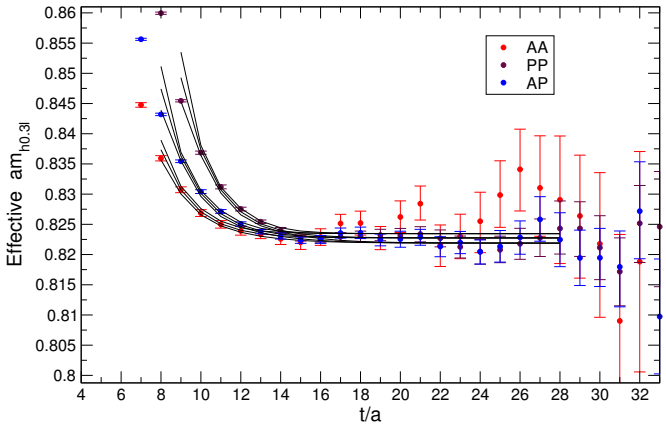


Figure 4.2: Heavy-light effective mass plot with $am_h = 0.3$ on the C0 ensemble. The two-point correlator has been fitted using a double exponential fit form, for $AA$, $PP$ and $AP$ channels simultaneously.

| Name | $[t_{\min}, t_{\max}]$ | $am_D$ | $af_D^{\text{bare}}$ | $m_D$ (GeV) | $f_D^{\text{ren}}$ (GeV) |
|---|---|---|---|---|---|
| C0 | 14 - 24 | 0.82298(74) | 0.16260(74) | 1.4233(34) | 0.2002(10) |
| | 14 - 24 | 0.90023(92) | 0.16486(93) | 1.5570(37) | 0.2030(12) |
| | 14 - 24 | 0.9736(11) | 0.1661(11) | 1.6838(42) | 0.2045(15) |
| C1 | 16 - 27 | 0.83122(95) | 0.1686(11) | 1.4836(45) | 0.2158(15) |
| | 16 - 27 | 0.9077(12) | 0.1709(14) | 1.6201(50) | 0.2188(19) |
| | 16 - 27 | 0.9805(15) | 0.1723(18) | 1.7498(56) | 0.2206(24) |
| C2 | 16 - 27 | 0.84125(69) | 0.17466(80) | 1.5014(44) | 0.2238(12) |
| | 16 - 27 | 0.91700(82) | 0.17654(99) | 1.6367(48) | 0.2262(14) |
| | 16 - 27 | 0.98891(96) | 0.1772(13) | 1.7650(52) | 0.2271(17) |
| M0 | 19 - 32 | 0.63073(66) | 0.11482(67) | 1.4876(47) | 0.2013(13) |
| | 19 - 32 | 0.72602(86) | 0.11609(91) | 1.7124(55) | 0.2036(17) |
| | 19 - 32 | 0.8146(11) | 0.1162(12) | 1.9213(63) | 0.2037(22) |
| | 19 - 32 | 0.8972(14) | 0.1153(16) | 2.1161(71) | 0.2021(29) |
| M1 | 17 - 30 | 0.63756(86) | 0.12121(84) | 1.5195(59) | 0.2152(17) |
| | 17 - 30 | 0.7326(11) | 0.1229(11) | 1.7460(68) | 0.2181(21) |
| | 17 - 30 | 0.8205(14) | 0.1229(14) | 1.9554(78) | 0.2183(25) |
| | 17 - 30 | 0.9020(17) | 0.1215(17) | 2.1497(88) | 0.2157(32) |
| M2 | 17 - 30 | 0.64267(79) | 0.12464(75) | 1.5317(58) | 0.2214(16) |
| | 17 - 30 | 0.73773(93) | 0.12651(92) | 1.7582(67) | 0.2247(18) |
| | 17 - 30 | 0.8258(12) | 0.1267(11) | 1.9681(77) | 0.2251(21) |
| | 17 - 30 | 0.9076(14) | 0.1254(14) | 2.1631(85) | 0.2228(25) |
| F1 | 20 - 40 | 0.53755(48) | 0.10000(42) | 1.4912(55) | 0.2110(12) |
| | 20 - 40 | 0.62004(60) | 0.10165(55) | 1.7200(64) | 0.2146(14) |
| | 20 - 40 | 0.69678(74) | 0.10223(73) | 1.9329(73) | 0.2158(17) |
| | 20 - 40 | 0.76870(90) | 0.10194(92) | 2.1324(81) | 0.2152(21) |
| | 20 - 40 | 0.8618(12) | 0.1002(12) | 2.3906(92) | 0.2115(26) |

Table 4.1: Fit results for $D$ meson masses and decay constants on all the ensembles. The correlator has been fitted simultaneously in the $AA, AP$ and $PP$ channels with the fit range as indicated. Generally $PP$ shows a later plateau as compared to the other two channels and so it has its fit range starting at $t_{\min} + 1$. The first two columns show results in lattice units. The renormalization factors used in obtaining the renormalized decay constants, in the last column, are taken from Table. 3.1.

| Name | $[t_{\min}, t_{\max}]$ | $am_{D_s}$ | $af_{D_s^{\text{bare}}}$ | $m_{D_s}$ (GeV) | $f_{D_s}$ (GeV) |
|---|---|---|---|---|---|
| C0 | 18 - 32 | 0.88232(13) | 0.18829(15) | 1.5260(34) | 0.23184(54) |
| | 18 - 32 | 0.95679(15) | 0.19100(18) | 1.6548(37) | 0.23520(56) |
| | 18 - 32 | 1.02780(17) | 0.19249(22) | 1.7776(39) | 0.23703(58) |
| C1 | 18 - 30 | 0.87670(43) | 0.18652(52) | 1.5647(45) | 0.23875(94) |
| | 18 - 30 | 0.95125(47) | 0.18924(60) | 1.6978(48) | 0.2422(10) |
| | 18 - 30 | 1.02230(51) | 0.19074(71) | 1.8246(52) | 0.2442(11) |
| C2 | 18 - 30 | 0.87815(44) | 0.18835(55) | 1.5673(45) | 0.24134(98) |
| | 18 - 30 | 0.95246(50) | 0.19080(67) | 1.7000(49) | 0.2445(11) |
| | 18 - 30 | 1.02322(57) | 0.19195(82) | 1.8262(52) | 0.2459(13) |
| M0 | 23 - 40 | 0.678191(92) | 0.13594(12) | 1.5996(48) | 0.23836(74) |
| | 23 - 40 | 0.77132(11) | 0.13833(16) | 1.8192(54) | 0.24256(78) |
| | 23 - 40 | 0.85820(14) | 0.13902(20) | 2.0242(60) | 0.24376(81) |
| | 23 - 40 | 0.93935(17) | 0.13824(27) | 2.2156(66) | 0.24239(86) |
| M1 | 18 - 30 | 0.67418(37) | 0.13568(32) | 1.6068(59) | 0.2409(10) |
| | 18 - 30 | 0.76724(38) | 0.13796(38) | 1.8286(67) | 0.2449(11) |
| | 18 - 30 | 0.85383(43) | 0.13840(46) | 2.0349(74) | 0.2457(12) |
| | 18 - 30 | 0.93437(51) | 0.13717(56) | 2.2269(81) | 0.2435(13) |
| M2 | 18 - 30 | 0.67496(39) | 0.13657(36) | 1.6086(59) | 0.2425(11) |
| | 18 - 30 | 0.76819(81) | 0.13899(41) | 1.8308(69) | 0.2469(11) |
| | 18 - 30 | 0.85499(47) | 0.13960(47) | 2.0377(74) | 0.2479(12) |
| | 18 - 30 | 0.93576(55) | 0.13852(56) | 2.2302(82) | 0.2460(13) |
| F1 | 27 - 42 | 0.57226(20) | 0.11356(21) | 1.5874(58) | 0.23976(99) |
| | 27 - 42 | 0.65276(24) | 0.11562(27) | 1.8108(66) | 0.2441(11) |
| | 27 - 42 | 0.72801(27) | 0.11631(33) | 2.0195(73) | 0.2456(11) |
| | 27 - 42 | 0.79869(31) | 0.11586(41) | 2.2156(80) | 0.2446(12) |
| | 27 - 42 | 0.89031(39) | 0.11350(53) | 2.4697(90) | 0.2396(14) |

Table 4.2: Fit results for $D_s$ meson masses and decay constants on all the ensembles. The correlator has been fitted simultaneously in the $AA, AP$ and $PP$ channels with the fit range as indicated. Generally $PP$ shows a later plateau as compared to the other two channels and so it has its fit range starting at $t_{\min}+1$. The first two columns show results in lattice units. The renormalization factors used in obtaining the renormalized decay constants, in the last column, are taken from Table. 3.1.

It is worth presenting a theoretical argument for the exponential growth in time of the noise to signal ratio, observed in the above figures. We have previously derived that the meson correlator goes as $C(t) \sim e^{-m_M t}$, for meson $M$. The variance of the correlator can be written as

$$\sigma_M^2 \propto \langle \big(O(x)O^\dagger(0)\big)^2 \rangle - C(t)^2 \cdot \tag{4.21}$$

For charm-light meson correlators, the quarks and anti-quarks produced by the square of $O(x)O^\dagger(0)$ come together in pairs to form an $\eta_c$ and a pion. Since the pion mass is small due to chiral symmetry, this combination is much lighter than $2m_D$. As a result the noise to signal ratio, $\frac{\sigma_M^2}{C(t)}$ grows rapidly with distance. This also explains why the charm-light meson correlators decay into noise more quickly than the charm-strange correlators, due to the error on the latter having the mass of $\eta_c + \bar{s}s$ in the exponent which is heavier than $\eta_c + \pi$, for more details see Ref. [97–99].

Before we close this section, we present the final results for the analysis of the masses and decays constants which were obtained after a global fit was performed. The global fit ansatz involves a simultaneous fit to the continuum limit, the pion mass dependence and heavy quark dependence. The ansatz for this fit, as well as the numerical work has been performed by other members of the collaboration and is not part of this work. For more details regarding the global fit see Ref. [72]. However, for completeness we include the final results: $f_D = 208.7(2.8)_{\text{stat}} \left(^{+2.1}_{-1.8}\right)_{\text{sys}}$ MeV and $f_{D_s} = 246.4(1.3)_{\text{stat}} \left(^{+1.3}_{-1.9}\right)_{\text{sys}}$ MeV and $f_{D_s}/f_D = 1.1667(77)_{\text{stat}} \left(^{+60}_{-46}\right)_{\text{sys}}$. Fig. 4.3 shows a comparison between our results and the previous determinations, in including the most recent FLAG report [5]. Our results are in good agreement with the literature.

## 4.3 Neutral meson mixing parameter $B$

In the first part of this section, we aim to derive an expression for the meson bag parameter, taking kaon as an example, from the corresponding three-point function. The details of this step are necessary to understand the shape of the numerical data plotted.

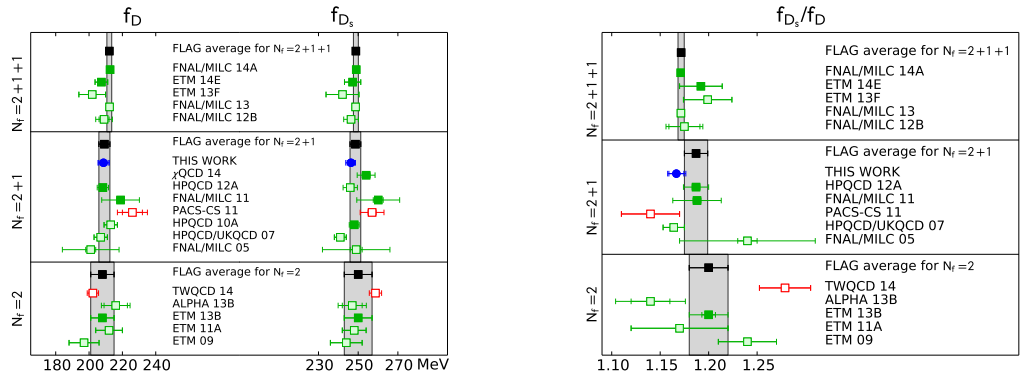


Figure 4.3: This figure shows our results, indicated by blue circles, as compared the most recent FLAG report [5].

### 4.3.1 The 3-point correlator

Using similar steps to Sec. 4.1.2, we can write an expression for the meson 3-point correlator. Recall that the three-point function in finite volume can be written as:

$$\begin{aligned}\langle O(t_y)Q(t_x)O(0)\rangle &= \frac{1}{Z}\mathrm{Tr}\left[e^{-(T-t_y)\hat{H}}O(0)e^{-(t_y-t_x)\hat{H}}Q(0)e^{-t_x\hat{H}}O(0)\right] \\ &= \frac{1}{Z}\sum_{n,l,m}\langle n|e^{-(T-t_y)\hat{H}}O(0)e^{-(t_y-t_x)\hat{H}}|m\rangle\langle m|Q(0)|l\rangle\langle l|^{-t_x\hat{H}}O(0)|n\rangle \\ &= \frac{1}{Z}\sum_{n,l,m}\langle n|O|m\rangle\langle m|Q|l\rangle\langle l|O|n\rangle e^{-(T-t_y)E_n}e^{-(t_y-t_x)E_m}e^{-t_xE_l}\ .\end{aligned} \tag{4.22}$$

for some choice of operator $O$. The lowest order contribution as $T$ becomes large is when $n = 0$, $l = K^0 = d\bar{s}$, $m = \bar{K}^0 = s\bar{d}$. The 4-fermi operator $Q_{\mathrm{AA+VV}}$ has the following form:

$$Q_{\mathrm{AA+VV}} = (\bar{s}\gamma_\mu d)(\bar{s}\gamma_\mu d) + (\bar{s}\gamma_\mu\gamma_5 d)(\bar{s}\gamma_\mu\gamma_5 d)\ . \tag{4.23}$$

Therefore, the the ground state matrix element of the operator $Q$ becomes,

$$\langle\bar{K}^0|Q_{\mathrm{AA+VV}}|K^0\rangle = \langle\bar{K}^0|(\bar{s}\gamma_\mu d)(\bar{s}\gamma_\mu d) + (\bar{s}\gamma_\mu\gamma_5 d)(\bar{s}\gamma_\mu\gamma_5 d)|K^0\rangle \tag{4.24}$$

One has to choose the creation or annihilation operator $O$ with the correct quantum numbers such as strangeness. For the kaon the operator $O$ can be chosen to be

$$O = \bar{d}\gamma_0\gamma_5 s \ , \tag{4.25}$$

which has the correct strangeness number, the axial structure is chosen to give cancellation of matrix elements once the full ratio for the bag parameter is constructed. As well as that, for the matrix element on the right, *i.e.* $\langle K^0|O|0\rangle$, $O$ must be such that in can create an $\bar{s}$ and a $d$ when acting on the vacuum. Similarly for the matrix element on the left hand side, *i.e.* $\langle 0|O|\bar{K}^0\rangle$.

The leading contribution to the ground state is

$$\langle 0|O|\bar{K}^0\rangle\langle\bar{K}^0|Q|K^0\rangle\langle K^0|O|0\rangle e^{-(t_y-t_x)E_{\bar{K}^0}} e^{-t_x E_{K^0}} \ . \tag{4.26}$$

In order to find the bag parameter which is directly related to the matrix element of the $Q$ operator, Eq. 1.72, the above equation needs to be divided by two two-point functions. This cancels the exponentials carrying the time dependance for certain values of time allowing for a constant fit to the plateau to be performed. Moreover, we choose the two point functions to be in the axial channel since this combination is what appears in the denominator of Eq. 1.72 or Eq. 1.77 for the bag parameter. This can be seen if we rewrite the decay constant according to Eq. 4.17 and cancel the meson mass.

### 4.3.2 Generic shape of the bag parameter plot

To gain a full understanding of the shape of the plot, we consider all the possible different time ranges and examine what happens in each region, indicated in Fig. 4.4.

1. For $0 < t_x < t_y < T/2$ and using translational invariance, we wish to find the combination,

$$\frac{\langle O(t_y)Q(t_x)O(0)\rangle}{\langle O^\dagger(t_y-t_x)O(0)\rangle\langle O^\dagger(t_x)O(0)\rangle} \tag{4.27}$$

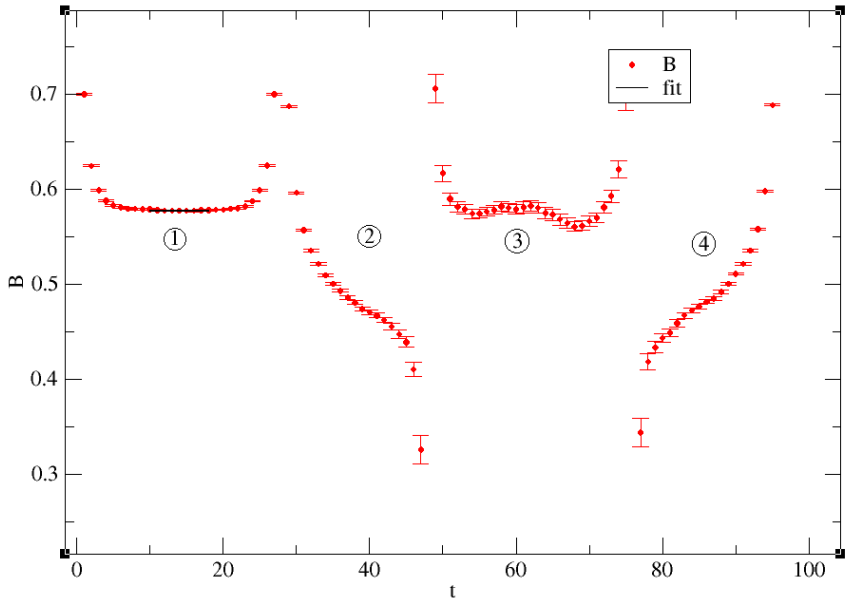


Figure 4.4: Generic shape of a bag parameter vs $t$ plot, for fixed $t_y$, here chosen to be $t_y = 28$. Here $t = t_x$ is the time dependence of the operator $Q$. The corresponding regions discussed are labelled 1-4 respectively.

For the ground state, ignoring the contribution of the first excited state, we have

$$C(t) = \frac{\langle 0|O|\bar{K}^0\rangle\langle\bar{K}^0|Q|K^0\rangle\langle K^0|O|0\rangle}{|\langle\bar{K}^0|\bar{s}\gamma_0\gamma_5 d|0\rangle|^2\ |\langle K^0|\bar{s}\gamma_0\gamma_5 d|0\rangle|^2} \times \frac{e^{-(t_y-t_x)E_{\bar{K}^0}} e^{-t_x E_{K^0}}}{\left(e^{-E_{\bar{K}^0}(t_y-t_x)} + e^{-E_{\bar{K}^0}(T-t_y+t_x)}\right)\left(e^{-E_{K^0}t_x} + e^{-E_{K^0}(T-t_x)}\right)} \tag{4.28}$$

in the given time range. This is because $T \gg t_y - t_x$, and so in the denominator of the above expression, the two terms without a $T$ in the exponent will dominate over the other ones. As a result, all time dependent terms in the numerator and denominator cancel with each other, resulting in a plateau in the plot which can be fitted to give the ground state value for the bag parameter. For example, in the case of the plot above, the time extend $T = 96$, $t_y = 28$ is fixed and $t_x$ is fitted over the range $t_x = 10 - 18$. The values away from the plateau in region (1) are due to the excited states.

2. Let us now consider the case where $0 < t_y < t_x < T/2$. From this region

onwards, the time ordering of the three-point function changes. In other words, we now have

$$\langle Q(t_x)O(t_y)O(0)\rangle = \frac{1}{Z}\sum_{n,l,m}\langle n|Q_x|m\rangle\langle m|O_y|l\rangle\langle l|O|n\rangle e^{-(T-t_x)E_n}e^{-(t_x-t_y)E_m}e^{-t_xE_l} \tag{4.29}$$

where the operators are now time independent, and this index is merely to remind the reader of the associated initial time dependance. Given that $O = \bar{d}\gamma_0\gamma_5 s$, we now have $|n\rangle = |\bar{K}^0\rangle = |\bar{d}s\rangle$ so that it is annihilated by $O$, $|l\rangle = |0\rangle$ and $|m\rangle = |K^0\rangle = |d\bar{s}\rangle$. Now, since $t_x > t_y$, with the correct time ordering $O^\dagger(T - t_x + t_y)$, the ratio becomes,

$$\begin{aligned} C(t) =& \frac{\langle \bar{K}^0|Q|K^0\rangle\langle K^0|O|0\rangle\langle 0|O|\bar{K}^0\rangle}{|\langle \bar{K}^0|\bar{s}\gamma_0\gamma_5 d|0\rangle|^2\ |\langle K^0|\bar{s}\gamma_0\gamma_5 d|0\rangle|^2} \\ &\times \frac{e^{-(T-t_x)E_{\bar{K}^0}}e^{-(t_x-t_y)E_{K^0}}}{\left(\underbrace{e^{-E_{\bar{K}^0}(T-t_x+t_y)}}_{a} + \underbrace{e^{-E_{\bar{K}^0}(T-T+t_x-t_y)}}_{b}\right)\left(\underbrace{e^{-E_{K^0}t_x}}_{c} + \underbrace{e^{-E_{K^0}(T-t_x)}}_{d}\right)} \end{aligned} \tag{4.30}$$

For this time range, term $(b)$ dominates over $(a)$ while $(c)$ dominates over $(d)$, in which case the time dependence in the numerator and denominator will not cancel which each other, as seen in the Fig. 4.4.

3. For $0 < t_y < T/2 < t_x < T/2+t_y$, term $(b)$ dominates over $(a)$ however now, $(d)$ dominates over $(c)$ cancelling the time dependence in the numerator giving a constant plateau as observed.

4. For $0 < t_y < T/2 < T/2+t_y < t_x$, $(a)$ and $(d)$ dominate and the expression is not longer time independent which is confirmed by the shape of the plot.

## 4.4 Numerical results for $B_{D_q}$ and $\xi$

The numerical results of the bare bag parameters,

$$B^{\text{bare}} = \frac{\langle M^0(\Delta T)|O_{\text{VV+AA}}(t)|\overline{M}^0(0)\rangle}{\frac{8}{3}\langle M^0(\Delta T - t)|A_0(0)\rangle\langle A_0(t)|\overline{M}^0(0)\rangle}. \tag{4.31}$$

for all the ensembles listed in Sec. 2.4 are presented in Table. 4.3. The notation is chosen to emphasize the time separation between the source and sink operators, $\Delta T$, which is fixed at a given value, while the time dependence of the $O_{\mathrm{VV+AA}}$ is simply denoted by $t$, over which a fit is performed. In the previous notation, these were denoted by $t_y$ and $t_x$ respectively. The numbers in Table. 4.3 are bare quantities. Representative plots of the bag parameter vs time for heavy-light and heavy-strange mesons, with $am_h = 0.3$ on the C0 ensemble have been shown in Fig. 4.5. These correspond to the region labelled by "1" in Fig. 4.4, *i.e.* where the time dependence cancels between the numerator and denominator of Eq. 4.31. The simulation data contains different values of $\Delta T$ from which the bag parameter can be extracted. For small source-sink separation, $\Delta T$, there may be not sufficient time for the plateau to be reached, and the fit to a constant may suffer from the effect of excited states. On the other hand, large $\Delta T$ contains less precise data as the noise grows with time separation, in particular, this is most visible for the heaviest data points. Therefore, we try to search for a particular $\Delta T$, such that a visible plateau is reached while the statistical error is small. The plots of bag parameters for different values of $\Delta T$ on the larger ensembles can be seen in Fig. 4.7, Fig. 4.8 and Fig. 4.9. We indeed observed the trend described above, with the error bars getting larger for large values of $\Delta T$. The particular choice of $\Delta T$ on each ensemble is given in the second column of Table 4.3, chosen in such a way that a plateau similar to those in Fig. 4.6 are visible on all the ensembles.

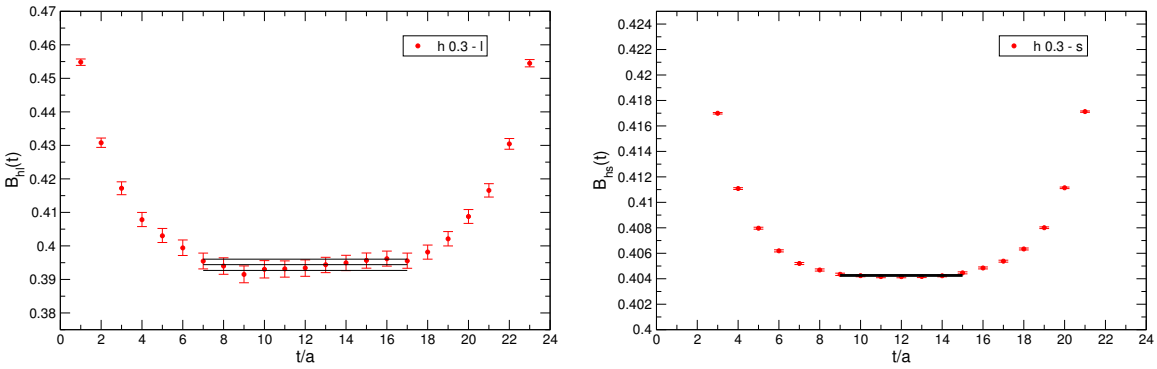


Figure 4.5: Heavy-light (left) and heavy-strange (right) bag parameter fits, for heavy quark mass $am_h = 0.3$, on the C0 ensemble.

| Name | $\Delta T/a$ | $[t_{\min}, t_{\max}]$ | $B_{hl}^{\text{bare}}$ | $[t_{\min}, t_{\max}]$ | $B_{hs}^{\text{bare}}$ |
|---|---|---|---|---|---|
| C0 | 24 | 7 - 17 | 0.3944(17) | 9 - 15 | 0.404259(71) |
| | 24 | 7 - 17 | 0.4015(23) | 9 - 15 | 0.411509(81) |
| | 24 | 7 - 17 | 0.4075(32) | 9 - 15 | 0.417930(96) |
| C1 | 24 | 7 - 17 | 0.39748(99) | 8 - 16 | 0.40418(27) |
| | 24 | 7 - 17 | 0.4054(13) | 8 - 16 | 0.41159(30) |
| | 24 | 7 - 17 | 0.4124(17) | 8 - 16 | 0.41815(35) |
| C2 | 24 | 7 - 17 | 0.39839(59) | 8 - 16 | 0.39839(59) |
| | 24 | 7 - 17 | 0.40619(71) | 8 - 16 | 0.40619(71) |
| | 24 | 7 - 17 | 0.41311(89) | 8 - 16 | 0.41311(89) |
| M0 | 28 | 9 - 19 | 0.3831(13) | 11 - 17 | 0.393369(77) |
| | 28 | 9 - 19 | 0.3939(19) | 11 - 17 | 0.404409(88) |
| | 28 | 9 - 19 | 0.4020(27) | 11 - 17 | 0.41332(11) |
| | 28 | 9 - 19 | 0.4083(38) | 11 - 17 | 0.42094(14) |
| M1 | 28 | 9 - 19 | 0.38543(92) | 11 - 17 | 0.39257(25) |
| | 28 | 9 - 19 | 0.3972(12) | 11 - 17 | 0.40377(27) |
| | 28 | 9 - 19 | 0.4068(16) | 11 - 17 | 0.41282(30) |
| | 28 | 9 - 19 | 0.4151(22) | 11 - 17 | 0.42055(36) |
| M2 | 28 | 9 - 19 | 0.3859(10) | 11 - 17 | 0.39206(24) |
| | 28 | 9 - 19 | 0.3975(13) | 11 - 17 | 0.40322(40) |
| | 28 | 9 - 19 | 0.4067(17) | 11 - 17 | 0.41218(47) |
| | 28 | 9 - 19 | 0.4145(22) | 11 - 17 | 0.41978(59) |
| F1 | 34 | 10 - 24 | 0.37714(92) | 13 - 21 | 0.38519(15) |
| | 34 | 10 - 24 | 0.3885(13) | 13 - 21 | 0.39635(17) |
| | 34 | 10 - 24 | 0.3975(18) | 13 - 21 | 0.40523(20) |
| | 34 | 10 - 24 | 0.4050(26) | 13 - 21 | 0.41269(25) |
| | 34 | 10 - 24 | 0.4139(40) | 13 - 21 | 0.42162(35) |

Table 4.3: Bag parameters for heavy-light and heavy-strange mesons on all ensembles for given $\Delta T$.

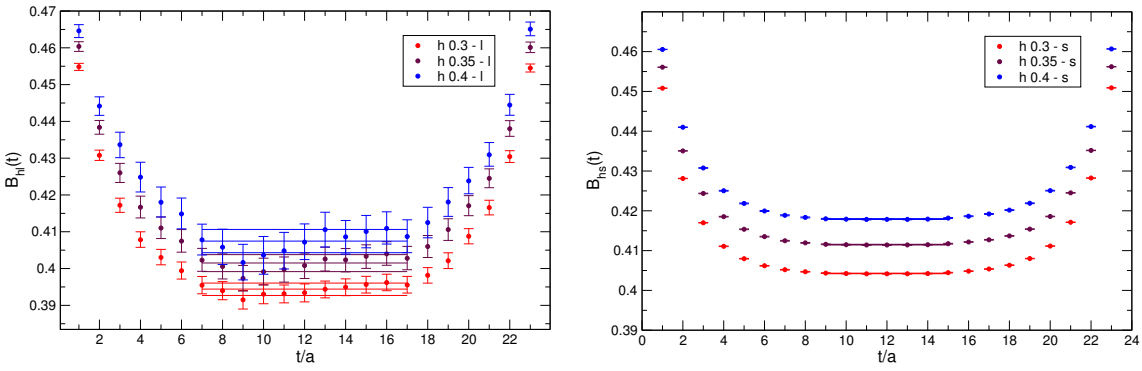


Figure 4.6: Heavy-light (left) and heavy-strange (right) bag parameter fits, for all heavy quark masses, on the C0 ensemble.

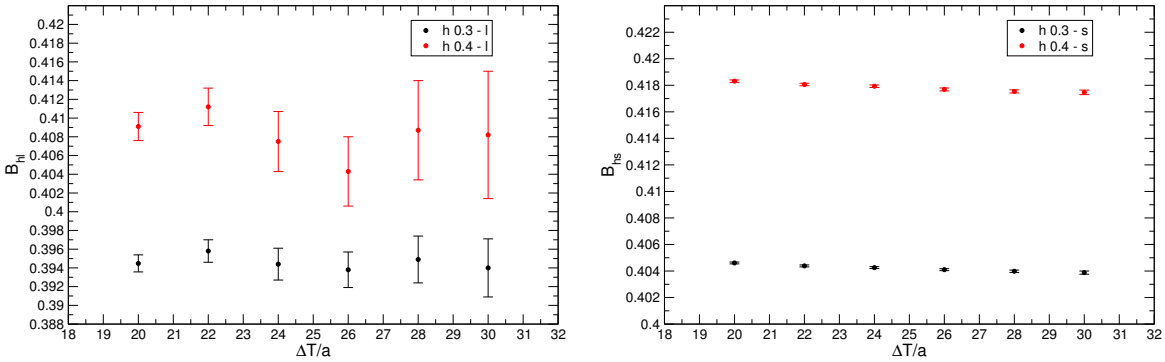


Figure 4.7: Heavy-light (left) and heavy-strange (right) bag parameter for different values of $\Delta T$ on the C0 ensemble. The mesons with the lightest, $am_h = 0.3$, and heaviest, $am_h = 0.4$, are chosen as representatives.

The results for heavy-light and heavy-strange bag parameters are plotted against inverse meson masses in lattice units, in Fig. 4.10. As can be observed from the plots, the bag parameter depends linearly on inverse meson mass, suggesting that very few terms in an HQET expansion are required to describe our data at the current, percent scale, precision. Final conclusions are deferred until we have performed the mass and continuum extrapolations analyses for this quantity.

Finally, we present the results for the $\xi$ parameter in the charm mass region, given our evaluation of the meson decay constants and bag parameters. Recall

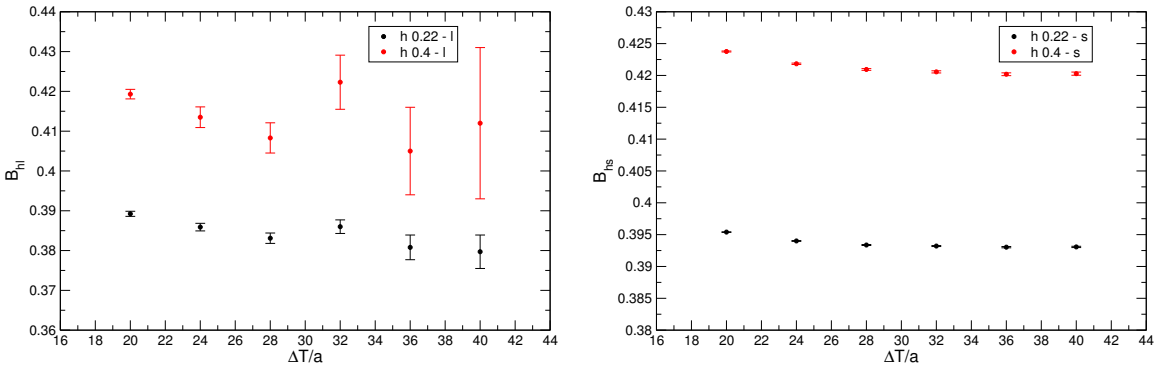


Figure 4.8: Heavy-light (left) and heavy-strange (right) bag parameter for different values of $\Delta T$ on the M0 ensemble. The mesons with the lightest, $am_h = 0.22$, and heaviest, $am_h = 0.4$, are chosen as representatives.

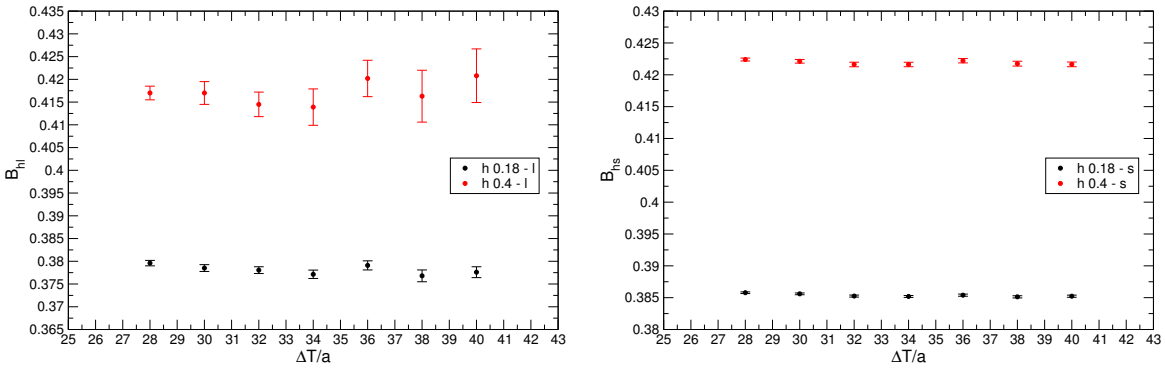


Figure 4.9: Heavy-light (left) and heavy-strange (right) bag parameter for different values of $\Delta T$ on the F1 ensemble. The mesons with the lightest, $am_h = 0.18$, and heaviest, $am_h = 0.4$, are chosen as representatives.

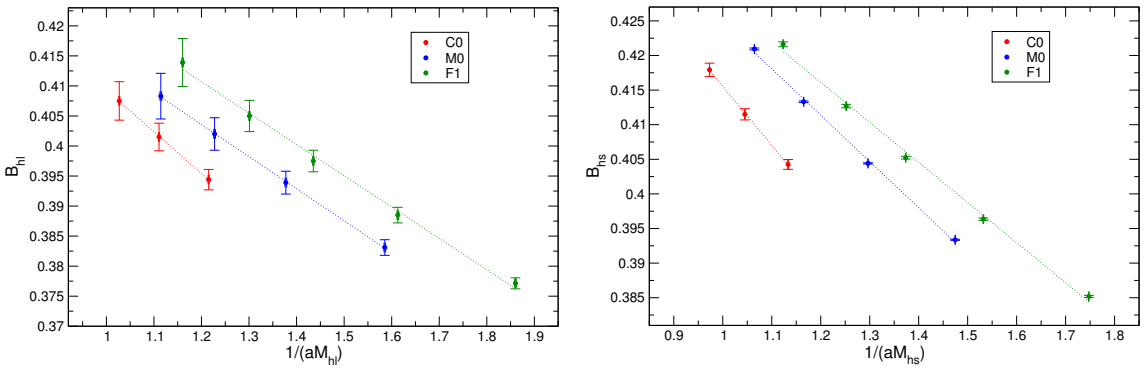


Figure 4.10: Heavy-light (left) and heavy-strange (right) bag parameter vs the corresponding inverse meson mass, in lattice units, on ensembles C0, M0, F1. Note that the dotted line is simply drawn to guide the eye and this is not how we fit the bag parameter in practice.

that the $\xi$ parameter is defined according to Eq. 1.80:

$$\xi = \frac{f_{B_s}\sqrt{B_{B_s}}}{f_{B_d}\sqrt{B_{B_d}}} \,, \tag{4.32}$$

As already stated Chapter. 1, this quantity is defined for B-mesons. Given that our simulations only covers the charm mass region, it is essential for the global fit to include an anzats for extrapolation to the B mass region, see Sec. 4.5. Fig. 4.11 summarizes our results so far. Note the insensitivity of $\xi$ to the heavy quark mass. The largest theoretical uncertainty in $\xi$ to date has arisen from the chiral extrapolation [100–102]. We emphasize that these small errors have been obtained directly at physical pion masses which removes the need for such extrapolation. The dependence on the lattice spacing will be removed by a continuum extrapolation in a global fit in future work.

## 4.5 Gauge link smearing

Since the $\xi$ parameter is a quantity which is defined for B mesons, an extrapolation to the heavy B mesons mass has to be included in a future global fit ansatz. As it can be observed in Fig. 4.11, this extrapolation is rather far at the moment which would lead to a less precise result for $\xi$. Therefore, it would be beneficial to find the optimal heavy domain wall fermion action that would give access to

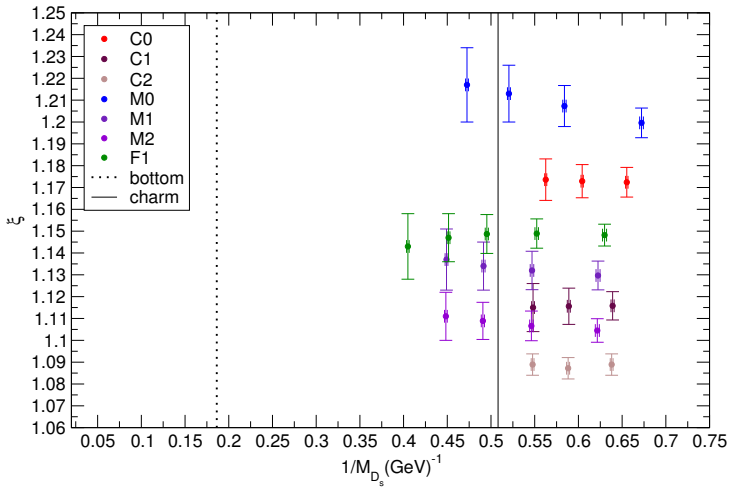


Figure 4.11: $\xi$ parameter on all ensembles vs inverse heavy-strange meson mass in physical units. The solid line represents the value of inverse physics $D_s$ meson mass, while the dotted line represent the value of inverse physical $B_s$ meson mass.

heavier quark masses i.e. closer to the physical point for B physics studies. In order to achieve this, we have tested the effect of gauge link smearing on the axial current renormalization factor $Z_A$ with heavy-heavy quarks. The tests involved generating propagators on a $16^3 \times 32$ lattice with $a^{-1} = 1.78$ and pion mass $m_\pi = 430$ MeV. Different stout smearing parameter $\rho$ and number of smearing hits [103] were used as well as altering the domain wall height $M_5$ in the action. We seek minimum amount of smearing while still maintaining the light quark mass near its physical point. The simulated heavy quark mass is $am_h = 0.45$. Fig. 4.12 shows the effect of different number of stout hits, with standard stout parameter $\rho = 0.1$. We observe that 3 hits of smearing reduces the residual mass to per mille level. Furthermore, it allows for simulation of even heavier masses whilst preserving the chiral properties of the domain wall formulation.

This study was then continued in more detail by other members of our collaboration to obtain the optimal heavy quark action on each of the ensembles C0 to F1 with smeared gauge links. Currently the second run of the charm project is underway with data being analysed in due course.

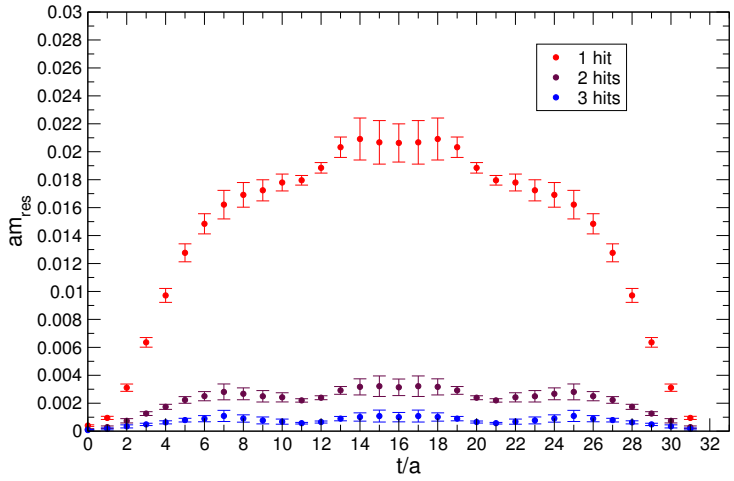


Figure 4.12: Effect of different number of levels (hits) of stout smearing on the residual mass with heavy quark input mass $am_h = 0.45$ and $M_5 = 1.0$ on a $16^3 \times 32$ lattice with $a^{-1} = 1.78$.

# Chapter 5

# Conclusions and Outlook

Interest in heavy quark physics as a probe to New Physics beyond the Standard Model has resulted in lattice QCD simulations to investigate their non-perturbative dynamics in recent years. Some of the quantities and observables that can be used to constrain the CKM matrix elements and hence act as probes to the SM were discussed in Chapter 1 of this thesis. In Chapter 2, we described some of the previous theoretical works, such as the domain wall formulation and the choice of parameters, used in the current RBC/UKQCD charm project simulations.

As discussed earlier, with a heavy quarks masses currently being the same order as the UV cut-off it is difficult identify the renormalization window clearly. This led us to develop a massive renormalization scheme to reshuffle lattice artefacts of $O(a^2m^2)$ in order to potentially remove some of these artefacts. In Chapter 3, we presented a mass dependent renormalization scheme, RI/mSMOM, for fermion bilinear operators in QCD with non-exceptional momentum kinematics similar to the standard RI/SMOM scheme. In contrast to RI/SMOM where the renormalization conditions are imposed at the chiral limit, this scheme allows for the renormalization conditions to be set at some mass scale $\overline{m}$, which we are free to choose. In the limit where $\overline{m} \to 0$, our scheme reduces to SMOM. Using a mass dependent scheme for a theory containing massive quarks has the benefit of preserving the continuum WI by taking into account terms of order $m/\mu$, which would otherwise violate the WI when a massless scheme is used. We have shown that the WIs for the case of both degenerate and non-

degenerate masses are satisfied non-perturbatively, giving $Z_V = 1$ and $Z_A = 1$. In order to gain a better understanding of the properties of the mSMOM scheme we have performed an explicit one-loop computation in perturbation theory using dimensional regularization. We also reperformed the 1-loop computation using the 't Hooft-Veltman convention for $\gamma_5$. These the results can be particularly useful for extending the renormalization conditions to the singlet quark flavor. The programme to generate vertex functions numerically, with an appropriate projector in the massive scheme, has be written. The vertex functions are now being generated. The renormalization factors will be extracted in the near future, in order to examine whether or not the new schemes allows for a smoother trajectory to the continuum limit.

In Chapter 4, lattice results for meson masses and decays constants as well as the bag and $\xi$ parameters near $D$ and $D_s$ meson regions were presented. The global fits for mesons masses and decay constants, in which the continuum limit dependence, the pion mass dependence and the heavy quark dependence where simultaneously fitted using an ansatz, were performed by other members of the collaboration. The details can be found in Ref. [72].

In terms of the future of this project, we have explored changes in the formulation of the domain wall action, such as gauge link smearing, in order to increase the reach in the heavy quark mass. An example was given in the last section of Chapter 4. After completely investigating the reach in heavy-light and heavy-strange meson masses using the parameters of the adapted action, by other members of the collaboration, the second large scale run for the RBC/UKQCD is on the way. This have allowed us to reach mesons heavier than the charm region, allowing to better constrict the extrapolation to the B sector.

# Appendix A

# Charge and Parity symmetries

Charge and parity symmetries are amongst discrete symmetry transformations. Under parity, the space-time coordinates transform as [104]:

$$x = (x^0, \boldsymbol{x}) \rightarrow x_P = (x^0, -\boldsymbol{x}) \cdot \tag{A.1}$$

The charged $W$-boson, under parity, transform as:

$$W_\mu^{(\pm)} \xrightarrow{P} W^{(\pm)\mu}(x_P) \ , \tag{A.2}$$

and under charge conjugation, $C$, as:

$$W_\mu^{(\pm)} \xrightarrow{C} -W^{(\mp)\mu}(x) \cdot \tag{A.3}$$

Putting the two transformations together,

$$W_\mu^{(\pm)}(x) \xrightarrow{CP} -W^{(\mp)\mu}(x_P) \cdot \tag{A.4}$$

In the chiral basis,

$$\gamma^\mu = \begin{pmatrix} 0 & \sigma^\mu \\ \\ \bar{\sigma}^\mu & 0 \end{pmatrix} , \tag{A.5}$$

where

$$\sigma^{\mu} \equiv (1, \underline{\sigma}) \quad \text{and} \quad \bar{\sigma}^{\mu} \equiv (1, -\underline{\sigma}) \cdot \tag{A.6}$$

Under parity, the Dirac spinor

$$\psi = \begin{pmatrix} \psi_L \\ \\ \psi_R \end{pmatrix} (x) \xrightarrow{P} \begin{pmatrix} \psi_R \\ \\ \psi_L \end{pmatrix} (x_P) \ , \tag{A.7}$$

*i.e.* ,

$$\psi(x) \xrightarrow{P} \gamma^0 \psi(x_P) \cdot \tag{A.8}$$

Under charge conjugation,

$$\psi(x) \xrightarrow{C} i\gamma^2\gamma^0 \bar{\psi}^T(x) \ , \tag{A.9}$$

leaving the space-time coordinate unaffected. Therefore, under $CP$

$$\psi = \begin{pmatrix} \psi_L \\ \\ \psi_R \end{pmatrix} (x) \xrightarrow{CP} \begin{pmatrix} -i\sigma^2 \psi_L^* \\ \\ i\sigma^2 \psi_R^* \end{pmatrix} (x_P) \cdot \tag{A.10}$$

# Appendix B

# Conventions

## B.1 Minkowski to Euclidean conventions

In this section the conventions for going from Minkowski to Euclidean space are stated and the fermion propagator is written as an example. Starting with the space-time 4-vector:

$$x_0^{\mathrm{M}} = -ix_4^{\mathrm{E}} \quad , \quad x^{i\mathrm{M}} = x_i^{\mathrm{E}} \ , \tag{B.1}$$

which means $x_i = -x_i^{\mathrm{E}}$ and we do not distinguish between upper and lower indices in Euclidean space. Similarly for momentum $k^\mu$ we have

$$k_0^{\mathrm{M}} = -ik_4^{\mathrm{E}} \quad , \quad k^{i\mathrm{M}} = k_i^{\mathrm{E}} \ . \tag{B.2}$$

The relation for the vector potential becomes

$$A_0^{\mathrm{M}} = iA_4^{\mathrm{E}} \quad , \quad A^{i\mathrm{M}} = -A_i^{E} \ . \tag{B.3}$$

Therefore the covariant derivative in Minkowski space

$$D_\mu = \partial_\mu + ig\not{A}_\mu \ , \tag{B.4}$$

maps to

$$D_0^{\mathrm{M}} = iD_4^{\mathrm{E}} \quad , \quad D^{i\mathrm{M}} = -D_i^{\mathrm{E}} \ , \tag{B.5}$$

and the Euclidean covariant derivative becomes

$$D_\mu^{\mathrm{E}} = \partial_\mu^{\mathrm{E}} + ig\mathscr{A}_\mu^{\mathrm{E}} \ . \tag{B.6}$$

The gamma matrices map in the following way:

$$\gamma_0^{\mathrm{M}} = \gamma_4^{\mathrm{E}} \quad , \quad \gamma^{1,2,3\ \mathrm{M}} = i\gamma_{1,2,3}^{\mathrm{E}} \ . \tag{B.7}$$

For convenience we also take

$$\psi^{\mathrm{M}} = \psi^{\mathrm{E}} \quad , \quad \overline{\psi}^{\mathrm{M}} = \overline{\psi}^{E} \ . \tag{B.8}$$

The fermionic part of the action in Minkowski space is

$$S^{\mathrm{M}}[\overline{\psi}, \psi] = \int d^4x \ \overline{\psi}\big(i\gamma^\mu D_\mu - m\big)\psi. \tag{B.9}$$

Using the maps defined above, the Euclidean action becomes

$$S^{\mathrm{E}}[\overline{\psi}, \psi] = \int d^4x^{\mathrm{E}} \ \overline{\psi}^{\mathrm{E}}\Big[\gamma_\mu^{\mathrm{E}} D_\mu^E + m\Big]\psi^{\mathrm{E}}, \tag{B.10}$$

where

$$iS^{\mathrm{M}} = -S^{\mathrm{E}}. \tag{B.11}$$

The inverse Fourier transform in Minkowski space is given by:

$$f(x_{\mathrm{M}}) = \int \frac{d^4p_{\mathrm{M}}}{(2\pi)^4} \ e^{-ip_{\mathrm{M}}.x_{\mathrm{M}}} \tilde{f}(p_{\mathrm{M}}). \tag{B.12}$$

The consistent inverse FT in Euclidean space is then

$$f(x_{\mathrm{E}}) = \int \frac{d^4p_{\mathrm{E}}}{(2\pi)^4} \ e^{ip_{\mathrm{E}}.x_{\mathrm{E}}} \tilde{f}(p_{\mathrm{E}}). \tag{B.13}$$

Therefore, analytics continuation implies that

$$\tilde{f}(p_{\mathrm{M}}) = -i\tilde{f}(p_{\mathrm{E}}). \tag{B.14}$$

The inverse fermionic propagator at tree-level, using Euclidean FT

$$\tilde{f}(p_{\mathrm{E}}) = \int d^4x_{\mathrm{E}}\ e^{-ip_{\mathrm{E}}.x_{\mathrm{E}}} f(x_{\mathrm{E}}). \tag{B.15}$$

becomes

$$S_E^{-1}(p) = (i\not{p}_{\mathrm{E}} + m). \tag{B.16}$$

One can check that

$$\mathcal{F}\big[\langle\psi(x)\overline{\psi}(0)\rangle\big]_{\mathrm{M}} = -i\mathcal{F}\big[\langle\psi(x)\overline{\psi}(0)\rangle\big]_{\mathrm{E}}, \tag{B.17}$$

is satisfied:

$$\frac{i}{\not{p}_M - m} = \frac{i}{-i\not{p}_E - m} = \frac{-i}{i\not{p}_E + m}. \tag{B.18}$$

## B.2 Fourier transform and derivatives on the lattice

In this section we introduce basic mathematical tools and conventions required for the formulation of Quantum Field Theory on the lattice.

Given lattice spacing $a$, the lattice coordinates can be written as:

$$x_\mu = n_\mu a \quad n = 0, 1, ... \quad \mu = 1, 2, ..., D \quad \text{in D dimensions} \tag{B.19}$$

for finite volume box of size $L = Na$, $n$ takes the values $n = 0, 1, ..., N-1$. For a smooth function $f(x)$ in $D$ dimensions one has, in the limit $a \to 0$:

$$\sum_x f(x) = a^D \sum_n \to \int d^D x\ f(x) \tag{B.20}$$

again, for a finite volume lattice of side $L$, the corresponding integral would range from 0 to $L$.

We define the forward and backward derivatives on the lattice as follows:

$$\nabla_\mu \phi(x) = \frac{\phi(x + a\hat{\mu}) - \phi(x)}{a} \tag{B.21}$$

$$\nabla^*_\mu \phi(x) = \frac{\phi(x) - \phi(x - a\hat{\mu})}{a} \tag{B.22}$$

so that $\nabla_\mu = \partial_\mu + \mathcal{O}(a)$. In principle, one can increase the accuracy of the calculations involved by defining derivatives in different ways. The Central Difference formulation takes the form

$$\nabla_{\text{mid}} \phi(x) = \frac{\phi(x + a) - \phi(x - a)}{2a} + \mathcal{O}(a^2) \tag{B.23}$$

which means that the central difference derivative will have smaller discretisation errors (since it is $\mathcal{O}(a^2)$) compared to the forward derivative ($\mathcal{O}(a)$). Therefore, one can see that there is an ambiguity in the way derivatives can be defined on the lattice. Having derivative formulations which contain higher orders of $a$ will naturally increase accuracy. The drawback however, is that it will become more computationally expensive. For the second derivative we have

$$\phi''(x) = \frac{\phi(x + a) - 2\phi(x) + \phi(x - a)}{a^2} + \mathcal{O}(a^2) \tag{B.24}$$

which can be easily proved by taylor expanding both sides up to order $a^4$.Note that the latter definition of the first derivative *i.e.* of order $\mathcal{O}(a^2)$ as in equation B.23, is the one that is used in Chapter 2 section 2.1.4 when constructing the fermion propagator. The same is used for the scalar field.

To construct the discretized inverse Fourier transform, let us start with recalling the integral representation of the Kronecker delta function (*i.e.* discrete),

$$\delta_{nn'} = \frac{1}{2\pi i} \oint \frac{z^n}{z^{n'+1}} \ , \tag{B.25}$$

which is simply due to the residue theorem. Making a change of variables $z = e^{ik}$

where $-\pi < k < \pi$ results in

$$\delta_{nn'} = \frac{1}{2\pi} \int_{-\pi}^{\pi} dk e^{ik(n-n')} \ . \tag{B.26}$$

Note that the limits make sense because if we set $n = n'$ on the LHS we get 1 from the delta and on the right hand side $\frac{2\pi}{2\pi} = 1$. Making another change of variable $k \to ak$ yields

$$\delta_{nn'} = \frac{a}{2\pi} \int_{-\pi/a}^{\pi/a} e^{ika(n-n')} dk \ . \tag{B.27}$$

Now consider the discretized Fourier transform which is of the form,

$$\tilde{f}(k) = a \sum_n f(na) e^{-ikna} \ . \tag{B.28}$$

Multiplying both sides of the equation by $e^{ikn'}$ and integrating with respect to $k$ from $-\pi/a$ to $\pi/a$ gives

$$\begin{aligned} \int_{-\pi/a}^{\pi/a} \tilde{f}(k) e^{ikna'} dk =& a \sum_n \int_{-\pi/a}^{\pi/a} e^{-ika(n-n')} f(na) dk \\ =& 2\pi \sum_n \delta_{nn'} f(na) = 2\pi f(n'a) \ . \end{aligned} \tag{B.29}$$

This yields the discretized inverse Fourier transform:

$$f(na) = \int_{-\pi/a}^{\pi/a} \frac{dk}{2\pi} \tilde{f}(k) e^{ikan} \ , \tag{B.30}$$

where we are in fact integrating over the first Brillouin zone. Generalization to higher dimensions is trivial. In all the above, the volume was considered to be infinite. If however, we wish to work in a finite volume we would need to impose certain boundary conditions. For periodic boundary conditions:

$$f(an + aN) = f(an) \ , \tag{B.31}$$

where there are $N$ points in total. Defining $n' = N + n$, we must have

$$\begin{aligned}\tilde{f}(k) =& a\sum_{n} f((N+n)a)e^{-ikna} = a\sum_{n'} f(n'a)e^{-ik(n'-N)a} \\ =& a\sum_{n'} f(n'a)e^{-ikn'a}e^{ikNa} \ .\end{aligned} \tag{B.32}$$

meaning $e^{ikaN} = e^{2i\pi m}$ where $m$ is an integer and so $k = \frac{2\pi m}{aN}$. Going back to Eq. B.30 and observing the limits, we conclude that $m$ must run from $\frac{-N}{2} + 1$ to $\frac{N}{2}$ since we cannot have more than $N$ points. Replacing $dk$ by its discretized equivalent *i.e.* the "fundamental" unit $k$ which is $k = 2\pi/aN$, we get

$$f(na) = \frac{1}{L}\sum_{m=-N/2+1}^{N/2} \tilde{f}(\frac{2\pi m}{L})e^{\frac{2\pi imn}{N}} \tag{B.33}$$

where we have used $L = aN$. The above can be easily generalised to $d$ dimensions.

## B.3 Free scalar field propagator

The continuum Euclidean action in 4 dimensions for the free scalar field reads as follows

$$\begin{aligned}S_E[\phi] =& \int d^4x \left(\frac{1}{2}\partial_\mu\phi(x)\partial_\mu\phi(x) + \frac{1}{2}m^2\phi^2(x)\right) \\ =& \frac{1}{2}\int d^4x \left(-\phi(x)\partial^2\phi(x) + m^2\phi^2(x)\right) ,\end{aligned} \tag{B.34}$$

Discretizing space-time and using B.24 for the definition of the derivative we get

$$\begin{aligned}
S_E[\phi] =& \frac{a^4}{2}\sum_x \left( -\phi(x)\sum_\mu \frac{\phi(x+a\hat{\mu}) - 2\phi(x) + \phi(x-a\hat{\mu})}{a^2} + m^2\phi^2(x) \right) \\
=& \frac{a^4}{2}\sum_x \left\{ \int_{kk'} \Big( -\frac{e^{ikx}}{a^2}\tilde{\phi}(k)\sum_\mu \left[ e^{ik'.(x+a\hat{\mu})} - 2e^{ik'.x} + e^{ik'.(x-a\hat{\mu})} \right]\tilde{\phi}(k') \right. \\
& \left. + m^2\tilde{\phi}(k)\tilde{\phi}(k')e^{i(k+k')x} \Big) \right\} \\
=& \frac{a^4}{2}\sum_x \left\{ \int_{kk'} e^{i(k+k').x} \left[ \frac{-1}{a^2}\tilde{\phi}(k)2\sum_\mu \cos(k'_\mu a) + \left( m^2 + \frac{8}{a^2} \right)\tilde{\phi}(k)\tilde{\phi}(k') \right] \right\} \\
=& \frac{1}{2}\int_{kk'} \delta(k+k') \left[ \frac{-1}{a^2}\tilde{\phi}(k)2\sum_\mu \cos(k'_\mu a) + \left( m^2 + \frac{8}{a^2} \right)\tilde{\phi}(k)\tilde{\phi}(k') \right] \\
=& \frac{1}{2}\int_k \left[ \phi(k) \left( m^2 + \frac{1}{a^2}\sum_\mu (2 - 2\cos(k_\mu a)) \right)\phi(k) \right] \\
=& \frac{1}{2a^2}\int_k \left[ \phi(k) \left( a^2m^2 + \sum_\mu (2 - 2\cos(k_\mu a)) \right)\phi(k) \right],
\end{aligned} \tag{B.35}$$

where $k.\hat{\mu} = k_\mu$ and $\int_{kk'}$ denotes $\frac{d^4kd^4k'}{(2\pi)^4(2\pi)^4}$. In the last line we have changed variables from $k \to -k$ and the integral is over the first Brillouin zone. The inverse scalar propagator on the lattice, in momentum space, takes the form:

$$D_S(k) = \frac{1}{m^2 + a^{-2}\sum_\mu (2 - 2\cos(k_\mu a))} \cdot \tag{B.36}$$

## B.4 Twisted boundary conditions

Here we discuss a different boundary condition for fermions on a finite lattice which turns out to be very useful [90]. The fact that momentum is quantized on the lattice, leads to limitations in different phenomenological applications. Take the 2-body hadron decay as an example. The energies of the decay products is related to the masses of the particles involved by 4-momentum conservation. However, they cannot take their physical value unless the masses are consistent with the momentum quantisation rule. This issue can be resolved by choosing

different boundary conditions. The momentum quantization rule for periodic boundary conditions is well-known:

$$\psi(x + \mathbf{e}_i L) = \psi(x) \quad , \quad i = 1, 2, 3 \ , \tag{B.37}$$

for spacial directions. Taking the Fourier transform

$$\int d^4p \ e^{+ip(x+\mathbf{e}_i L)} \tilde{\psi}(p) = \int d^4p \ e^{ipx} \tilde{\psi}(p) \quad , \quad i = 1, 2, 3 \tag{B.38}$$

which implies

$$e^{ip_i L} = 1 \quad \Longrightarrow \quad p_i = \frac{2\pi n_i}{L} \quad , \quad i = 1, 2, 3 \cdot \tag{B.39}$$

Now, define the $\theta$-boundary conditions as

$$\psi(x + \mathbf{e}_i L) = e^{i\theta_i} \psi(x) \ , \tag{B.40}$$

similar to above, taking the Fourier transform gives

$$e^{i(p_i - \theta_i/L)} = 1 \quad \Longrightarrow \quad p_i = \frac{\theta_i}{L} + \frac{2\pi n_i}{L} \quad , \quad i = 1, 2, 3 \cdot \tag{B.41}$$

In other words, the spacial momenta are still quantised for periodic boundary condition but also shifted by an arbitrary amount $\theta_i/L$ which is *continuous*. It is shown [90] that $\theta/L$ does indeed act as a true physical momentum, in particular the physical energy of the mesonic state can be written as

$$E_{ij}(\theta, a) = \sqrt{M_{ij}^2 + \left(\frac{\theta}{L}\right)^2} \ , \tag{B.42}$$

where $M_{ij}$ is the mass of the pseudoscalar meson made of an $i$ and a $j$ quark anti-quark pair. It is also shown that the continuum extrapolation gives the correct relativistic dispersion relations.

# Appendix C

# Renormalization

## C.1 Conventions

- The fermion propagator in position space is

$$S(x_3 - x_2) = \langle \psi(x_3)\bar{\psi}(x_2)\rangle, \tag{C.1}$$

and the Minkowski Fourier convention we use is

$$S(p) = \int d^4x e^{ip.x} S(x). \tag{C.2}$$

The Mikowski fermion propagator in momentum space is written as

$$S(p) = \frac{i}{\not{p} - m + i\epsilon - \Sigma(p)}\,, \tag{C.3}$$

and the fermion self-energy $\Sigma(p)$ is decomposed into

$$\Sigma(p) = \not{p}\Sigma_V(p^2) + m\Sigma_S(p^2)\,. \tag{C.4}$$

- The gluon propagator in Feynman gauge is

$$\frac{-ig^{\mu\nu}}{k^2 + i\epsilon}\,. \tag{C.5}$$

- Note that the one-loop self-energy $\Sigma(p)$ in this convention is

$$-i\Sigma(p) = -ig^2 C_2(F) \int \frac{\gamma_\alpha(\not{p} - \not{k} + m)\gamma^\alpha}{k^2\left[(p-k)^2 - m^2\right]} \,. \tag{C.6}$$

- The basis of the Clifford algebra is chosen to be:

$$\Gamma = 1(S),\ i\gamma^5(P),\ \gamma^\sigma(V),\ \gamma^\sigma\gamma^5(A),\ \sigma^{\mu\nu} = \frac{i}{2}\left[\gamma^\mu, \gamma^\nu\right](T)\ \cdot \tag{C.7}$$

- The vertex function in position space is

$$G_O^a(x_3 - x, x_2 - x) = \langle \psi(x_3) O_\Gamma^a(x) \bar{\psi}(x_2) \rangle \tag{C.8}$$

  where we have used translational invariance and $O_\Gamma^a = \bar{\psi}\Gamma\tau^a\psi$ is a flavor non-singlet fermion bilinear operator.

## C.2 Vector WI in Minkowski space

To derive the non-singlet vector WI in Minkowski space, we start by applying the vector transformation on fermions fields,

$$\delta\psi(x) = i\Big[\alpha_V(x)\tau^a\Big]\psi(x)\,, \quad \delta\overline{\psi}(x) = -i\overline{\psi}(x)\Big[\alpha_V(x)\tau^a\Big]\cdot \tag{C.9}$$

In what follows we suppress the flavor index for simplicity. The Lagrangian under consideration is,

$$\mathcal{L} = i\bar{\psi}\not{D}\psi - m\bar{\psi}\psi\ , \tag{C.10}$$

where the covariant derivative is as usual,

$$D_\mu = \partial_\mu + ig\not{A}_\mu\ \cdot \tag{C.11}$$

We choose the operator insertion to be

$$O(x_3, x_2) = \psi(x_3)\bar{\psi}(x_2)\ , \tag{C.12}$$

and evaluate the change in the expectation value $\delta\langle O(x_3, x_2)\rangle = 0$:

$$
\begin{aligned}
0 = \frac{\delta}{\delta\alpha(x)}\langle O(x_3,x_2)\rangle &= \frac{\delta}{\delta\alpha(x)}\left[\int \mathcal{D}[\bar\psi,\psi]e^{iS[\mathcal{L}]}O(x_3,x_2)\right] \\
&= \int \mathcal{D}[\bar\psi,\psi]e^{iS[\mathcal{L}]}\frac{\delta O(x_3,x_2)}{\delta\alpha(x)} \quad + i\int \mathcal{D}[\bar\psi,\psi]e^{iS[\mathcal{L}]}\frac{\delta S[\mathcal{L}]}{\delta\alpha(x)}O(x_3,x_2)\cdot
\end{aligned}
\tag{C.13}
$$

For the variation in the operator we have,

$$
\frac{\delta O(x_3,x_2)}{\delta\alpha(x)} = i\delta(x-x_3)\psi(x_3)\bar\psi(x_2) - i\delta(x-x_2)\psi(x_3)\bar\psi(x_2)\cdot \tag{C.14}
$$

For the variation of the action,

$$
\begin{aligned}
&\frac{\delta}{\delta\alpha(x)}\left[\int d^4x'(\bar\psi(x')\delta\alpha(x'))(\not\partial + ig\not A)\psi(x') - \bar\psi(x')(\not\partial + ig\not A)\Big(\alpha(x')\psi(x')\Big)\right] \\
=&\bar\psi(x)\not D\psi(x) - \frac{\delta}{\delta\alpha(x)}\left[\int d^4x'\Big(\partial_\mu\alpha(x')\Big)\bar\psi(x')\gamma^\mu\psi(x') + \alpha(x')\bar\psi(x')\gamma^\mu\Big(D_\mu\psi(x')\Big)\right] \\
=&\bar\psi(x)\not D\psi(x) + \frac{\delta}{\delta\alpha(x)}\left[\int d^4x'\alpha(x')\partial_\mu V^\mu(x')\right] - \bar\psi(x)\not D\psi(x) \\
=&\partial_\mu V^\mu(x)\cdot
\end{aligned}
\tag{C.15}
$$

The vector WI in Minkowski space then reads:

$$
i\delta(x-x_3)\langle\psi(x_3)\bar\psi(x_2)\rangle - i\delta(x-x_2)\langle\psi(x_3)\bar\psi(x_2)\rangle = -i\partial_\mu G^\mu_{\mathrm{V}}(x_3-x,x_2-x)\cdot \tag{C.16}
$$

Taking the Fourier transform, placing the operator at the origin $x=0$, *i.e.* an implicit $\int d^4x\delta(x)$, the LHS or Eq. C.16 becomes,

$$
\begin{aligned}
&\int d^4x_2d^4x_3\ \Big(i\delta(-x_3)S(x_3-x_2) - i\delta(-x_2)S(x_3-x_2)\Big)e^{ip_3.x_3}e^{-ip_2.x_2} \\
=&\int d^4x_2\ iS(-x_2)e^{-ip_2.x_2}\ -\ \int d^4x_3\ iS(x_3)e^{ip_3.x_3} \\
=&iS(p_2) - iS(p_3)\cdot
\end{aligned}
\tag{C.17}
$$

For the first term on the RHS of Eq. C.16 we have the following, which we will evaluate at $x = 0$ after differentiation,

$$\begin{aligned} & -i\partial_\mu \int d^4x_2 d^4x_3 \; G^\mu_{\rm V}(x_3 - x, x_2 - x) e^{ip_3.x_3} e^{-ip_2.x_2} \\ =& -i\partial_\mu \int d^4x'_2 d^4x'_3 \; G^\mu_{\rm V}(x'_3, x'_2) e^{ip_3.(x'_3+x)} e^{-ip_2.(x'_2+x)} \\ =& -i(ip_3 - ip_2)_\mu \int d^4x'_2 d^4x'_3 \; G^\mu_{\rm V}(x'_3, x'_2) e^{ip_3.x'_3} e^{-ip_2.x'_2} \\ =& -q.G_{\rm V}(p_3, p_2) \cdot \end{aligned} \tag{C.18}$$

We therefore have,

$$q.G_{\rm V}(p_3, p_2) = iS(p_3) - iS(p_2) \cdot \tag{C.19}$$

Multiplying on the left with $S(p_3)^{-1}$ and on the right with $S(p_2)^{-1}$, the vector Ward identity for the amputated vertex function in momentum space becomes,

$$q.\Lambda_{\rm V}(p_2, p_3) = iS(p_2)^{-1} - iS(p_3)^{-1} \cdot \tag{C.20}$$

## C.3 Vector and Axial WI in Euclidean space

Starting with the probe in Eq. C.12 and taking $\delta\langle O(x_3, x_2)\rangle = 0$ under the symmetry transformations under consideration are:

$$\delta\psi(x) = i\Big[\alpha_V(x)\tau^a\Big]\psi(x)\,, \quad \delta\overline{\psi}(x) = -i\overline{\psi}(x)\Big[\alpha_V(x)\tau^a\Big], \tag{C.21}$$

and

$$\delta\psi(x) = i\Big[\alpha_A(x)\tau^a\gamma^5\Big]\psi(x)\,, \quad \delta\overline{\psi}(x) = i\overline{\psi}(x)\Big[\alpha_A(x)\tau^a\gamma^5\Big]\,, \tag{C.22}$$

one has to compute the variation in the action and the probe in Euclidean space. In what follows we suppress the flavor index for simplicity. The Lagrangian under consideration in Euclidean space is:

$$\mathcal{L} = \bar{\psi}\not{D}\psi + m\bar{\psi}\psi \cdot \tag{C.23}$$

We have,

$$\begin{aligned} 0 &= \frac{\delta}{\delta\alpha(x)}\langle O(x_3,x_2)\rangle = \frac{\delta}{\delta\alpha(x)}\left[\int \mathcal{D}[\bar{\psi},\psi]e^{-S[\mathcal{L}]}O(x_3,x_2)\right] \\ &= \int \mathcal{D}[\bar{\psi},\psi]e^{-S[\mathcal{L}]}\frac{\delta O(x_3,x_2)}{\delta\alpha(x)} \quad - \int \mathcal{D}[\bar{\psi},\psi]e^{-S[\mathcal{L}]}\frac{\delta S[\mathcal{L}]}{\delta\alpha(x)}O(x_3,x_2)\ . \end{aligned} \tag{C.24}$$

For the variation in the operator according to Eq. C.21 we have,

$$\frac{\delta O(x_3,x_2)}{\delta\alpha(x)} = i\delta(x-x_3)\psi(x_3)\bar{\psi}(x_2) - i\delta(x-x_2)\psi(x_3)\bar{\psi}(x_2)\ , \tag{C.25}$$

and for the variation of the action,

$$\begin{aligned} &\frac{\delta}{\delta\alpha(x)}\left[\int d^4x' \ -i(\bar{\psi}(x')\delta\alpha(x'))(\not{\partial}+ig\not{\mathcal{A}})\psi(x') + i\bar{\psi}(x')(\not{\partial}+ig\not{\mathcal{A}})\Big(\alpha(x')\psi(x')\Big)\right] \\ &= -i\bar{\psi}(x)\not{D}\psi(x) + i\frac{\delta}{\delta\alpha(x)}\left[\int d^4x'\Big(\partial_\mu\alpha(x')\Big)\bar{\psi}(x')\gamma^\mu\psi(x') + \alpha(x')\bar{\psi}(x')\gamma^\mu\Big(D_\mu\psi(x')\Big)\right] \\ &= -i\bar{\psi}(x)\not{D}\psi(x) - i\frac{\delta}{\delta\alpha(x)}\left[\int d^4x'\alpha(x')\partial_\mu V^\mu(x')\right] + i\bar{\psi}(x)\not{D}\psi(x) \\ &= -i\partial_\mu V^\mu(x)\ . \end{aligned} \tag{C.26}$$

The Euclidean Vector WI in position space takes the form,

$$i\delta(x-x_3)\langle\psi(x_3)\bar{\psi}(x_2)\rangle - i\delta(x-x_2)\langle\psi(x_3)\bar{\psi}(x_2)\rangle = -i\partial_\mu G_V^\mu(x_3-x,x_2-x)\ . \tag{C.27}$$

Taking the Fourier transform, placing the operator at the origin $x = 0$, *i.e.* inserting $\int d^4x\delta(x)$, the LHS of Eq. C.27 becomes,

$$\begin{aligned} &\int d^4x_2d^4x_3\ \Big(i\delta(-x_3)S(x_3-x_2) - i\delta(-x_2)S(x_3-x_2)\Big)e^{-ip_3.x_3}e^{ip_2.x_2} \\ =&iS(p_2) - iS(p_3)\ . \end{aligned} \tag{C.28}$$

For the first term on the RHS of Eq. C.27, and evaluating at $x = 0$ after differentiation, we have the following,

$$\begin{aligned}
&-i\partial_\mu \int d^4x_2 d^4x_3 \; G^\mu_{\rm V}(x_3 - x, x_2 - x) e^{-ip_3.x_3} e^{ip_2.x_2} \\
=&-i\partial_\mu \int d^4x'_2 d^4x'_3 \; G^\mu_{\rm V}(x'_3, x'_2) e^{-ip_3.(x'_3+x)} e^{+ip_2.(x'_2+x)} \\
=&i(ip_3 - ip_2)_\mu \int d^4x'_2 d^4x'_3 \; G^\mu_{\rm V}(x'_3, x'_2) e^{-ip_3.x'_3} e^{+ip_2.x'_2} \\
=&q.G_{\rm V}(p_3, p_2)
\end{aligned} \tag{C.29}$$

Therefore, the vector WI in momentum space can be written as,

$$q.G_{\rm V}(p_3, p_2) = iS(p_2) - iS(p_3) \cdot \tag{C.30}$$

Multiplying on the left with $S(p_3)^{-1}$ and on the right with $S(p_2)^{-1}$, the vector Ward identity for the amputated vertex function in Euclidean momentum space becomes,

$$q.\Lambda_{\rm V}(p_2, p_3) = iS(p_3)^{-1} - iS(p_2)^{-1} \cdot \tag{C.31}$$

If we now instead choose to vary the fields according to Eq. C.22, for the variation in the prob we get,

$$\frac{\delta O(x_3, x_2)}{\delta\alpha(x)} = i\delta(x - x_3)\gamma^5\psi(x_3)\bar\psi(x_2) + i\delta(x - x_2)\psi(x_3)\bar\psi(x_2)\gamma^5 \ , \tag{C.32}$$

and for the variation of the action,

$$\frac{\delta}{\delta\alpha(x)}\Bigg[\int d^4x' \; i(\bar\psi(x')\delta\alpha(x')\gamma^5)(\not\partial + ig\not A)\psi(x') + i\bar\psi(x')(\not\partial + ig\not A)\Big(\alpha(x')\gamma^5\psi(x')\Big) \tag{C.33}$$

$$+ 2mi\delta\alpha(x')\bar\psi(x')\gamma^5\psi(x')\Bigg]$$

$$= i\bar\psi(x)\{\gamma^5, \gamma^\mu\}D_\mu\psi(x) - i\partial_\mu A^\mu + 2mi\bar\psi(x)\gamma^5\psi(x) \cdot \tag{C.34}$$

Therefore we have,

$$i\delta(x-x_3)\gamma^5\langle\psi(x_3)\bar{\psi}(x_2)\rangle + i\delta(x-x_2)\langle\psi(x_3)\bar{\psi}(x_2)\rangle\gamma^5 \tag{C.35}$$

$$= -i\partial_\mu\langle A^\mu\psi(x_3)\bar{\psi}(x_2)\rangle + 2mi\langle\bar{\psi}(x)\gamma^5\psi(x)\psi(x_3)\bar{\psi}(x_2)\rangle \cdot \tag{C.36}$$

In other words, the axial Ward identity in position space reads:

$$i\delta(x-x_3)\gamma^5 S(x_3-x_2) + i\delta(x-x_2)S(x_3-x_2)\gamma^5 \tag{C.37}$$

$$= -i\partial_\mu G^\mu_{\mathrm{A}}(x_3-x, x_2-x) + 2mG_{\mathrm{P}}(x_3-x, x_2-x) \cdot \tag{C.38}$$

Taking the Fourier transform, placing the operator at the origin $x = 0$, *i.e.* inserting an implicit $\int d^4x\delta(x)$, the LHS of Eq. C.37 becomes,

$$\begin{aligned}&\int d^4x_2 d^4x_3 \left(i\delta(-x_3)\gamma^5 S(x_3-x_2) + i\delta(-x_2)S(x_3-x_2)\gamma^5\right)e^{-ip_3.x_3}e^{ip_2.x_2}\\ =&i\gamma^5 S(p_2) + iS(p_3)\gamma^5 \cdot\end{aligned} \tag{C.39}$$

For the first term on the RHS of Eq. C.37, and evaluating at $x = 0$ after differentiation, we have the following:

$$\begin{aligned}&-i\partial_\mu \int d^4x_2 d^4x_3\ G^\mu_{\mathrm{A}}(x_3-x, x_2-x)e^{-ip_3.x_3}e^{ip_2.x_2}\\ =&-i\partial_\mu \int d^4x'_2 d^4x'_3\ G^\mu_{\mathrm{A}}(x'_3, x'_2)e^{-ip_3.(x'_3+x)}e^{+ip_2.(x'_2+x)}\\ =&i(ip_3-ip_2)_\mu \int d^4x'_2 d^4x'_3\ G^\mu_{\mathrm{A}}(x'_3, x'_2)e^{-ip_3.x'_3}e^{+ip_2.x'_2}\\ =&q.G_{\mathrm{A}}(p_3, p_2) \cdot\end{aligned} \tag{C.40}$$

giving,

$$-q.G_{\mathrm{A}}(p_3, p_2) = 2mG_{\mathrm{P}}(p_3, p_2) - i\gamma^5 S(p_2) - iS(p_3)\gamma^5 \cdot \tag{C.41}$$

Multiplying on the left with $S(p_3)^{-1}$ and on the right with $S(p_2)^{-1}$, the Ward identity for the amputated vertex function in momentum space becomes

$$-q.\Lambda_{\mathrm{A}}(p_2, p_3) = 2m\Lambda_{\mathrm{P}}(p_2, p_3) - iS(p_3)^{-1}\gamma^5 - i\gamma^5 S(p_2)^{-1} \cdot \tag{C.42}$$

## C.4 Computation of the basis integrals

In the following sections, we use dimensional regularization, setting $D = 4 - 2\epsilon$. We denote $\tilde{\mu}$ the scale introduced by dimensional regularization through the rescaling of the gauge coupling. $g \to g\tilde{\mu}^{\epsilon}$.

### C.4.1 Integral $I_{001} = I_{010}$

For the integral

$$I_{001} = g^2 \int_k \frac{1}{[(p_3 - k)^2 - m^2]} \ , \tag{C.43}$$

shifting $p_3 - k \to k$ gives and Wick rotating gives,

$$\begin{aligned} I_{001} =& - ig^2 \int_k \frac{1}{k^2 + m^2} = \frac{ig^2}{(4\pi)^2}\Gamma(\epsilon - 1)\left(m^2\right)^{1-\epsilon} = \frac{ig^2}{(4\pi)^2}\frac{\Gamma(\epsilon)}{\epsilon - 1}\left(m^2\right)^{1-\epsilon} \\ =& \frac{i\alpha}{4\pi} m^2 \left(\frac{1}{\epsilon} + 1 - \gamma_E\right)\left[1 - \epsilon \ln\left(\frac{m^2}{\tilde{\mu}^2}\right)\right] \\ =& \frac{i\alpha}{4\pi} m^2 \left[\frac{1}{\epsilon} + 1 - \gamma_E - \ln\left(\frac{m^2}{\tilde{\mu}^2}\right)\right] \cdot \end{aligned} \tag{C.44}$$

### C.4.2 Integral $I_{101} = I_{110}$

We wish to compute,

$$I_{101} = g^2 \int_k \frac{1}{k^2[(p_3 - k)^2 - m^2]} = g^2 \int_0^1 dxdy \ \int_k \frac{\delta(1 - x - y)}{(xk^2 + y[(p_3 - k)^2 - m^2])^2} \ , \tag{C.45}$$

where we have used Feynman parameterization in the last equality. In the denominator we have,

$$(x + y)k^2 - 2y(p_3.k) - y(\mu^2 + m^2) \cdot \tag{C.46}$$

Changing variables to $l = k - \frac{yp_3}{x+y}$ the denominator can be written as:

$$(x+y)\left[l^2 \underbrace{- \left(\frac{yp}{x+y}\right)^2 - (\mu^2+m^2)\frac{y}{x+y}}_{-M^2}\right] \cdot \tag{C.47}$$

The integral then becomes

$$I_{101} = g^2 \int_0^1 dxdy \ \frac{1}{(x+y)^2} \int_l \frac{\delta(1-x-y)}{(l^2-M^2)^2} \cdot \tag{C.48}$$

Performing the wick rotation $l^0 = il_E^0$, with $d = 4-2\epsilon$ dimensions and taking $g^2 = \alpha^2 \tilde{\mu}^{2\epsilon}$ where $\tilde{\mu}$ carries the dimensions,

$$\begin{aligned}
I_{101} =& ig^2 \int_0^1 dxdy \ \frac{\delta(1-x-y)}{(x+y)^2} \int_l \frac{1}{(l_E^2+M^2)^2} \\
=& \frac{i\alpha}{4\pi} \frac{\Gamma(\epsilon)}{\Gamma(2)} \int_0^1 dxdy \ \frac{\delta(1-x-y)}{(x+y)^2} \left(\frac{M^2}{\tilde{\mu}^2}\right)^{-\epsilon} \\
=& \frac{i\alpha}{4\pi} \left[\frac{1}{\epsilon} - \gamma_E\right] \int_0^1 dxdy \ \frac{\delta(1-x-y)}{(x+y)^2} \left[1 - \epsilon \ln\left(\frac{M^2}{\tilde{\mu}^2}\right)\right] \\
=& \frac{i\alpha}{4\pi} \int_0^1 dxdy \ \frac{\delta(1-x-y)}{(x+y)^2} \left[\frac{1}{\epsilon} - \gamma_E - \ln\left(\frac{M^2}{\tilde{\mu}^2}\right)\right] \\
=& \frac{i\alpha}{4\pi} \left[\left(\frac{1}{\epsilon} - \gamma_E\right) + 2 + \frac{m^2}{\mu^2} \ln\left(\frac{m^2}{m^2+\mu^2}\right) - \ln\left(\frac{m^2+\mu^2}{\tilde{\mu}^2}\right)\right] \cdot
\end{aligned} \tag{C.49}$$

### C.4.3 Integral $I_{011}$

For the integral,

$$\begin{aligned}
I_{011} =& g^2 \int_k \frac{1}{[(p_2-k)^2-m^2][(p_3-k)^2-m^2]} \\
=& g^2 \int_0^1 dxdy \ \int_k \frac{\delta(1-x-y)}{(x[(p_2-k)^2-m^2]+y[(p_3-k)^2-m^2])^2} \ ,
\end{aligned} \tag{C.50}$$

in the denominator we have,

$$(x+y)k^2 - 2k.(xp_2+yp_3) - (\mu^2+m^2)(x+y) \cdot \tag{C.51}$$

Making a change in variables, $l = k - \frac{xp_2+yp_3}{x+y}$, gives

$$(x+y)\left[l^2 \underbrace{-\left(\frac{xp_2+yp_3}{x+y}\right)^2 - (\mu^2+m^2)}_{-M^2}\right]\cdot \tag{C.52}$$

The integral then becomes,

$$g^2\int_0^1 dxdy\ \frac{1}{(x+y)^2}\int_l \frac{\delta(1-x-y)}{(l^2-M^2)^2}\ \ cdot t \tag{C.53}$$

Performing the wick rotation $l^0 = il_E^0$, working in $d = 4-2\epsilon$ dimensions and taking $g^2 = \alpha^2\tilde{\mu}^{2\epsilon}$ were $\tilde{\mu}$ carries the dimensions, a similar calculation as before gives

$$\begin{aligned}
I_{011} =& ig^2\int_0^1 dxdy\ \frac{\delta(1-x-y)}{(x+y)^2}\int_l \frac{1}{(l_E^2+M^2)^2}\\
=& \frac{i\alpha}{4\pi}\frac{\Gamma(\epsilon)}{\Gamma(2)}\int_0^1 dxdy\ \frac{\delta(1-x-y)}{(x+y)^2}\left(\frac{M^2}{\tilde{\mu}^2}\right)^{-\epsilon}\\
=& \frac{i\alpha}{4\pi}\left[\frac{1}{\epsilon}-\gamma_E\right]\int_0^1 dxdy\ \frac{\delta(1-x-y)}{(x+y)^2}\left[1-\epsilon\ln\left(\frac{M^2}{\tilde{\mu}^2}\right)\right]\\
=& \frac{i\alpha}{4\pi}\int_0^1 dxdy\ \frac{\delta(1-x-y)}{(x+y)^2}\left[\frac{1}{\epsilon}-\gamma_E-\ln\left(\frac{M^2}{\tilde{\mu}^2}\right)\right]\\
=& \frac{i\alpha}{4\pi}\left[\left(\frac{1}{\epsilon}-\gamma_E\right)-\int_0^1 dx\ \ln\left(\frac{(x_2p_2+(1-x_2)p_3)^2+\mu^2+m^2}{\tilde{\mu}^2}\right)\right]\\
=& \frac{i\alpha}{4\pi}\left[\left(\frac{1}{\epsilon}-\gamma_E\right)-\int_0^1 dx\ \ln\left(\frac{m^2-\mu^2\omega(-1+x)x}{\tilde{\mu}^2}\right)\right]\\
=& \frac{i\alpha}{4\pi}\left[\left(\frac{1}{\epsilon}-\gamma_E\right)-\ln\left(\frac{m^2}{\tilde{\mu}^2}\right)+2\right.\\
&\left.-\frac{i\sqrt{-4m^2-\mu^2\omega}}{\mu\sqrt{\omega}}\left(\ln\left(1-\frac{i\mu\sqrt{\omega}}{\sqrt{-4m^2-\mu^2\omega}}\right)-\ln\left(1+\frac{i\mu\sqrt{\omega}}{\sqrt{-4m^2-\mu^2\omega}}\right)\right)\right]\cdot
\end{aligned} \tag{C.54}$$

### C.4.4 Integral $I_{-111}$ and $I_{1-11}$

This integral has $k^2$ the numerator, hence the subscript $-1$:

$$I_{-111} = g^2 \int_k \frac{k^2}{[(p_2-k)^2-m^2][(p_3-k)^2-m^2]} \cdot \tag{C.55}$$

It can be computed by writing the numerator as a polynomial in $k$ and making a change of variable in the standard way. However, given that this integral does not belong to the minimal basis, it can be written as a linear combination of those in the basis which have already been computed. It is possible to write the integrand as:

$$k^2 = (p_2-k)^2 - p_2^2 - 2p_2.k = [(p_2-k)^2-m^2] - 2p.k + (m^2+\mu^2) \cdot \tag{C.56}$$

The first cancels the first propagator in the denominator to give integrals proportional to $I_{001}$ and the third term gives $I_{011}$. Both these integrals have been computed. The integral proportional to with $k^\mu$ in the numerator can be computed by writing it in terms of previously computed scalar integrals, using a similar method as Sec. 3.4.3. This can be done either by hand or automatically using Mathematica packages such as Fire-5 [83, 105]. The result is:

$$I_{-111} = I_{001} - \left(-m^2+\mu^2-\frac{\mu^2}{2}\right) I_{011} \cdot \tag{C.57}$$

Similarly, the integral $I_{1-11}$ can be written as,

$$I_{1-11} = g^2 \int_k \frac{(p_2-k)^2-m^2}{k^2[(p_3-k)^2-m^2]} = \frac{1}{2} I_{001} - \frac{1}{2}(m^2+\mu^2) I_{101} \cdot \tag{C.58}$$

## C.5 Integral with $k^\mu k^\nu$ in the numerator

The integral

$$I^{\mu\nu} = g^2 \int_k \frac{k^\mu k^\nu}{k^2[(p_2-k)^2-m^2][(p_3-k)^2-m^2]} \,, \tag{C.59}$$

can be written as a linear combinations of the possible scales in the problem, carrying the indices:

$$I^{\mu\nu} = Ag^{\mu\nu} + B(p_2^\mu p_2^\nu + p_3^\mu p_3^\nu) + C(p_2^\mu p_3^\nu + p_3^\mu p_2^\nu) \cdot \tag{C.60}$$

1. Contracting with $g^{\mu\nu}$, the RHS of Eq. C.60 becomes,

$$dA - 2\mu^2 B - \mu^2 C \cdot \tag{C.61}$$

The LHS becomes $g^2 \int_k \frac{1}{[(p_2-k)^2-m^2][(p_3-k)^2-m^2]} = I_{011}$, which we have already computed. Therefore,

$$V_1 \equiv g_{\mu\nu} I^{\mu\nu} = I_{011} \cdot \tag{C.62}$$

2. Contracting with $p_2^\mu p_2^\nu$ gives the RHS of Eq. C.60,

$$-\mu^2 A + \frac{5\mu^4}{4} B + C\mu^4 \ , \tag{C.63}$$

while the LHS becomes

$$p_2^\mu p_2^\nu I_{\mu\nu} = g^2 \int_k \frac{(p_2.k)^2}{k^2[(p_2-k)^2-m^2][(p_3-k)^2-m^2]} \cdot \tag{C.64}$$

Squaring $-2(p_2.k) = \Big[(p_2-k)^2 - m^2\Big] - (p_2^2 - m^2) - k^2$ gives,

$$\begin{aligned} 4(p_2.k)^2 = &\Big[(p_2-k)^2 - m^2\Big]^2 + (p_2^2-m^2)^2 + k^4 \\ &- 2\Big[(p_2-k)^2 - m^2\Big](p_2^2 - m^2) \\ &- 2\Big[(p_2-k)^2 - m^2\Big]k^2 \\ &+ 2\ (p_2^2 - m^2)k^2 \end{aligned} \tag{C.65}$$

Eq. C.64 takes the form:

$$\begin{aligned}
&p_2^\mu p_2^\nu I_{\mu\nu} = \frac{g^2}{4}\int_k \frac{(p_2.k)^2}{k^2[(p_2-k)^2-m^2][(p_3-k)^2-m^2]} \\
=&\frac{g^2}{4}\int_k \frac{(p_2-k)^2-m^2}{k^2[(p_3-k)^2-m^2]} + \frac{g^2}{4}(p_2^2-m^2)^2\int_k \frac{1}{k^2[(p_2-k)^2-m^2][(p_3-k)^2-m^2]} \\
+&\frac{g^2}{4}\int_k \frac{k^2}{[(p_2-k)^2-m^2][(p_3-k)^2-m^2]} - \frac{g^2}{2}(p_2^2-m^2)\int_k \frac{1}{k^2[(p_3-k)^2-m^2]} \\
-&\frac{g^2}{2}\int_k \frac{1}{[(p_3-k)^2-m^2]} + \frac{g^2}{2}(p_2^2-m^2)\int_k \frac{1}{[(p_2-k)^2-m^2][(p_3-k)^2-m^2]}\ .
\end{aligned} \tag{C.66}$$

All the integrals have already been computed. We have,

$$V_2 \equiv p_2^\mu p_2^\nu I_{\mu\nu} = \frac{1}{4}I_{1-11} + \frac{1}{4}(m^2+\mu^2)^2 I_{111} + \frac{1}{4}I_{-111} \tag{C.67}$$

$$+ \frac{1}{2}(m^2+\mu^2)I_{101} - \frac{1}{2}I_{001} - \frac{1}{2}(m^2+\mu^2)I_{011}\ . \tag{C.68}$$

3. Finally, Contracting with $p_2^\mu p_3^\nu$ gives, for the RHS of Eq. C.60,

$$\frac{-\mu^2}{2}A + \mu^4 B + \frac{5\mu^4}{4}C\ . \tag{C.69}$$

while the LHS gives

$$\begin{aligned}
&p_2^\mu p_3^\nu I_{\mu\nu} = g^2\int_k \frac{(p_2.k)(p_3.k)}{k^2[(p_2-k)^2-m^2][(p_3-k)^2-m^2]} \\
=&\frac{g^2}{4}\int_k \frac{\Big[[(p_2-k)^2-m^2]-k^2+(m^2-p_2^2)\Big]\Big[[(p_3-k)^2-m^2]-k^2+(m^2-p_3^2)\Big]}{k^2[(p_2-k)^2-m^2][(p_3-k)^2-m^2]}.
\end{aligned} \tag{C.70}$$

Therefore, using the symmetry between $p_2$ and $p_3$,

$$V_4 \equiv p_2^\mu p_3^\nu I_{\mu\nu} = -\frac{1}{2}I_{001} + \frac{1}{2}(m^2+\mu^2)I_{101} \tag{C.71}$$

$$-\frac{1}{2}(m^2+\mu^2)I_{011} + \frac{1}{4}I_{-111} + \frac{1}{4}(m^2+\mu^2)^2 I_{111}\ . \tag{C.72}$$

There for we have to solve for $A, B$ and $C$, in terms of $V_1, V_2$ and $V_3$:

$$\begin{cases} V_1 \equiv g_{\mu\nu} I^{\mu\nu} = dA - 2\mu^2 B - \mu^2 C \ , \\ V_2 \equiv p_{2\mu} p_{2\nu} I^{\mu\nu} = -\mu^2 A + \frac{5\mu^4}{4} B + C\mu^4 \ , \\ V_3 \equiv p_{2\mu} p_{3\nu} I^{\mu\nu} = \frac{-\mu^2}{2} A + \mu^4 B + \frac{5\mu^4}{4} C \ . \end{cases} \tag{C.73}$$

The answer is

$$\begin{cases} A = \frac{3\mu^2 V_1 + 8V_2 - 4V_3}{3(-2+d)\mu^2} \ , \\ B = \frac{4(3\mu^2 V_1 + (-2+5d)V_2 - 4(-1+d)V_3)}{9(-2+d)\mu^4} \ , \\ C = -\frac{2(3\mu^2 V_1 + 8(-1+d)V_2 + 2(8-5d)V_3)}{9(-2+d)\mu^4} \ . \end{cases} \tag{C.74}$$

In terms of the basis integrals:

$$\begin{aligned} A = \frac{(1+\epsilon)}{6\mu^2} \Big[ & -2I_{001} + I_{-111} + 2I_{1-11} + (\mu^2 - 2m^2) I_{011} \\ & + I_{111}(m^2+\mu^2)^2 + 2I_{101}(m^2+\mu^2) \Big] \ , \end{aligned} \tag{C.75}$$

$$\begin{aligned} B = \frac{1}{3\mu^4} \Big[ & \Big( -2I_{001} + I_{-111} + 3I_{1-11} - 2I_{011} m^2 + 2(m^2+\mu^2) I_{101} + (m^2+\mu^2)^2 I_{111} \Big) \\ & + \frac{2\epsilon}{3} \Big( -2I_{001} + I_{-111} + 2I_{1-11} + 2(\mu^2 - m^2) I_{011} \\ & + 2(\mu^2 + m^2) I_{101} + (m^2+\mu^2)^2 I_{111} \Big) \Big] \ , \end{aligned} \tag{C.76}$$

$$C = -\frac{1}{3\mu^4}\Bigg[2I_{1-11} + I_{011}\mu^2 + \frac{\epsilon}{3}\Big( - 2I_{001} + I_{-111} + 2I_{1-11} + I_{011}(-2m^2+\mu^2) + 2(m^2+\mu^2)I_{101} + (m^2+\mu^2)^2 I_{111}\Big)\Bigg] \cdot \tag{C.77}$$

## C.6 Fermion self-energy

To compute the fermion self-energy,

$$-i\Sigma = -g^2 C_2(F)\int_k \frac{\gamma_\alpha[\not{p}_2 - \not{k} + m]\gamma^\alpha}{k^2[(p_2-k)^2-m^2]} \ , \tag{C.78}$$

at 1-loop in perturbation theory, one can calculate of the coefficient $F$:

$$g^2\int_k \frac{k^\mu}{k^2[(p_2-k)^2-m^2]} = F p_2^\mu \cdot \tag{C.79}$$

which appears as part of the self-energy integral. Multiplying both sides by $p_{2\mu}$ gives, on the left hand side,

$$\begin{aligned} g^2\int_k \frac{p_2.k}{k^2[(p_2-k)^2-m^2]} &= -\frac{g^2}{2}\int_k \frac{[(p_2-k)^2-m^2] - p_2^2 + m^2 - k^2}{k^2[(p_2-k)^2-m^2]} \\ &= -\frac{1}{2}(\mu^2+m^2)I_{110} + \frac{1}{2}I_{001} \cdot \end{aligned} \tag{C.80}$$

This gives,

$$F = \frac{1}{2}\frac{\mu^2+m^2}{\mu^2}I_{110} - \frac{1}{2\mu^2}I_{001} \cdot \tag{C.81}$$

Putting it all the ingredients to Eq. C.78 together and using

$$\gamma^\mu\gamma_\mu = d \quad , \quad \gamma^\mu\gamma^\nu\gamma_\mu = (2-d)\gamma^\nu \ , \tag{C.82}$$

yields,

$$I = -C_2(F)\Bigg[\Big((-2+2\epsilon)\not{p}_2 + (4-2\epsilon)m\Big)I_{110} - \not{p}_2(-1+\epsilon)\left(\left(1+\frac{m^2}{\mu^2}\right)I_{110} - \frac{1}{\mu^2}I_{001}\right)\Bigg]. \tag{C.83}$$

Therefore,

$$-i\Sigma^{(1)} = \frac{-i\alpha}{4\pi}C_2(F)\Bigg[\frac{-\not{p}_2+4m}{\epsilon} + \not{p}_2\left(-1+\gamma_E+\frac{m^2}{\mu^2}+\frac{m^4}{\mu^4}\ln\left(\frac{m^2}{m^2+\mu^2}\right)+\ln\left(\frac{m^2+\mu^2}{\tilde{\mu}^2}\right)\right) + m\left(6-4\gamma_E+\frac{4m^2}{\mu^2}\ln\left(\frac{m^2}{m^2+\mu^2}\right)-4\ln\left(\frac{m^2+\mu^2}{\tilde{\mu}^2}\right)\right)\Bigg]. \tag{C.84}$$

## C.7 't Hooft-Veltman convention

### C.7.1 $\gamma$ matrices manipulation

We wish to prove the following useful identities:

$$\hat{\gamma}^\mu\hat{\gamma}^\nu\hat{\gamma}_\mu = (6-d)\hat{\gamma}^\nu\ , \tag{C.85}$$

$$\hat{\gamma}^\mu\bar{\gamma}^\nu\hat{\gamma}_\mu = (4-d)\bar{\gamma}^\nu\ , \tag{C.86}$$

$$\bar{\gamma}^\mu\bar{\gamma}^\nu\bar{\gamma}_\mu = -2\bar{\gamma}^\nu\ , \tag{C.87}$$

$$\bar{\gamma}^\mu\hat{\gamma}^\nu\bar{\gamma}_\mu = -4\hat{\gamma}^\nu\ . \tag{C.88}$$

Before we proceed note that

$$\hat{\gamma}^\alpha\hat{\gamma}_\alpha = \hat{g}_{\alpha\mu}\hat{g}^{\alpha\nu}\gamma^\mu\gamma_\nu = \hat{\delta}^\nu_\mu\gamma^\mu\gamma_\nu = (d-4)\ , \tag{C.89}$$

$$\bar{\gamma}^\alpha\bar{\gamma}_\alpha = \bar{g}_{\alpha\mu}\bar{g}^{\alpha\nu}\gamma^\mu\gamma_\nu = \hat{\delta}^\nu_\mu\gamma^\mu\gamma_\nu = 4\ . \tag{C.90}$$

Now,

$$\begin{aligned}\hat{\gamma}^\mu\hat{\gamma}^\nu\hat{\gamma}_\mu =&\hat{g}^{\mu\alpha}\hat{g}^{\nu\beta}\hat{g}_{\mu\sigma}\gamma_\alpha\gamma_\beta\gamma^\sigma\\ =&\hat{\delta}^\alpha_\sigma\hat{g}^{\nu\beta}\big(2g_{\alpha\beta}\gamma^\sigma-\gamma_\beta\gamma_\alpha\gamma^\sigma\big)\\ =&\hat{g}^{\nu\beta}\big(2\hat{g}_{\sigma\beta}\gamma^\sigma-\gamma_\beta\hat{\gamma}_\alpha\hat{\gamma}^\alpha\big)\\ =&2\hat{\delta}^\nu_\sigma\gamma^\sigma-(d-4)\hat{\gamma}^\nu\\ =&(6-d)\hat{\gamma}^\nu\ ,\end{aligned}\tag{C.91}$$

$$\begin{aligned}\hat{\gamma}^\mu\bar{\gamma}^\nu\hat{\gamma}_\mu =&\hat{\delta}^\alpha_\sigma\bar{g}^{\nu\beta}\big(2g_{\alpha\beta}\gamma^\sigma-\gamma_\beta\gamma_\alpha\gamma^\sigma\big)\\ =&2\bar{g}^{\nu\beta}\hat{g}_{\sigma\beta}\gamma^\sigma-\hat{\gamma}^\nu\hat{\delta}^\alpha_\sigma\gamma_\alpha\gamma^\sigma\\ =&0-(d-4)\bar{\gamma}^\nu\\ =&(4-d)\bar{\gamma}^\nu\ ,\end{aligned}\tag{C.92}$$

$$\begin{aligned}\bar{\gamma}^\mu\bar{\gamma}^\nu\bar{\gamma}_\mu =&\bar{g}^{\mu\alpha}\bar{g}^{\nu\beta}\bar{g}_{\mu\sigma}\gamma_\alpha\gamma_\beta\gamma^\sigma\\ =&\bar{\delta}^\alpha_\sigma\bar{g}^{\nu\beta}\big(2g_{\alpha\beta}\gamma^\sigma-\gamma_\beta\gamma_\alpha\gamma^\sigma\big)\\ =&2\bar{\gamma}^\nu-4\bar{\gamma}^\nu\\ =&-2\bar{\gamma}^\nu\ ,\end{aligned}\tag{C.93}$$

$$\begin{aligned}\bar{\gamma}^\mu\hat{\gamma}^\nu\bar{\gamma}_\mu =&\bar{g}^{\mu\alpha}\hat{g}^{\nu\beta}\bar{g}_{\mu\sigma}\gamma_\alpha\gamma_\beta\gamma^\sigma\\ =&\bar{\delta}^\alpha_\sigma\hat{g}^{\nu\beta}\big(2g_{\alpha\beta}\gamma^\sigma-\gamma_\beta\gamma_\alpha\gamma^\sigma\big)\\ =&2\bar{g}_{\sigma\beta}\hat{g}^{\nu\beta}\gamma^\sigma-\hat{\gamma}^\nu\bar{\delta}^\alpha_\sigma\gamma_\alpha\gamma^\sigma\\ =&-4\hat{\gamma}^\nu\ .\end{aligned}\tag{C.94}$$

Using the above results we can see that

$$\begin{aligned}\gamma_\alpha\bar{\gamma}^\mu\gamma^5\gamma^\alpha =&\bar{\gamma}_\alpha\bar{\gamma}^\mu\gamma^5\bar{\gamma}^\alpha+\hat{\gamma}_\alpha\bar{\gamma}^\mu\gamma^5\hat{\gamma}^\alpha\\ =&\gamma^5\bar{\gamma}_\alpha\bar{\gamma}^\mu\bar{\gamma}^\alpha-\gamma^5\hat{\gamma}_\alpha\bar{\gamma}^\mu\hat{\gamma}^\alpha\\ =&-2\gamma^5\bar{\gamma}^\mu-\gamma^5(4-d)\bar{\gamma}^\mu\\ =&(d-6)\gamma^5\bar{\gamma}^\mu\ ,\end{aligned}\tag{C.95}$$

and

$$\begin{aligned}\gamma_\alpha\hat{\gamma}^\mu\gamma^5\gamma^\alpha =&\bar{\gamma}_\alpha\hat{\gamma}^\mu\gamma^5\bar{\gamma}^\alpha+\hat{\gamma}_\alpha\hat{\gamma}^\mu\gamma^5\hat{\gamma}^\alpha\\ =&-\gamma^5\bar{\gamma}_\alpha\hat{\gamma}^\mu\bar{\gamma}^\alpha+\gamma^5\hat{\gamma}_\alpha\hat{\gamma}^\mu\hat{\gamma}^\alpha\\ =&4\gamma^5\big(\hat{\gamma}^\mu+(6-d)\hat{\gamma}^\mu\big)\\ =&(10-d)\gamma^5\hat{\gamma}^\mu\ .\end{aligned}\tag{C.96}$$

With four $\gamma$ matrices:

$$\begin{aligned}\bar{\gamma}_\alpha\bar{\gamma}^\mu\bar{\gamma}^\nu\bar{\gamma}^\alpha =&2\bar{g}^{\nu\alpha}\bar{\gamma}_\alpha\bar{\gamma}^\mu-\bar{\gamma}_\alpha\bar{\gamma}^\mu\gamma^\alpha\bar{\gamma}^\nu\\ =&2\bar{\gamma}^\nu\bar{\gamma}^\mu+2\bar{\gamma}^\mu\bar{\gamma}^\nu\\ =&4\bar{g}^{\mu\nu}\ ,\end{aligned}\tag{C.97}$$

$$\begin{aligned}\bar{\gamma}_\alpha\bar{\gamma}^\mu\hat{\gamma}^\nu\bar{\gamma}^\alpha =&\hat{\gamma}^\nu\bar{\gamma}_\alpha\bar{\gamma}^\mu\bar{\gamma}^\alpha\\ =&-2\hat{\gamma}^\nu\bar{\gamma}^\mu\\ =&2\bar{\gamma}^\mu\hat{\gamma}^\nu\ ,\end{aligned}\tag{C.98}$$

$$\begin{aligned}\bar{\gamma}_\alpha\hat{\gamma}^\mu\bar{\gamma}^\nu\bar{\gamma}^\alpha =&-\hat{\gamma}^\mu\bar{\gamma}_\alpha\bar{\gamma}^\nu\bar{\gamma}^\alpha\\ =&2\hat{\gamma}^\mu\bar{\gamma}^\nu\ ,\end{aligned}\tag{C.99}$$

$$\begin{aligned}\bar{\gamma}_\alpha\hat{\gamma}^\mu\hat{\gamma}^\nu\bar{\gamma}^\alpha =&-\bar{\gamma}_\alpha\hat{\gamma}^\mu\bar{\gamma}^\alpha\hat{\gamma}^\nu\\ =&4\hat{\gamma}^\mu\hat{\gamma}^\nu\ ,\end{aligned}\tag{C.100}$$

$$\begin{aligned}\hat{\gamma}_\alpha\bar{\gamma}^\mu\bar{\gamma}^\nu\hat{\gamma}^\alpha =&-\hat{\gamma}_\alpha\bar{\gamma}^\mu\hat{\gamma}^\alpha\bar{\gamma}^\nu\\ =&(d-4)\bar{\gamma}^\mu\bar{\gamma}^\nu\ ,\end{aligned}\tag{C.101}$$

$$\begin{aligned}\hat{\gamma}_\alpha\bar{\gamma}^\mu\hat{\gamma}^\nu\hat{\gamma}^\alpha =&2\hat{g}^{\nu\alpha}\hat{\gamma}_\alpha\bar{\gamma}^\mu-\hat{\gamma}_\alpha\bar{\gamma}^\mu\hat{\gamma}^\alpha\hat{\gamma}^\nu\\ =&-2\bar{\gamma}^\mu\hat{\gamma}^\nu-(4-d)\bar{\gamma}^\mu\hat{\gamma}^\nu\\ =&(d-6)\bar{\gamma}^\mu\hat{\gamma}^\nu\ ,\end{aligned}\tag{C.102}$$

$$\begin{aligned}\hat{\gamma}_\alpha\hat{\gamma}^\mu\bar{\gamma}^\nu\hat{\gamma}^\alpha =& -\hat{\gamma}_\alpha\hat{\gamma}^\mu\hat{\gamma}^\alpha\bar{\gamma}^\nu \\ =&(d-6)\hat{\gamma}^\mu\bar{\gamma}^\nu \ ,\end{aligned} \tag{C.103}$$

$$\begin{aligned}\hat{\gamma}_\alpha\hat{\gamma}^\mu\hat{\gamma}^\nu\hat{\gamma}^\alpha =&2\hat{g}^{\nu\alpha}\hat{\gamma}_\alpha\hat{\gamma}^\mu - \hat{\gamma}_\alpha\hat{\gamma}^\mu\hat{\gamma}^\alpha\hat{\gamma}^\nu \\ =&4\hat{g}^{\mu\nu} - 2\hat{\gamma}^\mu\hat{\gamma}^\nu - (6-d)\hat{\gamma}^\mu\hat{\gamma}^\nu \\ =&4\hat{g}^{\mu\nu} + (d-8)\hat{\gamma}^\mu\hat{\gamma}^\nu \ .\end{aligned} \tag{C.104}$$

Finally, we need to consider five $\gamma$ matrices. For the integrals under consideration, there two cases that need to be simplified: $\gamma_\alpha\gamma^\mu\hat{\gamma}^\sigma\gamma^5\gamma^\nu\gamma^\alpha$ and $\gamma_\alpha\gamma^\mu\bar{\gamma}^\sigma\gamma^5\gamma^\nu\gamma^\alpha$. The former combination appears in integral $\Lambda^{(1)}_{\hat{a}\ \mathrm{anom}}$, Eq. 3.160, and the latter in the re-computation of the axial vertex using the new convention for $\gamma_5$.

- $\underline{\gamma_\alpha\gamma^\mu\hat{\gamma}^\sigma\gamma^5\gamma^\nu\gamma^\alpha}$: For the cases we later consider, indices $\mu,\nu\sigma$ are implicitly summed with $\sigma \geq 4$. We have,

$$\begin{aligned}\gamma_\alpha\gamma^\mu\hat{\gamma}^\sigma\gamma^5\gamma^\nu\gamma^\alpha =&\gamma^5\Big[\bar{\gamma}_\alpha\bar{\gamma}^\mu\hat{\gamma}^\sigma\bar{\gamma}^\nu\bar{\gamma}^\alpha + \bar{\gamma}_\alpha\bar{\gamma}^\mu\hat{\gamma}^\sigma\hat{\gamma}^\nu\bar{\gamma}^\alpha - \bar{\gamma}_\alpha\hat{\gamma}^\mu\hat{\gamma}^\sigma\bar{\gamma}^\nu\bar{\gamma}^\alpha - \bar{\gamma}_\alpha\hat{\gamma}^\mu\hat{\gamma}^\sigma\hat{\gamma}^\nu\bar{\gamma}^\alpha \\ &- \hat{\gamma}_\alpha\bar{\gamma}^\mu\hat{\gamma}^\sigma\bar{\gamma}^\nu\hat{\gamma}^\alpha - \hat{\gamma}_\alpha\bar{\gamma}^\mu\hat{\gamma}^\sigma\hat{\gamma}^\nu\hat{\gamma}^\alpha + \hat{\gamma}_\alpha\hat{\gamma}^\mu\hat{\gamma}^\sigma\bar{\gamma}^\nu\hat{\gamma}^\alpha + \hat{\gamma}_\alpha\hat{\gamma}^\mu\hat{\gamma}^\sigma\hat{\gamma}^\nu\hat{\gamma}^\alpha\Big] \\ =&\gamma^5\Big[2\bar{\gamma}^\nu\bar{\gamma}^\mu\hat{\gamma}^\sigma - 2\bar{\gamma}^\mu\hat{\gamma}^\sigma\bar{\gamma}^\nu - 2\bar{\gamma}^\mu\hat{\gamma}^\sigma\hat{\gamma}^\nu + 2\hat{\gamma}^\mu\hat{\gamma}^\sigma\bar{\gamma}^\nu + 4\hat{\gamma}^\mu\hat{\gamma}^\sigma\hat{\gamma}^\nu \\ &+ (d-6)\bar{\gamma}^\mu\hat{\gamma}^\sigma\bar{\gamma}^\nu + 4\hat{g}^{\sigma\nu}\bar{\gamma}^\mu + (d-8)\bar{\gamma}^\mu\hat{\gamma}^\sigma\hat{\gamma}^\nu - 4\hat{g}^{\mu\sigma}\bar{\gamma}^\nu \\ &- (d-8)\hat{\gamma}^\mu\hat{\gamma}^\sigma\bar{\gamma}^\nu + 2\hat{\gamma}^\nu\hat{\gamma}^\mu\hat{\gamma}^\sigma - 4\hat{g}^{\mu\sigma}\hat{\gamma}^\nu - (d-8)\hat{\gamma}^\mu\hat{\gamma}^\sigma\hat{\gamma}^\nu\Big] \\ =&\gamma^5\Big[4\hat{g}^{\sigma\nu}\bar{\gamma}^\mu - 4\hat{g}^{\sigma\nu}\hat{\gamma}^\mu - 4\hat{g}^{\mu\sigma}\bar{\gamma}^\nu - 4\hat{g}^{\mu\sigma}\hat{\gamma}^\nu + 4\bar{g}^{\mu\nu}\hat{\gamma}^\sigma + 4\hat{g}^{\mu\nu}\hat{\gamma}^\sigma \\ &+ (d-6)\bar{\gamma}^\mu\hat{\gamma}^\sigma\bar{\gamma}^\nu + (d-10)\bar{\gamma}^\mu\hat{\gamma}^\sigma\hat{\gamma}^\nu - (d-10)\hat{\gamma}^\mu\hat{\gamma}^\sigma\bar{\gamma}^\nu \\ &- (d-14)\hat{\gamma}^\mu\hat{\gamma}^\sigma\hat{\gamma}^\nu\Big],\end{aligned} \tag{C.105}$$

where in the last line we have used

$$2\bar{\gamma}^\nu\bar{\gamma}^\mu\hat{\gamma}^\sigma = 4\bar{g}^{\mu\nu}\hat{\gamma}^\sigma - 2\bar{\gamma}^\mu\bar{\gamma}^\nu\hat{\gamma}^\sigma = 4\bar{g}^{\mu\nu}\hat{\gamma}^\sigma + 2\bar{\gamma}^\mu\hat{\gamma}^\sigma\bar{\gamma}^\nu \ , \tag{C.106}$$

and

$$\begin{aligned} 2\hat{\gamma}^\nu\hat{\gamma}^\mu\hat{\gamma}^\sigma =& 4\hat{g}^{\mu\nu}\hat{\gamma}^\sigma - 2\hat{\gamma}^\mu\hat{\gamma}^\nu\hat{\gamma}^\sigma \\ =& 4\hat{g}^{\mu\nu}\hat{\gamma}^\sigma - 4\hat{g}^{\nu\sigma}\hat{\gamma}^\mu + 2\hat{\gamma}^\mu\hat{\gamma}^\sigma\hat{\gamma}^\nu \ . \end{aligned} \tag{C.107}$$

If the sum over $\mu$ and $\nu$ is symmetric, such as the case in Sec. C.7.4, the above simplifies to the following:

$$\gamma^5\Big[ - 4\hat{g}^{\sigma\nu}\hat{\gamma}^\mu - 4\hat{g}^{\mu\sigma}\hat{\gamma}^\nu + 4\bar{g}^{\mu\nu}\hat{\gamma}^\sigma + 4\hat{g}^{\mu\nu}\hat{\gamma}^\sigma + (d-6)\bar{\gamma}^\mu\hat{\gamma}^\sigma\bar{\gamma}^\nu - (d-14)\hat{\gamma}^\mu\hat{\gamma}^\sigma\hat{\gamma}^\nu\Big]\cdot \tag{C.108}$$

This can be shown by proving that when $\mu$ is barred and $\nu$ is hatted, or vice versa, the sum of these terms vanishes leaving only symmetric sums in which $\mu$ and $\nu$ are either both barred or both hatted.

- $\underline{\gamma_\alpha\gamma^\mu\bar{\gamma}^\sigma\gamma^5\gamma^\nu\gamma^\alpha}$: The indices $\mu,\nu,\sigma$ are implicitly summed with another vectors or tensors but $\sigma$ only contains dimensions $\sigma \leq 3$. For our case of the axial current, the $\epsilon$ pole part only comes in as a coefficient of $g^{\mu\nu}$, so we only need to consider those term with the sum that are either both barred or hatted in $\mu$ and $\nu$ *i.e.*

$$\begin{aligned} &\gamma^5\Big[ - \bar{\gamma}_\alpha\bar{\gamma}^\mu\bar{\gamma}^\sigma\bar{\gamma}^\nu\bar{\gamma}^\alpha + \bar{\gamma}_\alpha\hat{\gamma}^\mu\bar{\gamma}^\sigma\hat{\gamma}^\nu\bar{\gamma}^\alpha + \hat{\gamma}_\alpha\bar{\gamma}^\mu\bar{\gamma}^\sigma\bar{\gamma}^\nu\hat{\gamma}^\alpha - \hat{\gamma}_\alpha\hat{\gamma}^\mu\bar{\gamma}^\sigma\hat{\gamma}^\nu\hat{\gamma}^\alpha\Big] \\ =&\gamma^5\Big[ - 2\bar{\gamma}^\nu\bar{\gamma}^\mu\bar{\gamma}^\sigma + 4\bar{g}^{\mu\sigma}\bar{\gamma}^\nu - 2\hat{\gamma}^\mu\bar{\gamma}^\sigma\hat{\gamma}^\nu - (d-4)\bar{\gamma}^\mu\bar{\gamma}^\sigma\bar{\gamma}^\nu - 2\hat{\gamma}^\nu\hat{\gamma}^\mu\bar{\gamma}^\sigma + (d-6)\hat{\gamma}^\mu\bar{\gamma}^\sigma\hat{\gamma}^\nu\Big] \\ =&\gamma^5\Big[ - 2\bar{\gamma}^\nu\bar{\gamma}^\mu\bar{\gamma}^\sigma + 4\bar{g}^{\mu\sigma}\bar{\gamma}^\nu + 2\hat{\gamma}^\mu\hat{\gamma}^\nu\bar{\gamma}^\sigma - (d-4)\Big(2\bar{g}^{\sigma\nu}\bar{\gamma}^\mu - \bar{\gamma}^\mu\bar{\gamma}^\nu\bar{\gamma}^\sigma\Big) - 2\hat{\gamma}^\nu\hat{\gamma}^\mu\bar{\gamma}^\sigma \\ &\quad - (d-6)\hat{\gamma}^\mu\hat{\gamma}^\nu\bar{\gamma}^\sigma\Big]\cdot \end{aligned} \tag{C.109}$$

When this expression multiplied by $g_{\mu\nu}$, it gives,

$$\begin{aligned}&\gamma^5\Big[-8+4+2(d-4)-2(d-4)+4(d-4)-2(d-4)-(d-6)(d-4)\Big]\bar{\gamma}^\sigma\\=&(-4-8\epsilon)\gamma^5\bar{\gamma}^\sigma\end{aligned} \tag{C.110}$$

### C.7.2 Reduction of scalar integrals to the minimal basis

Here we list all the possible scalar integrals required as ingredients to compute the new terms appearing in the axial WI using the 't Hooft-Veltman convention.

$$I_{-111} = I_{001} + (m^2 - \frac{\mu^2}{2})I_{011} \tag{C.111}$$

$$I_{1-11} = \frac{1}{2}I_{001} - \frac{1}{2}(m^2+\mu^2)I_{101} \tag{C.112}$$

$$I_{1-21} = \frac{(4-d)m^2 - 3d\mu^2}{4(d-1)}I_{001} + \frac{(d-4)(m^2+\mu^2)^2}{4(d-1)}I_{101} \tag{C.113}$$

$$I_{-211} = \frac{(-4+4d)m^2 - 3d\mu^2}{2(d-1)}I_{001} + \frac{(-4+4d)m^4 - (8+4d)m^2\mu^2 + (d-4)\mu^4}{4(d-1)}I_{011} \tag{C.114}$$

$$I_{-101} = (m^2-\mu^2)I_{001} \tag{C.115}$$

$$I_{-110} = (m^2-\mu^2)I_{001} \tag{C.116}$$

$$I_{0-11} = -\mu^2 I_{001} \tag{C.117}$$

$$I_{1-11} = \frac{1}{2}I_{001} - \frac{1}{2}(m^2+\mu^2)I_{101} \tag{C.118}$$

$$I_{0-11} = -\mu^2 I_{001} \tag{C.119}$$

### C.7.3 Derivation for $\Lambda^{(1)}_{\hat{b}\ \mathbf{anom}}$ and $\Lambda^{(1)}_{\hat{c}\ \mathbf{anom}}$ integrals

The last term in the axial WI Eq. 3.155, *i.e.* $-2g\langle\bar{\psi}(x)\gamma^5\hat{\gamma}^\mu\mathscr{A}_\mu\psi(x)\psi(x_3)\bar{\psi}(x_2)\rangle$, contributes at 1-loop as follows:

$$
\begin{aligned}
&(-ig)(-2g)\int d^4x\ \delta(x)\ d^4x_2\ e^{-ip_2.x}\ d^4x_3\ e^{ip_3.x}\ d^4z \\
&\qquad\qquad \bar{\psi}(z)\mathscr{A}_\rho(z)\gamma^\rho\psi(z)\bar{\psi}(x)\gamma^5\hat{\gamma}^\mu\mathscr{A}(x)_\mu\psi(x)\psi(x_3)\bar{\psi}(x_2) \\
=&(2ig^2)\int d^4x\ \delta(x)\ d^4x_2\ e^{-ip_2.x}\ d^4x_3\ e^{ip_3.x}\ d^4z \\
&\qquad S(x_3-z)\gamma^\rho S(z-x)\gamma^5\hat{\gamma}^\mu S(x-x_2)\Delta_{\rho\mu}(z-x) \\
=&(2ig^2)\int d^4x\ \delta(x)\ d^4x_2\ d^4x_3\ e^{-ip_2.x_2+ip_3.x_3}d^4z \\
&\qquad \int_{p,k_2,l,k_1} e^{-ip.(z-x)}e^{-ik_2.(x_3-z)}e^{-il.(z-x)}e^{-ik_1.(x-x_2)}S(k_2)\gamma^\rho S(l)\gamma^5\hat{\gamma}^\mu S(k_1)\Delta_{\rho\mu}(p) \\
=&(2ig^2)\int d^4x_2\ e^{-ip_2.x_2}\ d^4x_3\ e^{ip_3.x_3}\ d^4z \\
&\qquad \int_p e^{-ip.z}\int_{-k_2} e^{-ik_2.(x_3-z)}\int_l e^{-il.z}\int_{k_1} e^{ik_1.x_2}S(k_2)\gamma^\rho S(l)\gamma^5\hat{\gamma}^\mu S(k_1)\Delta_{\rho\mu}(p) \\
=&(2ig^2)\int_{p,k_2,l,k_1}\delta(p_3-k_2)\delta(-p_2+k_1)\delta(k_2-l-p)S(k_2)\gamma^\rho S(l)\gamma^\mu S(k_1)\Delta_{\rho\mu}(p) \\
=&(2ig^2)\int_p S(p_3)\gamma^\rho S(p_3-p)\gamma^5\hat{\gamma}^\mu S(p_2)\Delta_{\rho\mu}(p)\ \cdot
\end{aligned}
\tag{C.120}
$$

### C.7.4 Integral $I^{\mu\sigma\nu}$ for $\Lambda^{(1)}_{\hat{a}\ \mathbf{anom}}$

We are interested in the divergent part of the integral

$$
I^{\mu\sigma\nu} = \int_k \frac{k^\mu k^\sigma k^\nu}{k^2[(p_2-k)^2-m^2][(p_3-k)^2-m^2]}\ , \tag{C.121}
$$

that appears as in ingredient in the computation $\Lambda^{(1)}_{\hat{a}\ \mathrm{anom}}$. Note that the finite part goes to zero as $\hat{\gamma}\to 0$ at the end of the calculation. For simplicity, we denote the propagators in the denominator $k^2\to[1]$, $[(p_2-k)^2-m^2]\to[2]$, $[(p_3-k)^2-m^2]\to[3]$. Note that Eq. C.121 is symmetric under the exchange $p_2\leftrightarrow p_3$ and permutations of indices $\mu,\sigma,\nu$ and therefore is expected to be of the

form:

$$\begin{aligned} I^{\mu\sigma\nu} =& A\Big[g^{\mu\sigma}(p_2^\nu + p_3^\nu) + g^{\mu\nu}(p_2^\sigma + p_3^\sigma) + g^{\sigma\nu}(p_2^\mu + p_3^\mu)\Big] + B\Big[p_2^\mu p_2^\sigma p_2^\nu + p_3^\mu p_3^\sigma p_3^\nu\Big] \\ &+ C\Big[(p_2^\mu p_3^\sigma p_2^\nu + p_2^\nu p_3^\mu p_2^\sigma + p_2^\sigma p_3^\nu p_2^\mu) + (p_3^\mu p_2^\sigma p_3^\nu + p_3^\nu p_2^\mu p_3^\sigma + p_3^\sigma p_2^\nu p_3^\mu)\Big]\cdot \end{aligned} \tag{C.122}$$

We now contract this with $g_{\mu\sigma}p_{2\nu}$, $p_{2\mu}p_{2\sigma}p_{2\nu}$ and $p_{2\mu}p_{3\sigma}p_{2\nu}$ to reduce to a set of scalar integrals and solve a set of simultaneous equations in three variables to obtain coefficients $A, B$ and $C$.

1. Taking the scalar product with $g_{\mu\sigma}p_{2\nu}$ for the LHS gives

$$\begin{aligned} &\int_k \frac{p_2.k}{[(p_2-k)^2-m^2][(p_3-k)^2-m^2]} = -\frac{1}{2}\int_k \frac{[(p_2-k)^2-m^2]-k^2-(p_2^2-m^2)}{[(p_2-k)^2-m^2][(p_3-k)^2-m^2]} \\ &= -\frac{1}{2}I_{001} + \frac{1}{2}I_{-111} + \frac{1}{2}(p_2^2-m^2)I_{011} \\ &= -\frac{3\mu^2}{4}I_{011}\ , \end{aligned} \tag{C.123}$$

since $I_{-111} = I_{001} + (m^2 - \frac{\mu^2}{2})I_{011}$. On the RHS we have,

$$\begin{aligned} &A\ (d+2)(p_2^2 + p_2.p_3) + B\Big((p_2^2)^2 + p_3^2(p_2.p_3)\Big) \\ &+ C\Big(2(p_2.p_3)p_2^2 + (p_2.p_3)p_2^2 + 2(p_2.p_3)^2 + p_3^2p_2^2\Big) \\ =& -\frac{3\mu^2}{2}(d+2)\ A + \frac{3\mu^4}{2}B + 3\mu^4 C\cdot \end{aligned} \tag{C.124}$$

2. The scalar product of $p_{2\mu}p_{2\sigma}p_{2\nu}$ with the LHS of Eq. C.122 gives,

$$\begin{aligned}
&\int_k \frac{(p_2.k)^3}{k^2[(p_2-k)^2-m^2][(p_3-k)^2-m^2]} = \int_k \frac{(p_2.k)^3}{[1][2][3]} \\
&= \left(\frac{-1}{2}\right)^3 \int_k \frac{\Big([2]-[1]-(p_2^2-m^2)\Big)^3}{[1][2][3]} \\
&= \left(\frac{-1}{2}\right)^3 \left[\frac{3[1]}{[3]} - \frac{[1]^2}{[2][3]} - \frac{3[2]}{[3]} + \frac{[2]^2}{[1][3]} + \frac{6(p_2^2-m^2)}{[3]} - \frac{3[1](p_2^2-m^2)}{[2][3]}\right. \\
&\qquad \left. - \frac{3[2](p_2^2-m^2)}{[1][3]} + \frac{3(p_2^2-m^2)^2}{[1][3]} - \frac{3(p_2^2-m^2)^2}{[2][3]} - \frac{(p_2^2-m^2)^3}{[1][2][3]}\right] \\
&= \left(\frac{-1}{8}\right) \Big[3I_{-101} - I_{-211} - 3I_{0-11} + I_{1-21} + 6(p_2^2-m^2)I_{001} - 3(p_2^2-m^2)I_{-111} \\
&\qquad - 3(p_2^2-m^2)I_{1-11} + 3(p_2^2-m^2)^2 I_{101} - 3(p_2^2-m^2)^2 I_{011} - (p_2^2-m^2)^3 I_{111}\Big].
\end{aligned} \tag{C.125}$$

Writing the above integrals in therms of the minimal basis, App. C.7.2 yields,

$$\begin{aligned}
\int_k \frac{(p_2.k)^3}{[1][2][3]} = \left(\frac{-1}{8}\right) \Bigg[ & \\
& \left(\frac{(12-9d)m^2+3d\mu^2}{4(d-1)} + \frac{3}{2}m^2 - \frac{3}{2}\mu^2\right) I_{001} \\
& + \left(\frac{(4-4d)m^4+(8+4d)m^2\mu^2-(d-4)\mu^4}{4(d-1)} - \frac{9}{2}\mu^2(m^2+\mu^2)\right) I_{011} \\
& + \left(\frac{(d-4)(m^2+\mu^2)^2}{4(d-1)} + \frac{3}{2}(m^2+\mu^2)^2\right) I_{101} \\
& + (m^2+\mu^2)^3 I_{111}\Bigg].
\end{aligned} \tag{C.126}$$

The RHS of Eq. C.122 contracted with $p_{2\mu}p_{2\sigma}p_{2\nu}$ gives

$$\begin{aligned}&3Ap_2^2\bigg(p_2^2+p_2.p_3\bigg)+B\bigg((p_2^2)^3+(p_2.p_3)^3\bigg)+3C\bigg((p_2^2)^2(p_2.p_3)+p_2^2(p_2.p_3)^2\bigg)\\=&\frac{9\mu^4}{2}A-\frac{9\mu^6}{8}B-\frac{9\mu^6}{4}C\end{aligned} \tag{C.127}$$

3. The scalar product of $p_{2\mu}p_{3\sigma}p_{2\nu}$ with the LHS of Eq. C.122 gives,

$$\begin{aligned}&\int_k\frac{(p_2.k)^2(p_3.k)}{k^2[(p_2-k)^2-m^2][(p_3-k)^2-m^2]}=\int_k\frac{(p_2.k)^2(p_3.k)}{[1][2][3]}\\&=\left(\frac{-1}{2}\right)^3\int_k\frac{\bigg([2]-[1]-(p_2^2-m^2)\bigg)^2\bigg([3]-[1]-(p_3^2-m^2)\bigg)}{[1][2][3]}\\&=\left(\frac{-1}{8}\right)\Bigg[-I_{-211}+(\mu^2+m^2)^3I_{111}+3(\mu^2+m^2)I_{-111}+(\mu^2+m^2)I_{1-11}\\&\qquad+(\mu^2+m^2)^2I_{110}+I_{-110}+I_{1-10}+2(\mu^2+m^2)^2I_{101}+2I_{-101}\\&\qquad-3(\mu^2+m^2)^2I_{011}-I_{0-11}-6(\mu^2+m^2)I_{001}\Bigg].\end{aligned} \tag{C.128}$$

Writing the above integrals in therms of the minimal basis, App. C.7.2 yields,

$$\begin{aligned}&\frac{-1}{8}\Bigg[\left(\frac{(4-4d)m^2+3d\mu^2}{2(d-1)}+\frac{m^2}{2}-\frac{9\mu^2}{2}\right)I_{001}+\left(\frac{5}{2}(m^2+\mu^2)^2\right)I_{101}\\&\quad+\left(\frac{(4-4d)m^4+(8+4d)m^2\mu^2-(d-4)\mu^4}{4(d-1)}-\frac{9\mu^2}{2}(m^2+\mu^2)\right)I_{011}\\&\quad+(m^2+\mu^2)^3I_{111}\Bigg].\end{aligned} \tag{C.129}$$

The RHS of Eq. C.122 contracted with $p_{2\mu}p_{3\sigma}p_{2\nu}$ gives

$$\begin{aligned}
&\Big[2(p_2.p_3)(p_2^2+p_2.p_3)+p_2^2(p_2.p_3+p_3^2)\Big]A+\Big(p_2^2(p_2.p_3)p_2^2+(p_2.p_3)p_3^2(p_2.p_3)\Big)B\\
&+\Big(p_2^2p_3^2p_2^2+p_2^2(p_2.p_3)^2+(p_2.p_3)^2p_2^2+(p_2.p_3)^3+(p_2.p_3)p_2^2p_3^2+p_3^2p_2^2(p_2.p_3)\Big)C\\
&=3\mu^4A-\frac{3\mu^6}{4}B-\frac{21\mu^6}{8}C
\end{aligned} \tag{C.130}$$

Now, we use Mathematica to solve the set of simultaneous equations to obtain the coefficients $A, B, C$.

$$\begin{cases}
V_1\equiv g_{\mu\sigma}p_{2\nu}I^{\mu\sigma\nu}=-\frac{3\mu^2}{2}(d+2)\ A+\frac{3\mu^4}{2}B+3\mu^4C\\
V_2\equiv p_{2\mu}p_{2\sigma}p_{2\nu}I^{\mu\sigma\nu}=\frac{9\mu^4}{2}A-\frac{9\mu^6}{8}B-\frac{9\mu^6}{4}C\\
V_3\equiv p_{2\mu}p_{3\sigma}p_{2\nu}I^{\mu\sigma\nu}=3\mu^4A-\frac{3\mu^6}{4}B-\frac{21\mu^6}{8}C
\end{cases} \tag{C.131}$$

$$\begin{cases}
A=\frac{1}{12\epsilon}+\text{finite};\\
B=\text{finite};\\
C=\text{finite}\ \cdot
\end{cases} \tag{C.132}$$

Therefore,

$$\begin{aligned}
I^{\mu\sigma\nu}=&\frac{1}{12\epsilon}\Big[g^{\mu\sigma}(p_2^\nu+p_3^\nu)+g^{\mu\nu}(p_2^\sigma+p_3^\sigma)+g^{\sigma\nu}(p_2^\mu+p_3^\mu)\Big]\\
&+\text{finite}\ B\left(\frac{m^2}{\mu^2}\right)\Big[p_2^\mu p_2^\sigma p_2^\nu+p_3^\mu p_3^\sigma p_3^\nu\Big]\\
&+\text{finite}\ C\left(\frac{m^2}{\mu^2}\right)\Big[(p_2^\mu p_3^\sigma p_2^\nu+p_2^\nu p_3^\mu p_2^\sigma+p_2^\sigma p_3^\nu p_2^\mu)+(p_3^\mu p_2^\sigma p_3^\nu+p_3^\nu p_2^\mu p_3^\sigma+p_3^\sigma p_2^\nu p_3^\mu)\Big]
\end{aligned} \tag{C.133}$$

The only term in the above equation that we need to consider, is the divergent

one, proportional to the $g$'s. We use Eq. C.108 to obtain:

$$\begin{aligned}
&-2\frac{i\alpha}{4\pi}\frac{\gamma^5}{12\epsilon}\Big[-4-4(d-4)+4-(d-14)(d-4)\\
&\qquad\qquad -4(d-4)-4+4-(d-14)(d-4)\\
&\qquad\qquad -4-4+16+4(d-4)-4(d-6)-(d-14)(6-d)\Big](\hat{\not{p}}_2+\hat{\not{p}}_3)\\
&=-2\frac{i\alpha}{4\pi}\frac{\gamma^5}{12\epsilon}\times 36(\hat{\not{p}}_2+\hat{\not{p}}_3)=-\frac{i\alpha}{4\pi}\frac{6}{\epsilon}(\hat{\not{p}}_2+\hat{\not{p}}_3)\gamma^5
\end{aligned} \tag{C.134}$$

### C.7.5 Integral $I^{\mu\nu}$ for $\Lambda^{(1)}_{\hat{a}\ \mathbf{anom}}$

Having already computed the trip-k contribution to the integral,

$$\Lambda^{(1)}_{\hat{a}\ \mathrm{anom}}=-ig^2C_2(F)\int_k\frac{\gamma_\alpha[\not{p}_3-\not{k}+m](\hat{\not{p}}_2+\hat{\not{p}}_3-2\hat{\not{k}})\gamma^5[\not{p}_2-\not{k}+m]\gamma^\alpha}{k^2[(p_2-k)^2-m^2][(p_3-k)^2-m^2]}\ , \tag{C.135}$$

in Sec. C.7.4, it remain to collect other terms that could contain divergent parts. These are parts that would be proportional to $g^{\mu\nu}$. The relevant terms in the numerator are,

$$\begin{aligned}
&2\gamma_\alpha\not{p}_3\hat{\not{k}}\gamma^5\not{k}\gamma^\alpha+2m\gamma_\alpha\hat{\not{k}}\gamma^5\not{k}\gamma^\alpha\\
&+2\gamma_\alpha\not{k}\hat{\not{k}}\gamma^5\not{p}_2\gamma^\alpha+2m\gamma_\alpha\not{k}\hat{\not{k}}\gamma^5\gamma_\alpha\\
&+\gamma_\alpha\not{k}(\hat{\not{p}}_2+\hat{\not{p}}_3)\gamma^5\not{k}\gamma^\alpha\\
&=\big(\gamma_\alpha\gamma^\mu\hat{\gamma}^\sigma\gamma^5\gamma^\nu\gamma^\alpha\big)\Big[2p_{3\mu}k_\sigma k_\nu+2k_\mu k_\sigma p_{2\nu}+k_\mu(p_{2\sigma}+p_{3\sigma})k_\nu)\Big]\\
&+2m\Big[\Big(\gamma_\alpha\hat{\gamma}^\sigma\gamma^5\gamma^\mu\gamma^\alpha\Big)k_\sigma k_\mu+\Big(\gamma_\alpha\gamma^\mu\hat{\gamma}^\sigma\gamma^5\gamma^\alpha\Big)k_\mu k_\sigma\Big]\cdot
\end{aligned} \tag{C.136}$$

Let us first consider the term $k_\mu(p_{2\sigma}+p_{3\sigma})k_\nu$ and use Eq. C.105. We obtain,

$$\begin{aligned}
&\frac{i\alpha}{4\pi}\frac{\gamma^5}{4\epsilon}\Big[-8+16+4(d-4)-4(d-6)+(d-14)(d-6)\Big](\hat{\not{p}}_2+\hat{\not{p}}_3)\\
&=\frac{i\alpha}{4\pi}\frac{\gamma^5}{4\epsilon}\times 36(\hat{\not{p}}_2+\hat{\not{p}}_3)=\frac{i\alpha}{4\pi}\frac{9}{\epsilon}(\hat{\not{p}}_2+\hat{\not{p}}_3)\gamma^5\ \cdot
\end{aligned} \tag{C.137}$$

For $\big(2p_{3\mu}k_\sigma k_\nu\big)$, since $k_\sigma$ is contracted with $\hat{\gamma}^\sigma$, the only terms in Eq. C.105

that survive are those which have $\nu$ hatted as well *i.e.* ,

$$\gamma^5\Big[4\hat{g}^{\sigma\nu}\bar{\gamma}^\mu-4\hat{g}^{\sigma\nu}\hat{\gamma}^\mu-4\hat{g}^{\mu\sigma}\hat{\gamma}^\nu+4\hat{g}^{\mu\nu}\hat{\gamma}^\sigma+(d-10)\bar{\gamma}^\mu\hat{\gamma}^\sigma\hat{\gamma}^\nu-(d-14)\hat{\gamma}^\mu\hat{\gamma}^\sigma\hat{\gamma}^\nu\Big]\cdot \quad \text{(C.138)}$$

We therefore get,

$$\begin{aligned}
&2\frac{i\alpha}{4\pi}\frac{1}{4\epsilon}\gamma^5\Big[4(d-4)\bar{\not{p}}_3-4(d-4)\hat{\not{p}}_3-4\hat{\not{p}}_3+4\hat{\not{p}}_3+(d-10)(d-4)\bar{\not{p}}_3-(d-14)(d-4)\hat{\not{p}}_3\Big]\\
=&2\frac{i\alpha}{4\pi}\frac{1}{4\epsilon}\gamma^5\Big[(d-6)(d-4)\bar{\not{p}}_3-(d-4)(d-10)\hat{\not{p}}_3\Big]\\
=&2\frac{i\alpha}{4\pi}\frac{1}{4\epsilon}\gamma^5\Big[4\epsilon\bar{\not{p}}_3-12\epsilon\hat{\not{p}}_3\Big]=\frac{i\alpha}{4\pi}\times 2\gamma^5\bar{\not{p}}_3\ ,
\end{aligned} \quad \text{(C.139)}$$

where in the last equality we have used the fact that in the absence of $1/\epsilon$ poles, we can safely send $\hat{\not{p}}_3\to 0$. Similarly for the term $\big(2k_\mu k_\sigma p_{2\nu}\big)$, the only terms in Eq. C.105 that survive are those which have $\mu$ hatted *i.e.* ,

$$\gamma^5\Big[-4\hat{g}^{\sigma\nu}\hat{\gamma}^\mu-4\hat{g}^{\mu\sigma}\bar{\gamma}^\nu-4\hat{g}^{\mu\sigma}\hat{\gamma}^\nu+4\hat{g}^{\mu\nu}\hat{\gamma}^\sigma-(d-10)\hat{\gamma}^\mu\hat{\gamma}^\sigma\bar{\gamma}^\nu-(d-14)\hat{\gamma}^\mu\hat{\gamma}^\sigma\hat{\gamma}^\nu\Big]\cdot \quad \text{(C.140)}$$

This gives,

$$\begin{aligned}
&2\frac{i\alpha}{4\pi}\frac{1}{4\epsilon}\gamma^5\Big[-4\hat{\not{p}}_2-4(d-4)\bar{\not{p}}_2-4(d-4)\hat{\not{p}}_2+4\hat{\not{p}}_2-(d-10)(d-4)\bar{\not{p}}_2-(d-14)(d-4)\hat{\not{p}}_2\Big]\\
=&2\frac{i\alpha}{4\pi}\frac{1}{4\epsilon}\gamma^5\Big[-(d-6)(d-4)\bar{\not{p}}_2-(d-4)(d-10)\hat{\not{p}}_2\Big]\\
=&2\frac{i\alpha}{4\pi}\frac{1}{4\epsilon}\gamma^5\Big[-4\epsilon\bar{\not{p}}_2-12\epsilon\hat{\not{p}}_2\Big]=\frac{i\alpha}{4\pi}\times(-2)\gamma^5\bar{\not{p}}_2\ ,
\end{aligned} \quad \text{(C.141)}$$

which, again, in the absence of $1/\epsilon$ poles, we we have taken $\hat{\not{p}}_2\to 0$.

For the terms containing masses, we first have $2m\Big(\gamma_\alpha\hat{\gamma}^\sigma\gamma^5\gamma^\mu\gamma^\alpha\Big)k_\sigma k_\mu$. Given that one only need to consider the divergent parts and that these are proportional

to $g^{\sigma\mu}$, one only needs to choose terms with hatted $\mu$'s *i.e.*

$$\gamma^5\Bigg[-\bar{\gamma}_\alpha\hat{\gamma}^\sigma\hat{\gamma}^\mu\bar{\gamma}^\alpha+\hat{\gamma}_\alpha\hat{\gamma}^\sigma\hat{\gamma}^\mu\hat{\gamma}^\alpha\Bigg]=\gamma^5\Bigg[-4\hat{\gamma}^\sigma\hat{\gamma}^\mu+4\hat{g}^{\sigma\mu}+(d-8)\hat{\gamma}^\sigma\hat{\gamma}^\mu\Bigg]\cdot \quad \text{(C.142)}$$

Contracting the coefficient gives,

$$\frac{i\alpha}{4\pi}\frac{2m}{4\epsilon}\gamma^5\Bigg[-4(4-d)+4(4-d)+(d-8)(d-4)\Bigg]=\frac{i\alpha}{4\pi}\frac{2m}{4\epsilon}\gamma^5\times 8\epsilon=\frac{i\alpha}{4\pi}\gamma^5 4m \quad \text{(C.143)}$$

Similarly, for $2m\Big(\gamma_\alpha\gamma^\mu\hat{\gamma}^\sigma\gamma^5\gamma^\alpha\Big)k_\mu k_\sigma$, again we only choose hatted $\mu$'s in the sum over the indices which gives

$$\gamma^5\Bigg[-\bar{\gamma}_\alpha\hat{\gamma}^\mu\hat{\gamma}^\sigma\bar{\gamma}^\alpha+\hat{\gamma}_\alpha\hat{\gamma}^\mu\hat{\gamma}^\sigma\hat{\gamma}^\alpha\Bigg]=\gamma^5\Bigg[-4\hat{\gamma}^\mu\hat{\gamma}^\sigma+4\hat{g}^{\mu\sigma}+(d-8)\hat{\gamma}^\mu\hat{\gamma}^\sigma\Bigg]\cdot \quad \text{(C.144)}$$

Multiplying the coefficient,

$$\frac{i\alpha}{4\pi}\frac{2m}{4\epsilon}\gamma^5\Bigg[-4(4-d)+4(4-d)+(d-8)(d-4)\Bigg]=\frac{i\alpha}{4\pi}\frac{2m}{4\epsilon}\gamma^5\times 8\epsilon=\frac{i\alpha}{4\pi}\gamma^5 4m\cdot \quad \text{(C.145)}$$

Putting everything together from Sec. C.7.4 and this section, we obtain the final result for $\Lambda^{(1)}_{\hat{a}\ \text{anom}}$:

$$\begin{aligned}\frac{\Lambda^{(1)}_{\hat{a}\ \text{anom}}}{-iC_2(F)}=&g^2\int_k\frac{\gamma_\alpha[\not{p}_3-\not{k}+m](\hat{\not{p}}_2+\hat{\not{p}}_3-2\hat{\not{k}})\gamma^5[\not{p}_2-\not{k}+m]\gamma^\alpha}{k^2[(p_2-k)^2-m^2][(p_3-k)^2-m^2]}\\ =&\frac{i\alpha}{4\pi}\gamma^5\Bigg[-\frac{6}{\epsilon}(\hat{\not{p}}_2+\hat{\not{p}}_3)+\frac{9}{\epsilon}(\hat{\not{p}}_2+\hat{\not{p}}_3)+2\bar{\not{p}}_3-2\bar{\not{p}}_2+4m+4m\Bigg]\cdot\end{aligned} \quad \text{(C.146)}$$

Therefore,

$$\Lambda^{(1)}_{\hat{a}\ \text{anom}}=\frac{\alpha}{4\pi}\gamma^5 C_2(F)\Bigg[\frac{3}{\epsilon}(\hat{\not{p}}_2+\hat{\not{p}}_3)+2(\bar{\not{p}}_3-\bar{\not{p}}_2)+8m\Bigg]\cdot \quad \text{(C.147)}$$

## C.8 Minkowski to Euclidean convention for mSMOM

Following the conventions of Sec. B.1, the RI/mSMOM renormalization condition in Euclidean space are:

$$\lim_{M_R\to\overline{m}} \frac{1}{12p_{\mathrm{E}}^2}\mathrm{Tr}\left[iS_R^{\mathrm{E}}(p)^{-1}\ \not{p}^{\mathrm{E}}\right]\Big|_{p_{\mathrm{E}}^2=\mu^2} = -1\,, \tag{C.148}$$

$$\lim_{M_R\to\overline{m}} \frac{1}{12M_R}\left\{\mathrm{Tr}\left[S_R^{\mathrm{E}}(p)^{-1}\right]\big|_{p^2=\mu^2} + \frac{1}{2}\,\mathrm{Tr}\left[\left(iq\cdot\Lambda_{\mathrm{A},R}^{\mathrm{E}}\right)\gamma_5\right]\big|_{\mathrm{sym}}\right\} = 1\,, \tag{C.149}$$

$$\lim_{M_R\to\overline{m}} \frac{1}{12q^2}\mathrm{Tr}\left[(q\cdot\Lambda_{\mathrm{V},R})\ \not{q}\right]\big|_{\mathrm{sym}} = 1\,, \tag{C.150}$$

$$\lim_{M_R\to\overline{m}} \frac{1}{12q^2}\mathrm{Tr}\left[(q\cdot\Lambda_{\mathrm{A},R} + 2M_R\Lambda_{\mathrm{P},R})\,\gamma_5\ \not{q}\right]\big|_{\mathrm{sym}} = 1\,, \tag{C.151}$$

$$\lim_{M_R\to\overline{m}} \frac{1}{12i}\mathrm{Tr}\left[\Lambda_{\mathrm{P},R}\gamma_5\right]\big|_{\mathrm{sym}} = 1\,. \tag{C.152}$$

The conditions are now defined at the symmetric point,

$$p_2^2 = p_3^2 = q^2 = \mu^2. \tag{C.153}$$

The RI/mSMOM scheme for the heavy-light mixed case in Euclidean space now reads:

$$\lim_{\substack{m_R\to 0\\ M_R\to\overline{m}}} \frac{1}{12q^2}\mathrm{Tr}\left[(q\cdot\Lambda_{\mathcal{V},R} + (M_R - m_R)\Lambda_{\mathcal{S},R})\ \not{q}\right]\big|_{\mathrm{sym}} \tag{C.154}$$

$$= \lim_{\substack{m_R\to 0\\ M_R\to\overline{m}}} \frac{1}{12q^2}\mathrm{Tr}\left[\left(-i\zeta^{-1}S_{H,R}(p_2)^{-1} + i\zeta S_{l,R}(p_3)^{-1}\right)\ \not{q}\right]\,, \tag{C.155}$$

$$\lim_{\substack{m_R\to 0\\ M_R\to\overline{m}}} \frac{1}{12q^2}\mathrm{Tr}\left[(q\cdot\Lambda_{\mathcal{A},R} + (M_R + m_R)\Lambda_{\mathcal{P},R})\,\gamma_5\ \not{q}\right]\big|_{\mathrm{sym}} =$$

$$\lim_{\substack{m_R\to 0\\ M_R\to\overline{m}}} \frac{1}{12q^2}\mathrm{Tr}\left[\left(\ + i\gamma^5\zeta^{-1}S_{H,R}(p_2)^{-1} + i\zeta S_{l,R}(p_3)^{-1}\gamma^5\right)\gamma_5\ \not{q}\right]\,, \tag{C.156}$$

$$\lim_{\substack{m_R\to 0\\ M_R\to\overline{m}}} \frac{1}{12i}\mathrm{Tr}\left[\Lambda_{\mathcal{P},R}\gamma_5\right]\big|_{\mathrm{sym}} \tag{C.157}$$

$$= \lim_{\substack{m_R\to 0\\ M_R\to\overline{m}}} \left\{\frac{1}{12(M_R+m_R)}\left\{\mathrm{Tr}\left[\zeta^{-1}S_{H,R}(p)^{-1}\right]\big|_{p^2=-\mu^2} + \frac{1}{2}\,\mathrm{Tr}\left[(iq\cdot\Lambda_{\mathcal{A},R})\,\gamma_5\right]\big|_{\mathrm{sym}}\right\} +\right.$$

$$\frac{1}{12(M_R+m_R)}\left\{\mathrm{Tr}\left[\zeta S_{l,R}(p)^{-1}\right]\big|_{p^2=-\mu^2}+\frac{1}{2}\,\mathrm{Tr}\left[(iq\cdot\Lambda_{\mathcal{A},R})\,\gamma_5\right]\big|_{\mathrm{sym}}\right\}\Bigg\}\,. \tag{C.158}$$

# Bibliography


[1] CERN, *Restarting the LHCL Why 13 Tev?*, *CERN Document Server*.

[2] M. Artuso *et al.*, *B, D and K decays*, *Eur. Phys. J.* **C57** (2008) 309–492, [0801.1833].

[3] A. J. Buras and J. Girrbach, *Towards the Identification of New Physics through Quark Flavour Violating Processes*, *Rept. Prog. Phys.* **77** (2014) 086201, [1306.3775].

[4] G. Isidori and F. Teubert, *Status of indirect searches for New Physics with heavy flavour decays after the initial LHC run*, *Eur. Phys. J. Plus* **129** (2014), no. 3 40, [1402.2844].

[5] S. Aoki *et al.*, *Review of lattice results concerning low-energy particle physics*, *Eur. Phys. J.* **C77** (2017), no. 2 112, [1607.00299].

[6] Y. Nir, *Flavour Physics and CP Violation*, in *Proceedings, 7th CERN-Latin-American School of High-Energy Physics (CLASHEP2013): Arequipa, Peru, March 6-19, 2013*, pp. 123–156, 2015. 1605.00433.

[7] A. J. Buras, *Minimal flavour violation and beyond: Towards a flavour code for short distance dynamics*, *Acta Phys. Polon.* **B41** (2010) 2487–2561, [1012.1447].

[8] M. D. Schwartz, *Quantum Field Theory and the Standard Model*. Cambridge University Press, New York, 2014.

[9] **Particle Data Group** Collaboration, C. Patrignani *et al.*, *Review of Particle Physics*, *Chin. Phys.* **C40** (2016), no. 10 100001.

[10] **UTfit** Collaboration, D. Derkach, *Unitarity Triangle Fitter Results for CKM Angles*, in *7th International Workshop on the CKM Unitarity Triangle (CKM 2012) Cincinnati, Ohio, USA, September 28-October 2, 2012*, 2013. 1301.3300.

[11] *The CKM matrix and the unitarity triangle. Workshop, CERN, Geneva, Switzerland, 13-16 Feb 2002: Proceedings*, 2003.

[12] A. J. Buras, *Weak Hamiltonian, CP violation and rare decays*, in *Probing the standard model of particle interactions. Proceedings, Summer School in Theoretical Physics, NATO Advanced Study Institute, 68th session, Les Houches, France, July 28-September 5, 1997. Pt. 1, 2*, pp. 281–539, 1998. hep-ph/9806471.

[13] **CPLEAR** Collaboration, A. Apostolakis *et al.*, *A Determination of the CP violation parameter eta+- from the decay of strangeness tagged neutral kaons*, *Phys. Lett.* **B458** (1999) 545–552.

[14] J. H. Christenson, J. W. Cronin, V. L. Fitch, and R. Turlay, *Evidence for the $2\pi$ decay of the $k_2^0$ meson*, *Phys. Rev. Lett.* **13** (Jul, 1964) 138–140.

[15] **CPLEAR** Collaboration, A. Angelopoulos *et al.*, *Physics at CPLEAR*, *Phys. Rept.* **374** (2003) 165–270.

[16] A. J. Buras, D. Guadagnoli, and G. Isidori, *On $\epsilon_K$ Beyond Lowest Order in the Operator Product Expansion*, *Phys. Lett.* **B688** (2010) 309–313, [1002.3612].

[17] **RBC, UKQCD** Collaboration, N. H. Christ, T. Izubuchi, C. T. Sachrajda, A. Soni, and J. Yu, *Long distance contribution to the KL-KS mass difference*, *Phys. Rev.* **D88** (2013) 014508, [1212.5931].

[18] Z. Bai, N. H. Christ, T. Izubuchi, C. T. Sachrajda, A. Soni, and J. Yu, *$K_L - K_S$ Mass Difference from Lattice QCD*, *Phys. Rev. Lett.* **113** (2014) 112003, [1406.0916].

[19] N. H. Christ, X. Feng, G. Martinelli, and C. T. Sachrajda, *Effects of finite volume on the KL-KS mass difference*, *Phys. Rev.* **D91** (2015), no. 11 114510, [1504.01170].

[20] T. Inami and C. S. Lim, *Effects of Superheavy Quarks and Leptons in Low-Energy Weak Processes k(L) —¿ mu anti-mu, K+ —¿ pi+ Neutrino anti-neutrino and K0 ¡—¿ anti-K0*, *Prog. Theor. Phys.* **65** (1981) 297. [Erratum: Prog. Theor. Phys.65,1772(1981)].

[21] G. Buchalla, A. J. Buras, and M. E. Lautenbacher, *Weak decays beyond leading logarithms*, *Rev. Mod. Phys.* **68** (1996) 1125–1144, [hep-ph/9512380].

[22] J. Brod and M. Gorbahn, *Next-to-Next-to-Leading-Order Charm-Quark Contribution to the CP Violation Parameter $\epsilon_K$ and $\Delta M_K$*, *Phys. Rev. Lett.* **108** (2012) 121801, [1108.2036].

[23] J. Brod and M. Gorbahn, *$\epsilon_K$ at Next-to-Next-to-Leading Order: The Charm-Top-Quark Contribution*, *Phys. Rev.* **D82** (2010) 094026, [1007.0684].

[24] Y. Aoki *et al.*, *Continuum Limit of $B_K$ from 2+1 Flavor Domain Wall QCD*, *Phys. Rev.* **D84** (2011) 014503, [1012.4178].

[25] **ARGUS** Collaboration, H. Albrecht *et al.*, *Observation of B0 - anti-B0 Mixing*, *Phys. Lett.* **B192** (1987) 245–252.

[26] **CDF** Collaboration, A. Abulencia *et al.*, *Measurement of the $B_s^0 - \bar{B}_s^0$ Oscillation Frequency*, *Phys. Rev. Lett.* **97** (2006) 062003, [hep-ex/0606027].

[27] **BaBar** Collaboration, J. Beringer, *CP violation, B mixing and B lifetime results from the BaBar experiment*, in *Proceedings, 36th Rencontres de Moriond on QCD and High Energy Hadronic Interactions: Les Arcs, France, Mar 17-24, 2001*, pp. 197–200, 2002. hep-ex/0105073.

[28] **BaBar** Collaboration, S. A. Prell, *Measurements of CP violation, mixing and lifetimes of B mesons with the BABAR detector*, *AIP Conf. Proc.* **618** (2002) 15–26, [hep-ex/0112013]. [,15(2001)].

[29] **BaBar** Collaboration, C. Bozzi, *B mixing and lifetime measurements with the BaBar detector*, in *B physics and CP violation. Proceedings, International Workshop, BCP4, Ise-Shima, Japan, February 19-23, 2001*, pp. 144–149, 2001. hep-ex/0103046.

[30] **LHCb** Collaboration, R. Aaij *et al.*, *A precise measurement of the $B^0$ meson oscillation frequency*, *Eur. Phys. J.* **C76** (2016), no. 7 412, [1604.03475].

[31] **Belle** Collaboration, K. Abe *et al.*, *Observation of large CP violation in the neutral B meson system*, *Phys. Rev. Lett.* **87** (2001) 091802, [hep-ex/0107061].

[32] **BaBar** Collaboration, B. Aubert *et al.*, *Observation of CP violation in the $B^0$ meson system*, *Phys. Rev. Lett.* **87** (2001) 091801, [hep-ex/0107013].

[33] **LHCb** Collaboration, R. Aaij *et al.*, *Observation of $D^0 - \overline{D}^0$ oscillations*, *Phys. Rev. Lett.* **110** (2013), no. 10 101802, [1211.1230].

[34] A. J. Schwartz, *Charm Physics Prospects at Belle II*, *PoS* **CHARM2016** (2017) 042, [1701.07159].

[35] **LHCb** Collaboration, R. Aaij *et al.*, *Test of lepton universality using $B^+ \to K^+\ell^+\ell^-$ decays*, *Phys. Rev. Lett.* **113** (2014) 151601, [1406.6482].

[36] **LHCb** Collaboration, R. Aaij *et al.*, *Measurement of the ratio of branching fractions $\mathcal{B}(\bar{B}^0 \to D^{*+}\tau^-\bar{\nu}_\tau)/\mathcal{B}(\bar{B}^0 \to D^{*+}\mu^-\bar{\nu}_\mu)$*, *Phys. Rev. Lett.* **115** (2015), no. 11 111803, [1506.08614]. [Erratum: Phys. Rev. Lett.115,no.15,159901(2015)].

[37] **LHCb** Collaboration, R. Aaij *et al.*, *Measurements of the S-wave fraction in $B^0 \to K^+\pi^-\mu^+\mu^-$ decays and the $B^0 \to K^*(892)^0\mu^+\mu^-$ differential branching fraction*, *JHEP* **11** (2016) 047, [1606.04731].

[38] **BaBar** Collaboration, J. P. Lees *et al.*, *Evidence for an excess of $\bar{B} \to D^{(*)}\tau^-\bar{\nu}_\tau$ decays*, *Phys. Rev. Lett.* **109** (2012) 101802, [1205.5442].

[39] **Belle** Collaboration, M. Huschle *et al.*, *Measurement of the branching ratio of $\bar{B} \to D^{(*)}\tau^-\bar{\nu}_\tau$ relative to $\bar{B} \to D^{(*)}\ell^-\bar{\nu}_\ell$ decays with hadronic tagging at Belle*, *Phys. Rev.* **D92** (2015), no. 7 072014, [1507.03233].

[40] M. Bordone, G. Isidori, and A. Pattori, *On the Standard Model predictions for $R_K$ and $R_{K^*}$*, *Eur. Phys. J.* **C76** (2016), no. 8 440, [1605.07633].

[41] **LHCb** Collaboration, S. Bifani, *Search for new physics with $b \to sl^+l^-$ decays at LHCb*, *LHCb seminar at CERN* (18 April 2017).

[42] A. Vladikas, *FLAG: Lattice QCD Tests of the Standard Model and Foretaste for Beyond*, *PoS* **FPCP2015** (2015) 016, [1509.01155].

[43] P. A. Boyle, *Hierarchically deflated conjugate gradient*, 1402.2585.

[44] T. Blum, T. Izubuchi, and E. Shintani, *Error reduction technique using covariant approximation and application to nucleon form factor*, *PoS* **LATTICE2012** (2012) 262, [1212.5542].

[45] E. Shintani, R. Arthur, T. Blum, T. Izubuchi, C. Jung, and C. Lehner, *Covariant approximation averaging*, *Phys. Rev.* **D91** (2015), no. 11 114511, [1402.0244].

[46] J. Smit, *Introduction to Quantum Fields on a Lattice*. Cambridge University Press, 2002.

[47] B. Paladini and J. C. Sexton, *Asymptotic expansion of the lattice scalar propagator in coordinate space*, *Phys. Lett.* **B448** (1999) 76–84, [hep-lat/9805021].

[48] Wolfram, *Mathematica 9.0*, 2012.

[49] D. B. Kaplan, *Chiral Symmetry and Lattice Fermions*, in *Modern perspectives in lattice QCD: Quantum field theory and high performance computing. Proceedings, International School, 93rd Session, Les Houches, France, August 3-28, 2009*, pp. 223–272, 2009. 0912.2560.

[50] M. E. Peskin and D. V. Schroeder, *An Introduction to Quantum Field Theory*. Westview, 1995.

[51] P. H. Ginsparg and K. G. Wilson, *A Remnant of Chiral Symmetry on the Lattice*, *Phys. Rev.* **D25** (1982) 2649.

[52] P. Hasenfratz, V. Laliena, and F. Niedermayer, *The Index theorem in QCD with a finite cutoff*, *Phys. Lett.* **B427** (1998) 125–131, [hep-lat/9801021].

[53] V. A. Rubakov and M. E. Shaposhnikov, *Do We Live Inside a Domain Wall?*, *Phys. Lett.* **B125** (1983) 136–138.

[54] D. B. Kaplan, *A Method for simulating chiral fermions on the lattice*, *Phys. Lett.* **B288** (1992) 342–347, [hep-lat/9206013].

[55] V. Furman and Y. Shamir, *Axial symmetries in lattice QCD with Kaplan fermions*, *Nucl. Phys.* **B439** (1995) 54–78, [hep-lat/9405004].

[56] H. Neuberger, *More about exactly massless quarks on the lattice*, *Phys. Lett.* **B427** (1998) 353–355, [hep-lat/9801031].

[57] M. Luscher, *Exact chiral symmetry on the lattice and the Ginsparg-Wilson relation*, *Phys. Lett.* **B428** (1998) 342–345, [hep-lat/9802011].

[58] P. Hernandez, K. Jansen, and M. Luscher, *Locality properties of Neuberger's lattice Dirac operator*, *Nucl. Phys.* **B552** (1999) 363–378, [hep-lat/9808010].

[59] **RBC, UKQCD** Collaboration, D. J. Antonio *et al.*, *Localization and chiral symmetry in three flavor domain wall QCD*, *Phys. Rev.* **D77** (2008) 014509, [0705.2340].

[60] M. Luscher, *Chiral gauge theories revisited*, *Subnucl. Ser.* **38** (2002) 41–89, [hep-th/0102028].

[61] R. C. Brower, H. Neff, and K. Orginos, *Mobius fermions: Improved domain wall chiral fermions*, *Nucl. Phys. Proc. Suppl.* **140** (2005) 686–688, [hep-lat/0409118]. [,686(2004)].

[62] R. C. Brower, H. Neff, and K. Orginos, *Mobius fermions*, *Nucl. Phys. Proc. Suppl.* **153** (2006) 191–198, [hep-lat/0511031].

[63] R. C. Brower, H. Neff, and K. Orginos, *The Móbius Domain Wall Fermion Algorithm*, 1206.5214.

[64] **RBC, UKQCD** Collaboration, T. Blum *et al.*, *Domain wall QCD with physical quark masses*, *Phys. Rev.* **D93** (2016), no. 7 074505, [1411.7017].

[65] Y. Shamir, *Chiral fermions from lattice boundaries*, *Nucl. Phys.* **B406** (1993) 90–106, [hep-lat/9303005].

[66] C. Gattringer and C. B. Lang, *Quantum chromodynamics on the lattice*, *Lect. Notes Phys.* **788** (2010) 1–343.

[67] A. V. Manohar and C. T. Sachrajda, *Quark Masses*, .

[68] S. Hashimoto and T. Onogi, *Heavy quarks on the lattice*, *Ann. Rev. Nucl. Part. Sci.* **54** (2004) 451–486, [hep-ph/0407221].

[69] Y. Iwasaki and T. Yoshie, *Renormalization Group Improved Action for SU(3) Lattice Gauge Theory and the String Tension*, *Phys. Lett.* **B143** (1984) 449–452.

[70] Y. Iwasaki, *Renormalization Group Analysis of Lattice Theories and Improved Lattice Action: Two-Dimensional Nonlinear O(N) Sigma Model*, *Nucl. Phys.* **B258** (1985) 141–156.

[71] **RBC, UKQCD** Collaboration, R. Arthur *et al.*, *Domain Wall QCD with Near-Physical Pions*, *Phys. Rev.* **D87** (2013) 094514, [1208.4412].

[72] P. A. Boyle, L. Del Debbio, A. Juttner, A. Khamseh, F. Sanfilippo, and J. T. Tsang, *The decay constants* $\mathbf{f_D}$ *and* $\mathbf{f_{D_s}}$ *in the continuum limit of* $\mathbf{N_f = 2 + 1}$ *domain wall lattice QCD*, 1701.02644.

[73] P. A. Boyle, A. Juttner, C. Kelly, and R. D. Kenway, *Use of stochastic sources for the lattice determination of light quark physics*, *JHEP* **08** (2008) 086, [0804.1501].

[74] Y.-G. Cho, S. Hashimoto, A. Juttner, T. Kaneko, M. Marinkovic, J.-I. Noaki, and J. T. Tsang, *Improved lattice fermion action for heavy quarks*, *JHEP* **05** (2015) 072, [1504.01630].

[75] P. Boyle, A. Juttner, M. K. Marinkovic, F. Sanfilippo, M. Spraggs, and J. T. Tsang, *An exploratory study of heavy domain wall fermions on the lattice*, *JHEP* **04** (2016) 037, [1602.04118].

[76] G. Martinelli, C. Pittori, C. T. Sachrajda, M. Testa, and A. Vladikas, *A General method for nonperturbative renormalization of lattice operators*, *Nucl. Phys.* **B445** (1995) 81–108, [hep-lat/9411010].

[77] C. Sturm, Y. Aoki, N. H. Christ, T. Izubuchi, C. T. C. Sachrajda, and A. Soni, *Renormalization of quark bilinear operators in a momentum-subtraction scheme with a nonexceptional subtraction point*, *Phys. Rev.* **D80** (2009) 014501, [0901.2599].

[78] A. Vladikas, *Three Topics in Renormalization and Improvement*, in *Modern perspectives in lattice QCD: Quantum field theory and high performance computing. Proceedings, International School, 93rd Session, Les Houches, France, August 3-28, 2009*, pp. 161–222, 2011. 1103.1323.

[79] G. 't Hooft and M. J. G. Veltman, *Regularization and Renormalization of Gauge Fields*, *Nucl. Phys.* **B44** (1972) 189–213.

[80] P. Breitenlohner and D. Maison, *Dimensional Renormalization and the Action Principle*, *Commun. Math. Phys.* **52** (1977) 11–38.

[81] P. Boyle, L. Del Debbio, and A. Khamseh, *Massive momentum-subtraction scheme*, *Phys. Rev.* **D95** (2017), no. 5 054505, [1611.06908].

[82] V. A. Smirnov, *Feynman integral calculus*. 2006.

[83] A. V. Smirnov, *Algorithm FIRE – Feynman Integral REduction*, *JHEP* **10** (2008) 107, [0807.3243].

[84] F. Chavez and C. Duhr, *Three-mass triangle integrals and single-valued polylogarithms*, *JHEP* **11** (2012) 114, [1209.2722].

[85] J. C. Collins, *Renormalization*, vol. 26 of *Cambridge Monographs on Mathematical Physics*. Cambridge University Press, Cambridge, 1986.

[86] W. E. Caswell and A. D. Kennedy, *A SIMPLE APPROACH TO RENORMALIZATION THEORY*, *Phys. Rev.* **D25** (1982) 392.

[87] S. Weinberg, *New approach to the renormalization group*, *Phys. Rev.* **D8** (1973) 3497–3509.

[88] M. Testa, *Some observations on broken symmetries*, *JHEP* **04** (1998) 002, [hep-th/9803147].

[89] T. Blum *et al.*, *Quenched lattice QCD with domain wall fermions and the chiral limit*, *Phys. Rev.* **D69** (2004) 074502, [hep-lat/0007038].

[90] G. M. de Divitiis, R. Petronzio, and N. Tantalo, *On the discretization of physical momenta in lattice QCD*, *Phys. Lett.* **B595** (2004) 408–413, [hep-lat/0405002].

[91] C. T. Sachrajda and G. Villadoro, *Twisted boundary conditions in lattice simulations*, *Phys. Lett.* **B609** (2005) 73–85, [hep-lat/0411033].

[92] **RBC, UKQCD** Collaboration, R. Arthur and P. A. Boyle, *Step Scaling with off-shell renormalisation*, *Phys. Rev.* **D83** (2011) 114511, [1006.0422].

[93] L. G. Almeida and C. Sturm, *Two-loop matching factors for light quark masses and three-loop mass anomalous dimensions in the RI/SMOM schemes*, *Phys. Rev.* **D82** (2010) 054017, [1004.4613].

[94] M. Gorbahn and S. Jager, *Precise MS-bar light-quark masses from lattice QCD in the RI/SMOM scheme*, *Phys. Rev.* **D82** (2010) 114001, [1004.3997].

[95] J. Frison, P. Boyle, and N. Garron, *NPR step-scaling across the charm threshold*, *PoS* **LATTICE2014** (2015) 285, [1412.0834].

[96] O. Bar and M. Golterman, *Excited-state contribution to the axial-vector and pseudoscalar correlators with two extra pions*, *Phys. Rev.* **D87** (2013), no. 1 014505, [1209.2258].

[97] **Fermilab Lattice, MILC** Collaboration, A. Bazavov *et al.*, *Charmed and light pseudoscalar meson decay constants from four-flavor lattice QCD with physical light quarks*, *Phys. Rev.* **D90** (2014), no. 7 074509, [1407.3772].

[98] T. A. DeGrand and M. W. Hecht, *More about orbitally excited hadrons from lattice QCD*, *Phys. Rev.* **D46** (1992) 3937–3944, [hep-lat/9206011].

[99] G. P. Lepage, *Simulating heavy quarks*, *Nucl. Phys. Proc. Suppl.* **26** (1992) 45–56.

[100] A. Bazavov *et al.*, *Neutral B-meson mixing from three-flavor lattice QCD: Determination of the SU(3)-breaking ratio $\xi$*, *Phys. Rev.* **D86** (2012) 034503, [1205.7013].

[101] **HPQCD** Collaboration, E. Gamiz, C. T. H. Davies, G. P. Lepage, J. Shigemitsu, and M. Wingate, *Neutral B Meson Mixing in Unquenched Lattice QCD*, *Phys. Rev.* **D80** (2009) 014503, [0902.1815].

[102] **ETM** Collaboration, N. Carrasco *et al.*, *B-physics from $N_f = 2$ tmQCD: the Standard Model and beyond*, *JHEP* **03** (2014) 016, [1308.1851].

[103] C. Morningstar and M. J. Peardon, *Analytic smearing of SU(3) link variables in lattice QCD*, *Phys. Rev.* **D69** (2004) 054501, [hep-lat/0311018].

[104] L. Lellouch, R. Sommer, B. Svetitsky, A. Vladikas, and L. F. Cugliandolo, eds., *Modern perspectives in lattice QCD: Quantum field theory and high performance computing. Proceedings, International School, 93rd Session, Les Houches, France, August 3-28, 2009*, 2011.

[105] A. V. Smirnov, *FIRE5: a C++ implementation of Feynman Integral REduction*, *Comput. Phys. Commun.* **189** (2015) 182–191, [1408.2372].